JSCSEN 90(1)1-135(2025)

ISSN 1820-7421(Online)

Journal of the Serbian Chemical Society

Electronic version

VOLUME 90

No 1

BELGRADE 2025

Available on line at

www.shd.org.rs/JSCS/

The full search of JSCS is available through

DOAJ DIRECTORY OF OPEN ACCESS JOURNALS

www.doaj.org

The **Journal of the Serbian Chemical Society** (formerly Glasnik Hemijskog društva Beograd), one volume (12 issues) per year, publishes articles from the fields of chemistry. The **Journal** is financially supported by the **Ministry of Education, Science and Technological Development of the Republic of Serbia.**
Articles published in the **Journal** are indexed in **Clarivate Analytics products: Science Citation Index-Expanded™** – accessed *via* **Web of Science®** and **Journal Citation Reports®**.
Impact Factor announced on 28 June, 2023: **1.000; 5-year Impact Factor**: **1.100**.
Articles appearing in the **Journal** are also abstracted by: **Scopus, Chemical Abstracts Plus (CAplus℠), Directory of Open Access Journals, Referativnii Zhurnal (VINITI), RSC Analytical Abstracts, EuroPub, Pro Quest** and **Asian Digital Library.**

Publisher:	**Serbian Chemical Society**, Karnegijeva 4/III, P. O. Box 36, 1120 Belgrade 35, Serbia tel./fax: +381–11–3370–467, E-mails: **Society** – shd@shd.org.rs; **Journal** – jscs@shd.org.rs Home Pages: **Society** – http://www.shd.org.rs/, **Journal** – http://www.shd.org.rs/JSCS/
Internet Service:	Contents, Abstracts and full papers (from Vol 64, No. 1, 1999) are available in the electronic form at the Web Site of the **Journal** (http://www.shd.org.rs/JSCS/).
Former Editors:	**Nikola A. Pušin** (1930–1947), **Aleksandar M. Leko** (1948–1954), **Panta S. Tutundžić** (1955**–**1961), **Miloš K. Mladenović** (1962–1964), **Đorđe M. Dimitrijević** (1965–1969), **Aleksandar R. Despić** (1969–1975), **Slobodan V. Ribnikar** (1975–1985), **Dragutin M. Dražić** (1986–2006).
Editor-in-Chief:	BRANISLAV Ž. **NIKOLIĆ**, Serbian Chemical Society (E-mail: jscs-ed@shd.org.rs)
Deputy Editor:	DUŠAN **SLADIĆ**, Faculty of Chemistry, University of Belgrade
Sub editors:	
Organic Chemistry	DEJAN **OPSENICA**, Institute of Chemistry, Technology and Metallurgy, University of Belgrade JÁNOS **CSANÁDI**, Faculty of Science, University of Novi Sad
Biochemistry and Biotechnology	OLGICA **NEDIĆ**, INEP – Institute for the Application of Nuclear Energy, University of Belgrade
Inorganic Chemistry	BILJANA **GLIŠIĆ**, Faculty of Science, University of Kragujevac
Theoretical Chemistry	MATIJA **ZLATAR**, Institute of Chemistry, Technology and Metallurgy, University of Belgrade MILOŠ **MILIČIĆ**, Faculty of Chemistry, University of Belgrade
Physical Chemistry	LJILJANA **DAMJANOVIĆ-VASILIĆ**, Faculty of Physical Chemistry, University of Belgrade
Electrochemistry	SNEŽANA **GOJKOVIĆ**, Faculty of Technology and Metallurgy, University of Belgrade
Analytical Chemistry	RADA **BAOŠIĆ**, Faculty of Chemistry, University of Belgrade
Polymers	BRANKO **DUNJIĆ**, Faculty of Technology and Metallurgy, University of Belgrade
Thermodynamics	MIRJANA **KIJEVČANIN**, Faculty of Technology and Metallurgy, University of Belgrade
Chemical Engineering	TATJANA **KALUĐEROVIĆ RADOIČIĆ**, Faculty of Technology and Metallurgy, University of Belgrade
Materials	RADA **PETROVIĆ**, Faculty of Technology and Metallurgy, University of Belgrade
Metallic Materials and Metallurgy	ANA **KOSTOV**, Mining and Metallurgy Institute Bor, University of Belgrade
Environmental and Geochemistry	VESNA **ANTIĆ**, Faculty of Agriculture, University of Belgrade
History of and Education in Chemistry	DRAGICA **TRIVIĆ**, Faculty of Chemistry, University of Belgrade
English Language Editors:	LYNNE **KATSIKAS**, Serbian Chemical Society VLATKA **VAJS**, Serbian Chemical Society JASMINA **NIKOLIĆ**, Faculty of Technology and Metallurgy, University of Belgrade
Technical Editors:	VLADIMIR **PANIĆ**, Institute of Chemistry, Technology and Metallurgy, University of Belgrade, MARIO **ZLATOVIĆ**, Faculty of Chemistry, University of Belgrade
Journal Manager & Web Master:	MARIO **ZLATOVIĆ**, Faculty of Chemistry, University of Belgrade
Office:	VERA **ĆUŠIĆ**, Serbian Chemical Society

Editorial Board

From abroad: **R. Adžić**, Brookhaven National Laboratory (USA); **A. Casini**, University of Groningen (The Netherlands); **G. Cobb**, Baylor University (USA); **D. Douglas**, University of British Columbia (Canada); **G. Inzelt**, Etvos Lorand University (Hungary); **J. Kenny**, University of Perugia (Italy); **Ya. I. Korenman**, Voronezh Academy of Technology (Russian Federation); **M. D. Lechner**, University of Osnabrueck (Germany); **S. Macura**, Mayo Clinic (USA); **M. Spiteller**, INFU, Technical University Dortmund (Germany); **M. Stratakis**, University of Crete (Grecce); **M. Swart**, University de Girona (Cataluna, Spain); **G. Vunjak-Novaković**, Columbia University (USA); **P. Worsfold**, University of Plymouth (UK); **J. Zagal**, Universidad de Santiago de Chile (Chile).

From Serbia: **B. Abramović**, **V. Antić**, **R. Baošić**, **V. Beškoski**, **J. Csanadi**, **Lj. Damjanović-Vasilić**, **A. Dekanski**, **V. Dondur**, **B. Dunjić**, **M. Đuran, B. Glišić, S. Gojković**, **I. Gutman**, **B. Jovančićević**, **I. Juranić**, **T. Kaluđerović Radoičić**, **L. Katsikas**, **M. Kijevčanin**, **A. Kostov**, **V. Leovac**, **S. Milonjić**, **V.B. Mišković-Stanković**, **O. Nedić**, **B. Nikolić**, **J. Nikolić**, **D. Opsenica**, **V. Panić**, **M. Petkovska**, **R. Petrović**, **I. Popović**, **B. Radak**, **S. Ražić**, **D. Sladić**, **S. Sovilj**, **S. Šerbanović**, **B. Šolaja**, **Ž. Tešić**, **D. Trivić**, **V. Vajs, M. Zlatović**.

Subscription: The annual subscription rate is **150.00 €** including postage (surface mail) and handling. For Society members from abroad rate is **50.00 €**. For the proforma invoice with the instruction for bank payment contact the Society Office (E-mail: shd@shd.org.rs) or see JSCS Web Site: http://www.shd.org.rs/JSCS/, option Subscription.
Godišnja pretplata: Za članove SHD: **2.500,00 RSD**, za penzionere i studente: **1000,00 RSD**, a za ostale: **3.500,00 RSD**:za organizacije i ustanove: **16.000,00 RSD**. Uplate se vrše na tekući račun Društva: **205-13815-62**, poziv na broj **320**, sa naznakom "pretplata za JSCS".

Nota: Radovi čiji su svi autori članovi SHD prioritetno se publikuju.
Odlukom Odbora za hemiju Republičkog fonda za nauku Srbije, br. 66788/1 od 22.11.1990. godine, koja je kasnije potvrđena odlukom Saveta Fonda, časopis je uvršten u kategoriju međunarodnih časopisa (**M-23**). Takođe, aktom Ministarstva za nauku i tehnologiju Republike Srbije, 413-00-247/2000-01 od 15.06.2000. godine, ovaj časopis je proglašen za publikaciju od posebnog interesa za nauku. **Impact Factor** časopisa objavljen 28. juna 2023. godine je **1,000**, a petogodišnji **Impact Factor 1,100**.

Journal of the Serbian Chemical Society
JSCS-info@shd.org.rs • www.shd.org.rs/JSCS

J. Serb. Chem. Soc. Vol. 90, No. 1 (2025)

CONTENTS*

Published by the Serbian Chemical Society
Karnegijeva 4/III, P.O. Box 36, 11120 Belgrade, Serbia
Printed by the Faculty of Technology and Metallurgy
Karnegijeva 4, P.O. Box 35-03, 11120 Belgrade, Serbia

* For colored figures in this issue please see electronic version at the Journal Home Page: http://www.shd.org.rs/JSCS/

Journal of the Serbian Chemical Society
JSCS-info@shd.org.rs • www.shd.org.rs/JSCS
J. Serb. Chem. Soc. 90 (1) 1–12 (2025)
JSCS–5815
Original scientific paper
Published 1 February 2025

Investigating the therapeutic potential of monothiocarbohydrazones: A comprehensive *in vitro* evaluation of antioxidant, antimicrobial and cytotoxic activities

GORANA S. MRĐAN[1]*#, SANJA S. VLAISAVLJEVIĆ[1], PETAR N. KNEŽEVIĆ[2], ISIDORA N. NIKOLIĆ[2], DINA G. TENJI[2] and BORKO M. MATIJEVIĆ[1#]

[1]*University of Novi Sad, Faculty of Sciences, Department of Chemistry, Biochemistry and Environmental Protection, Novi Sad, Serbia and* [2]*University of Novi Sad, Faculty of Sciences, Department of Biology and Ecology, Novi Sad, Serbia*

(Received 1 February, revised 21 May, accepted 22 September 2024)

Abstract: Organic compounds, particularly those with nitrogen and sulphur heteroatoms, constitute over 99 % of clinically approved drugs. Among these, thiocarbohydrazones have been extensively studied, with a focus on symmetrical bis-substituted compounds. However, asymmetric and monosubstituted thiocarbohydrazones remain underexplored, despite their demonstrated high biological potential. This study presents an in-depth *in vitro* evaluation of the antioxidant, antimicrobial, and cytotoxic properties of eighteen previously synthesized and characterized monothiocarbohydrazones. The antioxidant potential was assessed using the DPPH assay, while the antimicrobial activity was determined against Gram-positive bacteria using a modified broth microdilution susceptibility method. The cytotoxic effect was evaluated on human hepatocellular carcinoma using the colorimetric MTT assay. The results reveal that the investigated monothiocarbohydrazones exhibit significant antioxidant and antimicrobial activities. Furthermore, their activity and cytotoxicity are influenced by the stereochemistry of the molecule and the nature and position of the substituents. These findings provide valuable insights for future *in vivo* examinations and underscore the potential of monothiocarbohydrazones in drug development.

Keywords: antimicrobial agents; antioxidant activity; biological activity; cytotoxicity; thiocarbohydrazones.

INTRODUCTION

Thiocarbohydrazones (TCHs) belong to a class of compounds obtained by condensation of thiocarbohydrazide with different types of carbonyl-based com-

* Corresponding author. E-mail: gorana.mrdjan@dh.uns.ac.rs
# Serbian Chemical Society member.
https://doi.org/10.2298/JSC240201089M

pounds. The first synthesis of these derivatives was reported in 1925,[1] but most studies were conducted from the late 1970s when thiocarbohydrazide became commercially available.[2] At the very beginning TCHs have mostly been used in analytical chemistry as spectrophotometric reagents for the determination of elements such as palladium, ruthenium, iridium, gallium, zinc, *etc*.[3–6] Today some of them are also used for analytical research,[7–9] but most studies on thiocarbohydrazones are concerning their potential biological activity. The majority of the compounds tested so far belong to bisubstituted TCHs mainly derived from isatin, pyridyl, salicylaldehyde and related carbonyl compounds. They have proven to be excellent antioxidant,[10–16] antimicrobial,[10,17–20] antiviral,[21] anticancer,[22–24] and antitumor[25] agents. On the other hand, monosubstituted TCHs are much less investigated, although some studies confirm their exceptional biological activity too, somewhere even more significant regarding analogous bisubstituted derivatives.[20–22] Continuing our work on monothiocarbohydrazones (mTCHs) where we have published synthesis and physicochemical characterization of eighteen compounds,[26] in this paper we present the results of the investigation on their potential biological activity. The antioxidant and antimicrobial activities of eighteen mTCHs were evaluated, along with their cytotoxic effects, using the human hepatocellular carcinoma HepG2 cell line, a standard model in toxicity assays, representing the liver, the primary organ responsible for biotransformation and detoxification of numerous xenobiotics.[27,28]

EXPERIMENTAL

Synthesis and structures of mTCHs

All thiocarbohydrazone derivatives tested within this paper were previously synthesized and characterized by Mrđan *et al.* 2021.[26] Structures and numbering of these compounds are presented in Table I.

TABLE I. Structures and numbering of thiocarbohydrazones

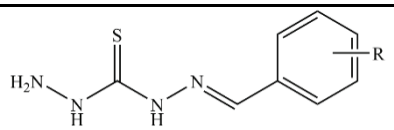

Compound	R
1	H
2/**3**/**4**	–OH
5/**6**/**7**	$–CH_3$
8/**9**/**10**	$–NO_2$
11/**12**/**13**	$–OCH_3$
14/**15**	–Cl
16/**17**	–Br
18	–F

Evaluation of antioxidant activity

The antioxidant activity of selected thiocarbohydrazones was evaluated using 2,2-diphenyl-1-picryl hydrazyl (DPPH) assay. The measurements were performed according to the early described spectrophotometric method with some modifications.[29] The stock solutions of TCHs were prepared in DMSO at a concentration of 5 mg mL^{-1}. After 30 min of incubation, the absorbance was measured at 515 nm. All the measurements were performed in triplicate. Results obtained were expressed as Trolox equivalent capacity per gram of dry weight of the tested solutions (mg TE/g d.w.).

Antimicrobial agents

Eighteen different compounds of mTCH were dissolved in 100 % dimethyl sulphoxide (DMSO) to prepare the stock solutions with a concentration of 20 mg mL^{-1}. The stock solutions were stored at room temperature. The final concentration of DMSO was not more than 1 % in broth.

Bacterial strains and culture conditions

Four reference Gram-positive bacteria: *Staphylococcus aureus* (ATCC 25923), *Listeria monocytogenes* (ATCC 19111), *Enterococcus faecalis* (ATCC 2912) and *Bacillus subtilis* (ATCC 6633) were used in antimicrobial tests. The overnight cultures were grown at 37 °C on Muller–Hinton agar (MHA), except *L. monocytogenes* and *E. faecalis* which were grown on Brain–Heart infusion agar (BHIA).

Antibacterial activity of monothiocarbohydrazones

The modified broth microdilution susceptibility method was used to determine the antibacterial activity of monothiocarbohydrazones (CLSI 2015). The serial dilutions of tested agents were prepared in a 96-well microtiter plate ranging from 128 to 2 μg mL^{-1} (DMSO concentration in the final volume was ≤ 0.8 %). The overnight cultures were used for preparing bacterial suspensions by adjusting the optical density of 0.5 using McFarland densitometer (Biosan, Latvia). Muller–Hinton (MHB) and Brain–Heart infusion broth (BHIB) were used in all experiments. The bacterial suspensions were diluted with MHB or BHIB (1:100 volume ratio) to achieve the inoculum density of approximately 2.0×10^6 CFU mL^{-1}. After the addition of equal volumes of the previously prepared inocula (1:1 volume ratio) to each well, the final bacterial count was approximately 1×10^6 CFU mL^{-1}. The microtiter plates were incubated for 24 h at 37 °C. Each experiment was performed in triplicate, in at least two independent repeats and results were presented as the geometric mean of the obtained values.

Cell culture

Human hepatocellular carcinoma HepG2 (European Collection of Authenticated Cell Cultures, ECACC 85011430, Salisbury, UK), cells were grown in minimum essential medium eagle (MEM, Sigma) growth medium, containing 10 % FBS (Gibco), sodium bicarbonate, penicillin/streptomycin, sodium pyruvate (0.11 g/L) and 10 mM HEPES buffer. The cell culture process followed conditions and protocol previously described by Vulin *et al.* 2022.[30]

Cytotoxicity assay

The cytotoxic effect of tested substances was assessed using a colorimetric MTT assay. For the experiments, HepG2 cells were seeded at a density of 20.000 cells/well in 96-well plates and incubated overnight before the treatment with test substances. After the 24 h incubation period, the test medium was replaced with MTT (final concentration 0.5 mg mL^{-1} in growth medium) and incubated for an additional 3 h, followed by the medium removal. The

formazan crystals were dissolved in 0.04 M HCl in isopropanol. The optical density was measured at 540 and 690 nm, using a Multiskan™ GO microplate spectrophotometer (Thermo Scientific). The activity of mitochondrial dehydrogenase (%) was calculated from the absorbances. The cell viability (*CV*) was expressed in percentages and calculated from the absorbances according to the formula:

$$CV = 100 - 100\frac{1 - A_{\text{Tested supstance}}}{A_{\text{Control}}} \quad (1)$$

where $A_{\text{Tested substance}}$ and A_{Control} represent the absorbances measured in the experimental and control wells, respectively. Hence, the values of the control are presented as 100 %.

Each concentration of all tested substances was examined in hexaplicates, in three independent experiments including treatment-free control (growth medium), solvent controls and blank wells (cell free wells). The final concentration of DMSO in treatments did not exceed 1 % and did not result in any background response.

EC_{50} value was calculated based on dose-response data using concentrations of the tested substances and the corresponding effects on cell growth in GraphPad Prism 6 (GraphPad Software, Inc., La Jolla, CA, USA). The dose-response curve was determined using the log inhibitor *vs*. normalized response-variable slope procedure.[31]

RESULTS AND DISCUSSION

Antioxidant activity of monothiocarbohydrazones

Many diseases occur as a result of oxidative stress, which represents an imbalance between free radicals and antioxidants present in the body. Antioxidants are substances that counteract and stop the action of free radicals by creating products that are non-toxic and do not cause damage to cellular structures or cells. One of the most used *in vitro* assays for the determination of the free-radical scavenging activity is the DPPH assay, applied in this paper. Eighteen compounds of monothiocarbohydrazones were tested and the results obtained are presented as mg of Trolox equivalents (TE) per g of dry weight (mg TE/g d.w.). The obtained values are shown in Table II.

TABLE II. Results of DPPH assay (mg TE/g d.w.) for monothiocarbohydrazones

Compound	Value	Compound	Value	Compound	Value
1	152.85±0.08	**7**	106.63±0.06	**13**	155.30±0.04
2	145.50±0.04	**8**	151.86±0.10	**14**	156.06±0.06
3	156.51±0.11	**9**	103.89±0.09	**15**	159.50±0.09
4	153.57±0.05	**10**	152.88±0.08	**16**	114.03±0.02
5	152.01±0.05	**11**	152.72±0.05	**17**	95.50±0.02
6	153.39±0.02	**12**	113.54±0.03	**18**	152.03±0.06

In general, all the examined compounds have shown great antioxidant activity in the range from 95 to 160 mg TE/g d.w.

It is well known that the effectiveness of a compound as an antioxidant can depend on its structure, i.e. the position and type of substituent present. As can be

seen from Table II the compounds **14** and **15** have shown the highest activity with chlorine as a substituent. The previous studies of structurally similar compounds have shown that derivatives with halogen substituents, especially chlorine, stand out with the highest activity.[10,14,32] Compound **18** with fluorine as a substituent has also exhibited significant activity, while the compounds with bromine (**16** and **17**) have less antioxidant power. Compounds **13** (4-OCH_3) and **3** (3-OH) also have great scavenging capacity, which is in agreement with studies where the compounds with these two functional groups also stand out as great antioxidants.[15,16,33]

Antimicrobial activity of monothiocarbohydrazones

Our previous studies showed that monothiocarbohydrazones are active only against Gram-positive bacteria, so in the present study, we focused on this group of microorganisms. It is known that gram-negative bacteria easily bypass the action of most drug molecules because of their unique outer membrane, that acts as a potent barrier restricting the entry of compounds into the cell. Low molecular weight and low lipophilicity are identified as two important parameters to enhance drug entry into Gram-negative bacteria.[34] Thus, high lipophilic nature of examined monothiocarbohydrazones could render them inactive in Gram-negative bacteria. As can be seen from Table III, the selected mTCHs showed activity

TABLE III. Susceptibility (*MIC* / μg mL^{-1}) of selected Gram-positive bacteria to monothiocarbohydrazones

mTCH	Bacteria			
	S. aureus (ATCC 25923)	*L. monocytogenes* (ATCC 19111)	*E. faecalis* (ATCC 2912)	*B. subtilis* (ATCC 6633)
1	>128	>128	>128	45
2	64	>128	>128	45
3	64	>128	>128	45
4	128	>128	>128	23
5	32	>128	>128	32
6	32	>128	>128	16
7	32	>128	>128	32
8	>128	>128	>128	>128
9	>128	>128	>128	>128
10	128	>128	>128	45
11	64	>128	>128	23
12	>128	>128	>128	64
13	>128	>128	>128	76
14	32	>128	>128	23
15	16	>128	>128	27
16	>128	>128	>128	>128
17	>128	>128	>128	54
18	32	>128	>128	64

against *S. aureus* and *B. subtilis*, but not against *L. monocytogenes* and *E. faecalis* at the highest applied concentration (128 μg mL^{-1}). This difference in susceptibility can be a consequence of different medium application since both resistant bacteria were grown using BHIA. As BHIA contains calf brain and beef heart extracts, it is possible that the extracts contain components that react with mTCHs and neutralize them. In order to confirm this assumption some of the compounds were examined again against *S. aureus* and *B. subtilis*, but now the bacterial suspension was prepared in BHIA, and the obtained results are presented in Table IV. *MIC* values were higher, compared to the previous results. It can be concluded that the use of BHIA leads to a decrease in mTCHs activity, probably due to the inhibition by broth components and this can be the reason why there is no activity against *L. monocytogenes* and *E. faecalis*. Considering that these two bacterial species grow poorly in MHA and that BHIA affects the activity of the given compounds, it is necessary to find an alternative broth that would support growth and not affect the activity of the compounds in order to precisely determine the *MIC* values.

TABLE IV. Susceptibility (*MIC* / μg mL^{-1}) of *S. aureus* and *B. subtilis* (BHIA) to selected mTCHs

mTCH	Bacteria	
	S.aureus (ATCC 25923)	*B. subtilis* (ATCC 6633)
3	128	>128
4	>128	>128
5	>128	>128
6	128	>128
7	>128	>128
11	>128	>128
14	128	128
18	>128	>128

The antibacterial activity of mTCHs against *S. aureus* and *B. subtilis* (Table III) can be ascribed to their lipophilic nature and easier penetration into the cells[17,35] and/or oxidation of thiono group by hydrogen peroxide and formation of toxic reaction compounds.[36,37] In general mTCHs have shown good activity against *S. aureus* and *B. subtilis.* The most active compounds were compounds **14** and **15** which have chlorine as a substituent. In previous studies[36,37] it has been proven that the compounds with halogen elements as substituents show high activity against bacteria. This trend also follows compound **18** with fluorine as a substituent (*MIC* 32 and 64 μg mL^{-1}), but it does not the compounds **16** and **17** that contain bromine. Significant activity have also shown the compounds **2**–**4** with OH-group as a substituent (2-OH, 3-OH and 4-OH, respectively) and com-

pounds **5**–**7** with CH_3-group as a substituent (2-CH_3, 3-CH_3 and 4-CH_3, respectively).

Cytotoxicity of monothiocarbohydrazones

The cytotoxicity of mTCHs was evaluated using the HepG2 cell line, with effective concentrations (EC_{50}) ranging from 20.12 to 138.04 μg mL^{-1} (Table V).

TABLE V. Effective concentrations (EC_{50}) of tested mTCHs for HepG2 cell line

Compd.	EC_{50} / μg mL^{-1}	r^2	Compd.	EC_{50} / μg mL^{-1}	r^2
1	36.22	0.960	**10**	88.94	0.901
2	34.67	0.980	**11**	50.12	0.926
3	109.65	0.950	**12**	44.17	0.980
4	138.04	0.962	**13**	70.78	0.880
5	28.84	0.994	**14**	133.80	0.939
6	43.71	0.936	**15**	27.54	0.970
7	29.51	0.986	**16**	32.20	0.980
8	20.12	0.990	**17**	29.76	0.980
9	36.16	0.840	**18**	120.23	0.963

The results showed that the cytotoxicity of thiocarbohydrazones varied depending on the nature of the substituents and other factors. The most cytotoxic compound was compound **8**, which had an $–NO_2$ group, with an EC_{50} of 20.12 μg mL^{-1}. This substituent is a strong electron-withdrawing group that can increase the intramolecular charge transfer and the lipophilicity of the thiocarbohydrazone molecule, which may enhance its cellular uptake and interaction with DNA. Moreover, this group can act as a redox-active centre that can induce oxidative stress in cells, leading to apoptosis.[40,41] However, the compounds **9** and **10** with the same $–NO_2$ group showed weaker cytotoxicity, suggesting other influencing factors.

The compounds **5**–**7**, with $–CH_3$ group as a substituent, also showed significant cytotoxicity in the lowest tested concentration (8 μg mL^{-1}). This group is a weak electron-donating group that can also increase the intramolecular charge transfer and the lipophilicity of the thiocarbohydrazone molecule, which may facilitate its cellular uptake and interaction with DNA.[42] In addition, this group can act as a methylating agent that can transfer a methyl group to nucleophilic sites on DNA, RNA or proteins, causing DNA damage and apoptosis.[39]

The least cytotoxic compound was **4**, which had an –OH group as a substituent. This group is a weak electron-donating group that can decrease the intramolecular charge transfer and the lipophilicity of the thiocarbohydrazone molecule, which may hinder its cellular uptake and the interaction with DNA.[40] Furthermore, this group can act as a hydrogen bond donor that can form intermole-

cular interactions with water molecules and increase the solubility of the thiocarbohydrazone compound, which may reduce its bioavailability and efficacy.[41]

These results suggest that the cytotoxicity of thiocarbohydrazones is influenced by several factors. Previous studies have reported that some of these factors, including the nature and position of the substituents, the stereochemistry and conformation of the molecules, the cell line used for testing and the metal complexation of the ligands may modulate the physicochemical and biological properties of thiocarbohydrazones and their metal complexes, affecting their molecular interactions and biological activities.[15,40–42] Thiocarbohydrazones have been tested for cytotoxicity on various, both cancer and non-cancer cell lines in different studies such as mouse fibroblast 3T3 cell line, human erythroleukemia HEL cell line, human normal keratinocyte NCTC-2544, MDA-MB-231 breast cancer and PC-3 human prostate adenocarcinoma cell lines, showing higher cytotoxic potential in cancer call lines.[43,44] Therefore, the difference between compounds with the same substituent on the same places suggest the need for further elucidation of the exact molecular targets and pathways involved in the cytotoxic effect.

CONCLUSION

In this paper, the results of the investigation on the potential biological activity of eighteen monothiocarbohydrazones were presented. The antioxidant and antimicrobial activity of mTCHs was evaluated, as well as their cytotoxic effect. Using the DPPH assay, it was concluded that all examined compounds have great antioxidant activity. The highest activity has shown compounds with chlorine as a substituent, in agreement with previous studies. Compounds with fluorine, methoxy and hydroxyl groups also show excellent activity. Antimicrobial examinations showed that mTCHs have activity against *S. aureus* and *B. subtilis*, but not against *L. monocytogenes* and *E. faecalis*. The results obtained showed that the use of BHIA leads to a decrease in mTCHs activity, probably due to the inhibition by broth components and that is probably the reason why there is no activity against *L. monocytogenes* and *E. faecalis.* The antibacterial activity of mTCHs can be ascribed to their lipophilic nature and easier penetration into the cells and/or oxidation of thiono group by hydrogen peroxide and the formation of toxic reaction compounds. Again, the most active compounds were compounds with chlorine, as well compounds with fluorine, hydroxyl, and methyl group. In the end, the cytotoxic effect of tested substances was assessed using a colorimetric MTT assay. Results obtained showed that the most cytotoxic compound was a compound with nitro group (*para* position). The compounds with methyl group as a substituent (all positions), also showed some significant cytotoxicity, while the least cytotoxic compound was a compound that had hydroxyl group as a substituent (also *para* position). This group is a weak electron-donating group

that can decrease the intramolecular charge transfer and the lipophilicity of the thiocarbohydrazone molecule, which may hinder its cellular uptake and interaction with DNA. These results suggest that the cytotoxicity of thiocarbohydrazones is influenced by several factors: the nature and position of the substituents, the stereochemistry and conformation of the molecules, the cell line used for testing, *etc*.

Acknowledgement. The authors acknowledge financial support of the Ministry of Science, Technological Development and Innovation of the Republic of Serbia (Grants No. 451-03-66/2024-03/200125 and 451-03-65/2024-03/200125).

И З В О Д

ИСПИТИВАЊЕ ТЕРАПЕУТСКОГ ПОТЕНЦИЈАЛА МОНОКАРБОХИДРАЗОНА: *IN VITRO* ПРОЦЕНА АНТИОКСИДАНТНЕ, АНТИМИКРОБНЕ И ЦИТОТОКСИЧНЕ АКТИВНОСТИ

ГОРАНА С. МРЂАН[1], САЊА С. ВЛАИСАВЉЕВИЋ[1], ПЕТАР Н. КНЕЖЕВИЋ[2], ИСИДОРА Н. НИКОЛИЋ[2], ДИНА Г. ТЕЊИ[2] и БОРКО М. МАТИЈЕВИЋ[1]

[1]Универзитет у Новом Саду, Природно–математички факултет, Департман за хемију, биохемију и заштиту животне средине, Нови Сад и [2]Универзитет у Новом Саду, Природно–математички факултет, Департман за биологију и екологију, Нови Сад

Органска једињења, посебно она која у свом саставу садрже атоме азота и сумпора, чине преко 99 % клинички одобрених лекова. Као једни од припадника поменутих једињења, симетрични бисупституисани деривати тиокарбохидразона су детаљно изучавани. Са друге стране, асиметрични и моносупституисани тиокарбохидразони нису довољно испитани, упркос њиховом израженом биолошком потенцијалу. У овом раду су приказани резултати *in vitro* процене антиоксидативних, антимикробних и цитотоксичних својстава осамнаест претходно синтетисаних и окарактерисаних монотиокарбохидразона. Антиоксидативни потенцијал је одређен применом DPPH теста, док је антимикробна активност испитана на Грам-позитивним бактеријама применом модификоване микродилуционе методе. Цитотоксични ефекат је испитан на ћелијама хуманог хепатоцелуларног карцинома применом колориметријског MTT теста. Добијени резултати показују да испитивани монотиокарбохидразони имају значајно антиоксидативно и антимикробно дејство. Такође је установљено да на њихову активност и цитотоксичност велики утицај имају структура испитиваног молекула, као и природа и положај присутног супституената. Ови резултати пружају добар увид за будућа *in vivo* испитивања и истичу потенцијалну примену монотиокарбохидразона у развоју лекова.

(Примљено 1. фебруара, ревидирано 21. маја, прихваћено 22. септембра 2024)

REFERENCES

1. P. C. Guha, S. C. Dey, *J. Indian Chem. Soc.* **2** (1925) 225 (https://ia902304.us.archive.org/18/items/sim_journal-of-the-indian-chemical-society_1925_2_index/sim_journal-of-the-indian-chemical-society_1925_2_index.pdf)
2. J. M. Cano Pavon, A. Garcia de Tores, C. Alcaraz, M. T. Siles Cordero, E. Vereda Alonso, *Quim. Anal. (Barcelona)* **13** (1994) 5 (https://scholar.google.com/scholar_lookup?journal=Quim.+Anal.&title=Analytical+applications+of+thiocarbohydrazones.+A+review&author=J.M.+Cano+Pavon&author=A.+Garcia+de+Torres&author=E.+Cristofol+Alcaraz&author=M.T.+Siles+Cordero&author=E.+Vereda+Alonso&volume=13&publication_year=1994&pages=5-10&)

3. D. Rosales, A. G. Asuero, J. L. G. Ariza, *Analyst* **111** (1986) 449 (https://dx.doi.org/10.1039/AN9861100449)
4. S. P. Chaudhury, S. C. Shome, *J. Indian. Chem. Soc*. **68** (1991) 430 (https://zenodo.org/record/6160571/files/430-431.pdf)
5. R. B. Lucena, E. Morales, J. L. Gomez-Ariza, *Farmaco* **49** (1994) 291 (https://pubmed.ncbi.nlm.nih.gov/8049011/)
6. R. B. Lucena, E. Morales, J. L. Gomez-Ariza, *Farmaco* **49** (1994) 297 (https://pascal-francis.inist.fr/vibad/index.php?action=getRecordDetail&idt=4270633)
7. S. B. Zanje, V. J. Suryavanshi, A. N. Kokare, A. A. Ghare, G. S. Kamble, P. N. Kamble, M. A. Anuse, *J. Anal. Chem.* **73** (2018) 438 (https://dx.doi.org/10.1134/S1061934818050131)
8. A. V. Sadlapurkar, U. B. Barache, A. B. Shaikh, S. H. Gaikwad, T. N. Lokhande, *Int. J. Environ. Anal. Chem.* **103** (2023) 3683 (https://dx.doi.org/10.1080/03067319.2021.1912333)
9. A. V. Sadlapurkar, U. B. Barache, A. B. Shaikh, P. C. Dhale, S. H. Gaikwad, T. N. Lokhande, *Chem. Data Collect.* **37** (2022) 100798 (https://dx.doi.org/10.1016/j.cdc.2021.100798)
10. G. Kiran, T. Maneshwar, Y. Rajeshwar, M. Sarangapani, *J. Chem.* **2013** (2013) 192039 (https://dx.doi.org/10.1155/2013/192039)
11. G. Mrđan, A. Tot, M. Vraneš, M. Rašeta, P. Knežević, T. Verbić, B. Matijević, *Bull. Chem. Soc. Jpn.* **95** (2022) 185 (https://dx.doi.org/10.1246/bcsj.20210326)
12. Y. Kaya, A. Ercag, A. Koca, *J. Mol. Struct.* **1102** (2015) 117 (https://dx.doi.org/10.1016/j.molstruc.2015.08.055)
13. Y. Kaya, A. Ercag, K. Kaya, *J. Coord. Chem.* **71** (2018) 3364 (https://dx.doi.org/10.1080/00958972.2018.1516872)
14. H. Muglu, M. S. Cavus, T. Bakir, H. Yakan, *J. Mol. Struct.* **1196** (2019) 819 (https://dx.doi.org/10.1016/j.molstruc.2019.07.002)
15. H. Yakan, T. K. Bakir, M. S. Cavus, H. Muglu, *Res. Chem. Intermed.* **46** (2020) 5417 (https://dx.doi.org/10.1007/s11164-020-04270-0)
16. T. K. Bakir, J. B. Lawag, *Res. Chem. Intermed.* **46** (2020) 2541 (https://dx.doi.org/10.1007/s11164-020-04105-y)
17. A. Bacchi, M. Carcelli, P. Pelagatti, C. Pelizzi, G. Pelizzi, F. Zani, *J. Inorg. Biochem.* **75** (1999) 123 (https://dx.doi.org/10.1016/S0162-0134(99)00045-8)
18. M. Shebl, S. M. E. Khalil, F. S. Al-Gohani, *J. Mol. Struct.* **980** (2010) 78 (https://dx.doi.org/10.1016/j.molstruc.2010.06.040)
19. M. T. Gabr, N. S. El-Gohary, E. R. El-Bendary, Ni Nanting, M. I. Shaaban, M. M. El-Kerdawy, *Synthetic Commun.* **48** (2018) 2899
20. (https://dx.doi.org/10.1080/00397911.2018.1520889)
21. A. R. Božić, S. K. Bjelogrlić, I. T. Novaković, N. R. Filipović, P. M. Petrović, A. D. Marinković, T. R. Todorović, I. N. Cvijetić, *ChemistrySelect* **3** (2018) 2215 (https://dx.doi.org/10.1002/slct.201702691)
22. K. Gangarapu, S. Manda, A. Jallapally, S. Thota, S. K. Karki, J. Balzarini, E. De Clercq, H. Tokuda, *Med. Chem. Res.* **23** (2014) 1046 (https://dx.doi.org/10.1007/s00044-013-0684-3)

23. A. Božić, A. Marinković, S. Bjelogrlić, T. R. Todorović, I. N. Cvijetić, I. Novaković, C. D. Muller, N. R. Filipović, *RSC Adv.* **6** (2016) 104763 (https://doi.org/10.2298/JSC161220045B)
24. J. Wang, Y. T. Wang, Y. Fang, Y. L. Lu, M.X. Li, *Toxicol. Res.* **8** (2019) 862 (https://doi.org/10.1039/C9TX00109C)
25. M. H. Assaleh, S. K. Bjelogrlic, N. Prlainovic, I. Cvijetic, A. Bozic, I. Arandjelovic, D. Vukovic, A. Marinkovic, *Arab. J. Chem.* **15** (2022) 103532 (https://doi.org/10.1016/j.arabjc.2021.103532)
26. M. T. Gabr, N. S. El-Gohary, E. R. El-Bendary, M. M. El-Kerdawy, Ni Nanting, *Eur. J. Med. Chem.* **128** (2017) 36 (https://doi.org/10.1016/j.ejmech.2017.01.030)
27. G. Mrdjan, Gy. Vastag, D. Škorić, M. Radanović, T. Verbić, M. Milčić, I. Stoiljković, O. Marković, B. Matijević, *Struct. Chem.* **32** (2021) 1231 (https://doi.org/10.1007/s11224-020-01700-y)
28. H. H. J. Gerets, K. Tilmant, B. Gerin, H. Chanteux, B. O. Depelchin, S. Dhalluin, F. A. Atienzar, *Cell. Biol. Toxicol.* **28** (2012) 69 (https://doi.org/10.1007/s10565-011-9208-4)
29. S. Yang, M. Ooka, R. J. Margolis, M. Xia, *Cell Reports Methods* **3** (2023) 100432 (https://doi.org/10.1016/j.crmeth.2023.100432)
30. C. J. Espin, G. Soler-Rivas, J. H. Wichers, *J. Agr. Food Chem.* **48** (2000) 648 (https://doi.org/10.1021/jf9908188)
31. I. Vulin, D. Tenji, I. Teodorovic, S. Kaisarevic, *Chem-Biol. Interact.* **365** (2022) 110082 (https://doi.org/10.1016/j.cbi.2022.110082)
32. J. L. Li, X.Y. Liu, J.T. Xie, Y.L. Di, F.X. Zhu, *J. Phytopathol.* **163** (2015) 239 (http://dx.doi.org/10.1111/jph.12312)
33. M. S. Cavus, H. Yakan, H. Muglu, T. Bakir, *J. Phys. Chem. Solids* **140** (2020) 109362 (http://dx.doi.org/10.1016/j.jpcs.2020.109362)
34. M. Demurtas, A. Baldisserotto, I. Lampronti, D. Moi, G. Balboni, S. Pacifico, S. Vertuani, S. Manfredini, V. Onnis, *Bioorg. Chem.* **85** (2019) 568 (https://doi.org/10.1016/j.bioorg.2019.02.007)
35. D. Saxena, R. Maitra, R. Bormon, M. Czekanska, J. Meiers, A. Titz, S. Verma, S. Chopra, *npj Antimicro. Resist.* **1** (2023) 17 (https://doi.org/10.1038/s44259-023-00016-1)
36. R. Tamaian, A. Mot, R. Silaghi-Dumitrescu, I. Ionut, A. Stana, O. Oniga, C. Nastasa, D. Benedec, B. Tiperciuc, *Molecules* **20** (2015) 22188 (http://dx.doi.org/10.3390/molecules201219841)
37. J. L. Stigliani, V. Bernardes–Génisson, *Ann. Pharm. Francaises* **77** (2019) 126 (http://dx.doi.org/10.1016/j.pharma.2018.11.004)
38. R. K. C. De Paiva, J. F. Da Silva, H. A. Moreira, O. G. Pinto, L. T. F. M. Camargo, P. L. F. Naves, A. J Camargo, L. Ribeiro, L. M. Ramos, *J. Brazil. Chem. Soc.* **30** (2019) 164 (http://dx.doi.org/10.21577/0103-5053.20180167)
39. S. Podunavac-Kuzmanović, D. Cvetković, D. Barna, *J. Serb. Chem. Soc.* **73** (2008) 967 (http://dx.doi.org/10.2298/JSC0810967P)
40. M. B. Halli, R. B. Sumathi, *Arab. J. Chem.* **10** (2017) S1748 (https://doi.org/10.1016/j.arabjc.2013.06.025)
41. C. Bonaccorso, T. Marzo, D. La Mendola, *Pharmaceuticals (Basel)* **13** (2020) 4 (http://dx.doi.org/10.3390/ph13010004)

42. S. M. Gomha, H. A. Abdelhady, D. Z. H. Hassain, A. H. Abdelmonsef, M. El-Naggar, M. M. Elaasser, H. K. Mahmoud, *Drug Des. Dev. Ther.* **15** (2021) 659 (http://dx.doi.org/10.2147/DDDT.S291579)
43. S. Bilginer, H. I. Gul, F. S. Erdal, H. Sakagami, S. Levent, I. Gulcin, C. T. Supuran, *J. Enzym. Inhib. Med. Chem.* **34** (2019) 1722 (http://dx.doi.org/10.1080/14756366.2019.1670657)
44. C. Bonaccorso, G. Grasso, N. Musso, V. Barresi, D. F. Condorelli, D. La Mendola, E. Rizzarelli, *J. Inorg. Biochem.* **182** (2018) 92 (http://dx.doi.org/10.1016/j.jinorgbio.2018.01.019)
45. Qurat-ul-Ain, M. Munira Taj, M. K. Khanlid, M. I. Choudhary, arXiv:2310.00939 [q-bio.BM] (2023) (https://doi.org/10.48550/arXiv.2310.00939).

Journal of the Serbian Chemical Society
JSCS-info@shd.org.rs • www.shd.org.rs/JSCS
J. Serb. Chem. Soc. *90* (1) 13–26 (2025)
JSCS–5816
Original scientific paper
Published 1 February, 2025

The interaction between 4-oxothiazolidine-2-ylidene thioamides and iodine: A regioselective two-component 4-oxothiazolidine-2-ylidene thioamide to thiazolo[3,2-*c*]pyrimidine transformation mediated by iodine

ALEKSANDAR RAŠOVIĆ*

Institute of Chemistry Technology and Metallurgy, University of Belgrade, Njegoševa 12, 11000 Belgrade, Serbia

(Received 9 December 2023, revised 6 June, accepted 30 December 2024)

Abstract: This study investigated the interaction between selected 4-oxothiazolidine-2-ylidene thioamides **2a**–**c** and iodine in acetone. The interaction followed two main reaction pathways: 1) iodine-mediated cyclization resulting in the formation of thiazolopyrimidine **7** and 2) electrophilic iodine attack on the thioamide sulfur atom, producing a complex mixture of iodine adducts. Due to the equilibrium of *Z*/*E* isomerization being strongly shifted to the *Z*-isomer in polar solvents, only the thioamide (*E*)-**2b** successfully formed thiazolopyrimidine **7**. The other two derivatives, (*Z*)-**2a** and (*Z*)-**2c**, followed the second reaction pathway. The factors influencing the heterocyclization of (*E*)-**2b** and its intermediates were thoroughly examined. This research provides the first description of an iodine-mediated heterocyclization leading to a thiazolopyrimidine scaffold. The literature on iodine-mediated heterocyclization leading to fused pyrimidines is limited, highlighting the significance of this study.

Keywords: 2-alkylidene-4-oxothiazolidine; heterocyclization; thiazolopyrimidine; push-pull effect.

INTRODUCTION

As previously reported, synthesized 4-oxothiazolidines **1** having an exocyclic C=C double bond at the C(2)-position (Scheme 1), proved to be an excellent heterocyclic scaffold displaying intrinsic reactivity through their versatile transformations that led to diverse heterocycles, such as 3,3aλ^4,4-trithia-1-azapentalenes,[1–4] 1,3-thiazines[1] and other thiazolidine derivatives.[5] Among them, the reactions involving their nucleophilic sites, *i.e.*, ring nitrogen atom, carbonyl

* Correspondence to this paper should be addressed to Dejan Opsenica, JSCS Organic Chemistry Sub-Editor, E-mail: jscs-oh@shd.org.rs
https://doi.org/10.2298/JSC231207001R

oxygen atom and carbon atoms C(5) and C(2'), having high affinity for electrophiles,[5] have also attracted great attention (Fig. 1; Scheme 2).

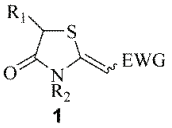

1

EWG = COPh, CO_2Et, CONHPh, $CONHCH_2CH_2Ph$, CN
R_1 = H, Me, CH_2CO_2Et
R_2 = H, Me

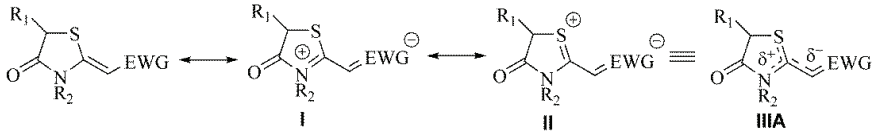

I **II** **IIIA**

Scheme 1. The structure of 2-alkylidene-4-oxothiazolidines.

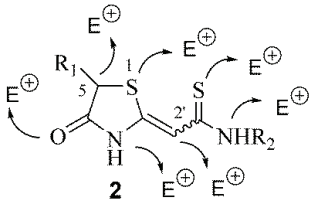

2

2a, R_1 = H, R_2 = H
2b, R_1 = CH_2COOEt, R_2 = H
2c, R_1 = H, R_2 = CH_2CH_2Ph,

Fig. 1. Nucleophilic sites in 4-oxothiazolidine-2-ylidene thioamides.

The high affinity of **1**, belonging to the biologically important thiazolidines[5,6] and the class of push-pull alkenes[7–10] to participate in the versatile heterofunctionalization reactions with electrophiles (Scheme 2), which led to the diverse thiazolidine derivatives, such as vinyl bromides **3**, pyridinium salts **4**, thiazolidine derivative **5**, possessing two exocyclic bonds, and fused bicyclic thiazolidine **6**,[5] has understood in the light of their push-pull effect, that is, the π-electron interaction between two electron donors (–NH and –S–) and one electron-withdrawing group (EWG; Scheme 1). As a result, the thiazolidine ring and the exocyclic C=C double bond of **1** are highly polarized, which can best described by the hybrid structure **IIIA** possessing nucleophilic sites, as summarized in Fig. 1. As reported previously, the 4-oxothiazolidine-2-ylidene thioamides **2** exhibit a larger push-pull effect than **1**.[10] Thus, compared with **1**, their structures are likely to be more highly polarized hybrid structure **IIIA** (Scheme 1). Furthermore, instead of exocyclic oxygen in thiazolidine analogues **1**, the nucleophilic site in **2** is exocyclic sulfur (Scheme 1; Fig. 1). All these show that the thiazolidines **2** could

be at the centre of the research interest regarding their reactivity toward potential electrophiles.

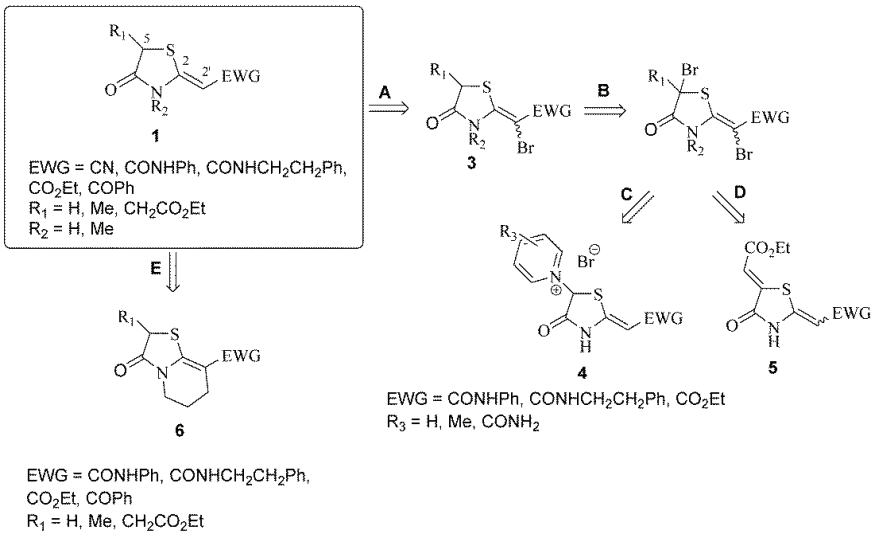

Scheme 2. The transformations of 2-alkylidene-4-oxothiazolidines **1** involving their nucleophilic sites.

Other main physicochemical properties of 2-alkylidene-4-oxothiazolidines arising from this so-called "push-pull effect" are: *i*) their low solubility in the versatile solvents (especially in nonpolar ones), *ii*) the significant lowering of the rotational barriers around the C(2)C(2') double bond,[10] resulting, as we showed previously and *iii*) the facile *Z*/*E* configurational isomerization.[10–12]

Since the factors above-mentioned, determining structural features of 2-alkylidene-4-oxothiazolidines, **1** and **2**, represent the main reason for their high potential reactivity, it was intriguing to continue the examination of their conversions leading to the functionally significant heterocyclic compounds. To choose the suitable electrophile for transformations of 4-oxothiazolidine-2-ylidine thioamides **2**, as the target substrate of this work, iodine seemed to be a good choice. That was supported by the iodine electron deficiency, resulting in its rich chemistry that involves the electrophilic iodination of organic compounds and its employment in the construction of versatile heterocyclic systems. In this sense, the iodine promotes cyclization of the many significant heterocycles, such as benzofurans, benzoxazoles and benzothiazoles, isoxazoles, pyrroles, thiophenes, indoles, pyrans, pyridines, isoquinolines, pyrimidines, *etc*.[13]

Therefore, concerning the **2a**/I_2 and **2b**/I_2 interaction in acetone, only the thioamide (*E*)-**2b** successfully formed a heterocyclic product. Thus, as outlined in Scheme 3, the two-component heterocyclization reaction between (*E*)-(5-ethoxy-

carbonylmethyl-4-oxothiazolidin-2-ylidene)ethanthioamide **2b** and acetone mediated by iodine led to the formation of thiazolo[3,2-*c*]pyrimidine **7**. However, despite its limitations, this transformation significantly contributed to a better understanding of the chemistry of 4-oxothiazolidines. That is especially true for reactions with electrophiles. Besides, it undoubtedly opens up applications for transformations of similar molecular systems. Moreover, this research describes an iodine-mediated heterocyclization leading to a thiazolopyrimidine scaffold as the biologically important class of heterocyclic compounds. Generally, the literature on iodine-mediated heterocyclization leading to fused pyrimidine scaffolds is limited, with just a few reports published thus far.[13–15]

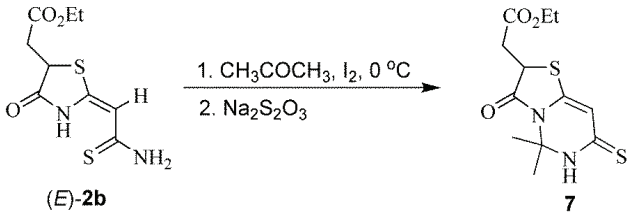

(*E*)-**2b** **7**

Scheme 3. The 2-alkylidene-4-oxothiazolidine to thiazolo[3,2-*c*]pyrimidine transformation is mediated by iodine.

EXPERIMENTAL

General

Melting points were determined on a Micro-Heiztisch Boetius PHMK apparatus or Büchi apparatus. Analytical thin-layer chromatography (TLC) was carried out by using Merck 60 F254 precoated silica gel plates (0.20 mm thickness), and the spots were visualized by iodine. Column chromatography was carried out on SiO_2 (silica gel 60 Å, 12-26, ICN Biomedicals). The NMR spectra were obtained using a Varian Gemini 2000 instrument (^{1}H at 200 MHz, ^{13}C at 50.3 MHz). Chemical shifts are reported in ppm on the δ scale from TMS as an internal standard in the solvents specified. Low-resolution mass spectra were recorded using a Finnigan MAT 8230 BE spectrometer at 70 eV (EI). Isobutane was used as the ionizing gas for the chemical ionization (CI) mass spectra. Elemental analyses were performed at the microanalysis laboratory at the Department of Chemistry, University of Belgrade. HRMS of ethyl 2-(5,5-dimethyl-3-oxo-7-thioxo-3,5,6,7-tetrahydro-2*H*-thiazolo[3,2-*c*]pyrimidin-2-yl) acetate **7** was carried out on 6210 TOF LC/MS coupled with HPLC 1200 Series Agilent Technologies.

Experimental procedures for synthesising starting compounds and their analytical and spectral data are provided in the Supplementary material to this paper.

*Synthesis of ethyl 2-(5,5-dimethyl-3-oxo-7-thioxo-3,5,6,7-tetrahydro-2*H*-thiazolo[3,2-*c*]pyrimidin-2-yl)acetate 7*

To a stirred suspension of (*E*)-(5-ethoxycarbonylmethyl-4-oxothiazolidin-2-ylidene)-ethanthioamide **2b** (0.10 g, 0.39 mmol) and acetone (10 mL) was added one molar equivalent of iodine (0.10 g, 0.39 mmol) at 0 °C (an ice bath). After 10 min, when was added another molar equivalent of iodine, the initially heterogeneous mixture became homogeneous. The reaction was prolonged at this temperature for an additional 2.5 h when TLC indicated the complete consumption of starting (*E*)-**2b**. Afterwards, the reaction mixture was kept in the ref-

rigerator for 48 h, heated to room temperature and evaporated. To the dryness, the dark residue was added CH_2Cl_2 (15 mL) and the obtained solution was extracted twice with 1.2 % $Na_2S_2O_3$ (20 mL). The collected extracts were dried under Na_2SO_4, filtered and evaporated to dryness. The filtered solution was concentrated under reduced pressure, and the resulting solid residue was chromatographed (toluene/ethyl acetate volume ratio, 10:0 → 6:1), affording the desired product as a yellow solid in moderate yield (0.059 g, 51 %).

Analytical and spectral data of compound **7** are given in the Supplementary material to this paper.

TABLE I. Selected ^{13}C- and ^{1}H-NMR (DMSO-d_6) chemical shifts (ppm) of ethyl thiazolo[3,2-*c*]pyrimidin-2-yl)acetate **7** and thiazolidine derivatives **2a**–**c**

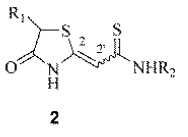

2

2a, R_1 = H, R_2 = H
2b, R_1 = CH_2COOEt, R_2 = H
2c, R_1 = H, R_2 = CH_2CH_2Ph

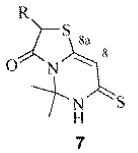

7

R = CH_2COOEt

Ent.	Compd.	Solvent	C=S	C=O_{lactam}	C(2')-*H*	C(2)	C(2')	$\Delta\delta_{C(2)=C(2')}$
1	(*Z*)-**2a**	DMSO-d_6	193.2	174.4	6.16	158.4	100.6	57.8
2	(*E*)-**2b**	DMSO-d_6	191.4	174.4	5.64	154.9	97.2	57.7
3	(*Z*)-**2c**	DMSO-d_6	190.4	174.3	6.21	156.1	101.2	54.9
4			C=S	C=O_{lactam}	C(8)-*H*	C(8)	C(8a)	$\Delta\delta_{C(8)=C(8a)}$
5	**7**	DMSO-d_6	184.5	172.2	5.73	146.8	101.0	45.8

RESULTS AND DISCUSSION

The structural assignment of **7** (Scheme 3; Table I) was made based on spectroscopic data (^{1}H- and ^{13}C-NMR, HRMS). Careful analysis of its NMR spectroscopic data revealed spectral features that correlated with the structure of ethyl thiazolo[3,2-*c*]pyrimidin-2-yl)acetate **7**. Further, the compound had the HRMS spectrum consistent with an elemental composition of $C_{12}H_{16}N_2O_3S_2$.

Regarding the comparison between the structural characteristics of thiazolodines **2a**–**c** and thiazolopyrimidine **7**, their selected experimental ^{1}H- and ^{13}C--NMR chemical shifts are presented in Table I (entries 1–3 for **2a**–**c**; entry 5 for **7**). In principle, compounds **2a**–**c** and **7** showed similar ^{1}H- and ^{13}C-NMR spectral characteristics for almost all identical structural motifs, including those for thioamide carbon atoms (column 4, DMSO-d_6; δ 190.4–193.2 ppm for **2a**–**c**; δ 184.5 ppm for **7**), lactam carbon atoms (column 5, DMSO-d_6; δ 174.3–174.4 ppm for **2a**–**c**; δ 172.2 ppm for **7**) and the olefinic protons (column 6, DMSO-d_6; δ 5.64–6.21 ppm for **2a**–**c**; δ 5.73 ppm for **7**). These results strongly indicated that thiazolodines **2a**–**c** and thiazolopyrimidine **7** belong to the structurally closely related compounds.

Furthermore, concerning the ^{13}C-NMR spectral data of olefinic carbon atoms of the C=C double bond of these compounds (Table I; C(2)C(2')/**2a**–**c**; C(8)C(8a)/**7**), they showed the low field position of the signal corresponding to the C(2) and C(8a) atoms at the donor side of **2a**–**c** and **7**, respectively (column 7, DMSO-d_6; δ 154.9–158.4 ppm for **2a**–**c**; δ 146.8 ppm for **7**) and the high field position of the signal assigned to their C(2') and C(8a) atoms at the acceptor side of the C=C double bond, respectively (column 8, DMSO-d_6; δ 97.2–101.2 ppm for **2a**–**c**; δ 101.0 ppm for **7**). This difference in the chemical shift values ($\Delta\delta_{C=C}$) of their olefinic carbon atoms is a characteristic feature of their push--pull character, *i.e.*, the significant charge polarization occurred within the C=C double bond. Therefore, since, as we proved previously,[10] experimentally determined $\Delta\delta_{C=C}$ values should increase with the increasing push-pull character of the double bond for the 2-alkylidene-4-oxothiazolidines possessing a similar EWG, the push-pull effect of the **7** is considerably lower than of the **2a**–**c** (column 9, DMSO-d_6; δ 54.9–57.8 ppm for **2a**–**c**; δ 45.8 ppm for **7**).

Since in both **7** and **2a**–**c**, the (Don)2−C=C−EWG fragments are very similar, the resultant significant reduction of the push-pull effect upon going from **2a**–**c** to **7** could be a result of the difference in the electron-donating ability of their donors (NH_{ring}/S_{ring}, **2a**–**c**; N_{ring}/S_{ring}, **7**; Scheme 4). In this sense, they have a much better electron-donating ability (increased base strength) in **2a**–**c** compared with **7** due to the better stabilization of **IIIA** than **IIIB** by the strong NH/S intramolecular hydrogen bonding in the (*E*)-**IIIA** and by the strong S_{exo}/S_{endo} intramolecular interaction in the (*Z*)-**IIIA**. Finally, due to a weaker push--pull effect in **7** compared to **2a**–**c,** the interaction between **7** and I_2 is significantly lower. That facilitated the (*E*)-**2b** to **7** heterocyclization and the refinement procedure of compound **7**.

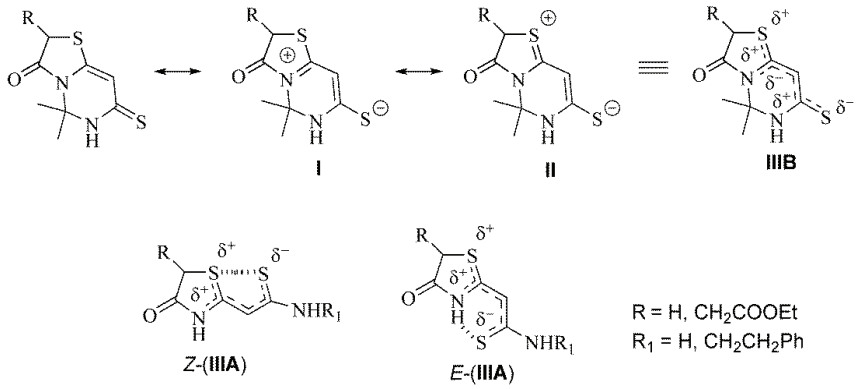

Scheme 4. The structures of thiazolo[3,2-*c*]pyrimidine **7** and thiazolidines **2a**–**c**.

During the planning of a synthetic strategy of 4-oxothiazolidine-2-ylidine thioamide **2** transformations with iodine, the two reaction paths were assumed: *i*) the iodine-mediated cyclization, affording to the heterocycles such as product **7**, containing a pyrimidine heterocyclic core (reaction path **1**; Schemes 3 and 5) and *ii*) the nucleophilic iodine attack on the thioamide sulfur atom, producing the complex mixture of iodine adducts **13**–**15**, respectively (reaction path 2; Scheme 6).

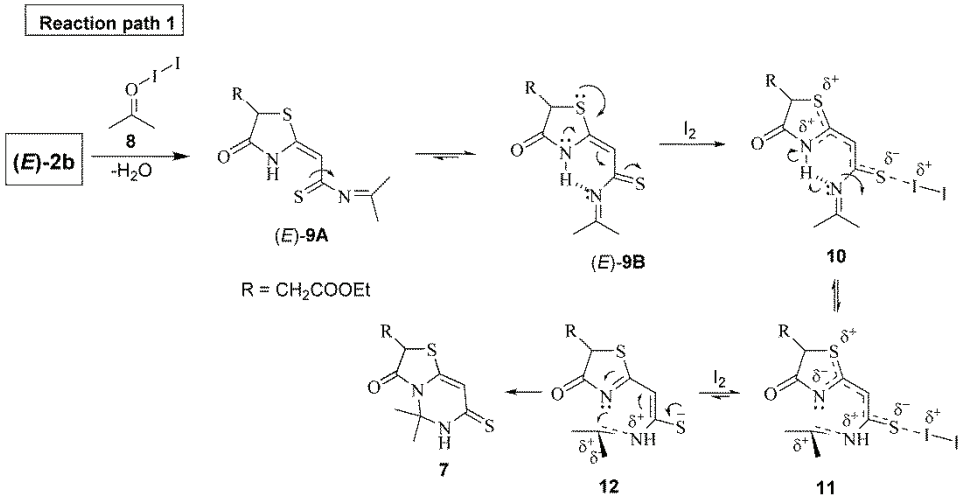

Scheme 5. The proposed reaction mechanism of 4-oxothiazolidine (*E*)-**2b** to thiazolo[3,2-*c*]pyrimidine **7** transformations.

Generally, the proposed undesired reaction path **2** (Scheme 6), as well as the performed synthetic route **1** in terms of iodine-promoted heterocyclization leading to **7** (Schemes 3 and 5), are based on the ability of the halogens X (typically, X is Cl, Br or I) that, as electron acceptor species, as the RX (Lewis acid), where the R ranges from another halogen atom to the large organic or inorganic residue interact with donor species D (Lewis base), yielding a subclass of the charge transfer (CT), or electron donor–acceptor (EDA) complex family (adducts).[16–27] In these so-called halogen-bonded (XB) complexes (adducts) RX···D, the donor species can be an anion or a neutral species possessing at least one nucleophilic region, *e.g.*, one or more electron lone pairs containing atoms (*e.g.*, electron donor atoms such as oxygen, nitrogen, sulfur, selenium or π-system). To those, the interaction of iodine with various Lewis bases, expressed *via* association constants (K_{XB}),[19,21,28,29] showed that the interactions between iodine and thioamides are medium to strong I_2/Lewis base interactions, which corroborates with the proposed reaction mechanisms in Schemes 5 and 6.

Regarding the potential trend in the behaviour of **2** under reaction conditions assumed in Scheme 6, which could lead to the complex mixture of iodine adducts,

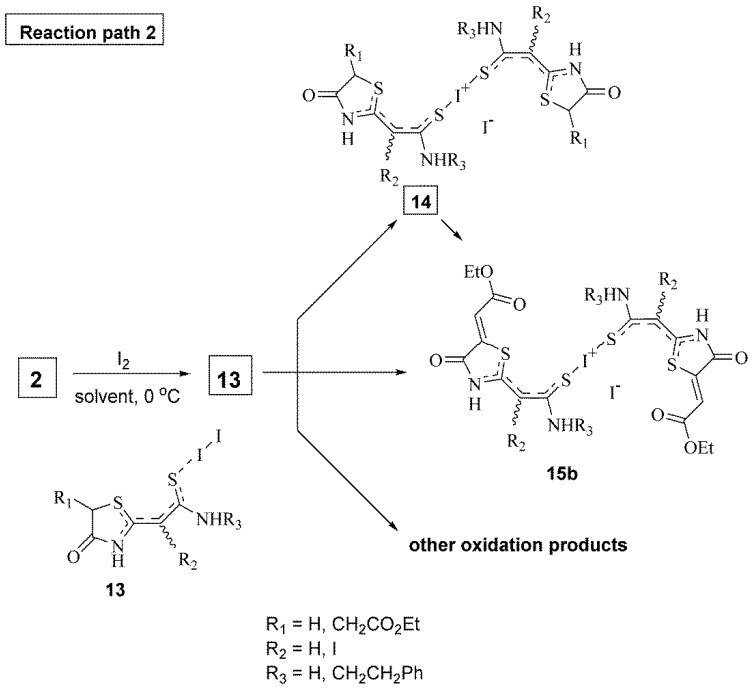

Scheme 6. The assumed **2**/I_2 interactions produce the complex mixture of iodine adducts.

all possible products have been proposed based on the literature data related to the medium (product **13**) to strong (products **14**/**15b** and more complex ones) thioamide/I_2 interactions.[16–25] The previously published data on the brominating reactions of thiazolidine derivatives 1 (products **3** and **5**; Scheme 2)[5] were patterns of potential ligands in the **14** and **15b**. Therefore, the possible formation of iodine adducts such as **13** and ionic species **14** and **15b**, which consist of iodine(I) cation coordinated with two thioamide ligands, respectively,[17,19–23,25] suggested in Scheme 6, or even more complex structures forming as a result of further oxidation transformations, such as disulfide cations,[16–19,24] could be the best rationalized in the light of the MO theory: the increased the donor–acceptor interaction, the greater the amount of negative charge transferred from the donor to the σ* anti-bonding orbital of I_2, and the greater the I–I bond lengthening,[21] leading to the **13** with reduced I–I bond order or even more complex adducts **14** and **15b** produced by I–I bond heterolytic cleavage.

The main factors that determined the possibility of occurrence of the 2-alkylidene-4-oxothiazolidine to thiazolo[3,2-*c*]pyrimidine transformation are: *i*) the nature of 4-oxothiazolidine derivatives, *i.e.*, their push-pull effect and their strong affinity toward electrophile species, *ii*) the iodine chemistry and, closely related with this, the halogen bonding[26,27] as the crucial one that, along with the push-

-pull effect of **2**, pulled in the direction of this transformation and, as a third factor, *iii*) the reaction conditions. In this sense, the mechanism of 4-oxothiazolidine (*E*)-**2b** to thiazolo[3,2-*c*]pyrimidine **7** heterocyclization (Scheme 5) can be rationalized by the series of steps involving an initial attack on the carbonyl carbon of iodine–acetone adduct **8** by the nucleophilic thioamide nitrogen atom of (*E*)-**2b**, which occurs with the loss of H_2O, giving rise to the like Schiff base **9**. The conformational change (*E*)-**9A** → (*E*)-**9B** produced a hydrogen-bonded six--membered chelate ring in the (*E*)-**9B**, which was transformed in the **10** by the addition of iodine. Then, the proton shifted from the lactam to the imine nitrogen atom in the **10** to give **11**. That followed the **11** → **12** transformations, which set the step for the cyclization. Thus, the final attack of the lactam nitrogen on the positively charged carbon atom of iminium ion **12** led to the formation of the pyrimidine ring in product **7**.

Additionally, to my knowledge, the (*E*)-**2b** → **7** reaction mechanism outlined in Scheme 5 represents a new one. Regarding this, a few steps have drawn particular attention, as follows, and described below: *i*) (*E*)-**2b** → (*E*)-**9** transformation, *ii*) the **10** → **11** rearrangements and *iii*) formation of vinylogous *N*-thioacyliminium ion **12** in the **11** → **12** transformations.

Concerning the (*E*)-**2b** → (*E*)-**9** reaction as the slowest step of the (*E*)-**2b** → **7** transformations, at first look, it seems that this type of transformation producing the Schiff bases like **9** is a widespread one, occurring among the numerous thioamides and carbonyl compounds. However, it is limited to only one report so far.[30]

Furthermore, the **10** → **11** rearrangements could be a crucial step in a complete (*E*)-**2b** → **7** transformations (Schemes 5 and 7). Since the hydrogen bond is an initial stage to proton-transfer reactions, which can proceed in the case of strong ones,[31] then compound **10** is one in which a strong hydrogen bond has established, leading to a very rapid proton transfer and the formation of product **11**.

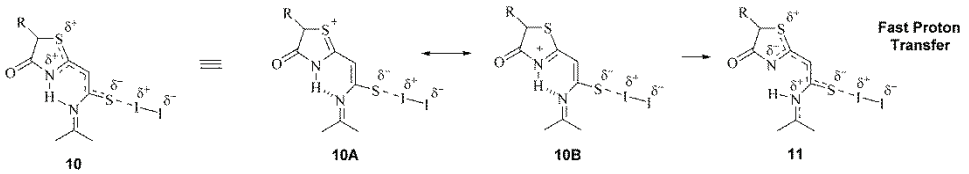

Scheme 7. Intramolecular proton transfer in the **11**.

This work has postulated that iminium ion **12** could be a key intermediate of the (*E*)-**2b** → **7** transformations (Scheme 5). Generally, the iminium ions, such as Mannich-intermediate **16**, *N*-acyl derivative **17**, carbamate **18**, amide **19**, *N*-tosyl cations **20**, hydrazonium cation **21** and vinylogous *N*-acyliminium ion **22**, are well known in the literature and they are involved in the construction of many

heterocyclic compounds (Scheme 8).[32–34] In this sense, the novel vinylogous *N*-thioacyliminium ion **12**, as well as the iodine adducts of an iminium ion like **10** and **11**, as the key intermediates in (*E*)-**2b** → **7** transformation present additional contributions in the field in terms of better understanding this type transformation (Scheme 5).

Scheme 8. The iminium ions.

In conclusion, for a series of reaction steps of the (*E*)-**2b** → **7** transformations (Scheme 5), one can conclude that is the strict regularity of the catalytic activity of iodine based on the principle of a switch-on/ turn-off act, *i.e.*, "act purposefully" according to the structural characteristics of the intermediates. In this way, the action of iodine results in the production of a series of intermediates ending with chelate intermediate **10**, where the activity of iodine culminates in the promotion of proton transfer from the thiolactam NH group to imino group to form intermediate **11**.

Finally, as described below, the difference in the interaction of **2a**–**c** with iodine in the presence of acetone can be explained by their different structural characteristics, closely related to their different behaviour in potential *Z*/*E* configurational isomerization in a polar solvent.

Our previous works described the basic principle of *Z*/*E* isomerization of thiazolidine derivatives **1** and **2**.[10–12] These results unequivocally proved that due to the push-pull effect, the facile *Z*/*E* configurational isomerization of **1**,**2** occurs spontaneously in solution due to the lowering of the rotational barrier around the C=C double bond. The direction of this isomerization dictates the solvent polarity. Thus, forming the stable solvent-solute intermolecular interactions and breaking the intramolecular hydrogen bond in the (*E*)-**1** and (*E*)-**2**, depicted in Scheme 9 as the structure **I**, the polar solvents shift the *Z*/*E* equilibrium to the left. On the other hand, in nonpolar solvents, intramolecular hydrogen bonding is favored, and in such conditions (*E*)-isomers become the dominant species.

Therefore, when considering the failed potential (*Z*)-**2a** to **7a** transformation *via* its counterpart (*E*)-**2a** (Scheme 9), the best explanation for this could be, as we previously proved, the trend to complete or complete shift to the left of the *Z*/*E* configurational isomerization of 2-alkylidene-4-ocoxothiazolidines **1** and **2**, occurring under polar solvent conditions.[10–12] In this sense, as in the case of most thiazolidine derivatives (*Z*)-**1**,[12] there is no evidence that (*Z*)-**2a** to (*E*)-**2a** transformation occurs under polar solvent conditions. Even if it happened to a

low extent in acetone, it probably would not lead to a valid amount of **7a** due to competition between (*Z*)-**2a** to **7a** and (*Z*)-**2a** to (*Z*)-**2a**/iodine adducts transformations *via* (*Z*)-**2b** → (*E*)-**2b** isomerization (Scheme 9). Regarding those, the behaviour of (*E*)-**2b**, under polar solvent conditions**,** constitutionally very similar to (*Z*)-**2a**, corroborates with the above conclusions and findings.[10] Concerning the (*Z*)-**2c**/iodine interaction, the (*Z*)-**2c** → **7c** transformation is impossible due to this compound belonging to secondary thioamides, and the formation of a Schiff base **9c** did not occur.

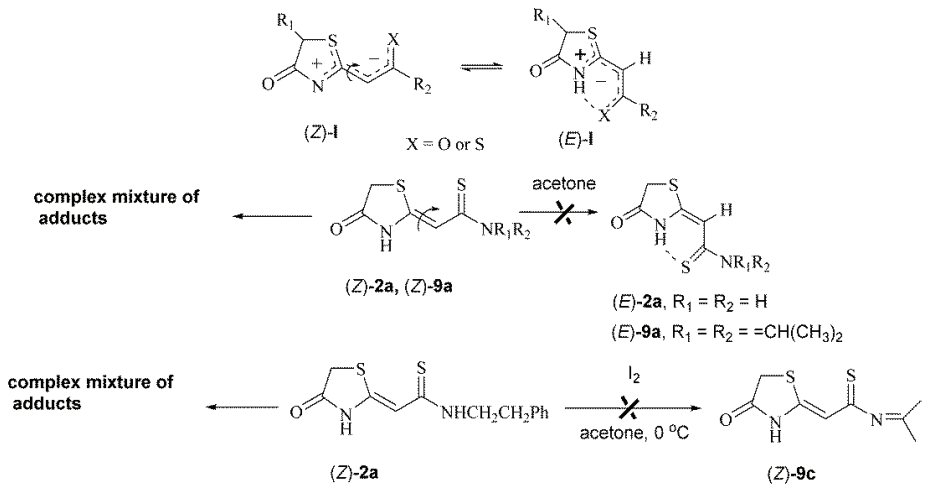

Scheme 9. Configurational isomerization of thiazolidines **1**,**2** and the interactions of the **2a** and **2c** derivatives with iodine in acetone.

Given the above-described, competitions between (*E*)-**2b** → **7** and (*Z*)-**-2b**,(*Z*)-**9** → (*Z*)-**2b**,(*Z*)-**9**/iodine adducts transformations *via* (*E*)-**2b**,(*E*)-**9** → (*Z*)-**-2b**,(*Z*)-**9** isomerizations could be reliable (Scheme 10). Thus, in that case, the

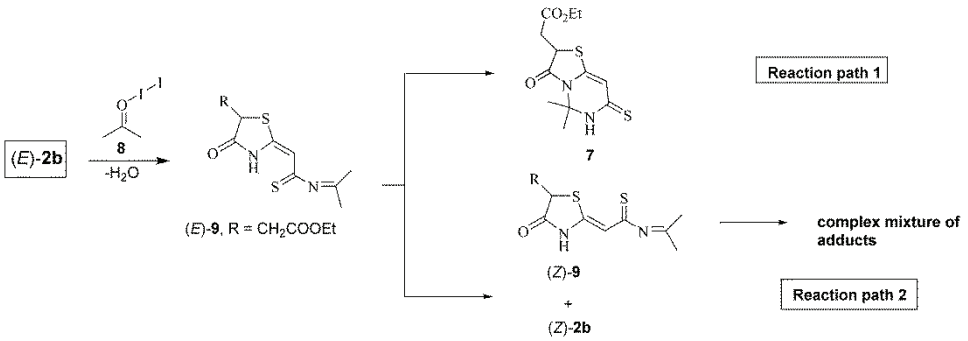

Scheme 10. Competition between reaction paths **1** and **2** in the interaction of thiazolidine (*E*)-**2b** with iodine.

regioselective 2-alkylidene-4-oxothiazolidine (*E*)-**2b** to thiazolopyrimidine **7** transformation should be a kinetically controlled reaction. Furthermore, based on the proposed reaction mechanism of the (*E*)-**2b** → **7** transformation (Scheme 5), it is powerfully guided by the electron deficiency of iodine, which strengthens the thiazolidine push-pull effect in the series iodine adduct intermediates such as **10** and **11**. The same should be for reaction path **2** (Scheme 6), affording to the complex mixture of the iodine adducts, which could take place between the precursor compounds (*Z*)-**2b** and (*Z*)-**9** with iodine, as the reactive species (Scheme 10).

CONCLUSION

In conclusion, the interaction between thioamides **2a**–**c** and iodine in acetone followed two main reaction pathways: 1) heterocyclization of thiazolidine (*E*)-**2b** to give a thiazolopyrimidine **7** (reaction path **1**) and 2) electrophilic iodine attack on the thioamide sulfur atom of derivatives (*Z*)-**2a** and (*Z*)-**2c**, producing a complex mixture of iodine adducts (reaction path **2**). The difference in the interaction of **2a**–**c** with iodine in the presence of acetone has been explained by their different structural characteristics, closely related to their different behaviour in potential *Z*/*E* configurational isomerization in a polar solvent, such as acetone. In such conditions, the equilibrium of *Z*/*E* isomerization has strongly shifted to the *Z*-isomer. Furthermore, this research thoroughly studied the (*E*)-**2b** to **7** transformations as the first description of an iodine-mediated heterocyclization leading to a thiazolopyrimidine scaffold.

SUPPLEMENTARY MATERIAL

Additional data and information are available electronically at the pages of journal website: https://www.shd-pub.org.rs/index.php/JSCS/article/view/12725, or from the corresponding author on request.

Acknowledgement. This research has been financially supported by the Ministry of Science, Technological Development and Innovation of the Republic of Serbia (Contract No: 451-03-66/2024-03/200026).

И З В О Д

ИНТЕРАКЦИЈА ИЗМЕЂУ 4-ОКСОТИАЗОЛИДИН-2-ИЛИДЕН ТИОАМИДА И ЈОДА: РЕГИОСЕЛЕКТИВНА ДВОКОМПОНЕНТНА ТРАНСФОРМАЦИЈА 4-ОКСОТИАЗОЛИДИН-2-ИЛИДЕН ТИОАМИДА У ТИАЗОЛО[3,2-*c*]ПИРИМИДИН ПОСРЕДОВАНА ЈОДОМ

АЛЕКСАНДАР РАШОВИЋ

Универзитет у Београду, Институт за хемију, технологију и металургију, Центар за хемију, Његошева 12, 11 000 Београд

Ова студија истраживала је интеракцију између одабраних 4-оксотиазолидин-2-илиден тиоамида **2a**–**c** и јода у ацетону. Интеракција је пратила два главна реакциона пута: 1) циклизација посредована јодом која је резултирала формирањем тиазолопиримидина **7** и 2) електрофилни напад јода на атом сумпора тиоамида, стварајући сложену смешу јодних адуката. Пошто је у поларним растварачима равнотежа *Z*/*E* изомеризације снажно поме-

рена према (*Z*)-изомеру, само је тиоамид (*E*)-**2b** успешно формирао тиазолопиримидин **7**. Друга два деривата, (*Z*)-**2a** и (*Z*)-**2c**, пратила су други реакциони пут. Фактори који утичу на хетероциклизацију (*E*)-**2b** и на њене интермедијере детаљно су испитани. Ово истраживање даје први опис хетероциклизације посредоване јодом која води до тиазолопиримидинске структуре. Литература о хетероциклизацији посредованој јодом којом се добијају кондензовани пиримидини је ограничена, што наглашава значај ове студије.

(Примљено 9. децембра 2023, ревидирано 6. јуна, прихваћено 30. децембра 2024)

REFERENCES

1. A. Rašović, P. J. Steel, E. Kleinpeter, R. Marković, *Tetrahedron* **63** (2007) 1937 (https://doi.org/10.1016/j.tet.2006.12.075)
2. R. Marković, A. Rašović, in *Comprehensive Heterocyclic Chemistry III*, A. R. Katritzky, Executive Ed., J. A. Joule, Vol. Ed., Elsevier Ltd., Oxford, 2008, p. 893 (https://doi.org/10.1016/B978-008044992-0.00411-9)
3. A. Rašović, A. Koch, E. Kleinpeter, R. Marković, *Tetrahedron* **69** (2013) 10849 (https://doi.org/10.1016/j.tet.2013.10.088)
4. A. Rašović, in *Comprehensive Heterocyclic Chemistry IV*, D. StC Black, J. Cossy, C. V. Stevens, Eds., R. A. Aitken, Vol. Ed., Elsevier Ltd., Oxford, 2022, p. 766 (https://doi.org/10.1016/B978-0-12-818655-8.00137-2)
5. M. Stojanović, Z. Džambaski, B. Bondžić, J. Aleksić, M. Baranac-Stojanović, *Curr. Org. Chem.* **18** (2014) 1108 (http://dx.doi.org/10.2174/1385272818091406241204 36)
6. M. Gajić, Z. Džambaski, B. S. Ilić, G. Kocić, B. P. Bondžić, A. Šmelcerović, *Chem. Biol. Interact.* **345** (2021) 109536 (https://doi.org/10.1016/j.cbi.2021.109536)
7. J. Sandström, *Top. Stereochem.* **14** (1983) 83 (https://doi.org/10.1002/9780470147238.ch2)
8. E. Kleinpeter, *J. Serb. Chem. Soc.* **71** (2006) 1 (https://doi.org/10.2298/JSC0601001K)
9. M. Baranac-Stojanović, U. Klaumünzer, R. Marković, E. Kleinpeter, *Tetrahedron* **66** (2010) 8958 (https://doi.org/10.1016/j.tet.2010.09.040)
10. A. Rašović, V. Blagojević, M Baranac-Stojanović, E. Kleinpeter, R. Marković, D. M. Minić, *New J. Chem.* **40 (**2016) 6364 (https://doi.org/10.1039/C6NJ00901H)
11. R. Marković, M. Baranac, N. Juranić, S. Macura, I. Cekić, D. Minić, *J. Mol. Struct.* **800** (2006) 85 (https://doi.org/10.1016/j.molstruc.2006.03.075)
12. R. Marković, A. Shirazi, Z. Džambaski, M. Baranac, D. Minić, *J. Phys. Org. Chem.* **17** (2004) 118 (https://doi.org/10.1002/poc.700)
13. P. T. Parvatkar, P. S. Parameswaran, S. G. Tilve, *Chem. Eur. J.* **18** (2012) 5460 (https://doi.org/10.1002/chem.201100324)
14. L.-Y. Zeng, C. Cai, *J. Comb. Chem.* **12** (2010) 35 (https://doi.org/10.1021/cc9000983)
15. M. Bakavoli, G. Bagherzadeh, M. Vaseghifar, A. Shiri, M. Pordel, M. Mashreghi, P. Pordeli, M. Araghi, *Eur. J. Med. Chem.* **45** (2010) 647 (https://doi.org/10.1016/j.ejmech.2009.10.051)
16. O. Foss, J. Johnsen, O. Tvedten, *Acta Chem. Scand.* **12** (1958) 1782 (https://doi.org/10.3891/acta.chem.scand.12-1782)
17. G. H.-Y. Lin, H. Hope, *Acta. Cryst.*, *B* **28** (1972) 643 (https://doi.org/10.1107/S0567740872002900)
18. A. J. Arduengo, E. M. Burgess, *J. Am. Chem. Soc.* **99** (1977) 2376 (https://doi.org/10.1021/ja00449a078)
19. C. Laurence, M. J. El Ghomari, J-Y. Le Questel, M. Berthelot, R. Mokhlisse, *J. Chem. Soc., Perkin Trans. 2* **7** (1998) 1545 (https://doi.org/10.1039/A803002B)

20. P. Deplano, J. R. Ferraro, M. L. Mercuri, E. F. Trogu, *Coord. Chem. Rev.* **188** (1999) 71 (https://doi.org/10.1016/S0010-8545(98)00238-0)
21. M. C. Aragoni, M. Arca, F. A. Devillanova, A. Garau, F. Isaia, V. Lippolis, G. Verani, *Coord. Chem. Rev.* **184** (1999) 271 (https://doi.org/10.1016/S0010-8545(98)00259-8)
22. P. D. Boyle, S. M. Godfrey, *Coord. Chem. Rev.* **223** (2001) 265 (https://doi.org/10.1016/S0010-8545(01)00386-1)
23. V. Daga, S. K. Hadjikakou; N. Hadjiliadis, M. Kubicki, J. H. Z. dos Santos, I. S. Butler, *Eur. J. Inorg. Chem.* **7** (2002) 1718 (https://doi.org/10.1002/1099-0682(200207)2002:7%3C1718::AID-EJIC1718%3E3.0.CO;2-S)
24. M. C. Aragoni, M. Arca, F. Demartin, F. A. Devillanova, A. Garau, F. Isaia, V. Lippolis, G. Verani, *J. Am. Chem. Soc.* **124** (2002) 4538 (https://doi.org/10.1021/ja012731k)
25. G. J. Corban, S. K. Hadjikakou, N. Hadjiliadis, M. Kubicki, E. R. T. Tiekink, I. S. Butler, E. Drougas, A. M. Kosmas, *Inorg. Chem*. **44** (2005) 8617 (https://doi.org/10.1021/ic0484396)
26. O. Hassel, *Nobel Lecture*, „*Structural Aspects of Interatomic Charge-Transfer Bonding*“, June 9, 1970 (https://www.nobelprize.org/prizes/chemistry/1969/hassel/lecture/)
27. G. Cavallo, P. Metrangolo, R. Milani, T. Pilati, A. Priimagi, G. Resnati, G. Terraneo, *Chem. Rev.* **116** (2016) 2478 (https://doi.org/10.1021/acs.chemrev.5b00484)
28. M. Breugst, D. von der Heiden, *Chem. Eur. J.* **24** (2018) 9187 (https://doi.org/10.1002/chem.201706136)
29. C. Laurence, J. Graton, M. Berthelot, M. J. El Ghomari, *Chem. Eur. J.* **17** (2011) 10431 (https://doi.org/10.1002/chem.201101071)
30. A. Jain, M. Gupta, A. Bhardwaj, T. R. Thapak, *Res. J. Chem. Sci.* **5** (2015) 39 (http://www.isca.me/rjcs/Archives/v5/i8/8.ISCA-RJCS-2015-112.php)
31. T. Steiner, *Angew. Chem. Int. Ed.* **41** (2002) 48 (https://doi.org/10.1002/1521-3773(20020104)41:1%3C48::AID-ANIE48%3E3.0.CO;2-U)
32. W. N. Speckamp, M. J. Moolenaar, *Tetrahedron* **56** (2000) 3817 (https://doi.org/10.1016/S0040-4020(00)00159-9)
33. J. Royer, M. Bonin, L. Micouin, *Chem. Rev.* **104** (2004) 2311 (https://doi.org/10.1021/cr020083x)
34. P. Wu, T. E. Nielsen, *Chem. Rev.* **117** (2017) 7811 (https://doi.org/10.1021/acs.chemrev.6b00806).

Journal of the Serbian Chemical Society
JSCS-info@shd.org.rs • www.shd.org.rs/JSCS
J. Serb. Chem. Soc. 90 (1) S1–S6 (2025) *Supplementary material*

SUPPLEMENTARY MATERIAL TO

The interaction between 4-oxothiazolidine-2-ylidene thioamides and iodine: a regioselective two-component 4-oxothiazolidine-2-ylidene thioamide to thiazolo[3,2-c]pyrimidine transformation mediated by iodine

ALEKSANDAR RAŠOVIĆ*

Institute of Chemistry Technology and Metallurgy, University of Belgrade, Njegoševa 12, 11000 Belgrade, Serbia

J. Serb. Chem. Soc. 90 (1) (2024) 13–26

SYNTHESIS, ISOLATED YIELDS, ANALYTICAL AND SPECTRAL DATA OF STARTING COMPOUNDS

General procedure for the preparation of 4-oxothiazolidine-2-ylidine thioamides 2a-c

The *push-pull* 2-alkylidene-4-oxothiazolidine **2a-c** derivatives were prepared according to the following general protocol previously reported[1] and slightly modified with respect to the amount of K_2CO_3, which was for this purpose used as the catalyst. To a suspension of the corresponding β-thioxonitrile **28** (0.01 mol) and freshly distilled α-mercaptoester (0.0172 mol; 72% molar excess) **27** in 16 mL of ethanol, a catalytic amount of K_2CO_3 was added (in 4.5 mol% of the starting material) (Table 1). **CAUTION**: *All reactions involving mercapto ester, owing to the unpleasant odor, should be carried out in a well-ventilated hood*. The mixture was heated and stirred in an oil bath at 75 °C for 3-4 h when TLC indicated the accomplishment of the reaction. After that, the reaction mixture was cooled down to room temperature and the precipitated products (*E*)-**2b** and (*Z*)-**2a** were collected by filtration, washed with ethanol and recrystallized from 96% ethanol and DMSO-water mixture (0.1 g, 7:5, v/v), respectively, to provide the final products (83-91%). Alternatively, in the case of the preparation of (*Z*)-**2c**, the filtered solution was concentrated under reduced pressure, and the residue was chromatographed by column chromatography on silica gel (toluene/ethyl acetate, 10:0 → 1:6) affording the desired product (61%). The structures of derivatives **2** were determined using the spectroscopic technique (^{1}H and ^{13}C NMR)[2] and elemental analysis.

* Correspondence to this paper should be addressed to Dejan Opsenica, JSCS Organic Chemistry Sub-Editor, E-mail: jscs-oh@shd.org.rs

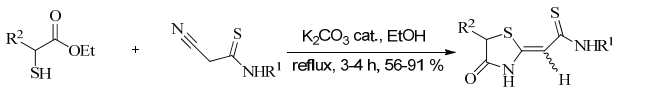

27 **28**

2a, R^1=H, R^2=H
2b, R^1=H, R^2=CH_2COOEt
2c, R^1=CH_2CH_2Ph, R^2=H

*(Z)-(4-Oxothiazolidin-2-ylidene)ethanthioamide (**2a**)*

According to the general procedure, the title compound was obtained from 1.46 g (14.6 mmol) of 2-cyanoethanthioamide, 3.02 g (25.1 mmol) of ethyl 2-mercaptoacetate and a catalytic amount of K_2CO_3 (0.25 g; 1.8 mmol) in ethanol (29 mL) as yellowish solid (2.31 g, 91%). M.P.: > 240 °C (decomposes after reaching this temperature). ^{1}H NMR (200 MHz, DMSO-d_6, δ): 3.61 (s, 2H, CH_2S), 6.16 (s, 1H, =CH), 8.44-8.65 (d, 2H, NH_{amide}), 11.51 (s, 1H, NH_{lactam}). ^{13}C NMR (50.3 MHz, DMSO-d_6, δ): 32.9 (CH_2S), 100.6 (=CH), 158.4 (C=), 174.4 (CO_{lactam}), 193.2 (C=S). MS (CI): *m/z* 175 $(M+1)^+$. Combustion analysis for $C_5H_6N_2OS_2$: Calculated. C 34.46, H 3.47, N 16.08; found: C 34.84, H 3.24, N 16.02.

*(E)-(5-Ethoxycarbonylmethyl-4-oxothiazolidin-2-ylidene)ethanthioamide (**2b**)*

According to the general procedure, the title compound was obtained from 1.20 g (12.0 mmol) of 2-cyanoethanthioamide, 4.27 g (20.7 mmol) of diethyl 2-mercaptosuccinate and a catalytic amount of K_2CO_3 (0.21 g; 1.5 mmol) in ethanol (19 mL) as yellow solid (2.59 g, 83%). M.P.: 208 °C. ^{1}H NMR (200 MHz, DMSO-d_6, δ): 1.18 (t, 3H, J = 7.2 Hz, CH_3), 3.05-3.09 (m, 2H, CH_AH_BCOO), 4.09 (q, 2H, J = 7.2 Hz, CH_2O), 4.45-4.51 (m, 1H, CH_XS), 5.64 (s, 1H, =CH), 8.81-8.87 (d, 2H, NH_{amide}), 13.28 (s, 1H, NH_{lactam}). ^{13}C NMR (50.3 MHz, DMSO-d_6, δ): 14.2 (CH_3), 36.3 (CH_2COO), 41.8 (CH_XS), 61.0 (CH_2O), 97.2 (=CH), 154.9 (C=), 170.4 (CO_{ester}), 174.4 (CO_{lactam}), 191.4 (C=S). MS (CI): *m/z* 261 $(M+1)^+$. Combustion analysis for $C_9H_{12}N_2O_3S_2$: Calculated. C 41.52, H 4.65, N 10.76; found: C 41.78, H 4.42, N 10.60.

*(Z)-(4-Oxothiazolidin-2-ylidene)-N-(2-phenylethyl)ethanthioamide (**2c**)*

From 0.20 g (1.0 mmol) of 2-cyano-*N*-phenethylethanthioamide, 0.19 g (1.9 mmol) of ethyl 2-mercaptoacetate and a catalytic amount of K_2CO_3 (0,03 g; 0,19 mmol) in ethanol (2 mL) after column chromatography the title compound was isolated as yellowish solid (0.16 g, 61%). M.P.: 170-172 °C. ^{1}H NMR (200 MHz, DMSO-d_6, δ): 2.86 (t, 2H, J = 7.0 Hz, CH_2Ph), 3.62-3.73 (m, 2H, NCH_2), the (s, 2H, CH_2S) signal is overlaped with the signal assigned to the (NCH_2) protons, 6.21 (s, 1H, =CH), 7.16-7.35 (m, 5H, Ph), 9.58 (t, 1H, J = 5.2 Hz, NH_{amide}), 11.51 (s, 1H, NH_{lactam}). ^{13}C NMR (50.3 MHz, DMSO-d_6, δ): 32.9 (CH_2S), 33.8 (CH_2Ph), 45.5 (NCH_2), 101.2 (=CH), 126.4 (*p*-Ph), 128.7 (*o*-Ph), 128.8 (*m*-Ph), 139.6 (C_{ipso}-Ph), 156.1 (C=), 174.3 (CO_{lactam}), 190.4 (C=S). MS (CI): *m/z* 279 $(M+1)^+$. Combustion analysis for $C_{13}H_{14}N_2OS_2$: Calculated. C 56.09, H 5.07, N 10.06; found: C 56.32, H 5.12, N, 9.83.

*Synthesis of 2-cyano-N-phenethylethanthioamide (**28b**)**

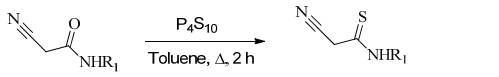

29 **28b** (59 %), R_1 = CH_2CH_2Ph

A mixture of 2-cyano-*N*-phenethylethanamide **29b** (0.70 g, 3.72 mmol) and P_4S_{10} (1.24 g, 2.80 mmol) in dry toluene (30 mL) was heated in an oil bath at 75 °C. **CAUTION:** *All reactions involving phosphorous decasulfide reagent, due to the unpleasant odor, should be carried out in a well-ventilated hood.* The mixture was stirred at this temperature for an additional 3 h when TLC indicated the complete consumption of 2-cyano-*N*-phenethylethanamide **29b**. After cooling to room temperature, the heterogeneous solution was filtered and concentrated under reduced pressure. The resulting residue was chromatographed by column chromatography on silica gel (toluene/ethyl acetate, 10:0 → 7:3) affording desired product as a yellow solid in moderate yield (0.45 g, 59%). M.P.: 93 °C. ^{1}H NMR (200 MHz, DMSO-d_6, δ): 2.89 (t, 2H, J = 7.2 Hz, CH_2Ph), 3.69-3.76 (m, 2H, NCH_2), 4.03 (s, 2H, CH_2), 7.18-7.37 (m, 5H, Ph), 10.49 (s, 1H, NH_{amide}). ^{13}C NMR (50.3 MHz, DMSO-d_6, δ): 32.9 (CH_2), 34.1 (CH_2Ph), 47.3 (NCH_2), 116.7 (CN), 126.6 (*p*-Ph), 128.7 (*o*-Ph), 128.8 (*m*-Ph), 138.9 (C_{ipso}-Ph), 190.3 (C=S). MS (CI): *m/z* 205 $(M+1)^+$. Combustion analysis for $C_{11}H_{12}N_2S$: Calculated. C 64.67, H 5.92, N 13.71; found: C 64.47, H 5.90, N 13.52.

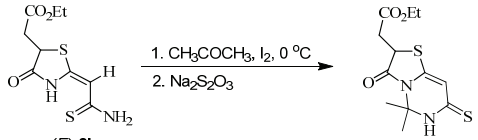

(*E*)-**2b** **7**

Yellow solid. M.P.: 145-147 °C. ^{1}H NMR ^{1}H NMR (200 MHz, DMSO-d_6, δ): 1.18 (t, 3H, J = 7.0 Hz, CH_3), 1.63 (s, 3H, CH_3), 1.77 (s, 3H, CH_3), 3.08-3.10 (m, 2H, CH_AH_BCOO), 4.09 (q, 2H, J = 7.0 Hz, CH_2O), 4.50-4.55 (m, 1H, CH_XS), 5.73 (d, 1H, J = 1.0 Hz, =CH), 9.54 (s, 1H, NH_{lactam}). ^{13}C NMR (50.3 MHz, DMSO-d_6, δ): 14.2 (CH_3), 25.6 (CH_3), 26.2 (CH_3), 36.1 (CH_2COO), 42.6 (CH_XS), 60.9 (CH_2O), 74.2 ($CNCH_3$), 101.0 (=CH), 146.8 (C=), 170.2 (CO_{ester}), 172.2 (CO_{lactam}), 184.5 (C=S). HRMS (TOF) *m/z*: calcd. for $C_{12}H_{16}N_2O_3S_2$ $[M+H]^+$: 301.06751, found: 301.06817.

* As the precursor of the (*Z*)-**2a** and (*E*)-**2b**, nitrile **28a** was used as a commercial compound. On the other side, the cyano-*N*-(2-phenyl)etanthioamide **28b**, i.e., the precursor of the (*Z*)-**2c** was prepared by the below described thionation procedure.

*Ethyl 2-(5,5-dimethyl-3-oxo-7-thioxo-3,5,6,7-tetrahydro-2H-thiazolo[3,2-c]pyrimidin-2-yl)acetate **7***

SPECTRAL DATA

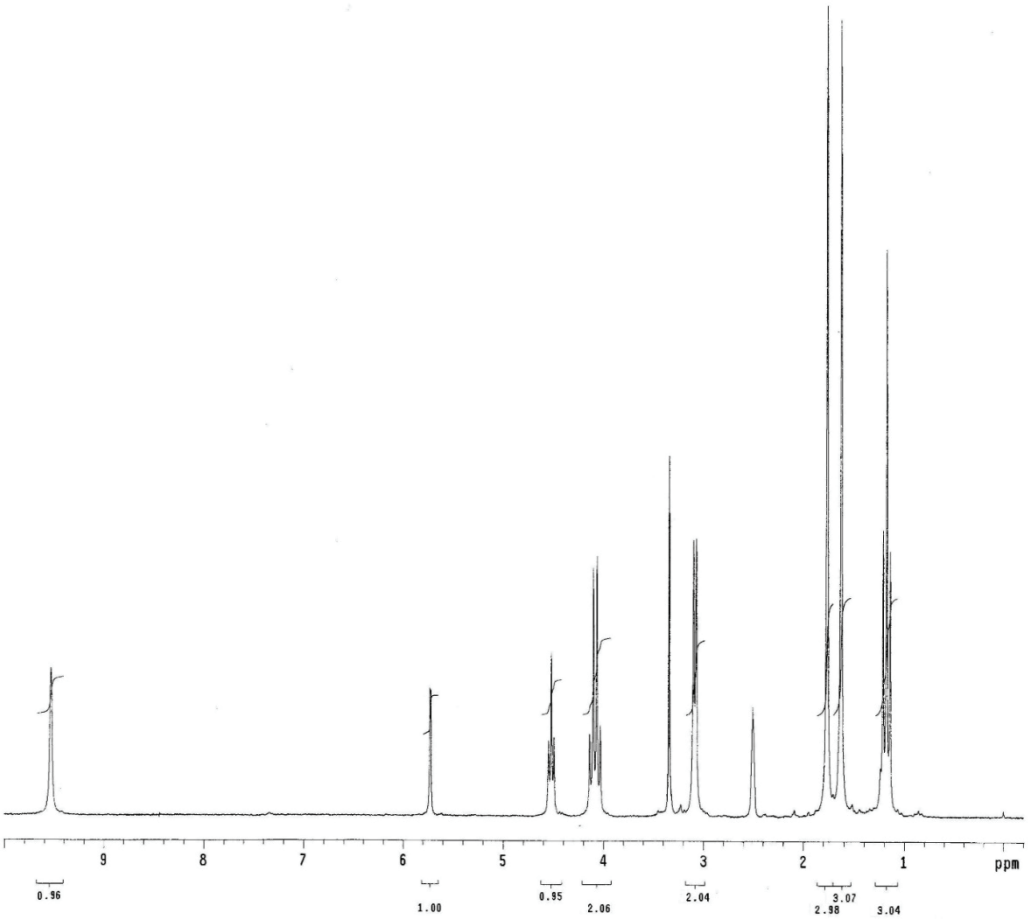

Fig. S-1. ^{1}H NMR spectrum of the thiazolopyrimidine **7**.

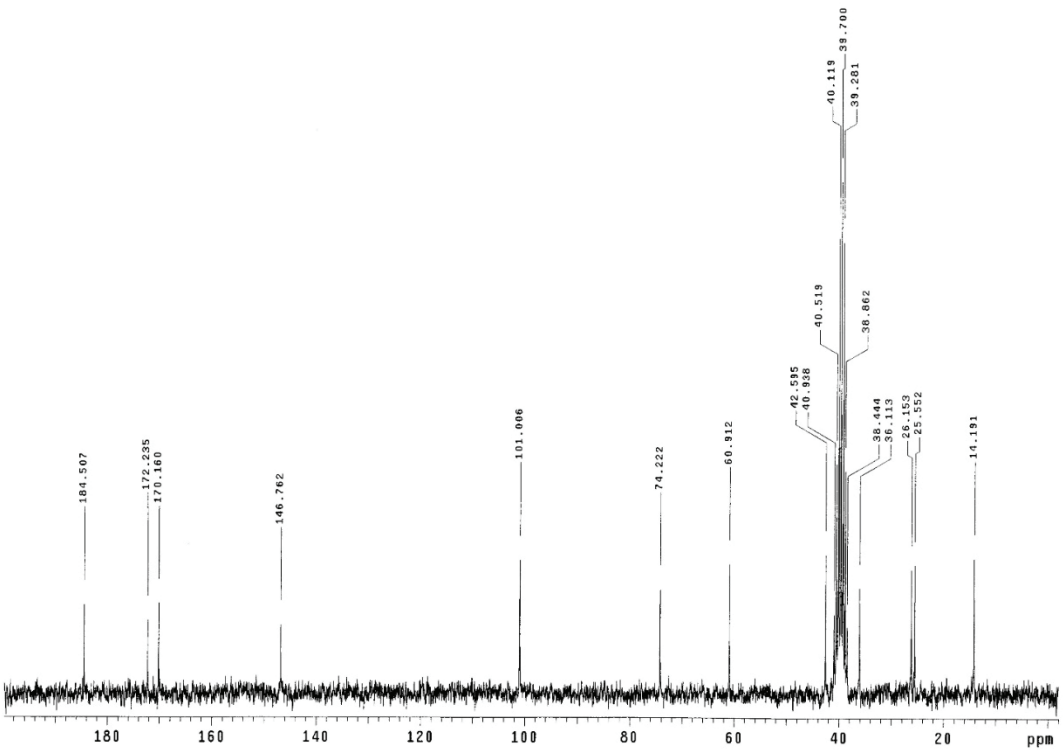

Fig. S-2. ^{13}C NMR spectrum of the thiazolopyrimidine **7**.

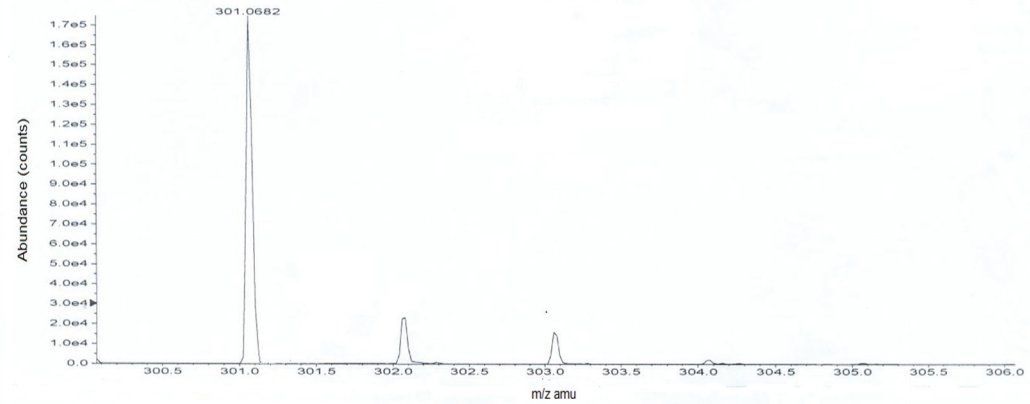

Formula	Compound name	Mass	Peak RT (min)	Peak area	Description
C12H16N2O3S2	--	300.06023	0.43	5.13012 E6	--

Species	Abundance (counts)	Ion Mass	Measured Mass	Error (mDa)	Error (ppm)	Ret. Time Error (min)
[M+H]+	176117.70	301.06751	301.06817	0.65630	2.18	--

Fig. S-3. HRMS (TOF) of the thiazolopyrimidine **7**.

REFERENCES

1. 1. R. Marković, M. Baranac, Z. Džambaski, M. Stojanović, P. J. Steel, *Tetrahedron* **59** (2003) 7803 (https://doi.org/10.1016/S0040-4020(03)01146-3)
2. A. Rašović, V. Blagojević, M Baranac-Stojanović, E. Kleinpeter, R. Marković, D. M. Minić, *New J. Chem.* **40** (2016) 6364 (https://doi.org/10.1039/C6NJ00901H).

Journal of the Serbian Chemical Society
JSCS-info@shd.org.rs • www.shd.org.rs/JSCS
J. Serb. Chem. Soc. *90* (1) 27–37 (2025)
JSCS–5817
Original scientific paper
Published 1 February, 2025

Zinc oxide nanoparticles: An experimental study of synthesis, characterization and biological activity

AULA M. AL HINDAWI[1], ZAHRAA M. ABD AL-AAMA[1], JUMAN KHALEEL AL-SABBAGH[2] and MOHAMMED AWAD[3,4]*

[1]*Department of Chemistry, College of Education for Pure Science, University of Kerbala, Karbala, Iraq,* [2]*College of Veterinary Medicine, University of Kerbala, Karbala, Iraq,* [3]*School of Engineering, Samarkand International University of Technology, Samarkand, Uzbekistan and* [4]*Department of Chemical Engineering, Toronto Metropolitan University, Toronto, Canada*

(Received 19 March, revised 22 April, accepted 24 August 2024)

Abstract: Zinc oxide (ZnO) nanosized structures were synthesized successfully using a benign method. The latter can be achieved by introducing sesame seed extract into the formation process of ZnO nanostructures as a reducing agent, converting zinc ions to Zn. The structural and optical properties of the prepared ZnO particles were studied using many techniques such as UV–Vis spectrophotometry, field emission scanning electron microscopy (FE-SEM), energy-dispersive X-ray spectroscopy (EDS), X-ray diffraction (XRD) and Fourier-transform infrared spectroscopy (FTIR). The estimated band gap energy of ZnO nanoparticles formed in the presence and absence of extract was found to be 3.94 and 3.88 eV, respectively, suggesting the effect of quantum confinement. The prepared particles have a flower-like shape with the appearance of small spherical particles. A Tauc plot was utilized to estimate the band gap energy of ZnO nanoparticles. The findings show that ZnO nanoparticles display bactericidal properties against *Staphylococcus hominins*, which are Gram-positive bacteria, and also on Gram-negative bacteria such as *Proteus mirabilis*, *E. coli*, *Acinetobacter baumannii*, *Pseudomonas aeruginosa* and *Klebsiella pneumonia*.

Keywords: ZnO-NPs; antibacterial activity; sesame seeds.

INTRODUCTION

Bacteria are known to be the cause of many infectious illnesses. The treatment of such diseases has become challenging due to their resistance to antibiotics.[1,2] To protect human society, new medications or techniques for killing these microorganisms must be developed. Nanotechnology is a developing area where the

* Corresponding author. E-mail: E-mail: mohammed.awad@torontomu.ca; mohammed.awad@siut.uz
https://doi.org/10.2298/JSC240319079A

nanostructures of varying shapes and sizes can be manufactured, offering potential applications as antibiotics.[3] Because of their tiny size at the nanoscale, the nanostructures can infiltrate bacteria cell walls and engage with the cell membrane subsequent to adhering to the cell wall.[3] Unlike their larger counterparts, these particles possess expansive surface areas, amplifying their reactivity and potential toxicity. Many metal oxide nanoparticles are incredibly damaging to certain types of bacteria. For example, titanium dioxide (TiO_2) nanoparticles can eliminate *Escherichia coli* bacteria.[4] Likewise, the nanoparticles of magnesium oxide (MgO) and calcium oxide (CaO) show the bactericidal effects against *Bacillus cereus*, *Bacillus globigii* and *E. coli*.[5,6]

Zinc oxide (ZnO) nanoparticles (NPs) are highly regarded as effective photocatalysts and antimicrobial agents because they can generate free radicals.[7] When ZnO particles encounter the solar radiation exceeding their band gap energy, electrons become energized to the conduction band (CB), leaving vacancies known as holes in the valence band (VB).[8] The photogenerated electrons and holes generated on the surface of ZnO lead to the creation of highly reactive oxygen species (ROS), like superoxide anion ($^{\bullet}O_2$) and hydroxyl radical ($^{\bullet}OH$). These extremely reactive oxygen species perform antibacterial and photodegradative activities by destroying bacteria's DNA and membrane. Moreover, studies show that Zn ion could damage the bacteria's cell membrane, changing the metabolic pathway. Yang *et al.* showed that the antibacterial effectiveness of ZnO-NPs at concentrations of 10 and 50 mg L^{-1} were 28.30 and 55.03 %, respectively. Their findings showed that increasing the concentration of ZnO-NPs increases the antibacterial effect due to their small size and high specific surface area.[9] This antibacterial activity of ZnO-NPs paves the way for use in many potential fields, such as in producing UV-blocking clothing, sunscreens, infant rash ointments, paints, drug delivery and even food preservatives.[10–12]

ZnO-NPs can be produced using various techniques, including co-precipitation,[13] sol–gel,[14,15] hydrothermal[16] and solochemical.[7] The size, shape, surface area, electronic states and surface charge of nanostructures majorly impact their biological activities. Therefore, the synthesis process must be chosen to produce nanosized materials with the best activity for the intended applications. This work is aimed to present a method to fabricate ZnO nanostructures using an eco-friendly and straightforward green method and chemical precipitation method. Their bacterial activity is examined against Gram-positive bacteria (*Staphylococcus hominis*) and Gram-negative bacteria (*Proteus mirabilis*, *E coli*, *Acinetobacter baumannii*, *Pseudomonas aeruginosa* and *Klebsiella pneumonia*). The basic idea behind this green synthesis is to use parts of plants such as seeds, leaves, and roots as reducing and stabilizing agents instead of chemical solvents and agents. The green synthesized ZnO-NPs were considered safe for pharmaceutical and biomedical applications.[17]

MATERIALS AND METHODS

Materials

In this project, zinc sulfate heptahydrate ($ZnSO_4 \cdot 7H_2O$, 99 %) was purchased from Thomas Baker. Scharlau supplied sodium hydroxide (NaOH, 99 %).

Preparation of sesame seed solution

The sesame seeds were purchased from the local market and crashed into tiny fragments. Five grams of sesame seeds were dissolved in de-ionized water (100 mL). A magnetic stirrer (set at 150 rpm) was used to stir the solution for a few minutes at 60 °C. After that, filter paper No. 1 was used to achieve filtration, and the filtrate was refrigerated (4 °C) before being used to prepare zinc oxide nanoparticles.

Preparation of ZnO-NPs

One mM of $ZnSO_4 \cdot 7H_2O$ was prepared and stirred for 60 min at 25 °C. After adding 50 mL of the sesame seed extract to the precursor solution, the latter was stirred for 10 min. Subsequently, NaOH (1 M) was gradually added until the pH of the solution reached 10 while maintaining 70 °C and stirring. A yellowish–white precipitate was observed at the bottom of the mixture flask, suggesting the formation of ZnO (capped-ZnO-NPs). The centrifuge was used to collect the residue, which was formed, for 20 min at 4000 rpm. Ultimately, the final product underwent 4 h of vacuum oven drying at 80 °C after being repeatedly cleaned with distilled water. A similar procedure was performed to form the uncapped-ZnO nanoparticles without the addition of the sesame seed extract.

Characterization techniques

Various characterization approaches were used to investigate the physicochemical properties of synthesized ZnO. UV-1800 Shimadzu spectrophotometer (Japan) was used to study the optical properties of zinc oxide nanostructures. The functional groups of the sesame seed extract were identified using the Fourier-transform infrared spectrum (FT-IR, Shimadzu). Using CuKα radiation (λ = 0.154056 nm) and a scanning range of 20 to 80°, the X-ray diffraction (XRD) patterns were recorded.

Biological activity of ZnO-NPs

Various strains of bacteria sourced from different medical cases, including skin infections, urinary tract infections, genital infections, tonsillitis and ear infections, were tested. These bacteria were identified through biochemical methods and VITEK2 analysis.

ZnO-NPs were prepared by dissolving 10 mg of ZnO powder in 100 mL distilled water. A pure culture of a bacterial organism that has been previously described (107 CFU) was used for the test. The inoculum was prepared by transferring five isolated colonies cultured on blood agar plates into 5 mL broth. This mixture was then incubated for 120 min to generate a moderately cloudy bacterial suspension. To acquire an inoculum from the standardized culture, a sterile swab was used and then transferred onto a Müeller–Hinton plate to dry.

Next, the diffusion test (Kirby–Bauer susceptibility test) was used to determine the bacterial sensitivity to antibacterial agents. After inoculating the medium agar with the bacterial isolates, pores are created on agar plates using a poorer cork before drying the plates. The solution of ZnO was added into the pores and incubated overnight (37 °C). A caliper was used to measure the inhibitory zones. According to the standard zones from the Clinical and Laboratory Standard Institute (CLSI), the organism's resistance was identified.[18]

RESULTS AND DISCUSSION

In Fig 1a, the appearance of the blue shift in the UV–Vis spectra of capped and uncapped-ZnO concerning their counterpart bulk (373 nm)[19] confirms the formation of ZnO at nanoscale levels. A large shift was observed when the sesame extract was introduced (capped-ZnO). A possible explanation for this shift is that adding the sesame extract prevents the further addition of atoms to the already existing particles. To estimate the energy of the band gap for the prepared ZnO--NPs, Tauc plot was used:[20,21]

$$\alpha h\nu = C(h\nu - E_g)^n \quad (1)$$

Herein, the band gap energy is E_g, the coefficient of absorption represented by α. The n indicates a direct electronic transition and equals 0.5, which denotes Tauc exponent,[22] the proportional constant is C and the energy photon is $h\nu$.

Extending the linear portion of the UV–Vis spectrum along the photon energy axis in Fig. 1b, the band gap energy is determined to be 3.94 and 3.88 eV for capped and uncapped-ZnO, respectively. This value exceeds bulk ZnO (3.37 eV)[23] due to elections confinement at the nanoscale.[24] The band gap energy value closely aligns with findings from prior experiments, conducted by Miri *et al.*[22]

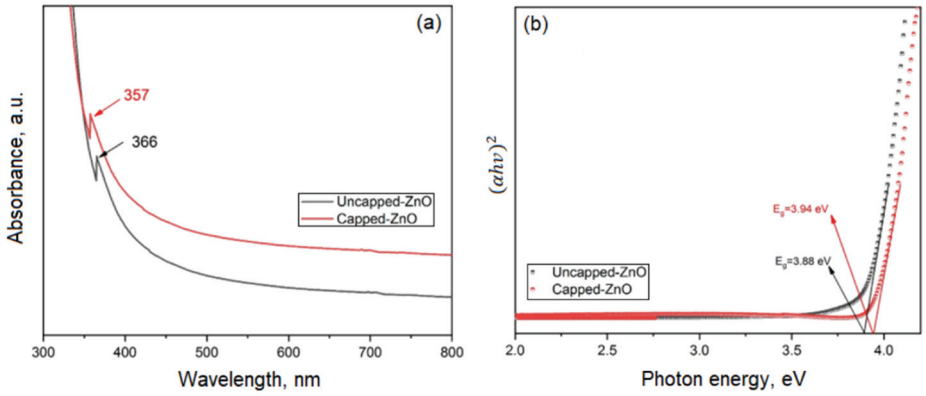

Fig. 1. a) UV–Vis spectrum of zinc oxide nanostructures formed in the presence of sesame seeds and b) the Tauc plot used to calculate the band gap (E_g), which equals 3.94 eV.

The field emission scanning electron microscopy (FE-SEM) examined the surface morphology of both capped and uncapped-ZnO nanostructures. Fig. 2a shows that introducing sesame seeds into the synthesis process of ZnO particles has no effect on the morphology of the prepared samples. Both methods give particles with flower-like shapes in addition to the appearance of small spherical particles. The energy-dispersive X-ray spectroscopy (EDS) was used to study the elements that could be present in the sample. The energy dispersive X-ray analysis (EDX) chart for capped-ZnO in Fig. 2c (uncapped-ZnO nanoparticles not shown

in Fig. 2c as the chart is similar to capped-ZnO) in Fig. 2b shows that the sample contains zinc and oxygen elements in its structure, confirming the formation of ZnO nanostructures. The appearance of the gold component in the chart is attributed to the coating process for the semiconductor to make the sample conductor.[25]

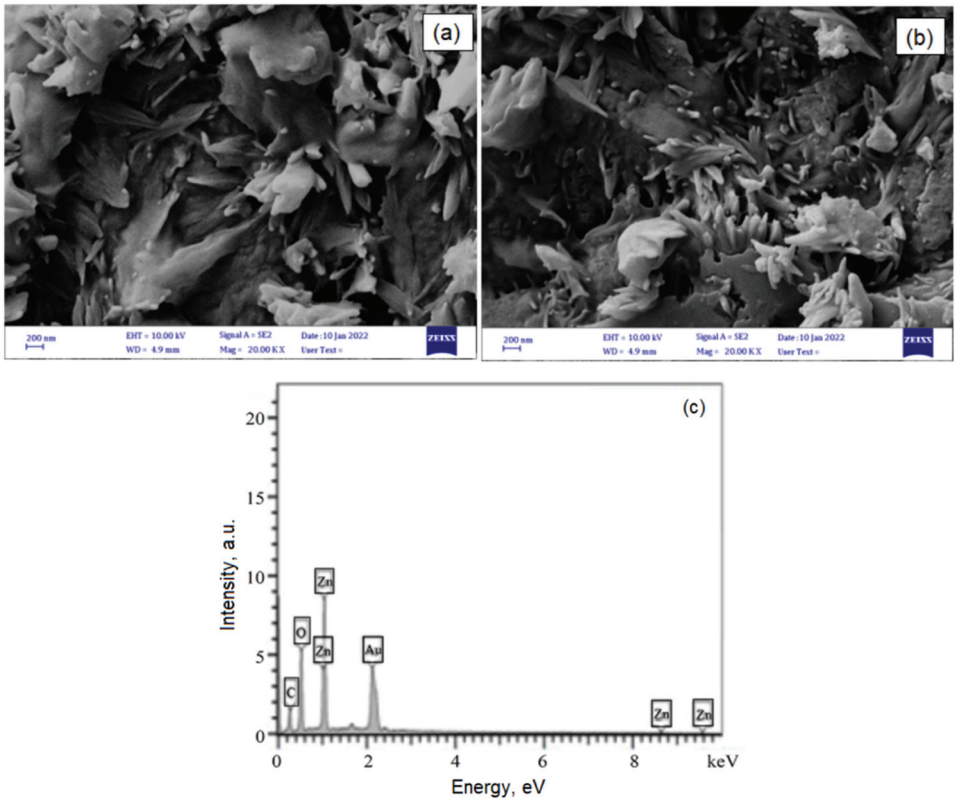

Fig. 2. a) The field emission scanning electron microscopy (FE-SEM) image of the prepared zinc oxide nanostructures in the presence of sesame seeds extract, b) FE-SEM image for uncapped-ZnO nanostructures and c) the energy dispersive X-ray analysis (EDX) chart showing the element in the capped-zinc oxide nanostructures sample.

The crystalline structure of the synthesized ZnO-NPs was examined using XRD. It is clear from Fig. 3 that the diffraction peaks appear at 30.03, 37.878, 48.21, 56.20, 63.69 and 67.24° correspond to 100, 002, 101, 102, 110 and 103 planes, respectively. This finding suggests that the as-prepared ZnO has a hexagonal wurtzite structure, which aligns with the previous studies.[26,27] The crystallite size was calculated for the highest intensity peak of 100 using Scherrer formula,[28,29] and it was found to be 20.2 nm. The interesting point here is that there was no effect seen at all on the crystalline properties of ZnO nanostructures

after introducing sesame seeds extract. Our speculation for this observation is that the bioactive components in the extract are attached to ZnO surface and form weak van der Waals forces, without any effect on the crystalline structures of ZnO.

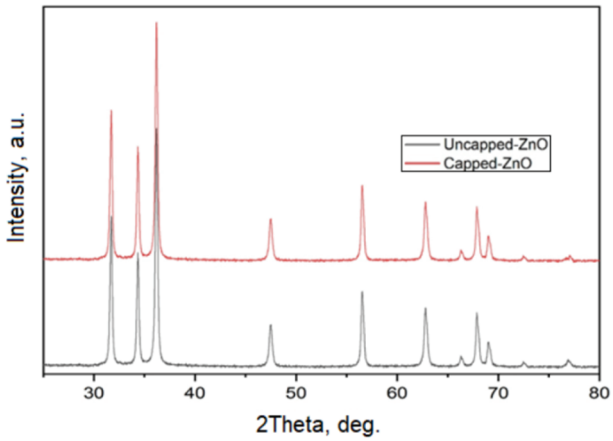

Fig. 3. X-ray diffraction (XRD) pattern for zinc oxide nanostructures prepared with sesame seed.

FTIR spectra for capped- and uncapped-ZnO nanostructures were measured between 500 and 4000 cm^{-1}. In both samples, the peak centered at 558 cm^{-1} is assigned to Zn–O vibration mode,[30] confirming the formation of ZnO-NPs (see Fig. 4). The spectrum of sesame seeds capped-ZnO exhibits several additional peaks which probably relates to the presence of bioactive constituents extracted from sesame seeds. For example, the peak appeared at 3340 cm^{-1} could be related to the presence of the OH group from the alkaloid compound on the ZnO surface, while the absorption band at ~2950 cm^{-1} corresponds to the C–H group.[31,32] The two peaks at 1527 and 1653 cm^{-1} is ascribed to N–H binding and C–O, respectively, which represent the sugars existed within ZnO nanostructures. A strong peak centered at ~880 cm^{-1} is assigned to (RCOOH), which is possibly related to phenolic compounds. The emergence of these peaks is ascribed to the presence of bioactive constituents extracted from sesame seeds. These components serve as reducing agents by supplying electrons, thereby facilitating the reduction of Zn^{2+} to Zn^{+} and subsequently to Zn (Zn nanoparticles).[33]

The antibacterial activity of prepared ZnO-NPs against different bacteria types was determined using a diffusion test for both capped, uncapped-ZnO nanoparticles and Zn ions alone. The appearance of clear zones on the Petri dishes indicates the ability of ZnO-NPs to inhibit the under-studying bacterial growth. The results found that uncapped ZnO-NPs had less effect as comparing to the capped ZnO--NPs with the sesame seeds extract; while Zn ions appear with no effect at all (Table I). Fig. 5a shows the antibiotic effect of ZnO nanocrystals against *Pseudo-*

monads aeruginosa (upper part), *Klebsiella pneumonia* (lower part) and Fig. 5b *E. coli* bacteria.

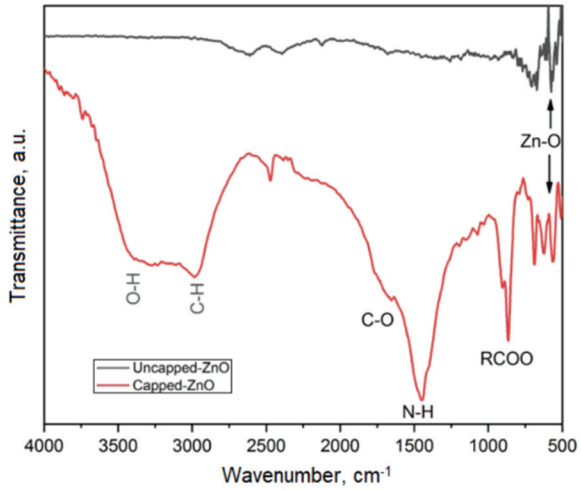

Fig. 4. Fourier-transform infrared spectroscopy (FTIR) for zinc oxide nanostructures.

TABLE I. The antibacterial effect of Zinc oxide nanoparticles (ZnO-NPs) was determined from the inhibition zones

No.	Bacterial isolates	Inhibition zone, mm
1	*Proteus mirabilis*	15
2	*Escherichia coli*	28
3	*Staphylococcus hominis*	22
4	*Acinetobacter baumannii*	18
5	*Pseudomonas aeruginosa*	25
6	*Klebsiella pneumoniae*	20

The rest of the chosen bacteria in this study and their inhibition zones, which formed around the particles, were calculated and presented in Table I. *E. coli* is more sensitive to the ZnO nanoparticles based on its inhibition zone (28 mm). It was known that the larger the inhibitory zone, the greater the sensitivity to the ZnO particles. According to a previous Klink *et al.*[34] study, the inhibition zone should be ≥10 mm for effectiveness. Although *P. mirabilis* shows a smaller inhibition zone (15 mm) than other strains, it is still considered adequate.

The best explanation for the antibiotic effect is that the small ZnO particles result in a high surface-to-volume ratio and more adherence to the Gram-positive and harmful bacteria. Several mechanisms for the antibacterial action of ZnO-NPs have been proposed. A possible mechanism is the adsorption of ZnO-NPs on the bacterial surface, which leads to product various intermediates and electrostatic interactions.[35]

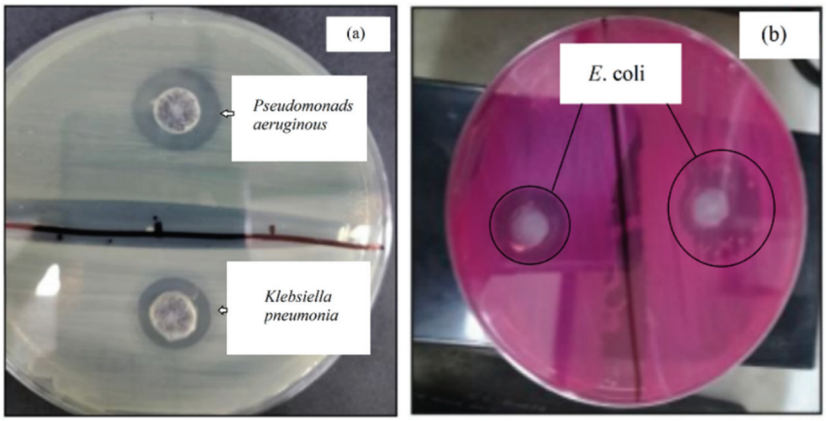

Fig. 5. The inhibition zones of zinc oxide nanoparticles against bacterial isolates: a) *Pseudomonas aeruginosa* (upper part) and *Klebsiella pneumonia* (lower part) bacteria; b) *Escherichia coli* bacteria.

On the other hand, Mendes *et al.*[17] have recently studied the membrane integrity of *P.s aeruginosa*, *E. coli*, *S. aureus* and *B. subtilis* cells. They noted cytoplasmic membrane disruption across all strains upon the introduction of ZnO particles due to their adhesion to bacterial surfaces. The negative charges on cell surfaces are primarily due to lipoteichoic acid within the membrane and teichoic acid in the peptidoglycan layer. The electrostatic interactions attract positive charges from ZnO nanocrystals to the cell surface. Consequently, the variance in the electrostatic gradient leads to surface damage to the cells.[36]

On the other hand, the reason why bacteria could resist ZnO ions, might be due to that, bacteria have developed sophisticated mechanisms to regulate the concentration of meta ions within their cells; this is achieved through efflux and influx pump systems, ensuring stable internal environment, zinc (Zn^{2+}) is a vital example of a metal ion that bacteria meticulously control.[37]

Several bacterial species, including *Staphylococci*, *Streptococci* and *E. coli*, possess genes dedicated to zinc transport; for example, in *S. aureus*, the ZntA and ZntR genes play a crucial role in zinc homeostasis; the ZntA protein, located in the cell membrane, acts as an efflux pump, actively removing excess zinc ions.[38] Meanwhile, the ZntR protein functions as an adjuster, adjusting the activity of the Znt operon (including ZntA) based on zinc availability.[39]

CONCLUSIONS

This study is concentrated on the formation and characterization of zinc oxide nanostructures using two methods: green and chemical precipitation. Various analytical techniques, such as UV–Vis spectrophotometry, FE-SEM, EDS, XRD and FTIR spectroscopy, were used to characterize the prepared ZnO-NPs. The findings show that capped and uncapped-ZnO are crystalline with a wurtzite structure, and

the crystalline size is 20.3 nm. No effect was observed on the morphology of ZnO after adding the extract. According to the calculated band gap, the quantum confinement effect becomes stringer after introducing the sesame seeds extract. Zinc oxide nanoparticles show an antibacterial effect against all the chosen bacteria, and *E. coli* exhibited an enormous sensitivity for ZnO-NPs.

ИЗВОД

НАНОЧЕСТИЦЕ ЦИНК-ОКСИДА: ЕКСПЕРИМЕНТАЛНА СТУДИЈА О СИНТЕЗИ, КАРАКТЕРИЗАЦИЈИ И БИОЛОШКОЈ АКТИВНОСТИ

AULA M. AL HINDAWI[1], ZAHRAA M. ABD AL-AAMA[1], JUMAN KHALEEL AL-SABBAGH[2] и MOHAMMED AWAD[3,4]

[1]Department of Chemistry, College of Education for Pure Science, University of Kerbala, Karbala, Iraq, [2]College of Veterinary Medicine, University of Kerbala, Karbala, Iraq, [3]School of Engineering, Samarkand International University of Technology, Samarkand, Uzbekistan u [4]Department of Chemical Engineering, Toronto Metropolitan University, Toronto, Canada

Честице цинк-оксида нановеличине су успешно синтетисане применом безбедног метода, коришћењем екстракта семена сусама као редукујућег агенса у току процеса формирања наноструктура ZnO, који преводи јоне цинка у Zn. Стуктурне и оптичке особине припремљених ZnO честица су испитане применом већег броја техника, ка о што су UV–Vis спектрофотометрија, скенирајућа електронска микроскопија са емисионим пољем (FE-SEM), спектроскопија X-зрака са расподелом енергије (EDS), дифракција X-зрака (XRD) и Фурије трансформишућа инфрацрвена спектроскопија (FTIR). Процењене енергетске разлике за ZnO наночестице настале у присуству и одсуству екстракта су биле 3,94 eV, односно 3,88 eV, сугеришући ефекат квантног ограничења. Добијене честице имају облик цвета и изгледају као мале сфере. Tauc дијаграм је коришћен за процену енергетске разлике ZnO наночестица. Резултати су показали да ZnO наночестице испољавају бактерицидну активност спрам Грам-позитивне бактерије *Staphylococcus hominins*, као и спрам Грам-негативних бактерија *Proteus mirabilis*, *E. coli*, *Acinetobacter baumannii*, *Pseudomonas aeruginosa* и *Klebsiella pneumonia*.

(Примљено 19. марта, ревидирано 22. априла, прихваћено 24. августа 2024)

REFERENCES

1. L. R. Thurlow, V. C. Thomas, L. E. Hancock, *J. Bacteriol.* **191** (2009) 6203 (https://doi.org/10.1128/JB.00592-09)
2. T. J. Foster, *FEMS Microbiol. Rev.* **41** (2017) 430 (https://doi.org/10.1093/femsre/fux007)
3. M. Ozdal, S. Gurkok, *ADMET DMPK* **10** (2022) 115 (https://doi.org/10.5599/admet.1172)
4. R. D. Desiati, M. Taspika, E. Sugiarti, *Mater. Res. Express* **6** (2019) 95059 (https://doi.org/10.1088/2053-1591/ab155c)
5. D. Sahu, N. R. Panda, *Curr. Nanosci.* **17** (2021) 162 (https://doi.org/10.2174/1573413716999200728175722)
6. C. Silva, F. Bobillier, D. Canales, F. Antonella Sepúlveda, A. Cament, N. Amigo, L. M. Rivas, M. T. Ulloa, P. Reyes, J. A. Ortiz, T. Gómez, C. Loyo, P. A. Zapata, *Polymers (Basel)* **12** (2020) 2132 (https://doi.org/10.3390/polym12092132)
7. R. C. De Souza, L. U. Haberbeck, H. G. Riella, D. H. B. Ribeiro, B. A. M. Carciofi, *Braz. J. Chem. Eng.* **36** (2019) 885 (https://doi.org/10.1590/0104-6632.20190362s20180027)

8. S. Yang, C. Feng, D. Spence, A. M. A. A. Al Hindawi, E. Latimer, A. M. Ellis, C. Binns, D. Peddis, S. S. Dhesi, L. Zhang, Y. Zhang, K. N. Trohidou, M. Vasilakaki, N. Ntallis, I. MacLaren, F. M. F. De Groot, *Adv. Mater.* **29** (2017) 1604277 (https://doi.org/10.1002/adma.201604277)
9. H. Yang, J. Zhang, Z. Li, J. Huang, J. Wu, Y. Zhang, H. Ge, Y. Zhao, *Nanomaterials* **13** (2023) 2033 (https://doi.org/10.3390/nano13142033)
10. C. Pushpalatha, J. Suresh, V. Gayathri, S. Sowmya, D. Augustine, A. Alamoudi, B. Zidane, N. H. Mohammad Albar, S. Patil, *Front. Bioeng. Biotechnol.* **10** (2022) 917990 (https://doi.org/10.3389/fbioe.2022.917990)
11. T. A. Singh, J. Das, P. C. Sil, *Adv. Colloid Interface Sci.* **286** (2020) 102317 (https://doi.org/10.1016/j.cis.2020.102317)
12. L. E. Román, J. Huachani, C. Uribe, J. L. Solís, M. M. Gómez, S. Costa, S. Costa, *Appl. Surf. Sci.* **469** (2019) 204 (https://doi.org/10.1016/j.apsusc.2018.11.047)
13. M. G. Kotresh, M. K. Patil, S. R. Inamdar, *Optik (Stuttgart)* **243** (2021) 167506 (https://doi.org/10.1016/j.ijleo.2021.167506)
14. S. Arya, P. Mahajan, S. Mahajan, A. Khosla, R. Datt, V. Gupta, S.-J. Young, S. K. Oruganti, *ECS J. Solid State Sci. Technol.* **10** (2021) 23002 (https://doi.org/10.1149/2162-8777/abe095)
15. I. Ben Amor, H. Hemmami, S. E. Laouini, M. S. Mahboub, A. Barhoum, *Catalysts* **12** (2022) 1611 (https://doi.org/10.3390/catal12121611)
16. M. M. El-Faham, A. M. Mostafa, E. A. Mwafy, *J. Phys. Chem. Solids* **154** (2021) 110089 (https://doi.org/10.1016/j.jpcs.2021.110089)
17. C. R. Mendes, G. Dilarri, C. F. Forsan, V. de M. R. Sapata, P. R. M. Lopes, P. B. de Moraes, R. N. Montagnolli, H. Ferreira, E. D. Bidoia, *Sci. Rep.* **12** (2022) 2658 (https://doi.org/10.1038/s41598-022-06657-y)
18. M. I. Khan, S. Shah, S. Faisal, S. Gul, S. Khan, Abdullah, S. A. Shah, W. A. Shah, *Micromachines* **13** (2022) 1 (https://doi.org/10.3390/mi13050668)
19. M. Zare, K. Namratha, S. Alghamdi, Y. H. E. Mohammad, A. Hezam, M. Zare, Q. A. Drmosh, K. Byrappa, B. N. Chandrashekar, S. Ramakrishna, X. Zhang, *Sci. Rep.* **9** (2019) 8303 (https://doi.org/10.1038/s41598-019-44309-w)
20. A. M. Al Hindawi, I. Joudah, S. Hamzah, Z. Tarek, *IOP Conf. Ser. Mater. Sci. Eng.* **571** (2019) 12069 (https://doi.org/10.1088/1757-899X/571/1/012069)
21. A. M. Al Hindawi, N. H. Obaid, I. Joudah, N. Shiltagh, K. Tahir, *Int. J. Pharm. Res.* **12** (2020) (https://doi.org/10.31838/ijpr/2020.12.02.0150)
22. A. Miri, M. Khatami, O. Ebrahimy, M. Sarani, *Green Chem. Lett. Rev.* **13** (2020) 27 (https://doi.org/10.1080/17518253.2020.1717005)
23. L. Alsaba, M. Ashoush, S. Elsayed, A. Eid, A. Abdelghany, *Al-Azhar Bull. Sci.* **30** (2019) 1 (https://doi.org/10.21608/absb.2019.86747)
24. Z. Turki, A. Al Hindawi, N. Shiltagh, *NanoWorld J.* **08** (https://doi.org/10.17756/nwj.2022-102)
25. A. Abed, A. Al Hindawi, H. Alesary, *NanoWorld J.* **08** (https://doi.org/10.17756/nwj.2022-103)
26. P. Shunmuga Sundaram, T. Sangeetha, S. Rajakarthihan, R. Vijayalaksmi, A. Elangovan, G. Arivazhagan, *Phys., B* **595** (2020) 412342 (https://doi.org/10.1016/j.physb.2020.412342)
27. W. Muhammad, N. Ullah, M. Haroon, B. H. Abbasi, *RSC Adv.* **9** (2019) 29541 (https://doi.org/10.1039/C9RA04424H)

28. A. Q. Abed, A. M. Al Hindawi, H. F. Alesary, *AIP Conf. Proc.* **2830** (2023) 20001 (https://doi.org/10.1063/5.0156826)
29. Z. T. Turki, A. M. Al Hindawi, N. M. Shiltagh, *AIP Conf. Proc.* **2834** (2023) 30008 (https://doi.org/10.1063/5.0161450)
30. N. Jayarambabu, B. S. Kumari, K. V. Rao, Y. T. Prabhu, *Int. J. Curr. Eng. Technol.* **4** (2014) 3411 (https://inpressco.com/wp-content/uploads/2014/09/Paper593411-3416.pdf)
31. M. Hraja, A. Al Hindawi, N. Shiltagh, *J. Turkish Chem. Soc.* **11** (2011) 565 (https://doi.org/10.18596/jotcsa.1356389)
32. P. J. Kanu, *Amer. J. Biochem. Mol. Biol.* **1** (2012) 145 (https://doi.org/10.3923/ajbmb.2011.145.157)
33. S. Alamdari, M. Sasani Ghamsari, C. Lee, W. Han, H.-H. Park, M. J. Tafreshi, H. Afarideh, M. H. M. Ara, *Appl. Sci.* **10** (2020) 3620 (https://doi.org/10.3390/app10103620)
34. M. J. Klink, N. Laloo, A. Leudjo Taka, V. E. Pakade, M. E. Monapathi, J. S. Modise, *Molecules* **27** (2022) 3532 (https://doi.org/10.3390/molecules27113532)
35. B. Abebe, E. A. Zereffa, A. Tadesse, H. C. A. Murthy, *Nanoscale Res. Lett.* **15** (2020) 190 (https://doi.org/10.1186/s11671-020-03418-6)
36. N. B. Raj, N. T. PavithraGowda, O. S. Pooja, B. Purushotham, M. R. A. Kumar, S. K. Sukrutha, C. R. Ravikumar, H. P. Nagaswarupa, H. C. A. Murthy, S. B. Boppana, *J. Photochem. Photobiol.* **6** (2021) 100021 (https://doi.org/10.1016/j.jpap.2021.100021)
37. J. K. Al-Sabbagh, A. Abd Al-Redha, M. A. Mohammad, *Ind. J. Public Health Res. Dev.* **11** (2020) 1123 (https://www.researchgate.net/publication/345508208)
38. C. C. Murdoch, E. P. Skaar, *Nat. Rev. Microbiol.* **20** (2022) 657 (https://doi.org/10.1038/s41579-022-00745-6)
39. B. Tartilán-Choya, C. Tejedor, R. Conde-Álvarez, P. María Muñoz, N. Vizcaíno. *Front. Vet. Sci.* **10** (2024) (https://doi.org/10.3389/fvets.2023.1323500).

Journal of the Serbian Chemical Society
JSCS-info@shd.org.rs • www.shd.org.rs/JSCS
J. Serb. Chem. Soc. *90* (1) 39–52 (2025)
JSCS–5818
Original scientific paper
Published 1 February, 2025

Monte Carlo optimization-based QSAR modelling of *Staphylococcus aureus* inhibitory activity of coumarin-1,2,3-triazole hybrids

KRISHNA N. MISHRA, HARISH C. UPADHYAY* and POONAM VERMA

Laboratory of Chemistry, Department of Applied Sciences, Rajkiya Engineering College (Affiliated with Dr. A.P.J. Abdul Kalam Technical University, Lucknow), Churk, Sonbhadra-231206, India

(Received 30 March, revised 22 September, accepted 12 November 2024)

Abstract: In this study, 51 coumarin-1,2,3-triazole hybrids with known minimum inhibitory concentration (*MIC*) values against *Staphylococcus aureus* were used for the generation of a Monte Carlo based optimized QSAR model on correlations and logic (CORAL) software. The entire dataset was divided into four different sets, namely the training set (Tr), the invisible training set (iTr), the calibration set (C) and the validation set (V) of three random splits. For each split, five models were generated using various combinations of SMILES, graphs and hybrid optimal descriptors with various connectivity indices. Finally, fifteen models were obtained from three random, non-identical splits. For the best model from each split, the correlation coefficient (r^2) ranged from 0.9672 to 0.8693, while the cross-validated correlation coefficient (Q^2) ranged from 0.9478 to 0.8250. The mean absolute error (*MAE*) for the best models was less than 0.065. Additionally, favourable values of the index of ideality of correlation (*IIC*) and correlation intensity index (*CII*) were reported, justifying the robustness, reliability and predictive potential of the developed models. Further, good and bad fingerprints were estimated based on correlation weights for structural attributes.

Keywords: CORAL software; antibacterial; structural attributes; index of ideality of correlation; correlation intensity index.

INTRODUCTION

Natural products have played a crucial role in the discovery of drugs for almost all types of diseases.[1] The natural products, as such and their semisynthetic analogs, contribute to more than half of the approved drugs of today.[2,3] Because of safety and compatibility, natural products are and will be at the center

* Corresponding author. E-mail: harishcu@recsonbhadra.ac.in
https://doi.org/10.2298/JSC240330094M

of the drug discovery process.[4] Traditional drug discovery methods often rely on trial-and-error approaches, which are time-consuming and resource-intensive.[5] However, due to dependence on several factors, it is not possible to estimate exactly, but on average, the development of a single drug from a new chemical entity may cost up to $1 billion over twelve to fifteen years.[5,6] While natural products continue to inspire drug discovery efforts, there is a growing recognition of the need for innovative approaches that integrate advances in computational biology, synthetic chemistry and biotechnology to overcome the limitations of traditional drug discovery.[7,8] By leveraging interdisciplinary approaches and cutting-edge technologies, researchers can harness the potential of natural resources more effectively and develop novel therapeutics with improved efficacy, safety and sustainability.[9] Computer-aided drug design (CADD) has emerged as a powerful tool in the field of pharmaceutical research that utilizes computational methods to facilitate the discovery and development of new drugs.[10] The CADD approach integrates principles from various disciplines, such as chemistry, biology and computer science, to expedite the drug discovery process.[11,12] CADD-based rational drug design approaches, *viz*., virtual screening by docking simulations, quantitative structure-activity relationship (QSAR) studies for lead optimization and prediction of bioactivities and *in silico* prediction of physiochemical characteristics of molecules in terms of absorption, distribution, metabolism and toxicity, help the researchers prioritize the most promising candidates for further experimental validation, significantly reducing the time and cost associated with traditional screening methods.[10]

QSAR studies play a pivotal role in drug discovery and development by enabling the rational design, optimization, and selection of potential drug candidates. QSAR models provide valuable insights into the relationship between the chemical structure of compounds and their biological activities.[13] QSAR modelling utilizes computational techniques to analyse the structural features of molecules and predict their pharmacological properties, thus facilitating the identification of potential drug candidates.[10] The application of QSAR studies is poised to revolutionize the drug discovery process, driving innovation and accelerating the development of new therapeutic agents to address unmet medical needs.[10] The most popular classic approach to QSAR modeling utilizes descriptors of molecular structure by using a simplified molecular input line entry system (SMILES) to correlate with the biological activity reported in wet lab experiments.[14] These models are formulated as a training set (for defining the model) and a test set or validation set (for checking the model with compounds of an external validation) and are often associated with one or more drawbacks.[14] A developed model must be robust enough to have high predictive power.[14] To validate a QSAR as scientifically legitimate and so enable its regulatory approval, the Organization for Economic Cooperation and Development (OECD) has

proposed five guidelines.[15] For any QSAR model, "appropriate measures of goodness-of-fit, robustness, and predictivity" must be established, according to Principle 4 of OECD.[15] It highlights the necessity for both the QSAR model's external validation (predictivity) and internal validation (as demonstrated by robustness and goodness-of-fit). The key to determining the trustworthiness of predictions is to determine whether the built models can be used with any confidence on new sets of data by using validation procedures.[13,15] The correlations and logic (CORAL), a freeware software for QSAR modelling uses the standardized SMILES-based optimal descriptors.[16] CORAL generates random models based on the Monte Carlo approach, and from a probabilistic perspective, the algorithms employed in CORAL can provide some answers to the limitations of classic QSAR modeling issues.[16] If the statistical quality of the model can be replicated in a series of attempts to create the model for both the training and validation sets, then a random model may be a reasonable predictor for an endpoint.[16,17] Following this logic, CORAL allows random splits to build a robust QSAR model. One can utilize the balance of correlations that is provided by the CORAL in addition to the conventional scheme that was previously dealt with.[16,17] The division of the training set into a calibration set and a sub-training/invisible training set is the fundamental concept of the balancing of correlations.[16] The calibration set serves as the basis for the initial validation of the model and the preliminary check assists in preventing overtraining. An additional measure to enhance predictability has involved analysing the balance of correlations with optimal slopes.[16] If the values of the cluster's slopes on the internal training and calibration sets are as close to each other as possible, the plot of the experimental versus calculated endpoint values will be perfect.[16,18]

Coumarins (2*H*-1-benzopyran-2-one) are a varied class of naturally occurring pharmacophores with a wide range of bioactivities, *viz*., anti-inflammatory, antioxidant, antinociceptive, hepatoprotective, antithrombotic, antiviral, antimicrobial, antituberculosis, anticancer, antidepressant, antihyperlipidemic, anti-Alzheimer, anticholinesterase and antiviral activities.[19,20] On the other hand, triazoles are five-membered heterocyclic compounds containing three nitrogen atoms that exist in two isomeric forms: 1,2,3-triazoles and 1,2,4-triazoles.[21,22] Commonly found in both natural and synthetic leads, 1,2,3-triazoles have a wide range of biological actions, including antitubercular, anticancer, antibacterial and antifungal properties.[21,22] Being enriched with electronegative nitrogen atoms that can interact in a variety of ways with biological targets, the 1,2,3-triazole ring system has emerged as a versatile and intriguing scaffold in medicinal chemistry, offering a myriad of pharmacological effects that contribute to its significance in drug discovery.[21,22] In recent attempts to synthesize multitargeting "hybrid molecules" there are enough reports on different coumarin-1,2,3-triazole--based molecular hybrids synthesized by coupling the coumarin to 1,2,3-triazole

as pharmacologically active segments, either in the presence or absence of tethering agents (spacer/linker).[21,22] Additionally, enough SAR has been identified in numerous series of potentially active coumarin hybrids with antibacterial, anticancer, antitubercular, antifungal, anti-Alzheimer, antidiabetic, antidepressant and antithrombotic properties that have been synthesized.[21,22]

In the given frame of context, from our recently published review encompassing the antibacterial coumarin-1,2,3-triazole hybrids, we collected data on coumarin-1,2,3-triazole hybrids with known activity against *Staphylococcus aureus* in terms of *MIC* values.[21] The collected data were used for the development of Monte Carlo optimization-based predictive QSAR modeling of *S. aureus* inhibitory activity of coumarin-1,2,3-triazole hybrids.

EXPERIMENTAL

Data collection

A total of 51 coumarin-1,2,3-triazole derivatives showing minimum inhibitory concentration (*MIC*) values in the range of 0.4 to 75 μg mL^{-1} against *S. aureus* were retrieved from the earlier published reports.[21,23-30] The molecular structures were drawn using ChemDraw v22, saved in ".cdxml" format, and then converted to simplified molecular-input line-entry system (SMILES) by using optical structure recognition (OSRA) online tool (https://cactus.nci.nih.gov/cgi-bin/osra/index.cgi). The input files for building the QSAR models corresponding to SMILES of the derivatives along with their *MIC* values were saved as text (.txt, also see Table S-I of the Supplementary material to this paper).

Descriptor calculation

Three types of descriptors: *i*) SMILES-based, *ii*) graph-based and *iii*) hybrid descriptors, which are combinations of SMILES and graphs, were calculated using CORAL software (http://www.insilico.eu/coral).[17]

SMILES-based descriptors. The optimal SMILES based descriptor were calculated as follows:

$$\begin{aligned}\mathrm{SMILES}_{DCW}(T, N_{\mathrm{epoch}}) = \alpha\sum CW(S_{\mathrm{k}}) + \beta\sum CW(SS_{\mathrm{k}}) + \gamma\sum CW(SSS_{\mathrm{k}}) + \\ + \delta CW(\mathrm{PAIR}) + xCW(\mathrm{BOND}) + yCW(\mathrm{NOSP}) + zCW(\mathrm{HALO}) + \\ + mCW(\mathrm{HARD})\end{aligned} \quad (1)$$

where T is the threshold used to classify molecular features into rare (noise) and active based on their frequency, and N_{epoch} is the number of iterations of the optimization process. *CW* represents the correlation weight for the above-mentioned eight types of structural attributes. S_{k}, SS_{k} and SSS_{k} are local SMILES attributes as representations of molecular fragments. PAIR, BOND, NOSP and HALO are global SMILES attributes, while the HARD index represents the association of BOND, NOSP and HALO attributes. The coefficients α, β, γ, δ, x, y, z and m are assigned binary values only, *i.e.*, 0 if the attribute is not used in building the model or 1 if the attribute is used in building the model. S_{k} represents the sole SMILES element *(e.g.*, Cl..., C..., N...), SS_{k} denotes the combination of two SMILES elements connected with each other, and they can be represented as C1... (..., =... O..., *etc*). SSS_{k} stands for the combination of the three SMILES elements, represented as C... C... (..., C... #... N..., *etc*). PAIR denotes the simultaneous presence of two SMILES atom compounds during descriptor calculation. The index BOND is related to the presence of three categories of chemical bonds

i.e., "=" double bond, "#" triple bond, and "@@" stereospecific chemical bond. NOSP indicates the presence or absence of nitrogen, oxygen, sulphur and phosphorous atoms. The index HALO is related to the presence or absence of only three halogen atoms, *i.e.*, fluorine, chlorine and bromine.

Graph-based descriptors. In CORAL, three types of graph-based descriptors, namely HSG (hydrogen-suppressed graph), HFG (hydrogen-filled graph), and GAO (graph of atomic orbitals), with many invariants, are available. The optimal graph-based descriptors are calculated as follows:

$$\text{Graph}_{DCW}(T, N_{\text{epoch}}) = \sum CW(A_{\text{k}}) + \alpha \sum CW({}^{0}EC_{\text{k}}) + \beta \sum CW({}^{1}EC_{\text{k}}) + \gamma \sum CW({}^{2}EC_{\text{k}}) + \delta \sum CW({}^{3}EC_{\text{k}}) \quad (2)$$

where CW is the correlation weight of the invariants of the molecular graph. The indexes A_{k} is the correlation weight of atomic elements, and ${}^{0}EC_{\text{k}}$, ${}^{1}EC_{\text{k}}$, ${}^{2}EC_{\text{k}}$ and ${}^{3}EC_{\text{k}}$ are the Morgan extended connectivity for each vertex in the molecular graph of the zero, first, second and third order, respectively. The coefficients α, β, γ and δ belong to invariants of molecular graphs, which can take up only binary values, *i.e.*, 0 if not used or 1 if used in model building.

Hybrid descriptors. Hybrid descriptors are the combination of SMILES-based and graph--based descriptors and are calculated as follows:

$$\text{Hybrid}_{DCW}(T, N_{\text{epoch}}) = \text{Graph}_{DCW}(T, N_{\text{epoch}}) + \text{SMILES}_{DCW}(T, N_{\text{epoch}}) \quad (3)$$

Monte Carlo optimization

A three-step process was chosen for the generation of a Monte Carlo-based optimized model. As required in the input format of CORAL software, the very first step entails preparing SMILES attributes from the molecular structures in various splits. The optimization of T and N_{epoch} values for each model independently is the second step. Here, N_{epoch} is the number of iterations in the Monte Carlo optimization, and T is the number of thresholds for classifying the molecular characteristics taken from the SMILES. Herein, values 1–4 of T and 15–60 of N_{epoch} were considered the most preferable combination.[31] The third and final step belongs to the calculation of descriptors (SMILES, graph and hybrid) and optimization of correlation weights (CW) using the balance correlation scheme of the Monte Carlo algorithm.[32] The entire dataset was divided into four different sets, namely the training set (Tr), the invisible training set (iTr), the calibration set (C) and the validation set (V) of three random splits. The distribution of compounds in training and various sets of three random splits have been provided in Table S-II of the Supplementary material. For each split, five models were generated using various combinations of SMILES, graphs and hybrid optimal descriptors with various connectivity indices. Finally, fifteen models were obtained from three random non-identical splits.

Mechanistic interpretation

Correlation weights (CW) for structural attributes (SAKs), *i.e.*, descriptors for SMILES, hybrids and fragments of local symmetry, were obtained in several probes of the Monte Carlo optimization for the best models (M4, M10 and M11). Structural attributes were classified into four types: promoters of increase, promoters of decrease, undefined and blocked. Those SAKs whose CW are positive indicate that these attributes of the derivatives of coumarin are promoters of an increase in MIC. SAKs with negative CW are responsible for decreasing the MIC of the derivatives. SAKs having both positive and negative correlation weights fall in the

undefined category, and all the attributes, where *CW* shows null values, fall under the blocked category.

RESULTS AND DISCUSSION

Several earlier published reports on the antibacterial activity of coumarin--1,2,3-triazole hybrids, have been compiled in the review by our group.[21] These reports comprise a preliminary screening of the antibacterial activity of the synthesized hybrid molecules against various Gram-positive and Gram-negative bacterial strains. The results of most of the preliminary screening have been published in terms of zone of inhibition or in *MIC* values. We collected the coumarin-1,2,3-triazole hybrids with antibacterial activities tested against *S. aureus* presented in *MIC* for the current study.[21] The descriptors of 51 molecules with known *MIC*s were calculated using CORAL software, which calculates SMILES--based, graph-based and hybrid descriptors, which are combinations of SMILES and graph-based descriptors. The literature reports highlight the outstanding forecasting capability of QSAR models on SMILES-based optimal descriptors as calculated by CORAL.[16,33] Using the Monte Carlo optimization method, the CORAL software allows the user to build QSAR models as a mathematical function of descriptors (also known as correlation weights of fragments of quasi--SMILES) with biological activity.[16] The entire dataset was divided into four different sets, namely the training set (Tr), the invisible training set (iTr), the calibration set (C) and the validation set (V) of three random non-identical splits: Split 1 (Tr = 16 compounds, iTr = 14 compounds, C = 11 compounds and V = 10 compounds); Split 2 (Tr = 15 compounds, iTr = 14 compounds, C = 11 compounds and V = 11 compounds); Split 3 (Tr = 11 compounds, iTr = 15 compounds, C = 14 compounds and V = 11 compounds; also see Table S-II). Each set aimed to solve an individual task. The training set aims to find the maximum correlation coefficient between endpoint and descriptor for compounds present. The invisible training set aimed at finding out whether the correlation is satisfactory for similar substances that are not involved in the training set. The calibration set identifies the starting point of overtraining. For each split, five models were generated using various combinations of SMILES, graph and hybrid optimal descriptors with various connectivity indices. Finally, fifteen models were generated after the search for the best preferable threshold value and N_{epoch} value for Monte Carlo optimization. The statistical parameters, correlation coefficient (r^2) cross-validated correlation coefficient (Q^2), standard error of estimation (s), Fischer ratio (F), mean absolute error (MAE), index of ideality of correlation (IIC) and correlation intensity index (CII), were calculated to evaluate the predictive potential of each model (Table I).

A developed QSAR model must, as always, be sufficiently robust to be able to forecast new molecular characteristics in an impartial, reliable and precise way.[9,14] The so-called five OECD principles, which are internationally defined,

are: *i*) a defined endpoint; *ii*) an unambiguous algorithm; *iii*) a defined domain of applicability; *iv*) suitable measures of robustness, predictivity and goodness-of--fit; *v*) a mechanistic interpretation, if feasible.[15,34] Considering OECD principles, the best models with higher predictive potential for each split are presented in Fig. 1, and their equations are depicted below:

Split 1.

$$pMIC = -4.1880389(\pm 0.1069537) + 0.1795520(\pm 0.0063400) \times DCW(1,40) \quad \text{(M4)}$$

Split 2.

$$pMIC = -4.4055993(\pm 0.0701103) + 0.1119546(\pm 0.0022489) \times DCW(1,40) \quad \text{(M10)}$$

Split 3.

$$pMIC = -5.1755729(\pm 0.1209286) + 0.1698881(\pm 0.0045733) \times DCW(1,70) \quad \text{(M11)}$$

TABLE I. Various models for *S. aureus* inhibitory activity using Monte Carlo optimization; *T*: threshold, *N*: N_{epoch}/Number of iterations, *n*: number of compounds in set, r^2: correlation coefficient, *s*: standard error of estimation, *MAE*: mean absolute error, *F*: Fischer ration, Tr: training set, iTr: invisible training set, C: calibration set, V: validation set

No.	Split	Parameter	*T*, *N*	Set	*n*	r^2	Q^2	*IIC*	*CII*	*s*	*MAE*	*F*
M1	1	SMILES	1, 40	Tr	16	0.4147	0.1668	0.5008	0.7502	0.455	0.347	10
				iTr	14	0.9052	0.8791	0.4884	0.9264	0.510	0.343	115
				C	11	0.7681	0.6661	0.8762	0.8670	0.362	0.284	30
				V	10	0.8036	0.7118	0.1263	0.8281	0.535	0.355	33
M2	1	SMILES	1, 25	Tr	16	0.9062	0.8655	0.9519	0.9312	0.182	0.137	165
		and HSG		iTr	14	0.9009	0.8741	0.7171	0.9272	0.479	0.389	109
		with 0		C	11	0.7638	0.6257	0.8736	0.8526	0.309	0.246	29
		ECk		V	10	0.2453	-0.5510	0.1673	0.3575	0.897	0.493	3
M3	1	SMILES	1, 50	Tr	16	0.8467	0.7969	0.7157	0.8887	0.233	0.188	77
		and HSG		iTr	14	0.8470	0.8167	0.8623	0.8694	0.362	0.304	66
		with 1		C	11	0.8959	0.8539	0.9465	0.9194	0.231	0.178	77
		ECk		V	10	0.2455	-0.2148	0.1270	0.5582	0.969	0.610	3
M4	1	SMILES	1, 40	Tr	16	0.8738	0.8250	0.7270	0.9184	0.211	0.161	97
		and HFG		iTr	14	0.8819	0.8493	0.9371	0.9177	0.473	0.353	90
		with 0		C	11	0.8732	0.8114	0.9343	0.9066	0.221	0.188	62
		ECk		V	10	0.3808	0.0753	0.3603	0.5537	0.766	0.482	5
M5	1	SMILES	1, 45	Tr	16	0.8871	0.8462	0.7325	0.9097	0.200	0.155	110
		and HFG		iTr	14	0.8793	0.8515	0.6968	0.8947	0.414	0.354	87
		with 1		C	11	0.6791	0.4856	0.8239	0.8121	0.340	0.272	19
		ECk		V	10	0.4852	0.2614	0.1450	0.5698	0.580	0.360	8
M6	2		1, 30	Tr	15	0.8593	0.8258	0.6180	0.8861	0.288	0.226	79
		SMILES		iTr	14	0.8711	0.8339	0.3429	0.9105	0.286	0.223	81
				C	11	0.6806	0.4677	0.8248	0.7768	0.434	0.301	19
				V	11	0.6524	0.2616	0.4050	0.7163	0.419	0.249	17
M7	2	SMILES	1, 70	Tr	15	0.8447	0.8099	0.6127	0.8804	0.303	0.230	71
		and HSG		iTr	14	0.8773	0.8443	0.2638	0.9136	0.250	0.181	86
		with 0		C	11	0.7032	0.5015	0.8384	0.8000	0.426	0.279	21
		ECk		V	11	0.6121	0.4713	0.5489	0.7854	0.415	0.299	14

TABLE I. Continued

No.	Split	Parameter	*T*, *N*	Set	*n*	r^2	Q^2	*IIC*	*CII*	*s*	*MAE*	*F*
M8	2	SMILES	1, 40	Tr	15	0.8519	0.8210	0.8076	0.8772	0.296	0.236	75
		and HSG		iTr	14	0.8973	0.8661	0.5188	0.9334	0.305	0.254	105
		with 1		C	11	0.7634	0.6097	0.8735	0.8201	0.284	0.207	29
		ECk		V	11	0.4633	0.1582	0.0625	0.6474	0.771	0.534	8
M9	2	SMILES	2, 25	Tr	15	0.8416	0.8015	0.6116	0.8806	0.306	0.246	69
		and HFG		iTr	14	0.8852	0.8598	0.4471	0.9171	0.302	0.237	93
		with 0		C	11	0.6644	0.4191	0.8149	0.8271	0.438	0.334	18
		ECk		V	11	0.6085	0.4633	0.2208	0.7015	0.801	0.572	14
M10	2	SMILES	1, 40	Tr	15	0.8693	0.8399	0.6216	0.9011	0.278	0.222	86
		and HFG		iTr	14	0.8923	0.8602	0.0793	0.9248	0.294	0.219	99
		with 1		C	11	0.7627	0.5970	0.8733	0.8364	0.330	0.240	29
		ECk		V	11	0.6788	0.3623	0.5865	0.7518	0.511	0.381	19
M11	3		1, 70	Tr	11	0.9672	0.9478	0.8195	0.9687	0.087	0.065	265
		SMILES		iTr	15	0.8475	0.8045	0.5932	0.8851	0.624	0.489	72
				C	14	0.8889	0.8500	0.9428	0.9397	0.355	0.275	96
				V	11	0.2995	-0.0298	0.5029	0.6025	0.737	0.563	4
M12	3	SMILES	1, 33	Tr	11	0.9579	0.9282	0.8156	0.9632	0.099	0.079	205
		and HSG		iTr	15	0.8301	0.7703	0.5334	0.8923	0.576	0.456	64
		with 0		C	14	0.8099	0.7314	0.8998	0.9394	0.420	0.326	51
		ECk		V	11	0.3844	0.0716	0.5218	0.6268	0.891	0.750	6
M13	3	SMILES	3, 15	Tr	11	0.8739	0.7521	0.5341	0.8810	0.171	0.128	62
		and HSG		iTr	15	0.7665	0.6942	0.5871	0.8499	0.543	0.418	43
		with 1		C	14	0.7612	0.6833	0.8725	0.8876	0.500	0.415	38
		ECk		V	11	0.3552	-0.2766	0.3893	0.5673	0.688	0.474	5
M14	3	SMILES	1, 23	Tr	11	0.9302	0.8892	0.8037	0.9414	0.127	0.093	120
		and HFG		iTr	15	0.8668	0.8322	0.5049	0.8942	0.761	0.535	85
		with 0		C	14	0.8469	0.7822	0.9195	0.9543	0.440	0.347	66
		ECk		V	11	0.3105	-0.0192	0.2676	0.6277	0.706	0.545	4
M15	3	SMILES	3, 75	Tr	11	0.8928	0.7935	0.7874	0.9286	0.158	0.130	75
		and HFG		iTr	15	0.7843	0.7114	0.4777	0.8490	0.436	0.317	47
		with 1		C	14	0.6740	0.5633	0.8205	0.8872	0.567	0.483	25
		ECk		V	11	0.3723	0.0122	0.2434	0.5971	0.649	0.462	5

The problem of overtraining in prediction models can be calculated by using the newly introduced parameters, *IIC* and *CII*, which increase the predictive potential of the model.[18,35] The *IIC* is based on the correlation coefficient and mean absolute error, while the *CII* indicates the statistical quality of linear regression models with a unique ability since it is a measure that is sensitive both to the value of the correlation coefficient and to the value of the mean absolute error (*MAE*).[35] Both *IIC* and *CII* can expose the drawbacks of the predictive model usually seen with others. Favorable statistical parameters are obtained for all the models from each split.

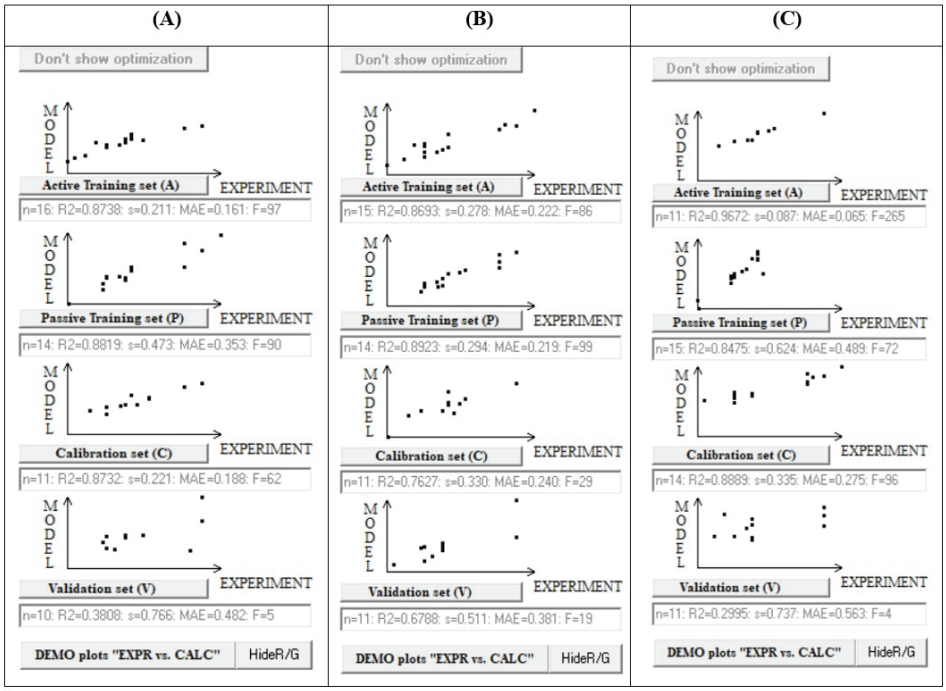

Fig. 1. Monte Carlo optimization based on best QSAR models from each split: M4 from Split 1 (A), M10 from Split 2 (B) and M11 from Split 3 (C).

Mechanistic interpretation

Correlation weights (*CW*) for structural attributes (SAKs) were estimated for both SMILES and hybrid descriptors using CORAL software. Structural attributes were classified into four types: promoters of increased activity, *i.e.*, good fingerprints (stable positive values), promoters of decreased activity, *i.e.*, bad fingerprints (stable negative values), undefined and blocked. SAKs having both positive and negative correlation weights fall in the undefined category, while all the attributes, where *CW* shows null values, fall under the blocked category. The data on *CW* for each structural attribute, which were obtained in several probes of the Monte Carlo optimization for the best models (M4, M10 and M11), are shown in supplemental Table S-III of the Supplementary material. The structural attributes of coumarin-1,2,3-triazole hybrids responsible for the increase in *MIC* value (Fig. 2) were c...3...c... (*i.e.*, presence of two aromatic cycles at three bond distances as can be seen in compound 42), c...2... (*i.e.*, presence of aromatic cycle followed by two bonds as can be seen in compounds 21 and 22), c...c...c... (*i.e.*, presence of three fused aromatic cycles as can be seen in compound 30), c...c...2... (*i.e.*, presence of branching on adjacent aromatic cycle as seen in compound 46), n...n... (*i.e.*, presence of adjacent nitrogen atoms as in the compound

4), O...=...(... (*i.e.*, presence of oxygen with double bonds as seen in the compound 7), c...(...Cl… (*i.e.*, presence of aromatic cycle and chlorine atom with branching as seen in compound 24) and c...(...N… (*i.e.*, presence of aromatic cycle and nitrogen atom with branching in between as can be seen in compound 31). On the other hand, among the hybrid descriptor correlation weights of Morgan's extended connectivity, the promoters responsible for the crucial increase in the inhibitory activity of the derivatives were found to be "EC0-O...1...", "EC1--C...6...", "EC1-C...9....", "EC1-N...5…", " EC1-Cl..6…", "EC1-O...4…", "EC1--N...2..." and "EC1-N...8..." of the model. "BOND10000000" constitutes the presence of a double bond is very important for compound's activity.

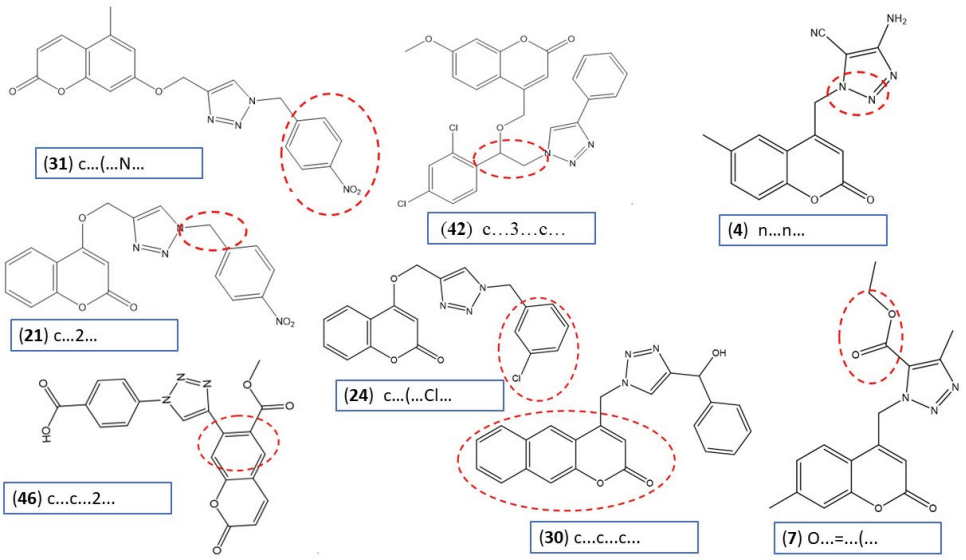

Fig. 2. Good fingerprints causing the increase in activity against *S. aureus*.

The structural attributes of coumarin-1,2,3-triazole hybrids responsible for the decrease in *MIC* value (bad fingerprints, Fig. 3) obtained from M4, M10, and M11 among SMILES descriptors were found to be c…(…=… (*i.e.*, presence of branching between aromatic carbon and double bonding as in compound 37), c...4...c... (*i.e.*, the presence of two aromatic cycles separated by four bonds as shown in compound 44) and c...(...C... (*i.e.*, the presence of branching between aromatic ring and aliphatic carbon as in compound 37). On the other hand, among hybrid descriptors correlation weights of Morgan's extended connectivity, the promoters responsible for the decrease of activity of the derivatives were found to be EC0-C...2..., EC1-C...10…

It can be seen that promoters of the decrease effect are not very much affected by the Morgan's extended connectivity in comparison to the promoters

of the increase. BOND11000000 (presence of a triple bond in the compound) and HALO00000000 (absence of a halogen atom) are detrimental to the inhibitory activity of bacteria.

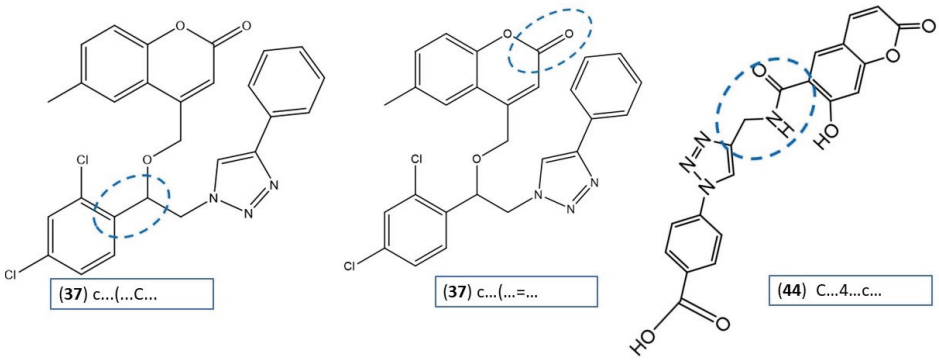

Fig. 3. Bad fingerprints causing the decrease in activity against *S. aureus*.

CONCLUSION

New 2D-QSAR models with good prediction ability were developed and validated for the prediction of the antibacterial activity of coumarin-1,2,3-triazole hybrids against *S. aureus* using the Monte Carlo optimization method. The consideration of additional statistical parameters such as the index of ideality of correlation and correlation intensity index gave clear insight into the improved predictability in all the QSAR models. Overall, among all the developed models, M11 may be considered best based on statistical parameters. The study provides a significant analysis of the important structural fingerprints required to be a potentially active substrate against *S. aureus*. Overall, the models will help design novel chemical entities with the coumarin-1,2,3-triazole moiety for the development of potent antibacterial drugs against *S. aureus*.

SUPPLEMENTARY MATERIAL

Additional data and information are available electronically at the pages of journal website: https://www.shd-pub.org.rs/index.php/JSCS/article/view/12871, or from the corresponding author on request.

Acknowledgements. The authors thank the Director of Rajkiya Engineering College, Sonbhadra, for his constant encouragement and for providing all types of facilities for this study. The financial support by the Council of Science and Technology Uttar Pradesh (Project No. 3027) is duly acknowledged.

И З В О Д

QSAR МОДЕЛОВАЊЕ ИНХИБИТОРНЕ АКТИВНОСТИ ХИБРИДА КУМАРИН-1,2,3--ТРИАЗОЛА НА *Staphylococcus aureus*, ЗАСНОВАНО НА МОНТЕ КАРЛО ОПТИМИЗАЦИЈИ

KRISHNA N. MISHRA, HARISH C. UPADHYAY и POONAM VERMA

Laboratory of Chemistry, Department of Applied Sciences, Rajkiya Engineering College (Affiliated with Dr. A.P.J. Abdul Kalam Technical University, Lucknow), Churk, Sonbhadra-231206, India

У овој студији су 51 кумаринski-1,2,3-триазолски хибриди са познатим минималним вредностима инхибирајућих концентрација (*MIC*) према *Staphylococcus aureus* искоришћени за генерисање, на Монте Карло заснованом, оптимизованог QSAR модела на *correlations and logic* (CORAL) софтверу. Целокупан скуп података је подељен на четири различита скупа података, наиме скуп за увежбавање (Tr), невидљиви скуп за увежбавање (iTr), скуп за калибрисање (C) и скуп за валидацију (V) из три случајне поделе. За сваку поделу, било је генерисано пет модела користећи различите комбинације SMILES, графова и хибридних оптималних дескриптора са различитим индексима повезаности, петнаест модела је добијено из три насумичне неидентичне поделе. За најбољи модел из сваке поделе, корелациони коефицијент (r^2) ишао је од 0,9672 до 0,8693, док унакрсно валидирани коефицијенти корелације (Q^2) ишли су од 0,9478 до 0,8250. Просечна апсолутна грешка (*MAE*) за најбоље моделе је била мања од 0,065. Додатно, саопштене су пожељне вредности индекса идеалности корелације (*IIC*) и индекс интензитета корелације (*CII*), потврђујући робусност, поузданост и потенцијал предвиђања развијених модела. Надаље, процењени су добри и лоши отисци прстију на основу корелационих тежина структурних атрибута.

(Примљено 30. марта, ревидирано 22. септембра, прихваћено 12. новембра 2024)

REFERENCES

1. G. M. Cragg, D. J. Newman, *Biochim. Biophys. Acta Gen. Subj.* **1830** (2013) 3670 (https://doi.org/10.1016/j.bbagen.2013.02.008)
2. D. J. Newman, G. M. Cragg, *J. Nat. Prod.* **83** (2020) 770 (https://doi.org/10.1021/acs.jnatprod.9b01285)
3. H. C. Upadhyay, *Lett. Drug Des. Discov.* **20** (2023) 373 (https://doi.org/10.2174/1570180820042301131444044)
4. H. C. Upadhyay, G. R. Dwivedi, M. P. Darokar, V. Chaturvedi, S. K. Srivastava, *Planta Med.* **78** (2012) 79 (https://doi.org/10.1055/s-0031-1280256)
5. M. Dickson, J. P. Gagnon, *Discov. Med.* **4** (2004) 172 (PMID: 20704981)
6. M. Dickson, J. P. Gagnon, *Nat. Rev. Drug. Discov.* **3** (2004) 417 (https://doi.org/10.1038/nrd1 382)
7. H. C. Upadhyay, G. R. Dwivedi, S. Roy, A. Sharma, M. P. Darokar, S. K. Srivastava, *ChemMedChem* **9** (2014) 1860 (https://doi.org/10.1002/cmdc.201402027)
8. H. C. Upadhyay, B. S. Sisodia, H. S. Cheema, J. Agrawal, A. Pal, M. P. Darokar, S. K. Srivastava, *Nat. Prod. Commun.* **8** (2013) 1591 (https://doi.org/10.1177/1934578x1300801123)
9. H. C. Upadhyay, M. Singh, O. Prakash, F. Khan, S. K. Srivastava, D. U. Bawankule, *SN Appl. Sci.* **2** (2020) 2069 (https://doi.org/10.1007/s42452-020-03798-5)
10. M. Xiang, Y. Cao, W. Fan, L. Chen, Y. Mo, *Comb. Chem. High Throughput Screen.* **15** (2012) 328 (https://doi.org/10.2174/138620712799361825)

11. S. Surabhi, B. Singh, *J. Drug Deliv. Therapeut.* **8** (2018) 504 (https://doi.org/10.22270/jddt.v8i5.1894)
12. G. R. Dwivedi, H. C. Upadhyay, D. K. Yadav, V. Singh, S. K. Srivastava, F. Khan, N. S. Darmwal, M. P. Darokar, *Chem. Biol. Drug. Des.* **83** (2014) 482 (https://doi.org/10.1111/cbdd.12263)
13. M. Rudrapal, D. Chetia, *J. Drug Deliv. Therapeut.* **10** (2020) 225 (https://doi.org/10.22270/jddt.v10i4.4218)
14. P. Gramatica, *QSAR Comb. Sci.* **26** (2007) 694 (https://doi.org/10.1002/qsar.200610151)
15. OECD, *OECD principles for the validation, for regulatory purposes, of (quantitative) structure-activity relationships models*, 2004
16. E. Benfenati, A. A. Toropov, A. P. Toropova, A. Manganaro, R. Gonella Diaza, *Chem. Biol. Drug. Des.* **77** (2011) 471 (https://doi.org/10.1111/j.1747-0285.2011.01117.x)
17. A. T. K. Baidya, K. Ghosh, S. A. Amin, N. Adhikari, J. Nirmal, T. Jha, S. Gayen, *New J. Chem.* **44** (2020) 4129 (https://doi.org/10.1039/c9nj05825g)
18. K. Bagri, A. Kumar, M. Nimbhal, P. Kumar, *Mol. Simul.* **46** (2020) 777 (https://doi.org/10.1080/08927022.2020.1770753)
19. T. G. Kraljević, A. Harej, M. Sedić, S. K. Pavelić, V. Stepanić, D. Drenjančević, J. Talapko, S. Raić-Malić, *Eur. J. Med. Chem.* **124** (2016) 794 (https://doi.org/10.1016/j.ejmech.2016.08.062)
20. Y. L. Fan, X. Ke, M. Liu, *J. Heterocycl. Chem.* **55** (2018) 791 (https://doi.org/10.1002/jhet.3112)
21. H. C. Upadhyay, *Curr. Top. Med. Chem.* **21** (2021) 737 (https://doi.org/10.2174/1568026621666210303145759)
22. K. N. Mishra, H. C. Upadhyay, *Frontiers Drug Discov.* **2** (2022) 1072448 (https://doi.org/10.3389/fddsv.2022.1072448)
23. J. M. Madar, L. A. Shastri, S. L. Shastri, R. Guda, M. Holiyachi, N. S. Naik, S. Dodamani, S. Jalapure, V. A. Sungar, *Chem. Data Collect.* **17**–**18** (2018) 219 (https://doi.org/10.1016/j.cdc.2018.09.005)
24. P. Yadav, B. Kumar, H. K. Gautam, S. K. Sharma, *J. Chem. Sci.* **129** (2017) 211 (https://doi.org/10.1007/s12039-016-1214-x)
25. S. Carmel Yesudass, P. Ranjan, H. P. Suresh, *J. Heterocycl. Chem.* **59** (2022) 309 (https://doi.org/10.1002/jhet.4385)
26. M. H. Shaikh, D. D. Subhedar, B. B. Shingate, F. A. Kalam Khan, J. N. Sangshetti, V. M. Khedkar, L. Nawale, D. Sarkar, G. R. Navale, S. S. Shinde, *Med. Chem. Res.* **25** (2016) 790 (https://doi.org/10.1007/s00044-016-1519-9)
27. S. M. Sutar, H. M. Savanur, C. Patil, G. M. Pawashe, G. Aridoss, K. M. Kim, R. G. Kalkhambkar, *Chem. Data Coll.* **28** (2020) 100480 (https://doi.org/10.1016/j.cdc.2020.100480)
28. A. V. Lipeeva, D. O. Zakharov, L. G. Burova, T. S. Frolova, D. S. Baev, I. V. Shirokikh, A. N. Evstropov, O. I. Sinitsyna, T. G. Tolsikova, E. E. Shults, *Molecules* **24** (2019) 2126 (https://doi.org/10.3390/molecules24112126)
29. M. N. Joy, Y. D. Bodke, S. Telkar, V. A. Bakulev, *J. Mex. Chem. Soc.* **64** (2020) 53 (https://doi.org/10.29356/jmcs.v64i1.1116)
30. X. M. Peng, K. V. Kumar, G. L. V. Damu, C. H. Zhou, *Sci. China Chem.* **59** (2016) 878 (https://doi.org/10.1007/s11426-015-0351-0)
31. P. Kumar, A. Kumar, J. Sindhu, *SAR QSAR Environ. Res.* **30** (2019) 63 (https://doi.org/10.1080/1062936X.2018.1564067)

32. A. A. Toropov, A. P. Toropova, *Toxicol. Mech. Methods* **29** (2019) 43 (https://doi.org/10.1080/15376516.2018.1506851)
33. A. A. Toropov, E. Benfenati, *Curr. Drug. Discov. Technol.* **4** (2007) 77 (https://doi.org/10.2174/157016307781483432)
34. A. Kumar, S. Chauhan, *Arch. Pharm. (Weinheim)* **350** (2017) e1600268 (https://doi.org/10.1002/ardp.201600268)
35. A. P. Toropova, A. A. Toropov, A. Roncaglioni, E. Benfenati, *Molecules* **28** (2023) 6587 (https://doi.org/10.3390/molecules28186587).

Journal of the Serbian Chemical Society
JSCS-info@shd.org.rs • www.shd.org.rs/JSCS
J. Serb. Chem. Soc. 90 (1) S7–S11 (2024) *Supplementary material*

SUPPLEMENTARY MATERIAL TO

Monte Carlo optimization-based QSAR modelling of *Staphylococcus aureus* inhibitory activity of coumarin-1,2,3-triazole hybrids

KRISHNA N. MISHRA, HARISH C. UPADHYAY* and POONAM VERMA

Laboratory of Chemistry, Department of Applied Sciences, Rajkiya Engineering College (Affiliated with Dr. A.P.J. Abdul Kalam Technical University, Lucknow), Churk, Sonbhadra-231206, India

J. Serb. Chem. Soc. 90 (1) (2024) 39–52

TABLE S-I. List of Compounds with SMILES along with their antibacterial activity against *S. aureus* expressed in pMIC (–logMIC in μg mL^{-1})

ID	SMILES	pMIC
1	Cc3ccc2c(Cn1nnc(N)c1C#N)cc(=O)oc2c3	0.39794
2	Cc3cc(C)c2c(Cn1nnc(N)c1C#N)cc(=O)oc2c3	0.09691
3	COc3ccc2oc(=O)cc(Cn1nnc(N)c1C#N)c2c3	-0.79588
4	N#Cc1c(N)nnn1Cc2cc(=O)oc4c2ccc3ccccc34	0.39794
5	Cc3ccc2oc(=O)cc(Cn1nnc(N)c1C#N)c2c3	0.39794
6	N#Cc1c(N)nnn1Cc3cc(=O)oc4ccc2ccccc2c34	-0.79588
7	CCOC(=O)c1c(C)nnn1Cc2cc(=O)oc3cc(C)ccc23	-0.49415
8	CCOC(=O)c1c(C)nnn1Cc2cc(=O)oc3cc(C)cc(C)c23	-1.39794
9	CCOC(=O)c1c(C)nnn1Cc2cc(=O)oc3ccc(OC)cc23	-0.79588
10	CCOC(=O)c1c(C)nnn1Cc2cc(=O)oc4c2ccc3ccccc34	0.09691
11	CCOC(=O)c1c(C)nnn1Cc2cc(=O)oc3ccc(C)cc23	0.09691
12	CCOC(=O)c1c(C)nnn1Cc3cc(=O)oc4ccc2ccccc2c34	0.39794
13	Cc3ccc2c(Cn1nnc(C)c1C(=O)O)cc(=O)oc2c3	-0.79588
14	Cc3cc(C)c2c(Cn1nnc(C)c1C(=O)O)cc(=O)oc2c3	-0.79588
15	COc3ccc2oc(=O)cc(Cn1nnc(C)c1C(=O)O)c2c3	-0.49415
16	Cc4nnn(Cc1cc(=O)oc3c1ccc2ccccc23)c4C(=O)O	0.69897
17	Cc3ccc2oc(=O)cc(Cn1nnc(C)c1C(=O)O)c2c3	0.09691
18	Cc4nnn(Cc2cc(=O)oc3ccc1ccccc1c23)c4C(=O)O	0.39794
19	CC[N+](CC)(CC)CCCCCCCCCCOCc4cn(Cc2cc(=O)oc3cc1OC(C)(C)CCc1cc23)nn4	-1.07918
20	Cc3cc(=O)oc4cc(OCC(O)Cn2nnc1ccccc12)ccc34	-1.20412
21	O=c4cc(OCc2cn(Cc1ccc(N(=O)=O)cc1)nn2)c3ccccc3o4	-0.90309
22	O=c4cc(OCc2cn(Cc1cccc(N(=O)=O)c1)nn2)c3ccccc3o4	-0.90309
23	O=c4cc(OCc2cn(Cc1ccc(Cl)cc1)nn2)c3ccccc3o4	-1.20412
24	O=c4cc(OCc2cn(Cc1cccc(Cl)c1)nn2)c3ccccc3o4	-0.90309

* Corresponding author. E-mail: harishcu@recsonbhadra.ac.in

ID	SMILES	pMIC
25	O=c4cc(OCc2cn(Cc1ccc(Br)cc1)nn2)c3ccccc3o4	-1.20412
26	COc4ccc3oc(=O)cc(Cn2cc(C(O)c1ccccc1)nn2)c3c4	-1.57403
27	Cc4ccc3oc(=O)cc(Cn2cc(C(O)c1ccccc1)nn2)c3c4	-1.273
28	CC(C)(C)c4ccc3oc(=O)cc(Cn2cc(C(O)c1ccccc1)nn2)c3c4	-0.96848
29	O=c5cc(Cn2cc(C(O)c1ccccc1)nn2)c4cc(Cc3ccccc3)ccc4o5	-1.273
30	O=c5cc(Cn2cc(C(O)c1ccccc1)nn2)c4cc3ccccc3cc4o5	-1.273
31	Cc3cc(OCc2cn(Cc1ccc(N(=O)=O)cc1)nn2)cc4oc(=O)ccc34	-0.90309
32	Cc3cc(OCc2cn(Cc1cccc(N(=O)=O)c1)nn2)cc4oc(=O)ccc34	-0.90309
33	Cc3cc(OCc2cn(Cc1ccc(Cl)cc1)nn2)cc4oc(=O)ccc34	-0.90309
34	Cc3cc(OCc2cn(Cc1cccc(Cl)c1)nn2)cc4oc(=O)ccc34	-1.20412
35	Cc3cc(OCc2cn(Cc1ccc(Br)cc1)nn2)cc4oc(=O)ccc34	-1.20412
36	Cc3cc(OCc2cn(Cc1ccccc1)cn2)cc4oc(=O)ccc34	-0.90309
37	Cc5ccc4oc(=O)cc(COC(Cn2cc(c1ccccc1)nn2)c3ccc(Cl)cc3Cl)c4c5	-1.20412
38	Cc5ccc4c(COC(Cn2cc(c1ccccc1)nn2)c3ccc(Cl)cc3Cl)cc(=O)oc4c5	-1.49485
39	O=c5cc(COC(Cn2cc(c1ccccc1)nn2)c3ccc(Cl)cc3Cl)c4cc(Cl)ccc4o5	-0.60206
40	O=c5cc(COC(Cn2cc(c1ccccc1)nn2)c3ccc(Cl)cc3Cl)c4ccc(Cl)cc4o5	-0.60206
41	COc5ccc4oc(=O)cc(COC(Cn2cc(c1ccccc1)nn2)c3ccc(Cl)cc3Cl)c4c5	-0.90309
42	COc5ccc4c(COC(Cn2cc(c1ccccc1)nn2)c3ccc(Cl)cc3Cl)cc(=O)oc4c5	-1.20412
43	O=c5cc(COC(Cn2cc(c1ccccc1)nn2)c3ccc(Cl)cc3Cl)c4ccc(Br)cc4o5	-1.20412
44	O=C(O)c4ccc(n3cc(CNC(=O)c2cc1ccc(=O)oc1cc2O)nn3)cc4	0.18709
45	COC(=O)c6cc5cc(C#CCCCCCCc4cn(C3(C(C)C)Oc2cc1oc(=O)ccc1cc2C3=O)nn4)c(=O)oc5cc6O	-1.83727
46	COC(=O)c2cc1ccc(=O)oc1cc2c4cn(c3ccc(C(=O)O)cc3)nn4	-0.79796
47	Cc4cc(=O)oc5cc(OCc3cn(C1CCCCC1Oc2cccnc2Cl)nn3)ccc45	-1
48	Cc4cc(=O)oc5cc(OCc3cn(C1CCCC1Oc2cccnc2Cl)nn3)ccc45	-1
49	Cc3cc(=O)oc4cc(OCc2cn(Cc1ccc(F)cc1)nn2)ccc34	-0.69897
50	Cc3cc(=O)oc4cc(OCc2cn(Cc1ccc(C#N)cc1)nn2)ccc34	-1.87506
51	CC[N+](CC)(CC)CCCCCCCCCCOCc4cn(Cc2cc(=O)oc3c(OC)c1OC(C)(C)CCc1cc23)nn4	-1.74036

TABLE S-II. Distribution of compounds in Training, Invisible training, Calibration, and Validation set in three random splits.

Split number	Training	Invisible training	Calibration	Validation
Split 1	3, 6, 8, 12, 17, 20, 21, 24, 26, 34, 36, 40, 46, 48, 50, 51	1, 9, 10, 11, 14, 16, 25, 29, 30, 33,37, 41, 45, 47	2, 4, 7, 13, 15, 28, 31, 35, 38, 43, 49	5, 18, 19, 22, 23, 27, 32, 39, 42, 44
Split 2	2, 4, 8, 13, 16, 26, 31, 34, 37, 42, 43, 44, 46, 47, 50	1, 6, 10, 11, 15, 17, 23, 25, 28, 29, 32, 39, 41, 48	3, 5, 7, 9, 14, 24, 27, 38, 40, 45, 49	12, 18, 19, 20, 21, 22, 30, 33, 35, 36, 51
Split 3	5, 6, 7, 13, 15, 23, 24, 28, 38, 39, 40	3, 9, 14, 19, 22, 25, 27, 29, 30, 35, 45, 46, 48, 49, 50	16, 17, 20, 31, 33, 34, 42, 43, 44, 51, 2, 10, 11, 12	1, 4, 8, 18, 21, 26, 32, 36, 37, 41, 47

TABLE S-III. Structural attributes (Good and bad fingerprints) of activity against *S. aureus* in three runs of Monte Carlo optimization

SAk	CWs P1	CWs P2	CWs P3	Defect [SAk]
Promoters of activity (M4)				
EC0-O...1...	1.3803	1.0059	0.3405	0.0000
c...3...c...	1.8324	1.1794	6.1565	0.0036
[xyyx0].....	0.4606	0.4647	4.9302	0.0000
c...2.....	0.9736	0.0192	1.9032	0.0031
[xyzyx0]....	0.9314	1.0758	1.0885	0.0066
n...n.....	1.3189	0.9413	2.9101	0.0031
O...=...(…	0.2947	0.1729	1.8528	0.0071
c...c...c...	1.4163	0.9521	2.0173	0.0029
BOND10000000	1.6066	1.9218	3.1289	0.0026
HALO00000000	1.3248	1.3766	0.0045	0.0081
NOSP01000000	1.5227	1.2056	2.2937	0.0151
c...c...2...	1.7570	2.1183	1.5168	0.0115
n...(...C...	1.3563	0.2484	2.0366	0.0198
o...(...O...	0.5513	0.2877	0.5311	0.0065
c...1...(...	0.0755	0.0070	0.8339	0.0123
C...1.....	1.2124	1.3100	0.3349	0.0094
c...3...4...	1.4420	0.9888	0.9371	0.0387
c...C...(...	1.6156	0.5518	1.6063	0.0157
[xyx4].....	0.7896	1.1156	0.9742	0.0120
n...1.....	0.5169	0.6534	1.4766	0.0189
n...C...(...	0.5010	1.1322	1.6241	0.0274
3...c...2...	1.6260	1.2054	0.9456	0.0289
C...(...=...	1.3359	1.4561	1.2091	0.0275
N...(.....	1.1769	1.1051	0.2718	0.0503
c...(...N...	1.1440	1.1733	0.9345	0.0503
Promoters of activity (M10)				
EC1-C...6...	0.9202	0.9533	0.8767	0.0000
EC1-C...9...	0.9054	1.3435	1.0562	0.0000
EC1-N...5…	0.4271	2.8375	1.4485	0.0000
[xyyx0].....	1.5770	1.8835	2.5635	0.0000
c...(...=...	0.1594	1.0513	1.1669	0.0133
BOND10000000	1.4929	2.5504	1.1049	0.0081
c...c...2...	1.2138	1.5640	0.8367	0.0039
[xyzyx0]....	0.4841	1.0311	0.4801	0.0077
1...c...(...	0.8316	1.3412	0.9746	0.0150
n...C...(...	1.3817	0.1151	0.6553	0.0153
3...c...(...	0.2742	0.9664	1.3977	0.0043
4...c...(...	0.4650	1.7684	1.4240	0.0275
C...1.....	0.0756	1.1968	0.8009	0.0196
C...c...2...	0.4792	3.0906	1.6450	0.0043
EC1-Cl..6…	0.6074	1.6550	0.8792	0.0101
NOSP11000000	0.0556	1.2363	1.2616	0.0303
3...(.....	0.2700	1.2395	0.5709	0.0502
C...O...(...	1.1106	0.8134	1.1900	0.0035

SAk	CWs P1	CWs P2	CWs P3	Defect [SAk]
EC1-O...4…	0.2074	1.1468	1.4376	0.0310
N...(.....	0.9440	0.2287	2.3996	0.0189
c...(...Cl..	0.3360	1.7833	1.2956	0.0117
c...(...N...	1.1713	1.6040	0.5362	0.0189
c...C...(...	0.1849	2.4469	1.5329	0.0208
n...1.....	1.3319	1.3245	0.1696	0.0251
n...c...2...	0.4277	0.4810	0.3850	0.0208
n...n...1...	1.0808	0.9214	1.1837	0.0251
(...N...(...	0.7168	1.0285	0.2306	0.0081
EC1-N...2...	0.4635	0.2711	0.5377	0.0163
O...(...O...	0.4204	0.6575	1.1037	0.0364
c...(...3...	0.1966	2.1458	1.3361	1.0000
c...o...4...	1.1627	1.5654	0.2008	1.0000
[xyx5].....	0.8728	0.9104	1.4503	1.0000
(...N...#...	0.0323	1.5227	0.7897	0.0442
3...2.....	0.7651	1.6091	1.2781	0.0442
4...c...2...	1.9553	1.8426	3.3051	1.0000
C...c...4...	1.0932	1.2439	0.8365	0.0442
C...n...1...	0.7667	1.3442	0.9407	0.0348
EC1-N...8...	1.5275	1.1218	1.2967	1.0000
c...1...C...	0.2776	1.1237	1.9595	0.0348
c...2...3...	1.0613	1.1736	1.1102	0.0442
	Promoters of activity (M11)			
c...(.....	1.1802	0.5233	1.0124	0.0000
c...1.....	2.1678	1.1924	1.1989	0.0034
c...2.....	0.8964	1.8132	0.4523	0.0037
c...c...3...	0.2430	0.3123	1.3495	0.0079
[xyyx0].....	11.8616	9.4184	6.5641	0.0000
n...n.....	2.9301	1.8750	4.2672	0.0000
1...c...(...	1.1262	3.4869	2.3150	0.0340
BOND10000000	7.3038	7.3199	6.9298	0.0076
c...1...c...	4.0590	5.3725	4.8629	0.0081
[xyzyx0]....	4.1982	5.7704	3.7127	0.0160
n...n...(...	2.2563	1.6402	1.6530	0.0087
=...O...(...	0.2761	0.3821	0.1549	0.0183
O...=...(...	0.8956	0.6069	0.9192	0.0183
c...(...O...	1.5929	0.5332	1.3473	0.0192
n...C...(...	1.8772	1.5804	2.7283	0.0357
n...C.....	1.4897	3.5828	0.3799	0.0357
n...(...1...	2.1957	2.1046	0.6110	0.0198
	Adversaries of activity (M4)			
EC0-C...3...	-0.0063	-0.0650	-0.7341	0.0000
EC0-C...4...	-0.0496	-0.1014	-0.8191	0.0000
EC0-H...1...	-0.1827	-0.4861	-0.0113	0.0000
EC0-N...2...	-2.1326	-0.3570	-2.7170	0.0000
C...(.....	-0.0407	-0.3134	-0.7258	0.0047
O...(.....	-0.0597	-0.2022	-0.8645	0.0047

SAk	CWs P1	CWs P2	CWs P3	Defect [SAk]
c...1.....	-0.3059	-0.2583	-0.7519	0.0037
n...(.....	-0.4778	-0.2105	-0.8867	0.0079
n...n...(...	-0.6126	-0.0923	-1.5594	0.0081
c...4...c...	-0.4408	-0.7683	-1.1420	0.0194
c...c...4...	-1.5229	-0.4043	-0.7252	0.0156
c...(...C...	-0.4640	-0.2863	-0.8204	0.0117
C...c...2...	-0.2957	-0.2947	-0.1831	0.0115
c...C...O...	-0.2511	-0.4756	-0.6577	0.0343
n...n...2...	-0.2690	-0.4488	-0.9846	0.0123
C...C.....	-0.4162	-0.0034	-0.0894	0.0292
NOSP11000000	-0.4989	-1.0109	-0.0582	0.0536
o...c...4...	-0.6194	-0.5333	-0.2237	0.0503
	Adversaries of activity (M10)			
EC1-C...7...	-0.3739	-0.2071	-0.3508	0.0000
EC1-H...4...	-0.3191	-0.1586	-0.2877	0.0000
c...c...(...	-0.4745	-0.2398	-0.3352	0.0000
=...(.....	-0.0985	-0.2175	-0.0736	0.0133
=...O...(...	-0.5946	-0.3410	-0.9036	0.0133
c...c...1...	-0.0411	-0.1527	-0.0192	0.0145
EC1-O...7...	-0.6302	-0.5737	-0.0433	0.0035
n...(...1...	-0.4972	-0.2252	-0.1054	0.0048
C...c...3...	-0.2623	-0.3367	-0.5491	0.0208
(...C...(...	-0.3545	-0.2937	-0.1888	0.0152
(...O...(...	-0.2777	-0.8833	-0.0415	0.0208
C...n...2...	-0.1559	-0.7780	-0.3644	0.0035
c...5...c...	-0.5686	-0.6239	-0.4424	0.0035
c...c...5...	-0.8525	-0.2827	-0.3115	0.0035
C...(...C...	-0.3105	-0.9544	-0.8406	0.0162
N...#...C...	-0.1494	-1.6585	-1.4759	0.0163
c...O.....	-0.8582	-2.3522	-1.0626	0.0081
o...c...1...	-0.4978	-0.4420	-0.4747	1.0000
	Adversaries of activity (M11)			
O...=.....	-0.8329	-1.3695	-1.4543	0.0000
c...3...c...	-2.3114	-0.1758	-1.6712	0.0038
c...c.....	-1.0851	-0.3990	-1.1745	0.0000
c...c...c...	-0.0236	-1.4852	-0.1720	0.0079
C...(.....	-0.6451	-1.2806	-0.6066	0.0047
O...(.....	-0.8947	-0.7138	-0.6053	0.0098
NOSP01000000	-0.2907	-0.1564	-0.9909	0.0069
c...(...C...	-1.6102	-1.2066	-1.3291	0.0098
O...C.....	-1.9894	-2.4534	-2.7427	0.0069
c...(...=...	-1.0120	-1.1744	-2.8074	0.0189
c...C.....	-0.9450	-0.9782	-0.4993	0.0109
HALO00000000	-1.0185	-1.3042	-0.7699	0.0139
n...n...2...	-2.7940	-0.4582	-0.4058	0.0117

Journal of the Serbian Chemical Society
JSCS-info@shd.org.rs • www.shd.org.rs/JSCS
J. Serb. Chem. Soc. *90* (1) 53–65 (2025)
JSCS–5819
Original scientific paper
Published 25 January, 2025

The lithium oxide solubility in molten fluoride system CeF_3–FLiNaK

IRINA ZAKIRYANOVA*, IRAIDA KORZUN, ELENA NIKOLAEVA and ANDREY BOVET

Institute of High-Temperature Electrochemistry, 20 Akademicheskaya Street, Yekaterinburg, Russia

(Received 4 March, revised 17 March, accepted 27 March 2024)

Abstract: Molten systems based on alkali metal halides with lithium oxide additives are promising as a working medium on pyrochemical reprocessing of nuclear waste. A mixture of alkali metal fluorides of eutectic composition (FLiNaK) is a suggested solvent due to the high solubility of actinide oxides, low viscosity, high boiling points, low vapor pressure and resistance to radiation damage. Thermal analysis, XRD, Raman spectroscopy and thermodynamic simulations were used to obtain evidences on the phase equilibria and liquidus points of the system (0.85 FLiNaK–0.15 CeF_3)–Li_2O, containing up to 8.8 mol. % lithium oxide. The solubility of lithium oxide in the fluoride melt FLiNaK––CeF_3 and the thermodynamic parameters of dissolution were obtained. The eutectic point (the Li_2O content is 3.1 mol. %, T_m = 489 °C) and two peritectic points (lithium oxide content are 3.2 and 4.2 mol. %, and liquidus points are 497 and 549 ºC, respectively) were found. Thermodynamic simulation results show an exothermic effect due to interaction between lithium oxide and fluoride melt. The interaction product oxyfluoride CeOF was detected by XRD analysis and Raman spectroscopy.

Keywords: lithium oxide; solubility; FLiNaK; cerium oxyfluoride; cerium fluoride; molten fluoride; phase diagram.

INTRODUCTION

Pyrochemical reprocessing of spent nuclear fuel is one of the most promising options for environmentally safe handling of nuclear waste. It involves the electrolytic reduction process that converts the uranium oxide into metal in a molten salt electrolyte.[1–6] Oxide–halide melts based on alkali metal halides with lithium oxide additives are tested as a working medium. During the electrolysis of these melts, the released at the indifferent cathode lithium reduces actinide oxides to

* Corresponding author. E-mail: optica96@ihte.ru
https://doi.org/10.2298/JSC240304038Z

the corresponding metals.[3,4,7] For the process to proceed successfully, the concentration of lithium oxide must be at least 3 mol. %.[7]

The solubility of lithium oxide in LiCl and LiCl–KCl melts has been well studied.[7–9] It reaches 11.5 mol. % (923 K) for the LiCl solvent,[5] and decreases as potassium chloride is introduced into the solvent. In a melt of eutectic composition (58.5 LiCl–41.5 KCl) at 823 K, the solubility of lithium oxide is 1.32 mol. %.[8] The result presented in the literature[7] is interesting: it turns out that the addition of $SrCl_2$ (7 wt. %) enhance the Li_2O solubility with respect to that in pure LiCl (from 8.8 to 9.1 wt. %).

There is little information on the solubility of lithium oxide in fluoride melts. It is reported in[10] that the solubility of lithium oxide in a melt of composition (0.8 LiF–0.2 CaF_2) at a temperature of 1058 K is 10.6 wt. %, and increases on temperature increasing, reaching 14.8 wt. % at 1133 K.

Another promising solvent is a mixture of alkali metal fluorides of the eutectic composition LiF–NaF–KF (46.5–11.5–42 mol. %)–FLiNaK. Despite the fact that molten alkali metal fluorides are among the most aggressive to structural materials, it is the melts that have huge advantages due to high thermal conductivity, low viscosity, high boiling points, low vapor pressure, the highest heat capacity and stability to radiation damage. Unfortunately, the solubility of lithium oxide in the FLiNaK melt is low and is estimated to not exceed 1 %.[11]

We may anticipate that the introduction of rare earth fluorides into a molten mixture of alkali metal fluorides will lead to an increase in the solubility of lithium oxide due to chemical interaction. The basis for this assumption are the results[12] indicating the solubility of rare-earth oxides in fluoride melts is extremely low, but abruptly increase when rare-earth fluoride is introduced into the melt. This result is associated with the interaction of the fluoride melt with rare-earth oxide during dissolution and the formation of oxide–fluoride complexes LnO_xF_y.[13]

In this work, as an example, we adopted the FLiNaK fluoride system with the addition of 15 mol. % cerium fluoride and studied the solubility of lithium oxide in this molten system.

First of all, when modeling the physicochemical behavior of plutonium compounds, cerium containing salts can be used as environmentally safe simulators.[14,15]

Next, the FLiNaK and FLiNaK–CeF_3 molten mixtures with small addition of Li_2O were simulated within the *ab initio* theory to obtain the local structure patterns.[16,17] The introduction of cerium ions (in CeF_3) into the oxide–fluoride melt, FLiNaK–Li_2O, leads to significant changes in the parameters of the local structure: in the FLiNaK–CeF_3–Li_2O melt, cerium ions displace lithium from the immediate environment of oxygen. The longest-lived configuration includes oxygen, surrounded by cerium and lithium cations. The average lifetime of an O–Ce

ion pair exceeds 10 ps, while the average lifetime of an O–Li ion pair decreases from 5 (in FLiNaK–Li_2O melt) to 1.1 ps. This change in the local structure and dynamics of ions of the oxide–fluoride molten system FLiNaK–CeF_3–Li_2O compared to the FLiNaK–Li_2O melt allows, in particular, to make a prediction about the higher solubility of lithium oxide in melts containing cerium fluoride, compared to its solubility in FLiNaK. And finally, using the HSC Chemistry 9 software package,[18] we calculated the thermodynamic parameters of possible reactions of interaction of cerium fluoride with lithium oxide:

$$Li_2O + 0.5CeF_3 = 0.5LiCeO_2 + 1.5LiF$$
$$\Delta G = -128 \text{ kJ mol}^{-1};\ k = 4.48\times10^7;\ 600\ ^\circ\text{C} \quad (1)$$
$$Li_2O + CeF_3 = CeOF + 2LiF$$
$$\Delta G = -332 \text{ kJ mol}^{-1};\ k = 7.24\times10^{19};\ 600\ ^\circ\text{C} \quad (2)$$

The calculation results showed negative values of the change of the Gibbs energy and large values of the thermodynamic reaction constant of the proposed reactions. It can be expected that the interaction of lithium oxide with CeF_3 dissolved in the fluoride melt will increase the solubility of lithium oxide.

The purpose of this study was to obtain information on the phase equilibria and liquidus points of the system (0.85 FLiNaK–0.15 CeF_3)–Li_2O, containing up to 8.8 mol. % lithium oxide; to determine the solubility of lithium oxide in the fluoride melt FLiNaK–CeF_3, and to estimate the thermodynamic parameters of dissolution.

EXPERIMENTAL

Experimental techniques

Certification of the starting fluoride systems, determination of phase transformations points and accompanying thermal effects were carried out on a synchronous thermal analyzer STA 449C Jupiter coupled (NETZSCH, Germany). The instrument was calibrated using reference samples of $RbNO_3$, $KClO_4$, Ag_2SO_4, CsCl, K_2CrO_4 and biphenyl $C_{10}H_{12}$ (NETZSCH). The mass of the initial samples was 10-13 mg, the heating rate was 5 °C min^{-1}. The temperature range for thermal analysis was 25–700 °C. To protect the device, measurements were carried out in a flow of protective gas (high purity Ar, 99.998 %). The gas flow rate was 20 ml min^{-1}. The sample was placed in a Pt–Rh crucible with a pierced lid. According to the technical characteristics of the device, the error in determining the temperature was less than 1 °C, the error in measuring mass was 10^{-6} g.

XRD analysis and Raman spectroscopy were used to certificate of CeF_3, Li_2O, and to identify reaction products. X-ray patterns were recorded using an automatic X-ray diffractometer Rigaku D/MAX-2200VL/PC (CuK_α radiation, Rigaku MiniFlex 600 diffractometer, Tokyo, Japan), phases were identified using MDI Jade 6.5 software.

Raman spectra were recorded using the U1000 Raman microscope–spectrometer (Renishaw, UK) over a range 50–1000 cm^{-1}, and Ava-Raman fiber-optic spectrometric complex (Avantes, Eerbeek, The Netherlands) over a range 150–5400 cm^{-1}.

Reagents preparation and certification

The eutectic mixture FLiNaK was prepared using extra pure LiF, NaF and potassium bifluoride KF·HF (Vekton Company, Saints Petersburg, Russia). It is known that when heated to 300–400 °C, the acid salt KF·HF decomposes with the formation of potassium fluoride and gaseous HF according to reaction: KF·HF → KF + HF↑.

The formation of hydrogen fluoride is a positive factor affecting the purity of the obtained FLiNaK.[19] The required weighed portions of the initial reagents (LiF, NaF and KF·HF) were heated in a glassy carbon crucible at a rate of 2.5 °C min^{-1} to a temperature of 750 °C and kept for 2 h, followed by cooling to room temperature. The melting point (460 °C) and enthalpy of melting of the obtained fluoride eutectic composition (414 J g^{-1}, Fig. 1a) are consistent with the reference data.[20]

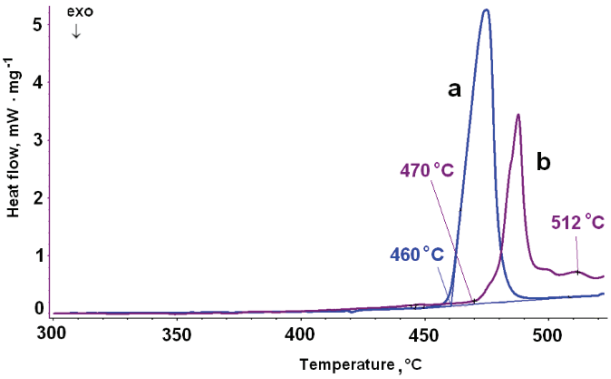

Fig. 1. The STA results: a) FLiNaK; b) 0.85 FLiNaK–0.15 CeF_3.

The methods of Raman spectroscopy and XRD analysis were used to certify pure CeF_3 (99.9 %, CAS 7758-88-5, CHIMKRAFT Company, Russia). It is known that cerium fluoride under normal conditions has a crystal lattice of D_{3d}^4 symmetry, containing six formula units per unit cell. The selection rules determine 17 active modes ($5A_{1g}$ + $12E_g$) in the Raman spectrum.[21] Some of them, apparently, had weak intensity and were not recorded. In accordance with the results,[21] in the recorded spectrum of CeF_3 (Fig. 2a), the vibration bands at 396, 240, 295, 314 cm^{-1} are associated with the A_{1g} vibration modes, whereas those recorded at 77, 145, 203, 225, 306, 319, 386 cm^{-1} are associated with E_g modes. Vibration bands related to other phases, as well as bands of adsorbed water, were not found. XRD analysis of the used CeF_3 reagent also confirmed its single-phase nature (Fig. 2b). FLiNaK–CeF_3 mixtures, containing 15 mol. % of cerium fluoride, were prepared in a glove box in an inert atmosphere (Ar, moisture and oxygen content did not exceed 10 ppm). The mixtures of a given composition were exposed in a glassy carbon crucible for 5 h at the temperatures exceeding the liquidus point (512 °C)[22] of the studied compositions by 150–200 °C.[22] The STA analysis results of obtained mixture are shown in Fig. 1b. The solidus and liquidus points are consistent with the reference data.[22]

Lithium oxide was obtained by thermal decomposition of anhydrous lithium hydroxide.[9] In the Raman spectrum over the range 150–5400 cm^{-1} of synthesized Li_2O, the only one vibration band was noted at 524 cm^{-1}, which is consistent with the data.[23,24] We note the active interaction of lithium oxide with water vapor and CO_2 in the air atmosphere. Fig. 3 shows the Raman spectra of a Li_2O sample recorded sequentially when it was kept in an air atmo-

sphere. The formation of lithium hydroxide (vibration band at 3667 cm^{-1}), crystalline hydrate, $LiOH·H_2O$ (3556 cm^{-1}) and lithium carbonate (195, 1093, 1465 cm^{-1}) were noticed. To prevent the formation of these impurities, the synthesized Li_2O was stored in a glove box in an inert atmosphere.

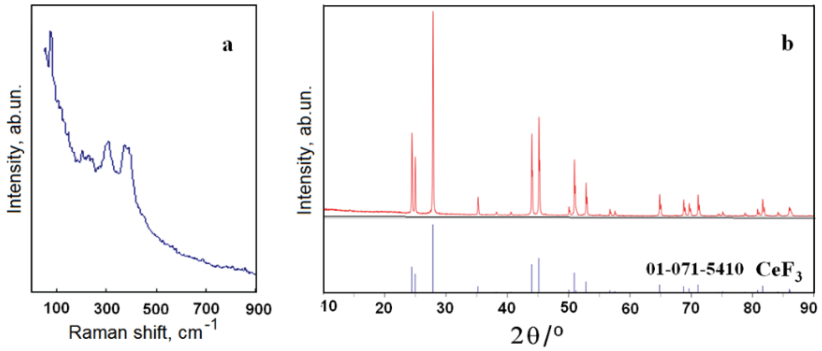

Fig. 2. Results of the cerium fluoride certification: a) Raman spectrum; b) XRD analysis.

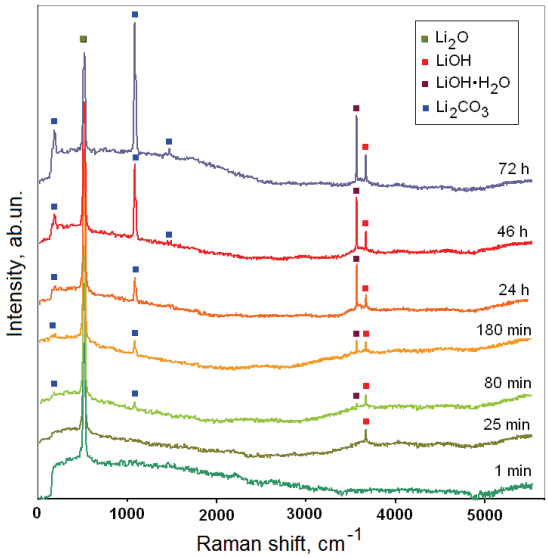

Fig. 3. Raman spectra of the Li_2O on various exposure times in the air atmosphere. Products of interaction with water vapor and CO_2 are marked.

RESULTS AND DISCUSSION

Phase equilibria and liquidus points of the (0.85 FLiNaK–0.15 CeF_3)–Li_2O system

As an example, Fig. 4 shows several DSC curves obtained on studying the thermal behavior of the (0.85 FLiNaK–0.15 CeF_3)–Li_2O system. It can be seen that the introduction of lithium oxide into the fluoride system affects the number

of thermal effects and the phase transformations points. Taking into account the complete set of data obtained, the phase diagram of the system (0.85 FLiNaK–0.15 CeF_3)–Li_2O, containing up to 8.8 mol. % lithium oxide, was constructed (Fig. 5).

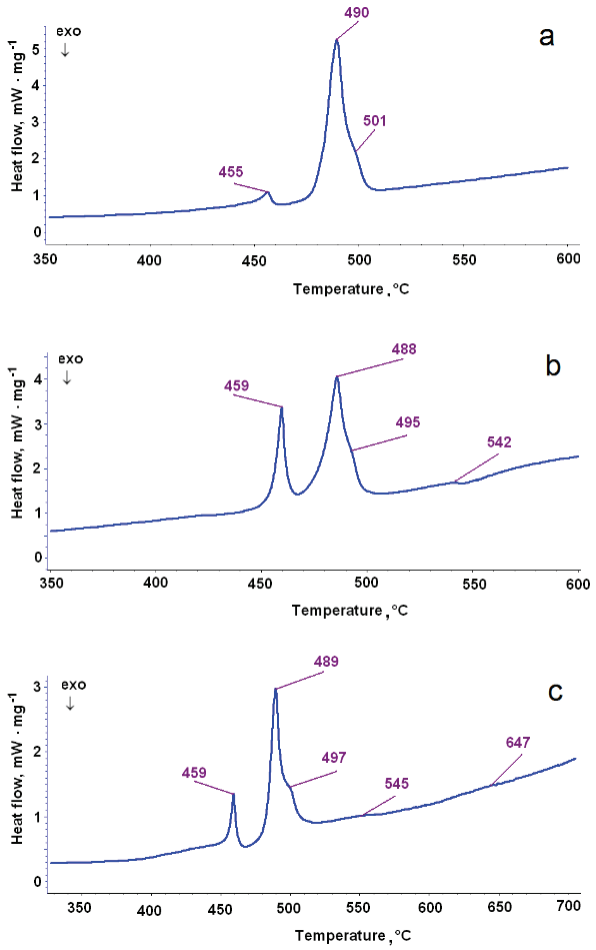

Fig. 4. DSC curves of the (0.85 FLiNaK–0.15 CeF_3)–Li_2O systems, containing 2.3 (a), 4.01 (b) and 8.8 mol. % (c) of lithium oxide.

In the system under study, the presence of a eutectic point was established (the Li_2O content is 3.1 mol. %, T_m = 489 °C), as well as two peritectic points (lithium oxide content 3.2 and 4.2 mol. %, and liquidus points 497 and 549 °C, respectively). The presence of the peritectic points indicates the formation in the system of thermally unstable incongruently melting compounds. The compositions of these compounds are outside the studied concentration range of the lith-

ium oxide. The solidus point of the system is 489 °C. An additional thermal effect was recorded at 456 °C, which can be associated with the polymorphic transformation of the oxyfluoride compound formed in the system. Using the XRD and Raman spectroscopy, a phase analysis of the frozen melts containing 3.5 mol. % Li_2O, was carried out (Figs. 6 and 7).

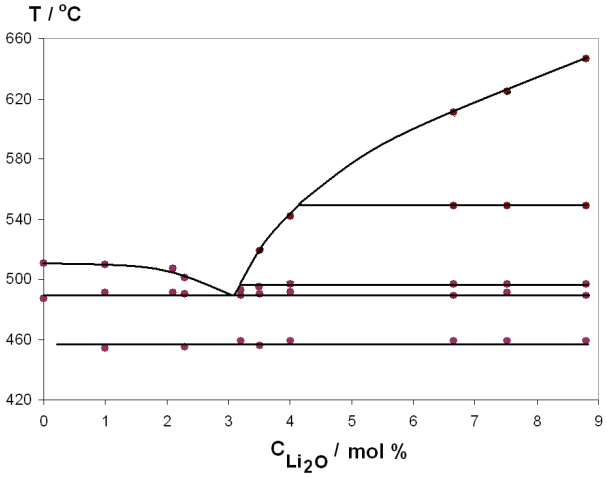

Fig. 5. Part of the phase diagram of the system (0.85 FLiNaK–0.15 CeF_3)–Li_2O.

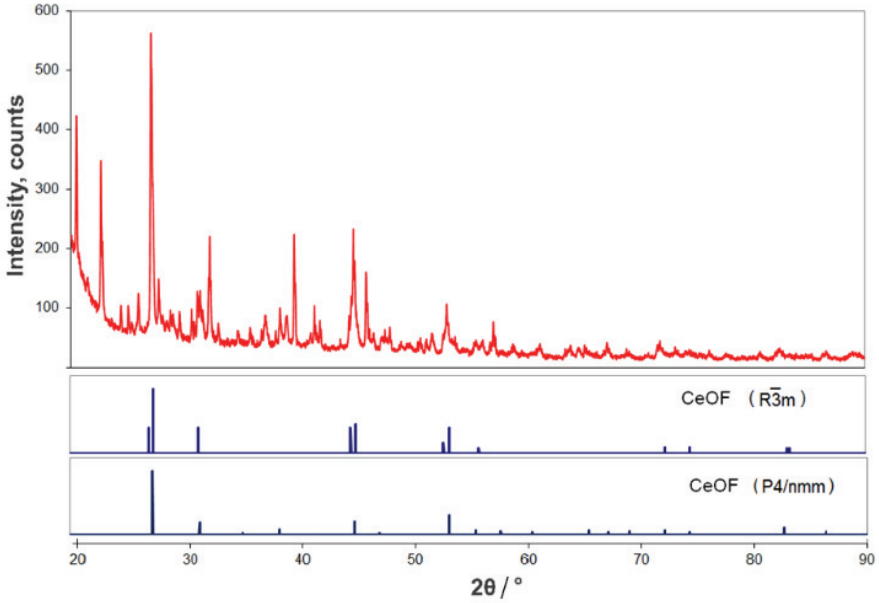

Fig. 6. XRD results of the frozen melt (0.85 FLiNaK–0.15 CeF_3)–Li_2O containing 3.5 mol. % of lithium oxide.

According to the XRD analysis, the presence of tetragonal (space symmetry group *P4*/*nmm*) and rhombohedral (space symmetry group *R3m*) oxyfluorides CeOF (Fig. 6) were established. The Raman microspectroscopy confirms these results: for different microparticles of the sample, vibration spectra of CeOF associated with *P4*/*nmm* and *R3m* space symmetry group[25,26] were recorded independently (Fig. 7).

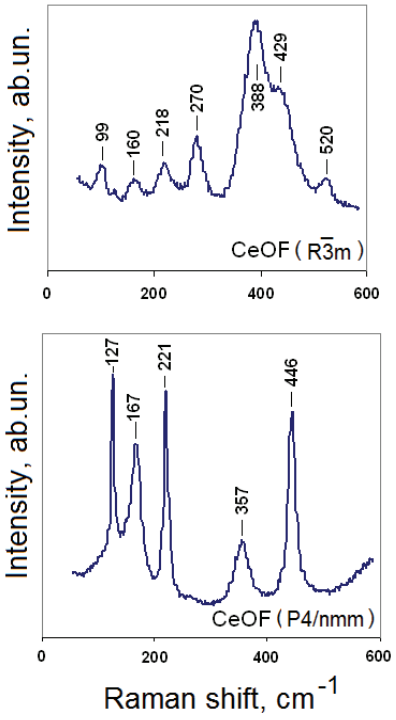

Fig. 7. Raman spectra of the different microparticles frozen melt (0.85 FLiNaK–0.15 CeF_3)–Li_2O containing 3.5 mol. % of lithium oxide.

The liquidus points of the oxide–fluoride system are presented in Table I. At first, the Li_2O additions decrease the temperature of initial crystallisation and then increase it. The change of the dependence flow may be due to the new solid phase which was the first to crystallise during the melt cooling. For the present instance it should be the CeOF. The coordinates of the points on the ascending branches of the liquidus curve correspond to the lithium oxide solubility (*S*) in the melt.

TABLE I. The liquidus points of the systems (0.85 FLiNaK–0.15 CeF_3)–Li_2O

Li_2O content, mol. %	0	1	2.1	2.3	3.2	3.5	4.01	6.62	7.52	8.8
T_{liq} / °C	512	510	507	501	493	519	542	611	625	647

Solubility of Li_2O in 0.85 FLiNaK–0.15 CeF_3 molten system

Using data on the liquidus points of the system (0.85 FLiNaK–0.15 CeF_3)––Li_2O, the lithium oxide solubility for different temperatures was calculated. The results are presented in Fig. 8. The Li_2O solubility increases exponentially on the temperature increasing according to the equation: $S = 0{,}078e^{0.0073T}$, where T is the temperature in °C and S is Li_2O solubility in mol. %.

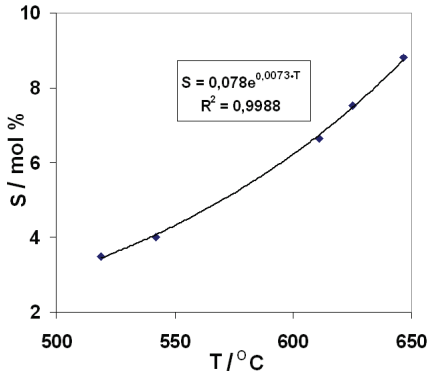

Fig. 8. The temperature dependence of Li_2O solubility in fluoride molten system 0.85 FLiNaK––0.15 CeF_3.

Fig. 9 shows the temperature dependence of Li_2O solubility related to the ln S–1/T coordinates over the temperatures 493–647 °C. It can be approximated by the linear equation: ln $S = A + B/T$, where A and B are empirical coefficients: ln $S = 2.7598 – 4811.9/T \pm 0.04$.

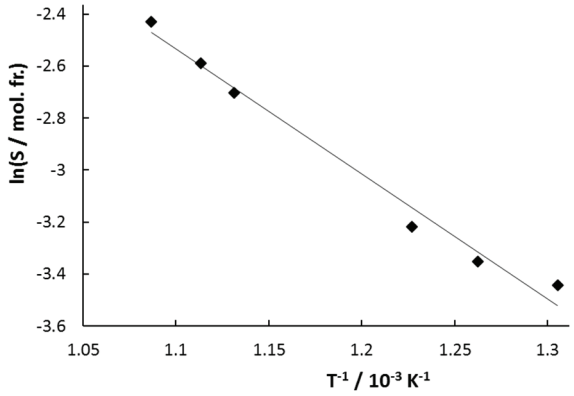

Fig. 9. The temperature dependence of Li_2O solubility in 0.85 FLiNaK–0.15 CeF_3 molten system related to the ln S–1/T coordinates.

The conditional value of the change in Gibbs energy of dissolution of 1 mol of the oxide, ΔG^*_{dis}, is determined by the equation:

$$\Delta G^*_{dis} = -RT\ln K^* \quad (3)$$

where $K^* = K/[f(Li_2O)]$ is the conditional equilibrium constant of the dissolution process. K^* is equal to the Li_2O solubility (S, mol. fr.). At the same time for the studied Li_2O concentration range (up to 8.8 mol. %) the Li_2O activity coefficients $f(Li_2O)$ are assumed to be unchangeable.

Thus, we have obtained the following equation of the temperature dependence of the conditional change in Gibbs energy of dissolution:

$$\Delta G^*_{dis} = \Delta H^* - T\Delta S^* = -RT(A + B/T) \quad (4)$$

Accordingly, it is possible to calculate the conditional values of the change in enthalpy ($\Delta H^* = -RB$) and entropy ($\Delta S^* = RA$) when 1 mol of lithium oxide is dissolved in the melt (Table II).

TABLE II. The thermodynamic characteristics of Li_2O dissolution in fluoride molten system 0.85 FLiNaK–0.15 CeF_3

T °C (K)	S mol. %	ΔG*sol J mol^{-1}	ΔH* kJ mol^{-1}	ΔS* J mol^{-1} K^{-1}	$\Delta G°_m$[18] J mol^{-1}	RTln (f(Li_2O)) J mol^{-1}	f(Li_2O)
500 (773)	3	22271			21644	–627	0.91
550 (823)	5	21124			20744	–380	0.95
600 (873)	6	19976	40.01	22.94	19774	–202	0.97
650 (923)	9	18829			18746	–83	0.99

Positive values of the enthalpy of dissolution indicate the endothermic effect of the process.

Based on these data, such thermodynamic parameters of dissolution as an excessive change in the Gibbs energy of mixing a liquid supercooled oxide with a molten solvent and the activity coefficients of Li_2O in the melt can also be determined.[27,28]

Let's consider the equilibrium of solid Li_2O(s) oxide and solution Li_2O(sol) in a 0.85 FLiNaK–0.15 CeF_3 melt at a constant temperature:

$$Li_2O(s) \leftrightarrows Li_2O(sol) \quad (5)$$

Given the equality of the chemical potentials of solid and dissolved Li_2O, we have written: $\mu°(Li_2O,s) = \mu(Li_2O,sol)$. Here $\mu(Li_2O,sol) = \mu°(Li_2O,liq) + RT\ln a(Li_2O,sol)$.

For the standard state for the solution, we take supercooled liquid lithium oxide at a given temperature, and:

$$\mu(Li_2O,sol) = \mu°(Li_2O,liq) + RT\ln N(Li_2O,sol) + RT\ln f(Li_2O,sol) \quad (6)$$

Here $N(Li_2O,sol)$ and $f(Li_2O,sol)$ are concentration and activity coefficients of Li_2O in the melt.

Thus, we can write the change of Gibbs energy, $\Delta G°_m(T)$, during Li_2O melting at temperature T by the equation:

$$\Delta G°_m(T) = \mu°(Li_2O,liq) - \mu°(Li_2O,s) = -RT\ln N((Li_2O,sol) - RT\ln f(Li_2O,sol) \quad (7)$$

The change of the Gibbs energy on the dissolution process is expressed by the equation:

$$\Delta G^*_{sol}(T) = -RT\ln S = \Delta G°_m(T) + RT\ln f(Li_2O,sol) \quad (8)$$

The $RT\ln f(Li_2O,sol)$ characterizes the excess changes of Gibbs energy of mixing of liquid overcooled oxide and a solvent melt.

The thermodynamic parameters of the Li_2O dissolution in 0.85 FLiNaK–0.15 CeF_3 molten system calculated in this way using[18] and experimental solubility values are shown in Table II. Small negative values of $RT\ln f(Li_2O,sol)$ indicate an exothermic interaction between lithium oxide and solvent when mixed. With increasing temperature, the value of $RT\ln f(Li_2O,sol)$ takes on more positive values, which indicates a decrease in the exothermic effect of the interaction. Accordingly, the activity coefficients $f(Li_2O,sol)$ have values slightly lower than unity, which increase with temperature.

CONCLUSION

Pyrochemical reprocessing of nuclear fuel is the promising option for environmentally safe handling of nuclear waste. Molten systems based on alkali metal fluorides (FLiNaK) with lithium oxide additives are suggested as a working medium. The data on the solubility of lithium oxide in fluoride melts is in demand. DSC analysis, XRD, Raman spectroscopy and thermodynamic simulations were used to obtain evidences on the phase equilibria and liquidus points of the system 0.85 (FLiNaK–0.15 CeF_3)–Li_2O, containing up to 8.8 mol. % lithium oxide. The eutectic point (the Li_2O content is 3.1 mol. %, T_m = 489 °C) and two peritectic points (lithium oxide content are 3.2 and 4.2 mol. %, and liquidus points are 497 and 549 °C, respectively) were found. Using the DSC results on the liquidus points, the solubility of lithium oxide was determined. The temperature dependence of Li_2O solubility (S, mol. %) is described by an equation: $S = 0{,}078e^{0.0073T}$. Thermodynamic simulation results show an exothermic effect due to interaction between lithium oxide and fluoride melt. The interaction product oxyfluoride CeOF was detected by XRD analysis and Raman spectroscopy.

Acknowledgments. The phase analysis was carried out by E. Vovkotrub and P. Mushnikov using the equipment of the Shared Access Center “Composition of Compounds” of the Institute of High Temperature Electrochemistry of the Ural Branch of the Russian Academy of Sciences. The preparation of lithium oxide was carried out by A. Mullabaev.

И З В О Д

РАСТВОРЉИВОСТ ЛИТИЈУМ-ОКСИДА У РАСТОПУ ФЛУОРИДА CeF_3–FLiNaK

IRINA ZAKIRYANOVA, IRAIDA KORZUN, ELENA NIKOLAEVA и ANDREY BOVET

Institute of High-Temperature Electrochemistry, 20 Akademicheskaya Street, Yekaterinburg, Russia

Растопи базирани на халогенидима алкалних метала уз додатке литијум оксида су потенцијално добра радна средина за пирохемијску додатну обраду нуклеарног отпада.

Смеша флуорида алкалних метала еутектичког састава (FLiNaK) је предложен растварач због високе растворљивости оксида актиноида, ниске вискозности, високих тачки кључања, ниског напона паре и отпорности на оштећења од радијације. Термална анализа, XRD, раманска спектроскопија и термодинамичке симулације су коришћене да би се добили докази о равнотежи фаза и температури топљења система (0,85 FLiNaK–0,15 CeF_3)–Li_2O, који садржи 8,8 mol. % литијум-оксида. Одређена је растворљивост литијум-оксида у растопу флуорида FLiNaK–CeF_3 као и термодинамички парамтери растварања. Нађене су еутектичка тачка (садржај Li_2O је 3,1 mol. %, T_m = 489 °C) и две перитактичке тачке (садржај литијум-оксида: 3,2 and 4,2 mol. % и тачке топљења: 497 и 549 °C, редом). Резултати термодинамичких симулација су показали егзотермни ефекат услед интеракција између литијум оксида и растопа флуорида. Производ интеракције је оксифлуорид CeOF који је детектован XRD анализом и раманском спектроскопијом.

(Примљено 4. марта, ревидирано 17. марта, прихваћено 27. марта 2024)

REFERENCES

1. H. Lee, G.-I. Park, K.-H. Kang, J.-M. Hur, J.-G. Kim, D.-H. Ahn, Y.-Z. Cho, E. H. Kim, *Nucl. Eng. Tech*. **43** (2011) 317 (https://doi.org/10.5516/NET.2011.43.4.317)
2. S. M. Jeong, B.H. Park, J.-M. Hur, C.-S. Seo, H. Lee, K.-C. Song, *Nucl. Eng. Tech*. **42** (2010) 183 (https://doi.org/10.5516/NET.2010.42.2.183)
3. E.-Y. Choi, C. Y. Won, D.-S.Kang, S.-W. Kim, *J. Radioanal. Nucl. Chem.* **304** (2015) 535 (https://doi.org/10.1007/s10967-014-3842-2)
4. Y. P. Zaikov, V. Y. Shishkin, A. M. Potapov, A. E. Dedyukhin, *J. of Physics: Conf. Series* **1475** (2020) 012027 (https://doi.org/10.1088/1742-6596/1475/1/012027)
5. M. Iizuka, T. Inoue, M. Ougier, J.-P. Glatz, *J. Nucl. Sci. Tech*. **44** (2007) 801 (https://doi.org/10.1080/18811248.2007.9711869)
6. B. H. Park, I. W. Lee, C. S. Seo, *Chem. Eng. Sci.* **63** (2008) 3485 (https://doi.org/10.1016/j.ces.2008.04.021)
7. D. Kim, S. Bae, J. Kim, T. Park, Y. Park, K. Song, *Asian J. Chem.* **25** (2013) 705 (http://dx.doi.org/10.14233/ajchem.2013.18)
8. Y. Kado, T. Goto, R. Hagiwara, *J. Chem. Eng. Data* **53** (2008) 2816 (https://doi.org/10.1021/je800540c)
9. A. Mullabaev, O. Tkacheva, V. Shishkin, V. Kovrov, Y. Zaikov, L. Sukhanov, Y. Mochalov, *J. Nucl. Mat*. **500** (2018) 235 (https://doi.org/10.1016/j.jnucmat.2018.01.004)
10. R. G. Reddy, S. G. Kumar, *Metal. Trans., B* **24** (1993) 1031 (https://doi.org/10.1007/BF02660994)
11. A. A. Maslennikova, P. N. Mushnikov, A. V. Dub, O. Y. Tkacheva, Y. P. Zaikov, Y.-L. Liu, W.-Q. Shi, *Materials* **16 (**2023) 4197 (https://doi.org/10.3390/ma16114197)
12. X. Guo, J. Sietsma, Y. Yang, *A Critical Evaluation of Solubility of Rare Earth Oxides in Molten Fluorides*, in *Rare Earths Industry*, Eds.: I. B. De Lima, W. L. Filho, Elsevir, 2016, p. 223 (https://doi.org/10.1016/B978-0-12-802328-0.00015-2)
13. A. L. Rollet, E. Veron and C. Bessada, *J. Nucl. Mater*. **429** (2012) 40 (https://doi.org/10.1016/j.jnucmat.2012.05.010)
14. O. Beneš, R. J. M. Konings, *J. Nucl. Mater*. **435** (2013) 164 (https://doi.org/10.1016/j.jnucmat.2012.12.005)
15. R. Marsac, F. Réal, N. Banik, M. Pédrot, O. Pourret, V. Vallet, *Dalton Trans*. **46** (2017) 13553 (https://doi.org/10.1039/C7DT02251D)
16. D. Zakiryanov, *J. Mol. Liq*. **384** (2023) 122265 (https://doi.org/10.1016/j.molliq.2023.122265)

17. D. Zakiryanov, *Molecular Simul.* (2023) 845 (https://doi.org/10.1080/08927022.2023.2193656)
18. HSC Chemistry 9 Software, Outokumpu Research Oy, Pori, 2007
19. G. Zong, Z. Zhang, J. Sun, J. Xiao, *J. Fluor. Chem.* **197** (2017) 134 (https://doi.org/10.1016/j.jfluchem.2017.03.006)
20. J. Derek, Y. Toshinobu, J. Janz, *J. Chem. Eng. Data* **27** (1982) 366 (https://doi.org/10.1021/je00029a041)
21. R. P. Bauman, S. P. S. Porto, *Phys. Rev*. **161** (1967) 842 (https://doi.org/10.1103/PhysRev.161.842)
22. P. N. Mushnikov, O. Y. Tkacheva, A. S. Kholkina, Y. P. Zaikov, V. Y. Shishkin, A. V Dub, *At. Energy* **131** (2022) 263 (https://doi.org/10.1007/s10512-022-00876-2)
23. F. S. Gittleson, K. Yao, D. G. Kwabi, S. Y. Sayed, W. Ryu, Y. Shao-Horn, A. D. Taylor, *ChemElectroChem* **2** (2015) 1446 (https://doi.org/10.1002/celc.201500218)
24. T. Osaka, I. Shindo, *Solid State Commun*. **51** (1984) 421 (https://doi.org/10.1016/0038-1098(84)90126-1)
25. E. M. Rodrigues, E. R. Souza, J. K. Monteiro, R. D. L. Gaspar, I. O. Mazali, F. A. Sigoli, *J. Mater. Chem*. **22** (2012) 24109 (https://doi.org/10.1039/c2jm34901a)
26. J. Hölsä, E. Säilynoja, H. Rahiala, J. Valkonen, *Polyhedron* **16** (1997) 3421 (https://doi.org/10.1016/S0277-5387(97)00065-X)
27. E. V. Nikolaeva, I. D. Zakiryanova, A. L. Bovet, I. V. Korzun, *Z. Naturforsch*. **71** (2016) 731 (https://doi.org/10.1515/zna-2016-0163)
28. E. V. Nikolaeva, I. D. Zakiryanova, I. V. Korzun, A. L. Bovet, B. D. Antonov, *Z. Naturforsch*. **70** (2015) 325 (https://doi.org/10.1515/zna-2014-0370).

Journal of the Serbian Chemical Society
JSCS-info@shd.org.rs • www.shd.org.rs/JSCS
J. Serb. Chem. Soc. *90* (1) 67–76 (2025)
JSCS–5820
Original scientific paper
Published 1 February, 2025

Analytical method development and validation of antifungal drugs in updated ointment formulation using UV spectroscopy and RP-HPLC

RETHINA KARUPPIAHYA[1], SUBA GEETHA ARUNACHALAM[1], SARAVANAN VENKATTAPURAM SAMPATH[1], SAMBATHKUMAR RAMANATHAN[1], ANANDA THANGADURAI SUBRAMANIAM[2], RAVIKUMAR RAMASAMY[1], ANUPRINCY PAULMURUGAN[1] and JAMBULINGAM MUNUSAMY[1]*

[1]*Department of Pharmaceutical Analysis, The Erode College of Pharmacy, Erode, Tamil Nadu, India and* [2]*Department of Pharmaceutical Analysis, JKKN College of Pharmacy, Kumarapalayam, Namakkal District, Tamil Nadu, India*

(Received 1 March, revised 12 March, accepted 18 August 2024)

Abstract: A precise, simple and validated reverse-phase high-performance liquid chromatography (RP-HPLC) method alongside spectrophotometric analysis has been established for the simultaneous quantification of clobetasol propionate, miconazole nitrate and salicylic acid in an updated ointment formulation. The impact of organic modifiers on the retention of the target compounds was assessed. The chromatographic analysis was conducted using a simple low-pressure gradient method with UV detection at 282 nm on a C18 column (5 µm, 4.6 mm×250 mm HSS). The mobile phase consisted of a mixture of methanol, acetonitrile and tetraethylamine acetate buffer at pH 4, adjusted with acetic acid in a 40:40:20 volume ratio, at a flow rate of 1.2 mL min^{-1}. The method demonstrated linearity in the 5–15 µg mL^{-1} concentration range for clobetasol propionate, 30–90 µg mL^{-1} for miconazole nitrate, and 15–45 µg mL^{-1} for salicylic acid. The limits of detection and quantification were determined to be 1.49 and 4.53 µg mL^{-1} for clobetasol propionate, 8.72 and 26.43 µg mL^{-1} for miconazole nitrate and 3.37 and 10.22 µg mL^{-1} for salicylic acid, respectively. The recoveries for drugs in formulation range from 95 to 99 %.

Keywords: clobetasol propionate; miconazole nitrate; salicylic acid; high-performance liquid chromatography; UV spectroscopy.

INTRODUCTION

Fungal infections present a notable challenge to skin wellness, impacting people across all age groups. From irritating nail infections to bothersome conditions such as jock itch, athlete's foot, and ringworm, the array of fungal ailments

* Corresponding author. E-mail: jambulingam48@gmail.com
https://doi.org/10.2298/JSC240301072K

calls for efficient treatment. If neglected, these infections can progress to more serious health issues, underscoring the importance of prompt intervention.[1]

Clobetasol propionate (Fig. S-2, of the Supplementary material to this paper) chemically designated as [(8*S*,9*R*,10*S*,11*S*,13*S*,14*S*,16*S*,17*R*)-17-(2-chloroacetyl)--9-fluoro-11-hydroxy-10,13,16-trimethyl-3-oxo-6,7,8,11,12,14,15,16-octahydrocyclopenta[*a*]phenanthren-17-yl]propanoate is a potent topical glucocorticoid.[2] It is an analogue of prednisolone, and it acts by binding glucocorticoid receptors in the cytoplasm, and activates gene transcription *via* the glucocorticoid receptor. This produces anti-inflammatory proteins and limits the activity of inflammatory mediators,[3] thus increasing the creation of phospholipase A2 suppressor proteins, which regulate the release of arachidonic acid, an inflammation precursor. Mainly used in the treatment of psoriasis, eczema, contact dermatitis, and lichen planus.[4]

Miconazole nitrate (Fig. S-3, Supplementary material) chemically named as 1-[2-(2,4-dichlorophenyl)-2-[(2,4-dichlorophenyl)methoxy]ethyl]imidazole; nitric acid and classified as an imidazole antifungal agent.[5,6] Miconazole nitrate inhibits the synthesis of ergosterol, a crucial component of fungal cell membranes, effective in the treatment of many fungal infections.[7,8]

Salicylic acid (Fig. S-1, Supplementary material) chemically named 2-hydroxybenzoic acid works as a keratolytic agent, it helps to break down and exfoliate dead skin cells.[9] This property makes it effective in treating conditions where there is an abnormal buildup of skin cells, such as acne, psoriasis and keratosis pilaris. Additionally, its anti-inflammatory and antimicrobial properties contribute to its usefulness in addressing various skin issues.[10,11]

Various formulations of clobetasol propionate, salicylic acid and miconazole nitrate are available for topical use, encompassing ointments, creams, gels, foams, cosmetic products and acne treatment preparations.[3,4,9,12]

A review of the literature showed that clobetasol propionate was determined using a variety of analytical techniques, including TLC-densitometric method,[13] RP-HPLC,[2,11,8] UV spectrophotometry[14] and UPLC-MS/MS.[15] Spectrofluorometric,[16] RP-HPLC,[5,7,8] UV Spectroscopy,[7] UPLC,[5] capillary zone electrophoresis,[17] LC–MS/MS[18] and gas chromatography-flame ionization detector (GC--FID)[19] were among the techniques used to analyze miconazole. LC–tandem mass spectrometry,[9] liquid chromatography with solid phase extraction,[20] TLC-densitometric techniques,[21] LC–MS/MS,[9] SPE-UHPLC–MS/MS,[22] UPLCMS/MS,[9] LC––MS/MS,[9] GC–MS,[9] spectrofluorimetry,[9] UV spectrometry,[9] liquid–liquid extraction-HPLC[9] and RP-HPLC[9,11] were among the methods used to analyse salicylic acid.

This article presents a comprehensive approach to treating skin conditions by combining antifungal and corticosteroid agents in topical formulation, namely an ointment. This synergistic strategy targets both fungal infections and inflammation, further enhanced by the addition of keratolytic agents to promote the skin cell

turnover and the absorption of active ingredients. Using a polyethylene glycol base ensures the optimal penetration and the patient compliance, resulting in efficient relief and accelerated recovery across various dermatological conditions.[23]

Furthermore, the article addresses a gap in analytical methods by proposing the development of an RP-HPLC and UV spectroscopy method to determine the percentage of drugs in the ointment, complementing the existing literature on salicylic acid with clobetasol propionate,[11] and miconazole nitrate with clobetasol propionate.[8] The integration of these analytical techniques promises a more comprehensive understanding and the evaluation of multifaceted formulations in dermatological care. The proposed method is reproducible, reliable and economical and permits the analysis of more samples in a short period of 15 min.

EXPERIMENTAL

Chemicals and reagent

Clobetasol propionate and miconazole nitrate were obtained as a gift sample from Ajanta Pharma, Hyderabad. The following analytical grade reagents like salicylic acid, acetonitrile and HPLC water were obtained from Merck (Vikhroli, Mumbai). Acetic acid, triethylamine, methanol, polyethylene glycol (PEG) 400 and polyethylene glycol (PEG) 4000 were obtained from Lobachemei Pvt. Limited, Mumbai.

Instrumentation

Spectroscopic analysis was performed using a Shimadzu UV-1900i double-beam spectrophotometer (Shimadzu, Japan) equipped with 1.0 cm quartz cells and data produced by the program Lab Solution version (1.13), data acquisition was performed using MATLAB, 6.2.1 version.

RP-HPLC was performed using a Shimadzu P-series PDA liquid chromatography system (Shimadzu, Japan) consisting of a column oven (CTO-10AS VP), a pump (LC-20ATD), a manual injector and a degasser (DGU20A3R/20A5R) and SPD 40 (photodiode array detector--UV–Vis detector) was used for UV detection. Then the chromatographic conditions were controlled by a software package named Lab Solutions.

Different column packing and mobile phases were tested to develop and formulate a method for the simultaneous determination of clobetasol propionate, miconazole nitrate and salicylic acid in ointment concerning the shape of peaks in the corresponding chromatogram. The final choice of the stationary phase consists of a C18 column (5µm, 4.6 mm×250 mm HSS), which shows great resolution and run time. The degassing of the mobile phase was performed by passing through a 0.45 µm membrane filter and sonicator. A flow rate of 1.2 mL min^{-1} was used for the separation, and an internal standard with UV detection at 282 nm was used as the detector wavelength, a column oven temperature of 30 °C was used with the injection volume of 20 µL.

Preparation of topical formulation

About 15 g of PEG 4000 and 31 mL of PEG 400, was stirred until the mixture had achieved a semisolid consistency at room temperature. Then the fusion technique was used to add the appropriate quantities of clobetasol propionate, miconazole nitrate and salicylic acid in succession, ensuring thorough incorporation and a uniform distribution[23] (Table S-I, Supplementary material).

Preparation of standards and sample stock solution (RP-HPLC and UV–Vis spectroscopy)

A standard stock solution of clobetasol propionate, miconazole nitrate and salicylic acid was prepared at a concentration of (1000 μg mL^{-1}). From this standard stock solution, the aliquots of different concentrations were prepared by the suitable dilutions using ethanol for spectroscopic measurements. In the same way sample solution was prepared for RP-HPLC using the diluent (acetonitrile:methanol at 50:50 volume ratio).

A combined standard stock solution was prepared by accurately weighing and transferring 10 mg of clobetasol propionate, 60 mg of miconazole nitrate and 30 mg of salicylic acid in a 100 mL volumetric flask. Add the required amount of diluent and sonicate to dissolve and make up the volume to 100 mL which may contain 100 μg mL^{-1} of clobetasol propionate, 600 μg mL^{-1} of miconazole nitrate and 300 μg mL^{-1} of salicylic acid. The final concentration was made to 50, 75, 100, 125 and 150 μg mL^{-1}, respectively by diluent. The final solutions were filtered using a membrane filter 0.45 μm of pore size.

The sample stock solution was prepared by accurately weighing 2 g of antifungal topical formulation which contains 0.01 g clobetasol propionate, 0.6 g of salicylic acid, 0.039 g of miconazole nitrate in a 100 mL volumetric flask, add 50 mL of ethanol and sonicate to dissolve. After lightly warming the solution to dissolve completely the volume was made with solvent ethanol for spectroscopic measurements (1000 μg mL^{-1}). From the sample stock solution, the final concentration was made to 20 μg mL^{-1} for spectroscopic analysis. In the same way sample solution was prepared for RP-HPLC using the diluent (acetonitrile:methanol at 50:50 volume ratio).

Spectrophotometric analysis

Wavelength selection. From the standard stock, 20 μg mL^{-1} of the solution was prepared and scanned from 200–400 nm. The maximum absorption was noted for clobetasol propionate at 239 nm, miconazole nitrate at 216 nm, and salicylic acid at 303 nm respectively. (Fig. S-4, Supplementary material).

MATLAB analysis

To achieve a concentration of 20 μg mL^{-1} for each analyte, dilutions were prepared from the standard stock solution. A 3×3 matrix was constructed using different wavelengths selected according to the maximum absorption of the compound in the UV spectrum (illustrated in Fig. 1), and MATLAB was employed to calculate the amount of drugs in the formulation.

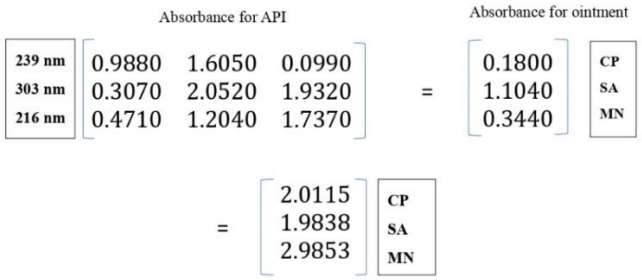

Fig. 1. A 3×3 matrix used for calculating drug content *via* MATLAB.

Chromatographic analysis

Linearity range. Typical linear concentrations were constructed with five samples of the combined stock solution. The linearity range was 5–15 μg mL^{-1} for clobetasol propionate, 30–

–90 μg mL^{-1} for miconazole nitrate, and 15–45 μg mL^{-1} for salicylic acid. The linear line was obtained by plotting the ratios of the peak areas of clobetasol propionate, miconazole nitrate, and salicylic acid *versus* their concentration in μg mL^{-1}. The regression equations were calculated by the Excel sheet.

The accuracy samples were prepared at 80, 100 and 120 % in the same way as linearity samples.

RESULTS AND DISCUSSION

Several evaluation parameters of formulated ointment were investigated and confirmed that the formulation passes the evaluation test for the topical application. The evaluation of physical parameters revealed that a white, uniform and consistent preparation with good homogeneity was found to have a pH of 4.9±0.06, indicating their potential suitability for dermatological care. The viscosity of formulation was performed at different speeds and values to adhere to the acceptance criteria for the skin application with 822,000 cps.

The spreadability of the new formulation was determined to be 17 cm^2 s^{-1}, which indicates the moderate to high spreadability rate. The drug content is measured using liquid chromatography with a high recovery of 96, 99 and 95 % for clobetasol propionate, miconazole nitrate and salicylic acid, respectively (Table S-II, Supplementary material).

Spectrophotometric analysis using MATLAB

Using a 3×3 matrix in MATLAB software, the drug concentration in an ointment was calculated. Each entry in the matrix indicates the amount of different drugs that are present. By using these measurements from MATLAB in conjunction with a series of calculations, the amount of drug in the topical formulation is calculated to be 98.6 % for clobetasol propionate, 92.2 % for miconazole nitrate, and 109.70 % for salicylic acid (Table S-III, Supplmentary material).

Method development

Several variables of the RP-HPLC method concerning their effect on the separation of clobetasol propionate, miconazole nitrate and salicylic acid were investigated. In comprehensive preliminary trials, a series of mobile phases with different pH in combination with different organic solvents were tested.

The chromatographic conditions for the simultaneous quantification of clobetasol propionate, salicylic acid and miconazole nitrate using RP-HPLC were patiently constructed after experimenting with several mobile phases, solvent–buffer ratios and pH conditions. The presence of organic modifiers in the mobile phase has a significant effect on the retention of analytes, which are mostly adsorbed onto the stationary phase. The systematic experimentation revealed that a mobile phase containing methanol, acetonitrile and tetraethylamine acetate buffer at pH 4, adjusted with acetic acid in a 40:40:20 volume ratio, provided the optimal retention times for the target compounds, all in less than 15 min.

Given the solubility of all drugs in a methanol and acetonitrile mixture, for the initial trials these solvents were used. However, the inclusion of a buffer became necessary due to the weak acid nature of salicylic acid and the weak base properties of miconazole, demanding a buffer with a pK_a value surpassing that of both drugs pH levels. Acetate buffer was thus incorporated into the mobile phase in varying compositions. Adjustments were meticulously made to pH, temperature and flow rate to perfect the method, ensuring precision, accuracy and suitability, which revealed better system suitability parameters (Table S-IV, Supplementary material).

Method validation

The International Council for Harmonisation of Technical Requirements for Pharmaceuticals for Human Use (ICH) provides guidelines for the validation of analytical procedures, commonly known as the ICH Q2(R1) guideline, which is used for validation of the optimized method.[24]

Linearity

The linearity was validated on samples of standard clobetasol propionate, miconazole nitrate and salicylic acid at five different concentrations (5–15, 30–90 and 15–45 μg mL^{-1}). The regression equations for clobetasol propionate, miconazole nitrate and salicylic acid were: $y = 4063.3x + 1899.1$, $y = 1181.7x + 1196.3$ and $y = 19107x + 20494$. The correlation coefficients were 0.9922, 0.9957 and 0.9954, respectively, where x represents concentration in μg mL^{-1}, y represents HPLC peak area, which was automatically tracked by an integrator of the HPLC equipment and R implies the correlation coefficient. The data entry and analysis were successfully carried out on a personal computer using Microsoft Excel (Office Home & Student 2021 Microsoft Co., Redmond, USA, 2021), Table S-V and Fig. S-5, Supplementary material).

Precision

The triplicate samples of each drug were prepared and analysed using the proposed RP-HPLC technique on the same day and three days apart. The related coefficients of variation were then calculated. Table I summarizes the method's intra- and inter-day variability. These findings support the method's high accuracy and consistency, both within and between analytical sessions. The method's accuracy is clear since the estimated relative standard deviations (*RSD*) are less than the maximum permissible value of 2 %, designated as RSD_{max}, as specified in Pharmacopoeias.

Accuracy

The accuracy was determined by calculating the percentage recovery of the observed concentration related to the predicted concentration. To test the method's accuracy, the recovery values were calculated for solutions containing 80, 100 and

120 % of the specified clobetasol propionate, miconazole nitrate and salicylic acid concentrations. Table II illustrates the findings. The procedure is amazingly precise, ensuring that dependable results are achieved.

TABLE I. Intra and inter-day precision data

Nominal conc. μg mL^{-1}	Intraday		Interday	
	Mean of observed peak area ± *SD*	*RSD* / %	Mean of observed peak area ± *SD*	*RSD* / %
Clobetasol propionate				
5	2574 ±219.6	0.8532	26468 ±477.2	1.8029
Miconazole nitrate				
30	41433.7 ±509.9	1.2308	41749 ±475.7	1.1395
Salicylic acid				
15	360081 ±5978.6	1.6603	361016 ±5840.2	1.6177

TABLE II. Accuracy data for ointment

Level	Sample μg mL^{-1}	Standard μg mL^{-1}	Nominal conc. μg mL^{-1}	Peak area	Recovery μg mL^{-1}	Recovery, %
Clobetasol propionate						
80	1	3	4	20130	3.99	99.75
100	1	4	5	23890	4.98	99.6
120	1	5	6	27420	5.91	98.5
Miconazole nitrate						
80	20	4	24	30519	23.96	99.83
100	20	10	30	37326	29.83	99.43
120	20	16	36	44389	35.91	99.75
Salicylic acid						
80	6	6	12	271455	11.98	99.83
100	6	9	15	325594	14.97	99.8
120	6	12	18	373902	17.92	99.55

Assay

A reversed-phase high-performance liquid chromatographic technique for simultaneous determination of clobetasol propionate, miconazole nitrate and salicylic acid concentration in an ointment has been developed. The active components were monitored by measuring the peak area of the ointment and the standard and the peak area ratio, when calculated, showed the great recovery rates and the assay success percentage. The specificity of the chromatographic technique was established by screening a placebo solution and an assay solution together.

The placebo solution was made in the same way as the examined solution but without the drugs (Table S-VI, Supplementary material). Figs. 2 and 3 shows the assay and the placebo chromatogram for sample and standard.

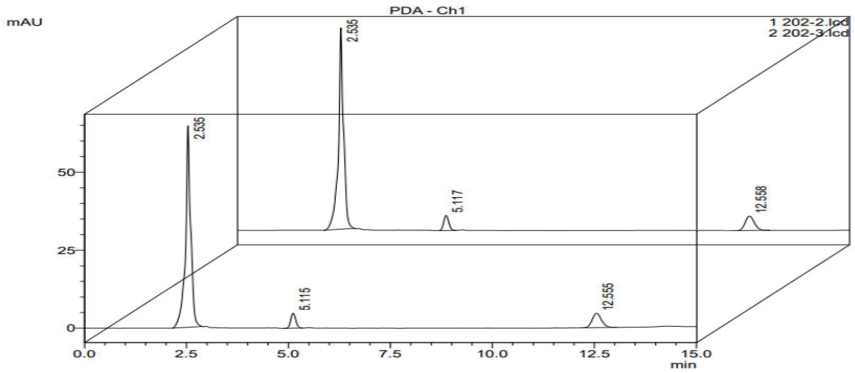

Fig. 2. Assay chromatogram for sample and standard (concentration of the combined standard and sample solution is 100 μg mL^{-1}).

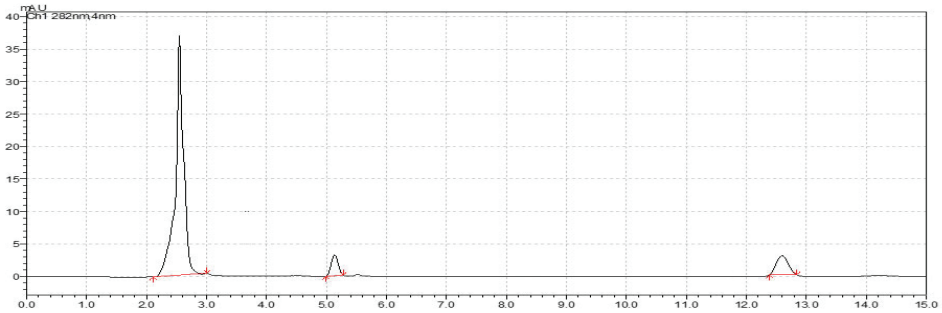

Fig. 3. Specificity chromatogram contains 50 μg mL^{-1} of combined standard solution.

Limit of detection and quantification

The detection and quantitation limits were calculated as *LOD* (k = 3.3) and *LOQ* (k = 10) and found to be 1.49 and 4.53 μg mL^{-1} for clobetasol propionate, 8.72 and 26.43 μg mL^{-1} for miconazole nitrate and 3.37 and 10.22 μg mL^{-1} for salicylic acid (Table S-VII, Supplementary material).

Robustness

The robustness of the RP HPLC method was assessed by introducing minor, stochastic alterations to the wavelength, temperature and flow rate. The variations were made to the flow rate (±0.1 mL min^{-1}), the temperature (±2 °C) and the wavelength (±2 nm). As the determined relative standard deviations (*RSD*) are below the maximum acceptable value of 2 % (RSD_{max}), as specified in Pharmacopoeias, the method's reliability is confirmed (Tables SVIII–S-X, Supplementary material).

CONCLUSION

The newly developed RP–HPLC and UV spectroscopy method, using the formulated formulation, provides a simple and precise procedure for simultaneously determining clobetasol propionate, miconazole nitrate and salicylic acid in an updated ointment. This approach was distinguished by its simplicity, speed and effectiveness. The validation data provided excellent precision and accuracy, confirming the suggested method's reliability.

SUPPLEMENTARY MATERIAL

Additional data and information are available electronically at the pages of journal website: https://www.shd-pub.org.rs/index.php/JSCS/article/view/12827, or from the corresponding author on request.

Acknowledgement. JM express his gratitude to his institution and staff for supporting his research.

И З В О Д

РАЗВОЈ АНАЛИТИЧКЕ МЕТОДЕ И ВАЛИДАЦИЈА АНТИФУНГАЛНИХ ЛЕКОВА У АЖУРИРАНОЈ ФОРМУЛАЦИЈИ МАСТИ ПРИМЕНОМ UV СПЕКТРОСКОПИЈЕ И RP-HPLC

RETHINA KARUPPIAHYA[1], SUBA GEETHA ARUNACHALAM[1], SARAVANAN VENKATTAPURAM SAMPATH[1], SAMBATHKUMAR RAMANATHAN[1], ANANDA THANGADURAI SUBRAMANIAM[2], RAVIKUMAR RAMASAMY[1], ANUPRINCY PAULMURUGAN[1] и JAMBULINGAM MUNUSAMY[1]

[1]*Department of Pharmaceutical Analysis, The Erode College of Pharmacy, Erode, Tamil Nadu, India u* [2]*Department of Pharmaceutical Analysis, JKKN College of Pharmacy, Kumarapalayam, Namakkal District, Tamil Nadu, India*

Прецизна, једноставна и валидирана метода реверсно-фазне течне хроматографије високих перформанси (RP-HPLC), заједно са спектрофотометријском анализом је успостављена за истовремену квантификацију клобетасол-пропионата, миконазол-нитрата и салицилне киселине у ажурираној формулацији састава масти за кожу. Извршена је процена утицаја органских модификатора на синтезу циљних једињења. Хроматографска анализа је урађена коришћењем једноставне методе градијента ниског притиска са UV детекцијом на 282 nm на C18 колони (5 μm, 4,6 mm×250 mm HSS). Мобилна фаза се састојала од смеше метанола, ацетонитрила и тетраетиламин ацетатног пуфера (pH 4), подешеног сирћетном киселином у запреминском односу 40:40:20, при брзини протока од 1,2 μg mL^{-1}. Метода је показала линеарност у опсегу концентрација од 5–15 μg mL^{-1} за клобетасол-пропионат, 30–90 μg mL^{-1} за миконазол-нитрат и 15–45 μg mL^{-1} за салицилну киселину. Одређене су границе детекције и квантификације: 1,49 и 4,53 μg mL^{-1} за клобетасол-пропионат, 8,72 и 26,43 μg mL^{-1} за миконазол-нитрат и 3,37 и 3,37 μg mL^{-1} за салицилну киселину. Добијени резултат за лекове у формулацији је у опсегу од 95 до 99 %.

(Примљено 1. марта, ревидирано 12. марта, прихваћено 18. августа 2024)

REFERENCES

1. S. H. Kim, S. H. Cho, S. K. Youn, J. S. Park, J. T. Choi, Y. S. Bak, Y. Bin Yu, Y. K. Kim, *Osong Public Heal. Res. Perspect.* **6** (2015) 341 (https://doi.org/10.1016/j.phrp.2015.10.012)

2. M. C. Fontana, M. O. Bastos, R. C. R. Beck, *J. Chromatogr. Sci.* **48** (2010) 637 (https://doi.org/10.1093/chromsci/48.8.637)
3. A. B. Nair, S. Kumar, P. Dalal, C. Nagpal, S. Dalal, R. Rao, N. Sreeharsha, S. Jacob, *Pharmaceutics* **14** (2022) 383 (https://doi.org/10.3390/pharmaceutics14020383)
4. L. N. Lili, A. Klopot, B. Readhead, G. Baida, J. T. Dudley, I. Budunova, *J. Invest. Dermatol.* **139** (2019) 2281 (https://doi.org/10.1016/j.jid.2019.04.021)
5. M. Tarek, H. A. Wagdy, E. S. Elzanfaly, S. M. Amer, *J. Chromatogr. Sci.* **57** (2019) 867 (https://doi.org/10.1093/chromsci/bmz082)
6. P. R. Sawyer, R. N. Brogden, R. M. Pinder, T. M. Speight, G. S. Avery, *Drugs* **9** (1975) 406 (https://doi.org/10.2165/00003495-197509060-00002)
7. A. F. Cartagena, T. Klein, A. Lyra, A. M. Urban, P. V. Farago, N. H. Campanha, *Lat. Am. J. Pharm.* **35** (2016) 1354 (http://www.latamjpharm.org/previous_issue.php?vol=35&num=6)
8. A. Karnik, V. Tambe, B. S. Kuchekar, *Ind. J. Pharm. Sci.* **84** (2022) 268 (https://doi.org/10.36468/pharmaceutical-sciences.920)
9. A. M. Abass, J. M. Rzaij, H. Ghalib Salman, W. Kadhum H.Al-Hashemi, *Open Access J. Chem.* **3** (2019) 22 (https://doi.org/10.22259/2637-5834.0303005)
10. J. C. Béani, *Ann. Dermatol. Venereol.* **129** (2002) 933
11. M. Bhuyian, D. H. Rashid, A. Islam, M. Tareque, *Br. J. Pharm. Res.* **7** (2015) 375 (https://doi.org/10.9734/bjpr/2015/18494)
12. A. Mazzotta, M. Esposito, I. Carboni, C. Schipani, S. Chimenti, *J. Dermatol. Treat.* **18** (2007) 84 (https://doi.org/10.1080/09546630601123835)
13. M. Dolowy, V. Kozik, A. Bak, J. Jampilek, K. Barbusinski, M. Thomas, A. Pyka-Pajak, *Molecules* **22** (2017) 1888 (https://doi.org/10.3390/molecules22111888)
14. N. Devi, S. Kumar, S. Rajan, J. Gegoria, S. Mahant, R. Rao, *Asian J. Chem. Pharm. Sci.* **1** (2016) 36 (https://doi.org/10.18311/ajcps/2016/7726)
15. Y.-T. Lu, R. Guan, J.-R. Zheng, T.-J. Hang, M. Song, *J. Pharm. Biomed. Anal.* **186** (2020) 113322 (https://doi.org/10.1016/j.jpba.2020.113322)
16. G. Magdy, E. Aboelkassim, R. A. El-Domany, F. Belal, *Sci. Rep.* **12** (2022) 21395 (https://doi.org/10.1038/s41598-022-25830-x)
17. M. A. Korany, H. M. Maher, S. M. Galal, M. A. A. Ragab, *J. AOAC Int.* **96** (2013) 1295 (https://doi.org/10.5740/jaoacint.11-343)
18. Y. Yu, J. Zhang, B. Shao, Y. Wu, H. Duan, H. Liu, *J. AOAC Int.* **94** (2011) 1650 (https://doi.org/10.5740/jaoacint.10-244)
19. S. Ashour, N. Kattan, *Int. J. Biomed. Sci.* **6** (2010) 13 (https://www.ncbi.nlm.nih.gov/pmc/articles/PMC3614734/)
20. E. Mikami, T. Goto, T. Ohno, H. Matsumoto, M. Nishida, *J. Pharm. Biomed. Anal.* **28** (2002) 261 (https://doi.org/10.1016/S0731-7085(01)00564-7)
21. L. Wulandari, G. Indrayanto, *J. Planar Chromatogr. – Mod. TLC* **16** (2003) 438 (https://doi.org/10.1556/JPC.16.2003.6.6)
22. Z. Márta, B. Bobály, J. Fekete, B. Magda, T. Imre, P. T. Szabó, *J. Pharm. Biomed. Anal.* **160** (2018) 99 (https://doi.org/10.1016/j.jpba.2018.07.016)
23. Y. Lu, Y. Xiao, M. Z. Yin, X. C. Zhou, L. S. Wu, W. Q. Chen, Y. Luo, Y. H. Kuang, W. Zhu, *Front. Med.* **7** (2021) (https://doi.org/10.3389/fmed.2020.560579)
24. P. Borman, D. Elder, in *ICH Qual. Guidel.*, Wiley, New York, 2017, pp. 127–166 (https://doi.org/10.1002/9781118971147.ch5).

Journal of the Serbian Chemical Society
JSCS-info@shd.org.rs • www.shd.org.rs/JSCS
J. Serb. Chem. Soc. 90 (1) S12–S17 (2025) *Supplementary material*

SUPPLEMENTARY MATERIAL TO

Analytical method development and validation of antifungal drugs in updated ointment formulation using UV spectroscopy and RP-HPLC

RETHINA KARUPPIAHYA[1], SUBA GEETHA ARUNACHALAM[1], SARAVANAN VENKATTAPURAM SAMPATH[1], SAMBATHKUMAR RAMANATHAN[1], ANANDA THANGADURAI SUBRAMANIAM[2], RAVIKUMAR RAMASAMY[1], ANUPRINCY PAULMURUGAN[1] and JAMBULINGAM MUNUSAMY[1]*

[1]*Department of Pharmaceutical Analysis, The Erode College of Pharmacy, Erode, Tamil Nadu, India and* [2]*Department of Pharmaceutical Analysis, JKKN College of Pharmacy, Kumarapalayam, Namakkal District, Tamil Nadu, India*

J. Serb. Chem. Soc. 90 (1) (2024) 67–76

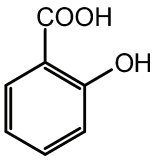

Fig. S-1. Salicylic acid

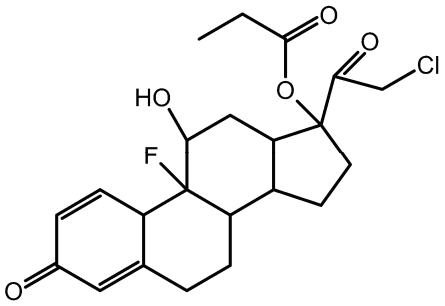

Fig. S-2. Clobetasol propionate

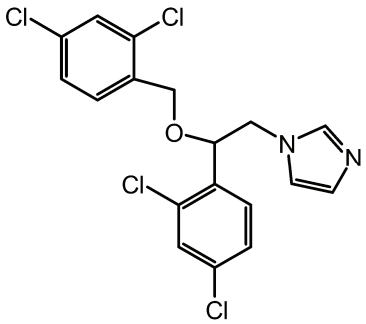

Fig. S-3. Miconazole nitrate

* Corresponding author. E-mail: jambulingam48@gmail.com

Table S-I. Data for formulation

Ingredients	Quantity(g) TF 1
Polyethylene glycol 400	35
Polyethylene glycol 4000	15
Clobetasol propionate	0.015
Miconazole nitrate	0.6
Salicylic acid	0.9

Table S-II. Data for evaluation parameters.

Evaluation parameters	Formulation code TF 1		
Appearance		White	
Homogeneity		Excellent	
Consistency		Semisolid	
pH		4.9 ± 0.06	
Viscosity		822000	
Spreadability		17 cm^2/s	
Drug content	CP 96%	MN 99%	SA 95%

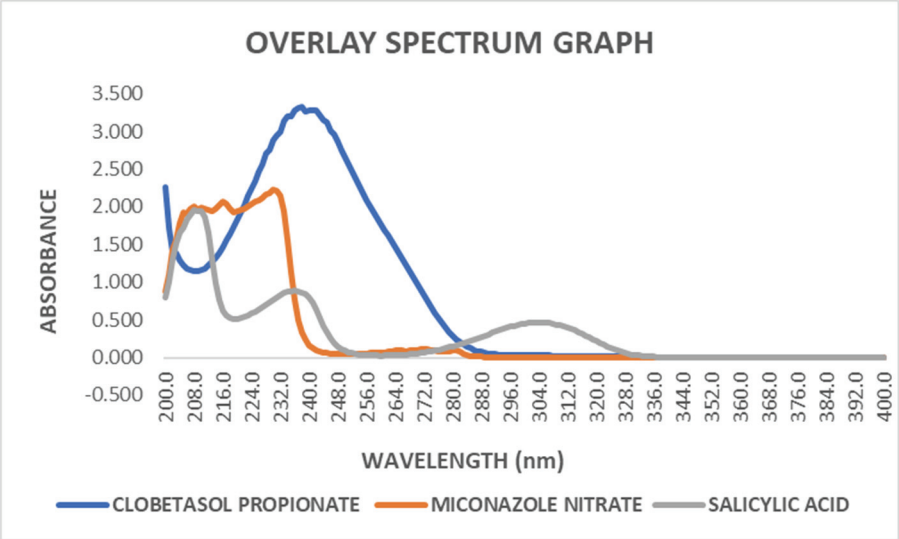

Fig. S-4. UV Spectrum overlay of clobetasol propionate (20 µg mL^{-1}), miconazole nitrate (20 µg mL^{-1}), salicylic acid (20 µg mL^{-1}).

Table S-III. Data for the amount of drug present in formulation using UV and MATLAB

Drug	Amount taken (μg mL^{-1})	Absorbance	Amount present (μg mL^{-1})	% Assay
CP	10	2.0115	9.86	98.6
MN	60	1.9838	55.32	92.2
SA	30	2.9853	32.911	109.70

Table S-IV. Data for system suitability parameters

Parameters	Observed results (mean ± SD) (n = 3)			% RSD		
	CP	MN	SA	CP	MN	SA
Retention time (Rt) in mins	5.128 ± 0.0097	12.595 ± 0.0244	2.539 ± 0.0054	0.1893	0.1935	0.2163
Area	42912 ± 14933.35	72337 ± 27396.39	597798 ± 214211.7	34.8	37.8732	35.833
Theoretical plates (N)	7,476 ± 266.97	15,362 ± 856.09	2871 ± 158.32	3.5713	5.5729	5.5148
Tailing factor (T)	1.064 ± 0.03724	1.092 ± 0.0206	0.901 ± 0.0451	3.4996	1.8924	5.0126
Capacity factor (K')	1.019 ± 0.002571	3.962 ± 0.0125	-	0.2522	0.3168	-
Resolution	12.127 ± 0.22150	23.2 ± 0.4675	-	1.8266	2.1014	-
HETP	20.086 ± 0.7216	9.787 ± 0.5101	52.374 ± 2.8575	3.5927	5.2127	5.4559

Table S-V. Linearity data for clobetasol propionate, miconazole nitrate, salicylic acid in RP-HPLC

Clobetasol propionate concentration (μg mL^{-1})	Clobetasol propionate peak area (n = 3)	Miconazole nitrate concentration (μg mL^{-1})	Miconazole nitrate peak area (n = 3)	Salicylic acid concentration (μg mL^{-1})	Salicylic acid peak area (n = 3)
5	25,500	30	40,085	15	3,31,393
7.5	33,022	45	54,898	22.5	4,52,794
10	40,568	60	68,046	30	5,92,080
12.5	52,929	75	89,774	37.5	7,58,835
15	62,539	90	1,08,881	45	8,53,890

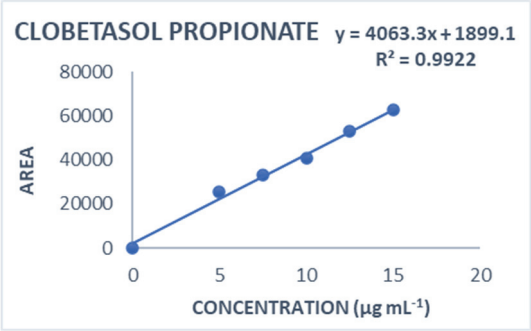

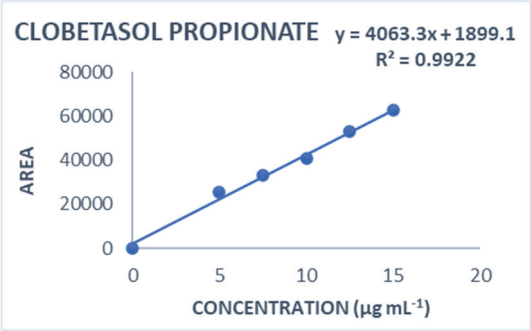

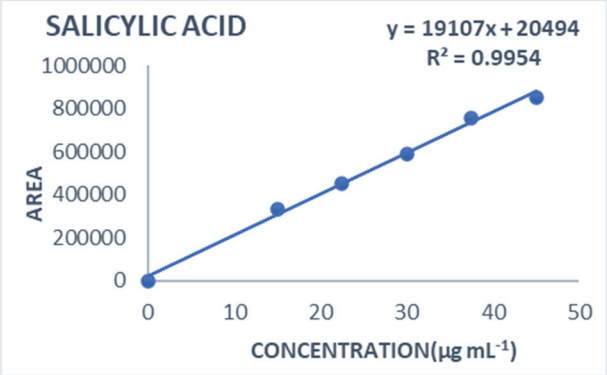

Fig. S-5. Data for linearity in RP-HPLC

Table S-VI. Data for assay of ointment

Drug	Amount taken (μg mL^{-1})	Peak area (n = 3)	Amount obtained (μg mL^{-1})	Amount obtained mean	SD	% RSD	% Assay
CP	10	41614 41132 41248	9.65 9.53 9.56	9.58	0.0624	0.651	95.8
MN	60	72382 72040 72199	60.03 59.74 59.88	59.88	0.1450	0.242	99.8
SA	30	568558 568915 567202	28.38 28.4 28.31	28.36	0.0472	0.166	94.5

Table S-VII. LOD and LOQ data for clobetasol propionate, miconazole nitrate, salicylic acid

Drug	Clobetasol propionate (μg mL^{-1})	Miconazole nitrate (μg mL^{-1})	Salicylic acid (μg mL^{-1})
LOD	1.49	8.72	3.37
LOQ	4.53	26.43	10.22

Table S-VIII. Robustness data for ±0.1 mL min^{-1} in flow rate

parameters	Peak area (n = 3) CP	MN	SA	Mean ± SD CP	MN	SA	% RSD CP	MN	SA
Minus flow rate (1.1 mL min^{-1})	40,620 41,293 41,477	72,770 72,382 72,040	5,67,480 5,67,278 5,69,550	41,130 ± 451.153	72,397 ± 365.241	5,68,103 ± 1257.49	1.1069	0.5045	0.22135
Plus, the flow rate (1.3 mL min^{-1})	41,623 40,892 41,154	71,521 71,856 71,541	5,68,254 5,69,001 5,68,819	41,223 ± 370.352	71,693 ± 187.905	5,68,691 ± 389.52	0.8984	0.26229	0.06849

Table S-IX. Robustness data for ±2 °C temperature

Parameters	Peak area (n = 3)			Mean ± SD			% RSD		
	CP	MN	SA	CP	MN	SA	CP	MN	SA
Minus temp. (28 °C)	41,518 41,271 40,785	71,652 70,458 71,431	5,70,445 5,70,629 5,71,112	41,191 ± 372.93	71,180 ± 635.24	5,70,729 ± 344.48	0.9054	0.89244	0.06036
Plus, temp. (32 °C)	41,145 39,918 41,391	71,121 72,644 72,718	5,73,696 5,72,581 5,65,393	40,818 ± 789.06	72,161 ± 901.42	5,70,557 ± 4506.48	1.9331	1.24919	0.78984

Table S-X. Robustness data for ±2 nm wavelength

Parameters	Peak area (n = 3)			mean ± SD			% RSD		
	CP	MN	SA	CP	MN	SA	CP	MN	SA
Minus wavelength (280 nm)	41,518 41,293 41,271	71,841 72,247 72,121	5,68,753 5,68,481 5,69,946	41,361 ± 136.69	72,070 ± 207.811	5,69,060 ± 779.258	0.3305	0.28835	0.13694
Plus, wavelength (285 nm)	40,892 40,785 41,623	71,950 72,148 72,382	5,75,985 5,76,672 5,78,581	41,100 ± 456.08	72,160 ± 216.25	5,77,079 ± 1345.082	1.1097	0.29968	0.23308

Journal of the Serbian Chemical Society
JSCS-info@shd.org.rs • www.shd.org.rs/JSCS
J. Serb. Chem. Soc. *90* (1) 77–94 (2025)
JSCS–5821
Original scientific paper
Published 28 January, 2025

Determination of indacaterol from inhaler capsules by square-wave voltammetry at the surface of the boron-doped diamond electrode

HEMN ABDULAZEEZ H. BARZANİ[1], HOSHYAR SAADİ ALİ[2] and YAVUZ YARDIM[3]*

[1]*Lebanese French University, College of Health Science, Department of Medical Laboratory Science, 44001 Erbil, Iraq,* [2]*Knowledge University, College of Science, Department of Medical Laboratory Science, Kirkuk Road, 44001, Erbil, Iraq and* [3]*Yuzuncu Yil University, Faculty of Pharmacy and Science, Department of Analytical Chemistry, 65080 Van, Turkey*

(Received 21 February, revised 4 April, accepted 23 September 2024)

Abstract: This research paper presents an electroanalytical investigation using the voltammetric method to quantify indacaterol maleate (IND) employing an unmodified boron-doped diamond (BDD) electrode. IND exhibited a distinct, irreversible oxidation peak at approximately 1.06 V (*vs*. Ag/AgCl) in a 0.1 mol L^{-1} phosphate buffer solution (PBS) with a pH of 2.5, as demonstrated by cyclic voltammetry (CV). A hypothetical mechanism for the electro-oxidation of IND, based on data gathered from CV investigations, was suggested. The square wave-adsorptive stripping voltammetric technique achieved acceptable linearity in PBS (pH 2.5) at approximately 0.90 V. The methodology demonstrated linearity within the concentration range of 1.0 to 30.0 μg mL^{-1} (equivalent to 1.97×10^{-6}–5.89×10^{-5} mol L^{-1}) and yielded a limit of detection (*LOD*) of 0.22 μg mL^{-1} (equivalent to 4.33×10^{-7} mol L^{-1}). The proposed method's applicability was assessed through the sensing of IND in drug formulations.

Keywords: indacaterol maleate; square-wave voltammetry; boron-doped diamond electrode; inhaler capsules.

INTRODUCTION

In the realm of medical research, it is widely acknowledged that inhaled bronchodilators hold a position of utmost importance as the fundamental symptomatic maintenance therapy for the effective management of chronic obstructive pulmonary disease (COPD). This particular ailment, which afflicts a significant portion of the population, is recognized for its characteristic slow and progressive development of airflow limitation.[1] COPD is characterized by its non-

* Corresponding author. E-mail: yavuzyardim2002@yahoo.com
https://doi.org/10.2298/JSC240221090B

-reversible nature and usually corresponds with an aberrant inflammatory reaction within the lungs triggered by exposure to harmful particles and gases.[2,3] Therapeutic interventions aimed at relaxing bronchial smooth muscle and improving lung function in patients with COPD have demonstrated rapid, productive, and durable therapeutic results.[4,5]

Indacaterol maleate (IND), 5-[2-[(5,6-diethyl-2,3-dihydro-1*H*-inden-2-yl)-amino]-1-hydroxyethyl]-8-hydroxyquinolin-2(1*H*)-one, $C_{24}H_{28}N_2O_3 \cdot C_4H_4O_4$, molecular weight 508.6 as a maleate salt (392.49 as a base). The compound exhibits a water solubility of approximately 7.9×10^{-3} g L^{-1}, a log *P* value of 4.0 and pK_a values of 9.8 for the essential group and 8.5 for the acidic group. Functioning as a long-acting β2-agonist (LABA), it stimulates *β*2-receptors, increasing intracellular cyclic adenosine monophosphate (cAMP) levels.[6] Recently approved in the European Union, this novel medication is a pre-metered single-unit dose capsule-based ultra-long-acting *β*2-agonist for once-daily oral inhalation. It has gained approval from the United States Food and Drug Administration (FDA) for COPD management,[7,8] leading to improved bronchial muscle tissue smoothness. This once-daily regimen, containing an FDA-approved LABA dose, enhances health status, reduces dyspnea and lowers exacerbations in COPD patients.[9–11]

The deposition of inhaled medications in the pulmonary system is influenced by factors such as particle dimensions, inhalation apparatus structure, patient maneuver proficiency and airflow dynamics.[12,13] Various pharmacokinetic techniques assess lung deposition and therapeutic equivalency of inhaled treatments, using human plasma or urine as experimental samples.[14,15] Another method evaluates the effects of inhalation strategies and flow rates. IND, a recently developed long-acting *β*2-agonist, exhibits prolonged action due to its strong binding affinity to lipid raft domains in the airway membrane, impacting comparative lung deposition and systemic exposure upon inhalation.[16]

IND, administered at a daily dosage of 150–300 μg, demonstrates a slow dissociation rate from receptors.[17] Swift absorption upon oral administration results in extensive dispersion throughout the body, with an apparent volume of distribution of 10±4 L kg^{-1}. Plasma protein binding percentages range from 94.1 to 95.3 % and 95.1 to 96.2 %.[17] Extensive metabolic processes lead to the formation of the phenolic *O*-glucuronide. Primary adverse effects, especially in overdose cases, include nasopharyngitis, tremor, cough, upper respiratory tract infection, headache, tachycardia, palpitations, nausea, hypokalemia, vomiting, sleepiness, acidosis, cardiac arrhythmias, metabolic issues and hyperglycemia. IND's notable safety contributes to enhanced patient compliance and therapeutic effectiveness. Recent studies indicate potential advantages of IND in COPD management.[18,19]

Drug combinations, such as IND and glycopyrronium, are employed for the symptomatic management of chronic obstructive pulmonary disorder in adults. It

is crucial to emphasize consulting local prescribing information to obtain specific details on contraindications, special cautions, and precautions related to these medications. In this context, it is imperative to employ analytical methodologies that effectively substantiate the pharmacological attributes, therapeutic effectiveness and tolerability investigations concerning IND.[20] A limited range of physicochemical approaches has been documented for the quantification of IND in biological fluids and pharmacological formulations. Some involve high-performance liquid chromatography (HPLC) with various detectors,[21–27] ultra-performance liquid chromatography-diode array detector (UPLC-DAD),[28] ion-pairing chromatographic (IPC),[29] spectrophotometry,[30–32] capillary electrophoresis (CE),[33,34] potentiometry[35] and voltammetry.[36] However, only one study has shown that IND examination can be conducted using voltammetric approaches.[36]

In analytical chemistry, a critical application involves the analysis of pharmaceutical and clinical specimens.[37] Determining chemicals in various matrices is vital in pharmaceutical and medical sciences. For reliability and sensitivity, analytical techniques for such analyses should be applicable across a wide range of concentrations, quick, simple (suitable for non-experts) and cost-effective.[38] Electrochemical techniques, particularly voltammetric approaches, have gained prominence in drug and clinical analyses due to their benefits, including simplification, cost-effectiveness, rapid evaluation and high sensitivity. Understanding the oxidation and reduction mechanisms of pharmacologically relevant chemicals is equally crucial.[39]

A boron-doped diamond (BDD) electrode is a type of carbonaceous electrode material with unique properties, including a wide operational range in both cathodic and anodic directions. The research focuses on key aspects, such as investigating low background current, analyzing low signal-to-noise ratio, developing a process suitable for corrosive conditions, and establishing a repeatable response for electrochemical evaluations, all commonly observed in BDD. The wide operational range of the electrode material allows the analysis of electroactive compounds often inaccessible using conventional carbon and metal electrodes.[40] In contrast to many electrode materials like glassy carbon, BDD electrodes have limited capacity for modifications using modifying chemicals. This limitation stems from the restricted adsorption of both the sample and the modifying agent on the surfaces of BDD electrode materials.[41]

According to available data, a singular electroanalytical technique for detecting IND has been documented. The primary objective of this study is to establish a viable approach for IND analysis using a voltammetric modality that is cost-effective, expeditious and easy to apply. The effectiveness of the methodology was demonstrated through its application in a pharmaceutical formulation specimen under ideal conditions.

EXPERIMENTAL

Chemicals

The standard reference of IND maleate (ReagentPlus®, 99.81 %), purchased from ChemScene LLC (USA), was obtained. Due to its limited solubility in water, IND stock solutions were prepared by dissolving in ethanol to a concentration of 1.0 mg mL^{-1} and refrigerating until intended use. IND stock solutions were produced in the selected electrolytes at a reduced concentration. Ultra-pure water from a Milli-Q water purifying system (Millipore, resistivity ≥ 18.2 MΩ cm) was used for preparation. Analytical-grade materials, including 0.1 mol L^{-1} acetate buffer solution (ABS) at pH 4.7, 0.1 mol L^{-1} phosphate buffer solution (PBS) at pH 2.5 and 7.4, and 0.04 mol L^{-1} Britton–Robinson (BR) buffer among pH 2.0–8.0, were utilized. Voltammetric investigations conducted in aqueous buffer solutions were found to be independent of the presence of ethanol. The concentration of ethanol in the voltammetric cell was consistently kept below 10 % of the total volume.

Apparatus and analytical procedure

Using an electrochemical analyzer, specifically the μAutolab type III manufactured by Metrohm Autolab B.V. in the Netherlands, electrochemical measurements were conducted. The obtained data were collected and processed using GPES software, version 4.9. Baseline correction and smoothing of the peaks observed in the square wave voltammograms were performed using the Savicky–Golay method with a peak width of 0.01 V. For the electrochemical measurements, a three-electrode glass cell system with a 10 mL volume, maintained at ambient temperature, was employed. The cell configuration included a boron-doped diamond (BDD) working electrode, provided by Windsor Scientific Ltd., UK, with a boron content of 1000 ppm and a diameter of 3 mm. A platinum wire served as the auxiliary electrode, and an Ag/AgCl electrode immersed in a 3 mol dm^{-3} NaCl solution, specifically the RE-1 model from BAS, USA, functioned as the reference electrode. All electrode potentials in the paper are referred to Ag/AgCl scale. The impact of employing BDD electrode pretreatment methodologies on IND signals was examined. At the beginning of each experimental day, the BDD electrode underwent treatment, subjecting it to an anodic potential of 1.8 V for 180 s, followed by exposure to a cathodic potential of –1.8 V for an equivalent duration. The activation procedure began with anodic polarization to cleanse the fouled BDD surface, restoring its reactivity for subsequent use. Subsequently, cathodic polarization was applied to regenerate the primarily hydrogen-terminated electrode surface, inducing its hydrophobic characteristics. To mitigate potential detriment to the electrode surface, a rudimentary manual cleansing procedure was executed before each electrochemical assessment. The BDD electrode was gently abraded using a moistened, sleek polishing cloth (BAS velvet polishing pad) for less than 60 s, followed by a thorough water rinse.[44] This implemented methodology ensures the attainment of a pristine electrode surface, preventing any potential adsorption of IND or its oxidation byproducts.

The CV approach in the anodic direction (from 0.2 to 1.4 V) was employed to assess the electrochemical behavior and reaction mechanism of IND on the surface of a boron-doped diamond (BDD) electrode in the selected supporting electrolyte. Subsequently, square wave voltammetry (SWV) was used within a potential range of 0.25 to 1.30 V to identify the optimal conditions, including the supporting electrolyte (at various pH levels), and to compare differential pulse voltammetry (DPV), accumulation variables and SWV parameters, all aimed at enhancing the sensitivity for IND detection. Additionally, the analytical capability of the

developed methodology, the influence of interfering substances, and the practical applicability of the technique were evaluated.

To perform SW-AdSV sensing of IND, a three-electrode configuration was immersed in a voltammetric cell containing IND solutions and phosphate buffer solution (PBS) at pH 2.5. The voltammetric cell, under open-circuit conditions with a deposition time of 30 s, received a voltage application and was stirred at 500 rpm. After 10 s of equilibration, anodic scanning was recorded within the potential range of 0.25 to 1.3 V. The electrochemical analyses were conducted in triplicate, and the detection of IND in actual samples was carried out using the standard addition methodology.

Preparation of samples

The IND sample was obtained from a local pharmacy in the form of inhaler capsules (Inbroxa®, Deva Co., Türkiye), each containing 150 μg (195 μg IND maleate). The mass of ten capsules was precisely measured. After carefully extracting the outer shell of the capsules, the mass of the empty capsules was determined. The net weight per capsule was calculated by subtracting the weight of the empty capsules from the overall net weight. An appropriate amount of powder, equivalent to 1.0 mg of IND maleate, was quantified and placed in a 1-mL test tube, then saturated with the requisite volume of ethanol. Continuous agitation for approximately 15 min ensured complete dissolution. An appropriate volume of the solution (50 μL) was transferred to an electrochemical cell containing 10 mL of phosphate buffer solution (PBS) at pH 2.5 and was examined on the same day of preparation using the developed method. The content of IND in the sample was determined using the standard addition method, by adding IND at concentrations of 1.0, 2.5, 5.0, 7.5, 10 and 15 μg mL^{-1} to the product. Consequently, SW-AdS voltammograms were recorded after each addition.

RESULTS AND DISCUSSION

Investigation of the electrochemical behavior of IND on the boron-doped diamond electrode

Applying the CV method to the BDD electrode allowed us to evaluate the electrochemical properties of IND. Using a voltage scanning rate of 100 mV s^{-1}, three sequential cyclic voltammograms (CVs) for 100 μg mL^{-1} (1.97×10^{-4} mol L^{-1}) of IND were recorded between 0.2 and 1.40 V in 0.1 mol L^{-1} PBS at pH 2.5. The IND compound exhibited a distinct anodic peak (I_p) at a potential of approximately 1.06 V, following the completion of the initial cycle in the anodic direction (depicted in Fig. 1A). If the reversed scan does not exhibit a reduction peak, it indicates that the IND electrode reactions at the BDD electrode surface are irreversible, distinguishing them from other surface reactions. During the acquisition of sequential CVs, a decrease in the oxidation signal was observed, and potentially attributed to the adsorption of IND and/or its oxidation products on the surface of the BDD electrode, leading to deactivation, possibly through fouling. The investigation focused on exploring the influence of potential scan rate (v) on the anodic peak current of 100 μg mL^{-1} IND, employing CV in a 0.1 mol L^{-1} PBS solution (pH 2.5) to ensure that the anodic peak current could be clearly observed and measured with sufficient sensitivity and accuracy. The volt-

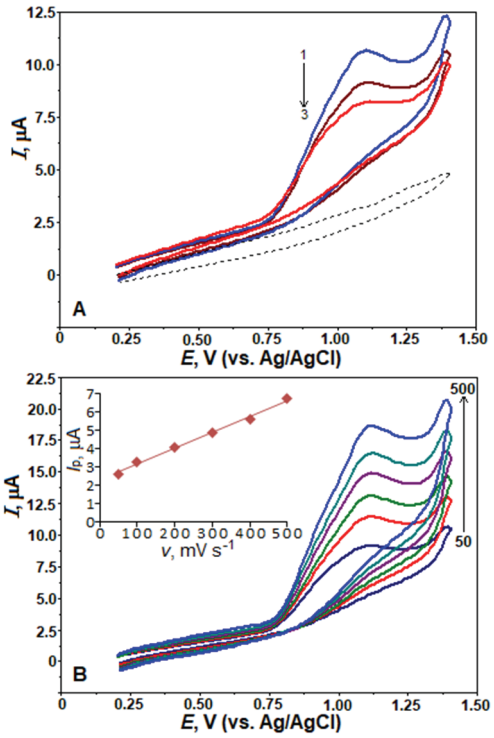

Fig. 1. A) The first three cycles (1–3) of cyclic voltammograms of 100 µg mL^{-1} IND, scan rate 100 mV s^{-1} (the dashed lines indicate the background current); B) cyclic voltammograms of 100 µg mL^{-1} IND recorded at 50, 100, 200, 300, 400 and 500 mV s^{-1} (the inset shows the linear relationship between I_p *versus* v).

age scan rate varied from 50 to 500 mV s^{-1}, as shown in Fig. 1B. The peak current responses increased as v was raised, indicating the irreversibility of the electrode process, which is evident from the voltammograms where the oxidation peak potentials of IND shifted to slightly more positive values with increased scan rates. The relationship between the peak currents (I_p) and the v was linear, as depicted by the equation I_p (µA) = 0.008v (mV s^{-1}) + 1.623, r = 0.993 (n = 6). This suggests that the electrode process is controlled by adsorption. Furthermore, a linear relationship was also evident when I_p was plotted against the square root of the scan rate ($v^{1/2}$), following the equation I_p (µA) = 0.290$v^{1/2}$ (mV s^{-1}) – – 0.693, r = 0.992, indicating the involvement of a diffusion mechanism alongside adsorption. The plot of log I_p versus log v, which is represented by the equation log I_p (µA) = 0.581log v (mV s^{-1}) – 0.806, r = 0.996, further confirms this behaviour. The slope of approximately 0.59 suggests that the oxidation of IND is governed by both diffusion and adsorption processes, a dual mechanism corroborated by data from our group and others, not only for boron-doped diamond electrodes,[40] but also for various carbon-based electrode materials.[42,43] To find the quantity of electrons (n) engaged in the IND oxidation phenomenon at the BDD electrode, the n value was computed utilizing the equation αn = 47.7/ /(E_p – $E_{p/2}$), where E_p – $E_{p/2}$ was determined to be 52 mV. In an entirely irrev-

ersible electrode process, the α (charge transfer coefficient) is conventionally regarded as 0.5. Upon analysis, it was determined that the n value, denoting the stoichiometric coefficient, amounted to 1.83, which approximates to 2. This finding aligns with the observations reported in a prior investigation pertaining to the oxidation mechanism of IND.[36] Although the primary objective of this investigation does not encompass a comprehensive examination of the mechanism underlying the electrochemical oxidation of IND, an assessment will be conducted utilizing the CVs obtained at the BDD electrode. Furthermore, by examining the voltammetric behaviour of IND at a titanium(IV) oxide nanoparticle (TiO_2-NPs) and the ionic liquid (IL) *n*-hexyl-3-methylimidazolium hexafluorophosphate modified carbon paste electrode (referred to as TiO_2-NPs–––IL-MCPE), it is possible to propose a preliminary oxidation reaction scheme for IND at a BDD electrode (as shown in Scheme 1).

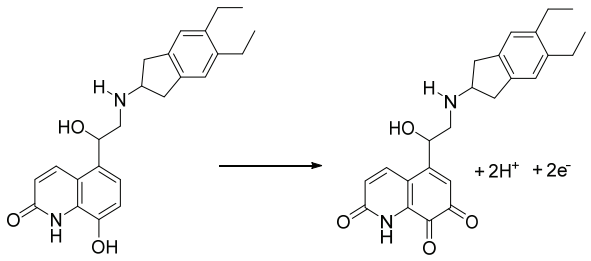

Scheme 1. Proposed oxidation reaction scheme for IND on the BDD electrode.

The SW mode stripping waveform was employed in the subsequent stage of the study due to its improved sensitivity, lower consumption of electroactive molecules and quicker examination rate. Preliminary examinations revealed that the untreated BDD electrode was ineffective in countering passivation challenges, especially when confronted with high IND concentrations. The repeatable and sensitive response of the BDD surface could be compromised by the electrochemical oxidation of this compound, leading to potential passivation without pretreatment. SW-AdSV was employed to examine the efficacy of three distinct methodologies for a concentration of 30 μg mL^{-1} (5.89×10^{-5} mol L^{-1}) of IND under open-circuit conditions, with an accumulation duration of 30 s. This period was chosen because it was sufficient for effective accumulation. The concentration was selected because SWV is a very sensitive technique compared to CV, enabling effective manipulation and examination of the reaction on the BDD electrode surface in PBS at a pH of 2.5. Initially, anodic pretreatment (APT) was implemented on the BDD electrode surface, involving subjecting the electrode to a potential of 1.8 V for 180 s in a solution of 0.5 mol L^{-1} H_2SO_4. Secondly, the evaluation assessed the effects of cathodic pretreatment (CPT) on the BDD electrode surface, involving applying a potential of –1.8 V for 180 s in a 0.5 mol L^{-1}

H_2SO_4 solution. In due course, the BDD electrode surface underwent anodic pretreatment followed by cathodic pretreatment. During the preceding pretreatment protocol, the BDD electrode surface underwent necessary preparations. Notably, the most discerning outcomes were achieved through this procedure for the analysis of IND, as depicted in Fig. 2. Henceforth, this protocol was perpetuated in the subsequent segments of the investigation.

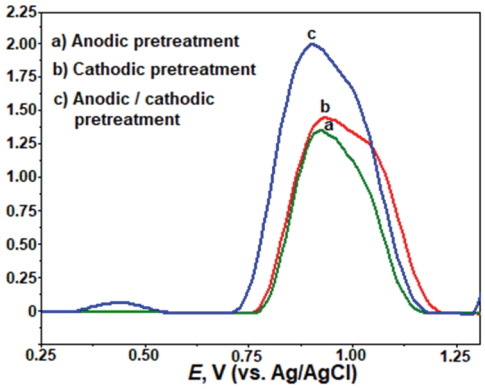

Fig. 2. The electrochemical pretreatments were employed to acquire the SW voltammograms at a concentration of 30.0 μg mL^{-1} of IND in a 0.1 mol L^{-1} PBS solution at a pH of 2.5. The BDD electrode was used for this purpose. During the open-circuit condition, the duration of accumulation is 30 s. The parameters for SWV are as follows: ΔE_s = 10 mV; ΔE_{sw} = 40 mV; f = 50 Hz.

To determine the optimal medium, the SW-AdSV technique was applied to investigate how various pH levels influence the oxidation peak current responses of IND at the BDD electrode interface. SW-AdSVs were recorded within a potential range of 0.25 to 1.30 V, utilizing a BR buffer with a pH spanning from 2.0 to 8.0. These measurements were conducted for a 30.0 μg mL^{-1} solution of IND, as depicted in Fig. 3A. As observed in Fig. 3A, the peak current densities exhibited a decline upon reaching a pH of 5.0, followed by an increment until reaching a pH of 7.0, and subsequently experienced a decline once again. Upon examining the anodic peak potentials within the pH range of 2.0–8.0, a discernible shift towards more negative values was observed with an increase in pH. The given equation illustrates the linear relationship between the pH values within the range of 2.0 to 8.0 and the anodic peak potentials of IND. It can be expressed as E_p (V) = –0.067pH + 1.083, r = 0.992.

The equation mentioned above demonstrates the pH-dependent nature of the IND oxidation on the BDD electrode. Based on experimental results, it can be inferred that the electrode reaction involved an equimolar exchange of protons and electrons. This is supported by the observed slope of 0.067 V/pH, which closely aligns with the expected value of 0.059 V. The observed anodic peak of IND in this investigation is likely attributed to the oxidation of the hydroxyl moiety within the molecular structure. A plausible mechanism outlining the electrooxidation of IND was presented in the Scheme 1. Fig. 3B illustrates the SW-AdSV signals obtained in different electrolyte solutions. Oxidation peak

potentials of 0.89, 0.77 and 0.57 V were observed, along with anodic peak currents of 2.09, 1.62 and 1.82 μA in 0.1 mol L^{-1} PBS pH 2.5, ABS pH 4.7 and PBS pH 7.4, respectively. The obtained outcomes are consistent with those achieved in the BR buffer. As can be seen from Fig. 3A and B, the most distinctive SW--AdSV signal of 30 μg mL^{-1} IND on the BDD electrode with the maximum peak current and the best shaped peak was obtained at PBS pH 2.5. Hence, this buffer was used for further studies.

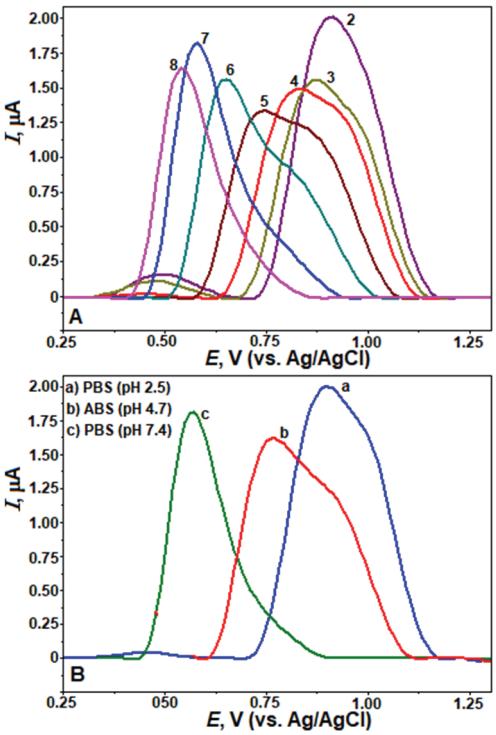

Fig. 3. SW-AdS voltammograms of 30 μg mL^{-1} IND in BR buffer pH 2.0–8.0 (A), and in various supporting electrolytes at different pH values (B) on BDD electrode. Other operating conditions were as indicated in Fig. 2.

A comparative analysis was performed to assess the relative sensitivity of two pulse approaches, namely DPV and SWV, in detecting the anodic peak currents of IND. The experimental findings revealed that the anodic peak currents of IND measured by SWV were approximately 5.58 times greater than those obtained by DPV (Fig. 4). Henceforth, further investigation shall be conducted employing the SWV methodology.

Considering the adsorptive properties of IND on the BDD electrode, we investigated the effect of accumulation time (t_{acc}) and deposition potential (E_{acc}) on 20.0 μg mL^{-1} IND. This concentration was chosen to ensure that the adsorptive properties of IND were clearly observable, facilitating a thorough investigation of the effects of t_{acc} and d E_{acc} on the electrochemical behavior of IND, while

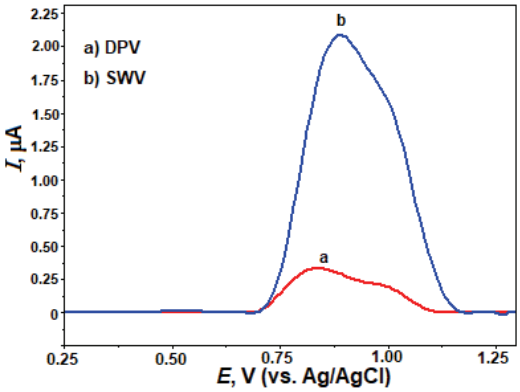

Fig. 4. DPAdS (a) and SW-AdS (b) voltammograms of 30 µg mL^{-1} IND in 0.1 mol L^{-1} PBS at pH 2.5 on the BDD electrode. DPV parameters: modulation amplitude, 50 mV; step potential, 8 mV and modulation time 0.05 s. Other operating conditions were as indicated in Fig. 2.

adhering to the ideal experimental conditions. Utilizing the open-circuit condition, an investigation was conducted to examine the impact of t_{acc} on the signal related to the anodic peak within the time frame of 0–150 s. It was observed that the peak currents increased up to 30 s. After reaching this point, they remained approximately constant, indicating that the electrode surface might have reached saturation. Therefore, t_{acc} of 30 s was selected for all the SW-AdSV experiments. Subsequently, the peak currents showed a state of near-constant stability, indicating that the IND had achieved saturation on the BDD electrode (Fig. 5A).

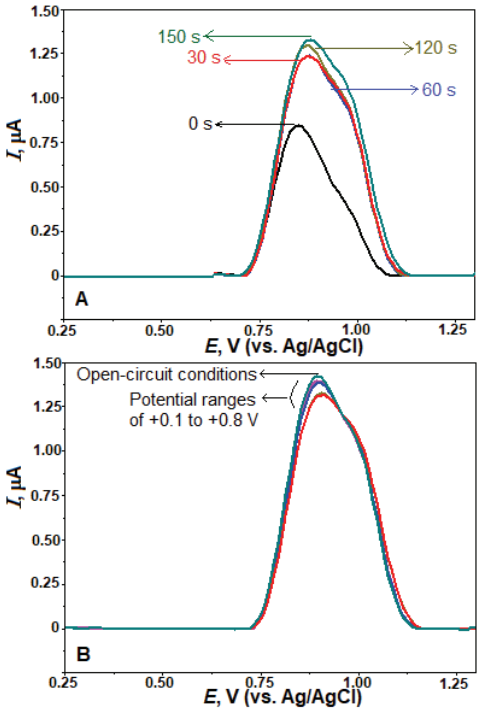

Fig. 5. SW-AdS voltammograms for 20 µg mL^{-1} IND recorded in PBS (pH 2.5) after different accumulation period, t_{acc} in the range 0–150 s at open-circuit condition (A) and after different accumulation potentials, E_{acc} at open-circuit condition or over the potential range 0.1 to 0.8 V using t_{acc} at 30 s (B). The other operating conditions as indicated in Fig. 2.

Conversely, the anodic peak current was evaluated at the specified E_{acc} by subjecting the system to voltage values ranging from 0.1 to 0.8 V or by maintaining open-circuit conditions for a duration of 30 s. The current associated with the IND peak remained relatively constant throughout its operating range, indicating that this parameter had a negligible effect on the determination of the compound (Fig. 5B). Accordingly, the oxidation peak currents were ascertained while the system was in an open-circuit state. Consequently, endeavors were undertaken to enhance the impact of pulse parameters under the given conditions (frequency, f, 25–125 Hz; step potential, ΔE_s, 8–18 mV; square-wave amplitude, ΔE_{sw}, 30–80 mV). The optimization was conducted through the manipulation of a singular parameter while keeping all other variables in a state of constancy. Maximum sensitivity and best peak shape were obtained via the following parameters: f = = 75 Hz; ΔE_s = 12 mV and ΔE_{sw} = 50 mV (Fig. 6A–C).

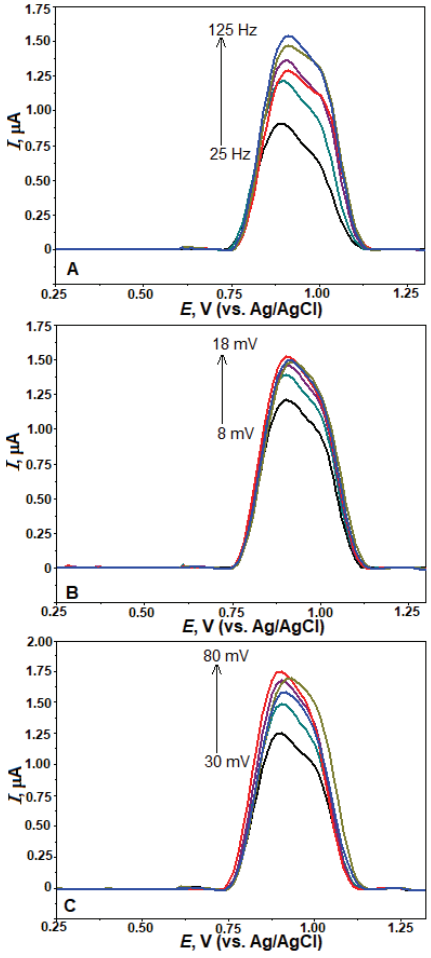

Fig. 6. SW-AdS voltammograms for 20 μg mL^{-1} IND were recorded in PBS (pH 2.5) using different frequencies (f, between 25-125 Hz) (A), step potentials, ΔE_s, 8–18 mV (B) and pulse amplitudes ΔE_{sw}, 30–80 mV (C) on the BDD electrode. The accumulation duration under open-circuit conditions was 30 s.

Analytical applications

The results presented thus far were utilized to assess the analytical performance by observing the concentration oxidation peaks of IND. Fig. 7 displays the voltammetric responses, while Table I elucidates the corresponding analytic parameters. The limits of detection (*LOD*) and quantification (*LOQ*) were determined using analytical curve data in the following manner: the *LOD* was calculated by multiplying three times the standard deviation of the peak currents (from ten runs) for the lowest concentration within the linear range and then dividing it by the slope of each calibration curve.

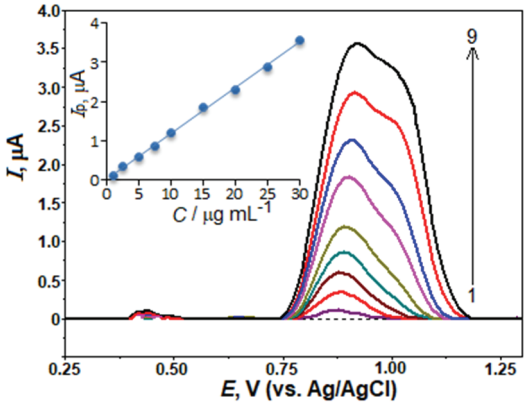

Fig. 7. SW-AdSW voltammograms for the IND concentrations of 1.0, 2.5, 5.0, 7.5, 10.0, 15.0, 20.0, 25.0 and 30.0 μg mL^{-1} (1–9) for the oxidation peaks in 0.1 mol L^{-1} PBS at pH 2.5 on the BDD electrode. The depiction of background current is represented by the delineation of dotted lines. The IND quantification calibration charts are visually presented in the inset. During the open-circuit condition, the duration of accumulation is 30 s, and the SWV parameters: ΔE_s = = 12 mV; ΔE_{sw} = 50 mV; f = 75 Hz.

Repeatability (intra-day precision) was investigated by conducting six tests on the same day, while intermediate precision (inter-day precision) was determined by conducting three assays on five separate days for 1.0 μg mL^{-1} IND under ideal experimental conditions (Table I). The positive outcomes demonstrate that the BDD electrode is an effective electrochemical sensor for accurately determining the amounts of IND in samples taken from the wild.

TABLE I. Analytical variables determined for the oxidation peak of IND by utilizing SW-AdSV on the BDD electrode; E_p = peak potential; LWR = linear working range; LRE = linear regression equation; r = correlation coefficient; *LOQ* = limit of quantification; *LOD* = limit of detection

Analytical parameter	Value
E_p	+0.90 V
LWR	1.0–30.0 μg mL^{-1} (1.97×10^{-6}–5.89×10^{-5} mol L^{-1})
LRE	I_p (μA) = 0.118C (μg mL^{-1}) + 0.011
r	0.999
LOQ	0.73 μg mL^{-1} (1.44×10^{-6} mol L^{-1})
LOD	0.22 μg mL^{-1} (4.33×10^{-7} mol L^{-1})
Intra-day repeatability (*RSD* / %, n = 10)	4.83
Inter-day repeatability (*RSD* / %, n = 5)	5.58

To the best of our knowledge, previous studies have not employed bare electrodes for determining IND. Our analysis, utilizing non-modified BDD electrodes, produced results showing lower sensitivity in terms of the limit of detection compared to prior findings[36] (see Table II). However, the suggested methodology exhibits enhanced practicality, cost-effectiveness, and efficiency in measuring IND compared to earlier research endeavors. Additionally, the use of non-modified BDD electrodes eliminates the need for complex electrode modifications, reducing both the time and costs associated with electrode preparation.

TABLE II. A contrast of the IND's linear range and detection limit with the previously reported work; TiO_2-NP–IL-MCPE: titanium (IV) oxide nanoparticles ionic liquid carbon paste electrode, BDDE: boron-doped diamond electrode

Electrode	Linear range (mol L^{-1})	LOD / mol L^{-1}	Ref.
TiO_2-NP–IL-MCPE	2×10^{-9}–2×10^{-5}	5×10^{-10}	36
BDDE	1.97×10^{-6}–5.89×10^{-5}	4.33×10^{-7}	This work

It is essential to highlight that the presence of electroactive chemicals has the potential to disrupt the peak of the analyte in both drug formulations and biological samples. The evaluation of IND determination selectivity on the BDD electrode involved investigating the impact of various molecules and ions commonly found in pharmaceutical formulations or urine specimens. This was accomplished by observing the alterations in the IND signal when these substances were introduced to a solution containing 1.0 μg mL^{-1} IND at concentration ratios of 1:1, 1:10 and 1:25 (IND:interfering compound) under ideal conditions. The determination of the tolerance limit was assessed through the quantification of the concentration at which an average deviation of ±5 % was observed in the oxidation signal of IND. The experimental findings revealed that the presence of a 25-fold surplus of anions and cations (chloride, nitrate, sodium, potassium, magnesium, calcium, copper, iron and aluminum) did not exert a noteworthy influence on the anodic response of IND. Furthermore, it was noted that the impacts of substances commonly present in pharmaceutical compositions, such as microcrystalline cellulose, gelatine, and lactose monohydrate, on the anodic currents response of IND were inconsequential when a 25-fold surplus was employed. The investigation focused on the effects of ascorbic acid (AA), dopamine (DOP) and uric acid (UA), which are commonly found in urine samples. The experimental findings indicate that the oxidation peak currents of IND were influenced by the separate solutions of DOP, AA, as well as UA while equimolar concentration was employed (Fig. 8). As a result, the direct use of the developed method for IND determination may be limited when analyzing real biological samples, such as plasma or urine. If needed, this issue can be addressed before the voltammetric measurement of IND by employing appropriate sep-

aration techniques. However, this limitation does not apply when analyzing pharmaceutical samples.

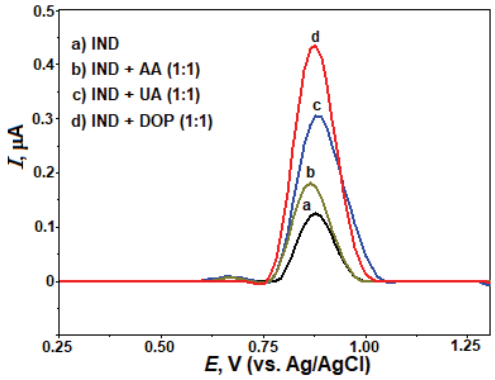

Fig. 8. SW-AdS voltammograms of 1.0 µg mL^{-1} IND (a) in the presence of equimolar concentration ascorbic acid (b), uric acid (c) and dopamine (d) in 0.1 mol L^{-1} PBS at pH 2.5. Other operating conditions as indicated in Fig. 7.

In consideration of these findings, a range of standard addition techniques were employed to assess the concentration of the IND compound in the sample. The samples were prepared as described in the Experimental (*Preparation of samples*). In Fig. 9, we present a graphical representation of the standard addition technique applied to evaluate the oxidation signal of IND. Additionally, we provide a set of sample SW voltammograms for reference.

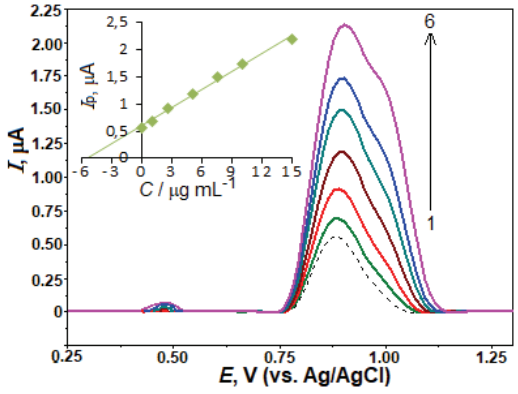

Fig. 9. SW-AdSV of the diluted drug sample (dashed lines) and evaluated by using standard additions of 1.0 and 15.0 µg mL^{-1} IND (1–6) in 0.1 mol L^{-1} PBS at pH 2.5. Inset depicts the result of analysis by standard addition method. Other operating conditions as indicated in Fig. 7.

Standard solutions of IND (ranging from 1.0 to 15.0 µg mL^{-1}) were prepared in an appropriate electrolyte solution and introduced into a voltammetric cell containing 10 mL of the sample solution. The voltammetric responses were then recorded to confirm the reliability of the established methodology for practical use. To quantify the recovered IND, we compared the concentrations of the spiked and unadulterated compounds. After carefully diluting the samples, we determined that the inhaler capsules contained 203.58 µg of IND maleate (with a relative standard deviation of 2.9 %). This value is 4.4 % higher than the manu-

facturer's stated label value of 195.0 μg, indicating that the measured amount is very close to the labeled value. The proximity of the measured value to the labeled value is considered close, as it falls within a 5 % range, which is generally acceptable in quality control assessments. The determined values for IND recovery are presented in Table III. As a result, the proposed methodology ensures the accuracy of voltammetric determination of IND in the commercial pharmaceutical formulation sample.

TABLE III. The inhaler capsule samples were subjected to analysis using SWV on the BDD electrode after treatment with standard solutions of the active pharmaceutical ingredient (IND)

Added[a], μg mL^{-1}	Expected[b], μg mL^{-1}	Found[c], μg mL^{-1}	Recovery ± *RSD*, %
0	-----	5.22	-
1.0	6.22	6.24	100.3 ± 4.7
2.5	7.72	7.94	102.9 ± 3.8
5.0	10.22	10.66	104.3 ± 3.6

[a]IND concentration in the electrochemical cell containing 10 mL of PBS; [b]the value to be obtained after adding IND to the electrochemical cell containing 10 mL of PB; [c]the average of three replicate measurements

CONCLUSIONS

Developing a novel and alternative electroanalytical approach for IND evaluation required the use of the SW-AdSV methodology, paired with the BDD electrode. The anti-fouling features of the BDD electrode, achievable through a quick and easy cleaning approach, are crucial to highlight in this context. These characteristics allow the electrode to be utilized for an extended amount of time while maintaining consistent responses. The BDD electrode provided an electrochemical method for IND measurement that did not require any modifications and effectively replaced the need for modified electrodes. The results revealed an anodic peak corresponding to IND when using CV at a positive potential of approximately 1.06 V in a pH 2.5 PBS as the supporting electrolyte. Additionally, the evaluated analytical parameters demonstrated good sensitivity, with a *LOD* of 4.33×10^{-7} and satisfactory repeatability (*RSD* = 4.83 %). The developed technique was tested for the evaluation of IND in a commercially available pharmaceutical composition and demonstrated excellent recoveries. Furthermore, the provided method has the potential for immediate use without the need for waste formation, complex sample extraction, increased chemical consumption, or expensive instrumentation. Evidently, the BDD electrode offers a straightforward, speedy, and cost-effective method for the routine pharmaceutical examination of IND.

И З В О Д

ОДРЕЂИВАЊЕ ИНДАКАТЕРОЛА НА ПОВРШИНИ БОРОМ ДОПИРАНЕ ДИЈАМАНТСКЕ ЕЛЕКТРОДЕ, У КАПСУЛАМА ЗА ИНХАЛАЦИЈУ, КОРИШЋЕЊЕМ ВОЛТАМЕТРИЈЕ ПРАВОУГАОНИХ ТАЛАСА

HEMN ABDULAZEEZ H. BARZANİ[1], HOSHYAR SAADİ ALİ[2] и YAVUZ YARDIM[3]

[1]Lebanese French University, College of Health Science, Department of Medical Laboratory Science, 44001 Erbil, Iraq, [2]Knowledge University, College of Science, Department of Medical Laboratory Science, Kirkuk Road, 44001, Erbil, Iraq и [3]Yuzuncu Yil University, Faculty of Pharmacy and Science, Department of Analytical Chemistry, 65080 Van, Turkey

У овом раду је приказано електроаналитичко испитивање помоћу волтаметријске методе за квантификацију индакатерол малеата (IND) употребом немодификоване дијамантске електроде допиране бором (BDD). Применом цикличне волтамерије IND је показао јасан, иреверзибилан пик оксидације на приближно 1,06 V (у односу на Ag/AgCl) у 0,1 mol L^{-1} раствору фосфатног пуфера (PBS), pH 2,5. Предложен је хипотетички механизам електрооксидације IND на основу података добијених цикличном волтаметријом. Применом адсорпционе стрипинг волтаметрије правоугаоних таласа постигнута је прихватљива линеарност у PBS раствору на pH 2,5 на приближно 0,90 V. Добијена је линеарност у опсегу концентрација од 1,0 to 30,0 μg mL^{-1} (еквивалентно $1{,}97\times10^{-6}$–$5{,}89\times10^{-5}$ mol L^{-1}) и граница детекције од 0,22 μg mL^{-1} (еквивалентно 4.33×10^{-7} mol L^{-1}). Применљивост предложене методе је процењена одређивањем IND у формулацијама лекова.

(Примљено 21. фебруара, ревидирано 3. априла, прихваћено 23. септембра 2024)

REFERENCES

1. C. F. Vogelmeier, G. J. Criner, F. J. Martinez, A. Anzueto, P. J. Barnes, J. Bourbeau, B. R. Celli, R. Chen, M. Decramer, L. M. Fabbri, P. Frith, D. M. G. Halpin, M. V. López Varela, M. Nishimura, N. Roche, R. Rodriguez-Roisin, D. D. Sin, D. Singh, R. Stockley, J. Vestbo, J. A. Wedzicha, A. Agusti, *Am. J. Respir. Crit. Care. Med*. **195** (2017) 557 (http://dx.doi.org/10.1164/rccm.201701-0218PP)
2. R. A. Pauwels, A.S. Buist, P. M. Calverley, C. R. Jenkins, S. S. Hurd, *Am. J. Respir. Crit. Care Med*. **163** (2001) 1256 (http://dx.doi.org/10.1164/ajrccm.163.5.2101039)
3. N. M. Siafakas, P. Vermeire, N. A. Pride, P. Paoletti, J. Gibson, P. Howard, D. S. Postma, *Eur. Respir. J.* **8** (1995) 1398 (http://dx.doi.org/10.1183/09031936.95.08081398)
4. S. P. Newman, *Ther. Deliv* .**8** (2017) 647 (http://dx.doi.org/10.4155/tde-2017-0037)
5. D. E. Lowe, S. M. Ernst, C. Zito, J. Ya, I. J. Glomski, *Infect. Immun*. **81** (2013) 4408 (http://dx.doi.org/10.1128/iai.00484-13)
6. G. R. Greenstein, *Res. Rev.* **21 (**2007) 40 (https://doi.org/10.1108/09504120710775534)
7. M. Cazzola, M. G. Matera, J. Lötvall, *Expert Opin. Investig. Drugs* **14** (2005) 775 (http://dx.doi.org/10.1517/13543784.14.7.775)
8. B. A. Chowdhury, S. M. Seymour, T. M. Michele, A. G. Durmowicz, D. Liu, C. J. Rosebraugh. *New Engl. J. Med.* **365** (2011) 2247 (http://dx.doi.org/10.1056/NEJMp1109621)
9. K. M. Beeh, J. Beier, *Adv. Ther.* **26** (2009) 691 (http://dx.doi.org/10.1007/s12325-009-0044-3)
10. R. Dahl, D. Jadayel, V. K. Alagappan, H. Chen, D. Banerji, *Int. J. Chron. Obstruct. Pulmon. Dis.* **2013** (2013) 501 (http://dx.doi.org/10.2147/COPD.S49615)

11. D. P. Tashkin, *Expert Opin. Pharmacother*. **11** (2010) 2077 (http://dx.doi.org/10.1517/14656566.2010.499358)
12. J. Haughney, D. Price, N. C. Barnes, J. C. Virchow, N. Roche, H. Chrystyn, *Respir. Med.* **104** (2010) 1237 (http://dx.doi.org/10.1016/j.rmedc.2010.10.004)
13. J. Shur, S. Lee, W. Adams, R. Lionberger, J. Tibbatts, R. Price, *AAPS J.* **14** (2012) 667 (http://dx.doi.org/10.1208/s12248-012-9379-9)
14. H. Chrystyn, *Br. J. Clin. Pharmacol.* **51** (2001) 289 (https://doi.org/10.1046/j.1365-2125.2001.01304.x)
15. D. Acerbi, G. Brambilla, I. Kottakis, *Pulm. Pharmacol. Ther.* **20** (2007) 290 (http://dx.doi.org/10.1016/j.pupt.2006.05.005)
16. B. J. Lipworth, C. M. Jackson, *Br. J. Clin. Pharmacol.* **48** (1999) 866 (http://dx.doi.org/10.1046/j.1365-2125.1999.00098.x)
17. J. Dwivedi, D. Patel, K. Patel, D. Meshram, *Int. J. Phar. Chem. Res.* **3** (2017) 447 (https://www.ijpacr.com/files/21-07-2017/06.pdf)
18. J. Jiang, L. Li, H. Yin, R. Woessner, C. Emotte, R. Li, H. Pei, *Eur. J. Drug. Metab. Pharmacokin.* **40** (2015) 203 (http://dx.doi.org/10.1007/s13318-014-0197-6)
19. M. Cazzola, L. Calzetta, C. P. Page, M.G. Matera, *Expert Opin. Drug. Metab. Toxicol.* **10** (2014) 129 (http://dx.doi.org/10.1517/17425255.2014.865723)
20. J. E. Frampton, *Drugs* **74** (2014)465 (http://dx.doi.org/10.1007/s40265-014-0194-8).
21. W. G. Ammari, Z. Al-Qadhi, M. Khalil, R. Tayyem, S. Qammaz, G. Oriquat, H. Chrystyn, *J. Aerosol Med. Pulm. Drug. Deliv*. **28** (2015) 202 (http://dx.doi.org/10.1089/jamp.2014.1153)
22. V. Gajula, K. Thejomoorthy, *Int. J. Pharm. Drug. Anal*. **9** (2021) 71 (http://dx.doi.org/10.47957/ijpda.v9i2.464)
23. C. Emotte, O. Heudi, F. Deglave, A. Bonvie, L. Masson, F. Picard, O. Kretz, *J. Chromatogr., B* **895** (2012)1 (http://dx.doi.org/10.1016/j.jchromb.2012.02.025)
24. S. Zayed, F. Fouad, F. Belal, *J. Iranian Chem. Soc.* **18** (2021) 1251 (http://dx.doi.org/10.1007/s13738-020-02107-6)
25. Y. A. Salem, D. T. El-Sherbiny, D. R. El-Wasseef, S. M. El-Ashry, *Int. J. Pharm. Sci. Res.* **6** (2015) 1324 (http://www.ijpsr.info/docs/IJPSR15-06-11-101.pdf)
26. N. M. A. El-Abasawy, K. A. M. Attia, A. A. Abouserie, A. El-Olemy, A. O. Elsayed, *World. J. Pharm. Pharm. Sci.* **7** (2018) 166 (https://www.wjpps.com/Wjpps_controller/abstract_id/8580)
27. S. Zayed, F. Belal, *Chem. Cent. J.* **11** (2017) 36 (http://dx.doi.org/10.1186/s13065-017-0264-6)
28. M. Tarek, N. S. Ghoniem, M. A. Hegazy, H. A. Wagdy, *J. Chromatogr. Sci.* **62** (2024) 676 (http://dx.doi.org/10.1093/chromsci/bmad072)
29. Y. A. Salem, M. E. Hammouda, N. M. Saleh, M. A. A. El-Enin, S. M. El-Ashry, *Spectrochim. Acta, A* **204** (2018) 464 (http://dx.doi.org/10.1016/j.saa.2018.06.078)
30. S. M. El-Ashry, D. R. El-Wasseef, D. T. El-Sherbiny, Y. A. Salem, *Luminescence* **30** (2015) 891 (http://dx.doi.org/10.1002/bio.2838)
31. D. R. Acharya, D. B. Patel, V. V. Patel, *J. Drug Deliv. Ther.* **2** (2012) (http://dx.doi.org/10.22270/jddt.v2i1.49)
32. M. F. A. Ghany, L. A. Hussein, N. Magdy, H. Z. Yamani, *Spectrochim. Acta, A* **157** (2016) 251 (http://dx.doi.org/10.1016/j.saa.2016.01.002)
33. T. Güray, M. Tunçel, U.D. Uysal, *J. Food Drug Anal*. **26** (2018) 842 (http://dx.doi.org/10.1016/j.jfda.2017.08.002)

34. S. Zayed, F. Belal, *Microchem. J.* **155** (2020) 104779 (http://dx.doi.org/10.1016/j.microc.2020.104779)
35. M. El Dosoky, *Al-Azhar*, *J. Pharm. Sci.* **57** (2018) 104 (http://dx.doi.org/10.21608/ajps.2018.46632)
36. S. A. Atty, M. F. A. Ghany, L. A. Hussein, N. Magdy, H. Z. Yamani, *J. Iranian Chem. Soc.* **17** (2020) 383 (http://dx.doi.org/10.1007/s13738-019-01778-0)
37. H. A. Barzani, H. Saadi Ali, C. Şahin, M. Kıran, Y. Yardım, *Electroanalysis* **34** (2022) 1280 (http://dx.doi.org/10.1002/elan.202100608)
38. P. T. Pınar, H. A. Barzani, H. S. Ali, Y. Yardım, *Monatsh. Chem.* **154** (2023) 1225 (http://dx.doi.org/10.1007/s00706-023-03126-8)
39. H. A. Barzani, Y. Yardım, *Diam. Relat. Mater.* **132** (2023) 109658 (http://dx.doi.org/10.1016/j.diamond.2022.109658)
40. H. S. Ali, Y. Yardım, *Food Chem.* **441** (2024) 138262 (http://dx.doi.org/10.1016/j.foodchem.2023.138262)
41. T. Kondo, *Curr. Opin. Electrochem.* **32** (2022) 100891 (http://dx.doi.org/10.1016/j.coelec.2021.100891)
42. S. S. Shankar, B. E. Kumara Swamy, K. R. Mahanthesha, T. V. Sathisha, C. C. Vishwanath. *Anal. Bioanal. Electrochem.* **5** (2013) 19 (https://www.yumpu.com/en/document/view/28386629/acetanilide-modified-carbon-paste-electrode-for-the-electrochemical-)
43. L. P. Silva, F. C. Vicentini, B. C. Lourencao, G. G. Oliveira, M. R. V. Lanza, O. Fatibello-Filho. *J. Solid State Electrochem.* **20** (2016) 2395e2402 (https://doi.org/10.1007/s10008-016-3143-5)
44. S. K. Kamal, Y. Yardım. *Maced. J. Chem. Chem. Eng.* **41** (2022) 163 (http://dx.doi.org/10.20450/MJCCE.2022.2565).

Journal of the Serbian Chemical Society
JSCS-info@shd.org.rs • www.shd.org.rs/JSCS
J. Serb. Chem. Soc. 90 (1) 95–107 (2025)
JSCS–5822
Original scientific paper
Published 1 February, 2025

Monte Carlo optimization based QSAR modeling of the cytotoxicity of acrylic acid-based dental monomers

MIRJANA BOŠKOVIĆ[1], SAŠA STANKOVIĆ[1], JELENA V. ŽIVKOVIĆ[2] and ALEKSANDAR M. VESELINOVIĆ[2]*

[1]*Department for Prosthetic Dentistry, Faculty of Medicine, University of Niš, Bulevar Dr Zorana Đinđića 81, 18000 Niš, Serbia and* [2]*Departmant of Chemistry, Faculty of Medicine, University of Niš, Bulevar Dr Zorana Đinđića 81, 18000 Niš, Serbia*

(Received 1 March; revised 15 April; accepted 2 June 2024)

Abstract: Acrylic acid derivatives are extensively utilized as initial monomers in dental materials. Nevertheless, these substances exhibit cytotoxicity towards different cell types, a phenomenon that must be reduced in future materials. The primary objective of this research is to establish a QSAR model for the prediction of cytotoxic effects and to identify molecular fragments and descriptors with mechanistic interpretations that play a role in cytotoxic effects. The Monte Carlo optimization technique employed QSAR models that are not reliant on conformation. These models utilized both molecular graph-based and SMILES-based descriptors. By employing a variety of statistical methodologies, an assessment of the predictive capabilities and resilience of the established QSAR models was achieved. The demonstrated numerical values used for their validation underscore the strong suitability of these QSAR models. The Monte Carlo optimization technique effectively identified molecular fragments represented in QSAR modeling through the use of SMILES notation, elucidating their impact on cytotoxicity, both positively and negatively. Given that the majority of molecular databases adhere to this molecular structure conformation, the featured QSAR models can serve as a rapid and precise screening tool for novel dental monomers.

Keywords: QSAR; cytotoxicity; dental material; composite resin; SMILES; Monte Carlo optimization.

INTRODUCTION

Numerous dental procedures necessitate the utilization of polymers, which are composed of methacrylate-based monomers, including monomethacrylates or dimethacrylates.[1,2] Some of the most frequently employed monomers in this con-

* Corresponding author. E-mail: aveselinovic@medfak.ni.ac.rs
https://doi.org/10.2298/JSC240301057B

text include urethane dimethacrylate (UDMA), triethylene glycol dimethacrylate (TEGDMA), 2-hydroxyethyl methacrylate (HEMA), bisphenol-A glycidil dimethacrylate (Bis-GMA), as well as other more recent functionalized monomers.[1–3] The biocompatibility of these materials holds significant relevance for clinical applications, considering that oral tissues come into direct contact with them.[4] In dental practice, direct restorations involving dental adhesives and resin composites involve interaction with sensitive dentin-pulp complexes and acrylic acid-based monomers. This interaction can result in the diffusion of monomers from the restorative material through dentinal tubules, potentially causing adverse effects on pulp cells and compromising tooth vitality.[5,6] Literary sources indicate certain biological effects, such as the mutagenicity of various monomers and the genotoxicity and estrogenicity of Bis-GMA.[7] The primary mechanism underlying the free-radical polymerization reaction in dental materials is associated with methacrylate-based monomers. This chemical process may be linked to incomplete monomer conversion, resulting in the presence of unreacted monomers.[8] Given that these unreacted monomers have the potential to leach into nearby aqueous environments and enter the body, they may pose risks of toxicity.[9] Incomplete polymerization not only has the potential to result in the removal of monomers from the formed polymer but can also contribute to the natural degradation of the matrix. The degradation of the resin phase in composites within the oral environment may take place through processes like hydrolysis and aging, which can lead to the release of monomers as a result of the breakdown of the organic matrix.[9,10] Resin composite biodegradation may be linked to allergic reactions, bone loss or irritation of the oral mucosa.[12] The physicochemical characteristics of dental materials, particularly concerning the molecular size of monomers, their chemical compositions and the presence of various functional groups, are the primary factors contributing to biodegradation and the subsequent leaching of materials.[13,14] In the realm of dental materials research, biocompatibility investigations tied to quality control hold immense significance. To achieve this goal, cytotoxicity testing, which assesses cellular responses and the potential for cell death in response to new material formulations, plays a vital role in the development of novel dental materials. Minimizing and preventing cytotoxic effects are paramount, particularly in specialized fields such as endodontics and operative dentistry.[15]

One of the primary challenges with studies on cytotoxic effects is that they require a substantial amount of labor and time.[16] To streamline and enhance the screening of novel molecules in the development of materials, a practical solution is the adoption of in silico-based modeling approaches, such as quantitative structure–activity relationships (QSAR).[17] In contemporary QSAR studies, models are constructed by utilizing a variety of molecular descriptors derived from a specific molecule's structure. These descriptors have their own advantages and

limitations. Subsequently, they are transformed into a mathematical equation that correlates the biological activities of the examined molecules with their chemical attributes (molecular descriptors).[18,19] The development of a QSAR model necessitates not only a strong predictive capacity, robustness and goodness of fit but also a well-defined domain of applicability. Additionally, QSAR modeling is subject to regulation by the Organization for Economic Co-Operation and Development (OECD), which has established several criteria that must be met for a QSAR model to be deemed valid. One of the key criteria involves the mechanistic interpretation of molecular descriptors, which pertains to the utilization of descriptors linked to molecular structure and relevant molecular fragments.

In recent years, a Monte Carlo optimization method, where the analyzed activity is regarded as a random event, has gained prominence as a promising approach in QSAR modeling. This approach relies on a conformation-independent methodology and employs optimal descriptors derived from topological molecular characteristics, as well as molecules represented in the simplified molecular input line entry system (SMILES) notation.[20,21] The described method offers a significant advantage over more commonly used approaches due to its simplicity and efficiency. Additionally, this method can identify molecular fragments (calculated as SMILES notation descriptors) that influence the studied activity and can be linked to the chemical structures of the compounds under investigation The primary objective of this research is to create a conformation-independent QSAR model utilizing the Monte Carlo optimization method for predicting the cytotoxic effects of acrylic acid-based monomers. Furthermore, another key goal of this research was to identify SMILES notation descriptors linked to molecular fragments that exert both positive and negative impacts on cytotoxic effects.

EXPERIMENTAL

To initiate the development of suitable QSAR models, a total of 39 acrylic acid-based dental monomers were initially drawn using ACD/ChemSketch software version 11.0. These molecules were subsequently transformed into SMILES notation using the same software.[22] The chemical structures of the compounds utilized for QSAR modeling, along with their corresponding SMILES notations, can be found in Table S-I (Supporting material to this paper). In this QSAR modeling, the pertinent cytotoxic effect activity was assessed using pIC_{50} values against Hela S3 cell lines, data from the literature were converted to pIC_{50} values, calculated as pIC_{50} = –log IC_{50}. Once we completed the construction of the relevant database, we proceeded to perform three distinct random divisions of the main molecule database into two sets: the training set, comprising 29 compounds (75 %), and the test set, comprising 10 compounds (25 %). We also assessed the normality of the activity distribution, following the method outlined in the published literature.[23]

To create conformation-independent QSAR models, we utilized the CORAL software (correlation and Logic, http://www.insilico.eu/coral), which is founded on the Monte Carlo method and its algorithm, considering the relevant activity as a random occurrence. We con-

sidered two categories of molecular descriptors derived from the molecular graph and SMILES notation. Concerning molecular graphs, we defined invariants as local graph invariants, including the Morgan extended connectivity index of increasing order (EC0), path numbers of lengths 2 and 3 (p2, p3), valence shells of ranges 2 and 3 (s2, s3), and the code of nearest neighbors (NNCk). In recent years, the SMILES notation has gained prominence as one of the most convenient representations, particularly in the field of chemoinformatics. SMILES notation is regarded as an appealing alternative to the traditional molecular graph representation. This characteristic is of great significance in medicinal chemistry because establishing correlations between molecular fragments and molecular graph-based descriptors can be quite complex.

The local SMILES attribute, entitled the "SMILES atom", is a SMILES string fragment with one ('C', 'N', '=') or two ('Cl', 'Br', '@@') symbols which cannot be decomposed further for conducting individual analyses. The calculation of DCW, one of the simplest local molecular descriptors, is performed with a mathematical function of the mentioned SMILES atoms. In essence, the approach translates every character found in the SMILES string into a numerical descriptor. To cite an example, the propionic acid molecule represented by the SMILES notation as "CCC(=O)O" can be considered. In this specific case, the calculation of the DCW could be performed on the basis of the individual CW characters:

$$DCW(\text{“CCC(=O)O”}) = CW(\text{“C”}) + CW(\text{“C”}) + + CW(\text{“C”}) + CW(\text{“(“}) + \\ + CW(\text{“=“}) + CW(\text{“O”}) + CW(\text{“)”}) + CW(\text{“O”}) \quad (1)$$

While valuable information is obtained from single atom-based local SMILES descriptors, in order to reveal more complex local chemical environments, one needs to go beyond individual atoms. Molecular fragments which significantly contribute to the overall molecular properties may be defined by combining two or three consecutive SMILES atoms. *DCW*s can then be calculated by using such fragments, further enhancing the information content available for QSAR modeling. For instance, propionic acid represented by the SMILES notation as "CCC(=O)O" could be considered. Through the combination of consecutive SMILES atoms, the following molecular fragments can be defined:

$$DCW(\text{“CCC(=O)O”}) = CW(\text{“CC”}) + CW(\text{“CC”}) + CW(\text{“C(“}) + \\ + CW(\text{“(=“}) + CW(\text{“=O”}) + CW(\text{“O)”}) + CW(\text{“)O”}) \quad (2)$$

When consecutive SMILES atoms are combined in order to define molecular fragments, there are significant advantages, although it is crucial to make certain considerations. For example, fragments such as "CO" and "OC" (or "CCO" and "OCC") are to be treated as distinct entities, which might lead to unreliable QSAR models and inaccurate representations. A normalized combination of SMILES atoms is applied in order to address this particular issue. The utilization of this approach ensures that the fragments are identified and consistently encoded irrespective of the order in which the atoms occur. In order to achieve this, specific algorithms need to be used, or it could be achieved by administering the SMILES notation canonization, which defines a unique order on the basis of the atomic symbols.[20,21] Global SMILES attribute based descriptors encompass broader characteristics of the whole molecule, such as whether specific functional groups or atom combinations are present or absent.[20,21] The information available for QSAR modeling can significantly be enriched through the incorporation of both local and global SMILES-based descriptors. What is more, SMILES notation-based molecular descriptors present a mechanistic interpretation, considering that this particular feature is in correlation with molecular fragments.[20,21] The numerical value of every SMILES notation descriptor that a molecule has contributes to the correlation weight of the

said molecule (*DCW*), which is defined as the sum of all the defined correlation weights (*CW*) of SMILES descriptors:

$$DCW(T,N_{epoch}) = zCW(\text{ATOMPAIR}) + xCW(\text{NOSP}) + yCW(\text{BOND}) + tCW(\text{HALO}) + rCW(\text{HARD}) + \alpha\Sigma CW(S_k) + \beta\Sigma CW(SS_k) + \gamma\Sigma CW(SSS_k) \quad (3)$$

where z, x, y, t, α, β and γ are numbers 1 (yes) or 0 (no), while their values determine whether the specific SMILES descriptor is used in the development of the model. Symbol S_k represents one SMILES notation symbol (or two that are inseparable), and is related to the local descriptors. These local descriptors also represent linear combinations of two or three SMILES atoms, represented by symbols SS_k and SSS_k, respectively. This study includes the following global SMILES notation-based descriptors: HALO, ATOMPAIR, BOND, HARD and NOSP, all defined in accordance with the published methodology.[20,21] The molecules' *DCW* was calculated by using Eq. (4) because the QSAR model development in this study was performed by combining both the SMILES notation (global and local) and the local graph invariant descriptors, considering that this hybrid molecular descriptor approach ensures the development of more accurate and robust QSAR models than the ones based on a single type of descriptor:

$$DCW(T,N_{epoch}) = \Sigma CW(S_k) + \Sigma CW(SS_k) + \Sigma CW(SSS_k) + \Sigma CW(EC0_k) + \Sigma CW(PT2_k) + \Sigma CW(PT3_k) + \Sigma CW(VS2_k) + \Sigma CW(VS3_k) + \Sigma CW(NNC_k) \quad (4)$$

In addition to the aforementioned symbols: S_k, SS_k and SSS_k, Eq. (2) uses the following symbols as well: the Morgan connectivity index of the zero order (with the hydrogen suppressed graph) – $EC0_k$, paths in the lengths of 2 and 3 – $PT2_k$ and $PT3_k$; valence shells 2 and 3 – $VS2_k$ and $VS3_k$; nearest neighbors – NNC_k. The calculation of all the above-defined molecular descriptors was made with the CORAL software (http://www.insilico.eu/coral). In this study, we employed all SMILES notation-based descriptors, encompassing local, global and HARD-index descriptors. A notable characteristic of the resulting QSAR model, developed using the Monte Carlo method, is the calculation of correlation weight (*CW*), which assigns a numerical value to each of the optimal descriptors utilized.[21] The methodology for accomplishing this process involves the generation of appropriate random numbers and assessing the fraction of numbers that conform to certain properties. In this process, *CW* values are randomly allocated to all employed optimal descriptors, encompassing both molecular graph-based and SMILES notation-based descriptors, in each individual Monte Carlo run. The Monte Carlo optimization procedure is then extended to compute the numerical data for the correlation weights, which aim to maximize the correlation coefficient between the studied activity and the employed optimal descriptors. In this context, the Monte Carlo method relies on two parameters: threshold (T) and the number of epochs (N_{epoch}).

In the creation of QSAR models, we explored values ranging from 0 to 10 for T and from 0 to 70 for Nepoch. The process of identifying the most predictive combination of T and N_{epoch} was determined based on a methodology outlined in published references.[24-26] The primary objective of any QSAR modeling process is to create a robust model that can predict the properties of new molecules with objectivity, reliability, and precision. To assess the quality of the developed QSAR models, we employed the following methods: internal validation using the training set, external validation using the validation set and data randomization through a *Y*-scrambling test. We accomplished this by employing various statistical parameters, including the correlation coefficient (r^2), cross-validated correlation coefficient (q^2), standard error of estimation (s), mean absolute error (*MAE*), Fischer ratio (F), root-mean-square error (*RMSE*), R_m^2, and *MAE*-based metrics.[23,27-31] Recently, a novel criterion known

as the index of ideality of correlation (*IIC*) has been proposed for evaluating the predictive capacity of QSAR models.[25,26] This criterion takes into account not only the correlation coefficient but also the distribution of data points relative to the diagonal line, in the coordinates of observed and calculated values for the studied endpoint. The set of correlation weights: *CW*(*x*) are coefficients producing a maximal value of the target function within the Monte Carlo optimization procedure and the target function can be defined as:

$$TF = R_{\text{training}} + R_{\text{invisible-training}} - \left| R_{\text{training}} - R_{\text{invisible-training}} \right| \times \text{Const.} \quad (5)$$

where R_{training} is the correlation coefficient between endpoint and the *DCW*(*T**, *N**) for compounds in the training set, the $R_{\text{invisible-training}}$ corresponds to the same parameter in the invisible training set; praxis has shown that Const. = 0.1 is a more or less satisfactory choice for manifold computational experiments with different endpoints. However, while keeping the value of Const. invariant, the target function can be modified as:

$$TF_{\text{m}} = TF + IIC \times \text{Const.} \quad (6)$$

with the IIC parameter calculated as the following form:

$$IIC_{\text{test}} = r_{\text{test}} \times \frac{\min({}^{-}MAE_{\text{test}}, {}^{+}MAE_{\text{test}})}{\max({}^{-}MAE_{\text{test}}, {}^{+}MAE_{\text{test}})} \quad (7)$$

where, using the differences:

$$\Delta_k = \text{Observed}_k - \text{Calculated}_k \quad (8)$$

With data available for all Δ_k values in the test set, it is possible to compute the sum of negative and positive Δ_k values, akin to the calculation of mean absolute error (*MAE*):

$${}^{-}MAE_{\text{test}} = \frac{1}{{}^{-}N} \sum\nolimits_{k=1}^{{}^{-}N} |\Delta_k|, \quad \Delta_k < 0, \; {}^{-}N \text{ is the number of } \Delta_k < 0 \quad (9)$$

$${}^{+}MAE_{\text{test}} = \frac{1}{{}^{+}N} \sum\nolimits_{k=1}^{{}^{+}N} |\Delta_k|, \quad \Delta_k \geq 0, \; {}^{-}N \text{ is the number of } \Delta_k \geq 0 \quad (10)$$

RESULTS AND DISCUSSION

The concept of the applicability domain (*AD*) plays a pivotal role in guiding the selection of molecules.[32–34] To establish the *AD*, we followed a published methodology and confirmed that all molecules in this study fell within the defined *AD* range, with no outliers identified.[21] Utilizing the least squares method, we present the most optimal QSAR models for the studied activity, with respect to the *T* and N_{epoch} values, in the form:

$$\text{Split 1: p}IC_{50} = -0.3378(\pm 0.0938) + 0.0194(\pm 0.0005) \times DCW(4,9) \quad (11)$$

$$\text{Split 2: p}IC_{50} = 0.2293(\pm 0.0350) + 0.0411(\pm 0.0005) \times DCW(1,6) \quad (12)$$

$$\text{Split 3: p}IC_{50} = 0.3749(\pm 0.0353) + 0.0326(\pm 0.0005) \times DCW(1,18) \quad (13)$$

The values of the statistical metrics used to assess the quality of the developed QSAR models for predicting the cytotoxicity of acrylic acid-based dental monomers are presented in Table S-I. These metrics suggest that the method employed was successful in creating a QSAR model with good reproducibility, which was further validated using the concordance correlation coefficient. The

predictability of the developed QSAR model was assessed based on the values presented in Table S-II of the Supplementary material, confirming the model's validity. Additionally, the model was classified as valid using *MAE*-based metrics. We conducted the ultimate evaluation of the developed QSAR models, both for the training and the test set, using the index of ideality of correlation and obtained values that indicate the high predictive potential of the developed QSAR models. Furthermore, we conducted *Y*-randomization, involving the random shuffling of *Y* values in 1000 trials across ten separate runs, to gauge the robustness of the developed QSAR models.[23] The values shown in Table S-III of the Supplementary material suggest that there was no chance correlation among the developed models. Among the statistical methods used, the most favorable QSAR model was derived from the first split. Notably, the best model was achieved with a *T* value of 4, and the most suitable N_{epoch} value was determined to be 9. The most successful Monte Carlo optimization runs (with the highest r^2 values) for the developed QSAR models from all splits are visually depicted in Figs. 1–3.

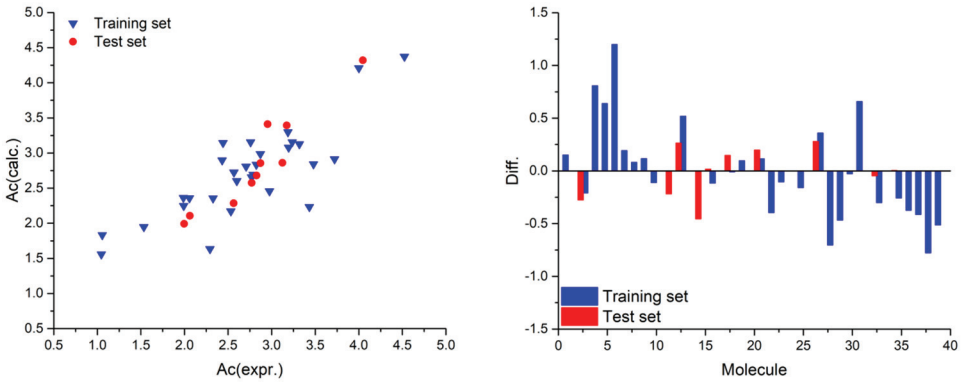

Fig. 1. Graphical presentation of the best Monte Carlo optimization run (the highest value for r^2) for the developed QSAR model for Split 1. (*Ac*(expr.) – experimental value for molecule pIC_{50}; *Ac*(calc.) – calculated value for molecule pIC_{50} using developed QSAR model; Diff. = *Ac*(expr.) – *Ac*(calc.).

One of the primary objectives of this study was to identify molecular fragments, characterized as the SMILES notation's optimal descriptors, that exert both positive and negative effects on the studied activity.[21,35–37] The complete list of molecular descriptors, which are derived from both the SMILES notation and the molecular graph, can be found in Table S-IV of the Supplementary material. An illustration of the calculation of a molecule's summarized correlation weight (*DCW*) and the studied activity (pIC_{50}) is provided in Table I. In this example, molecular graph-based descriptors were excluded to facilitate a more straightforward interpretation.

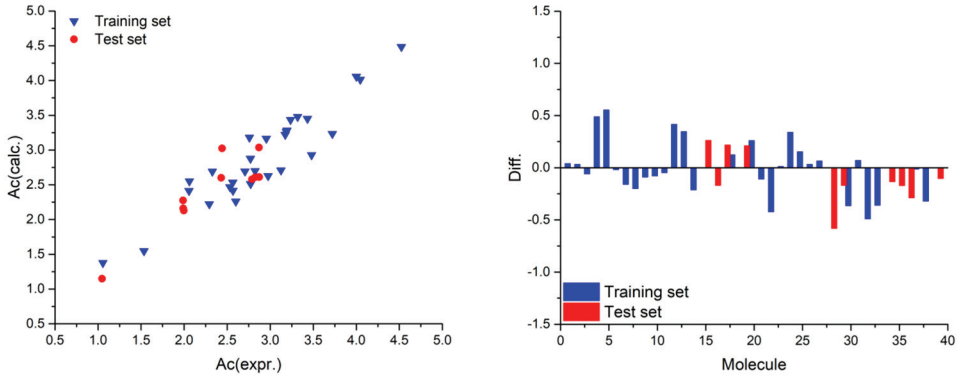

Fig. 2. Graphical presentation of the best Monte Carlo optimization run (the highest value for r^2) for the developed QSAR model for Split 2. (*Ac*(expr.) – experimental value for molecule pIC_{50}; *Ac*(calc.) – calculated value for molecule pIC_{50} using developed QSAR model; Diff. = *Ac*(expr.) – *Ac*(calc.).

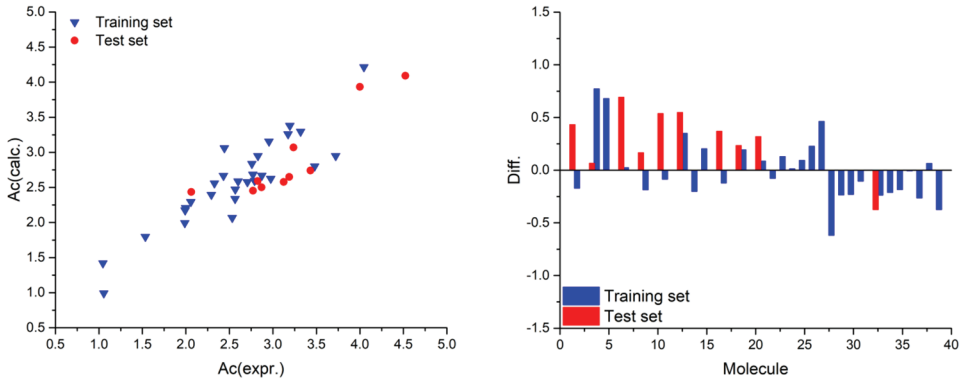

Fig. 3. Graphical presentation of the best Monte Carlo optimization run (the highest value for r^2) for the developed QSAR model for Split 3. (*Ac*(expr.) – experimental value for molecule pIC_{50}; *Ac*(calc.) – calculated value for molecule pIC_{50} using developed QSAR model; Diff. = *Ac*(expr.) – *Ac*(calc.).

Following the published methodology, we categorized the obtained SA_ks as promoters of the cytotoxicity of acrylic acid-based dental monomers.[21,35–37] In Table II, we have listed selected SAKs along with their mechanistic interpretations, while the complete list can be found in Table S-II. We have provided an analysis of the contribution of molecular fragments to the cytotoxicity of acrylic acid-based dental monomers in Fig. 4. In the presented figure, green denotes groups that have a positive influence, while red denotes groups that have a negative influence on the studied effect. As mentioned, each SA_K contributes its *CW* value.

TABLE I. Example of *DCW* calculation

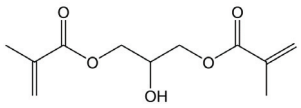

IUPAC name: [2-hydroxy-3-(2-methylprop-2-enoyloxy)propyl]--2-methylprop-2-enoate
SMILES notation: OC(COC(=O)C(=C)C)COC(=O)C(=C)C
DCW = 57.88841
pIC_{50}(calc.) = 2.6094

SA_k	*CW*(SA_k)	SA_k	*CW*(SA_k)	SA_k	*CW*(SA_k)	SA_k	*CW*(SA_k)
1000100000	2.0407	BOND10000	1.411	Cmax.0.....	0.0745	O...=.....	–0.9669
(.....	2.3831	C...(.....	–0.8598	HALO00000	3.1001	O...C...(...	1.0934
(...C...(...	–0.5923	C...(...=...	–0.916	Nmax.0.....	1.8318	O...C.....	–0.922
++O---B2=	2.9389	C...(...C...	1.4187	NOSP01000	1.9941	Omax.5.....	0
=...(.....	–0.7396	C.....	–0.8583	O...(.....	–0.6732	Smax.0.....	2.3577
=.....	–0.0911	C...=...(...	–0.9573	O...(...C...	2.1158	O...=...(...	–0.5599
=...C...(...	2.1233	C...=.....	4.2232	O.....	–0.5305		
=...O...(...	–0.4744	C...O...C...	–0.6593				

TABLE II. Mechanistic interpretation of selected SA_ks

Promoters of pIC_{50} increase		Promoters of pIC_{50} decrease	
(...(..... (.....	Simple molecular branching and complex	(...O...(...	Complex molecular branching with oxygen atom involving
		++++N---B2==	Presence of independent nitrogen atom and double bond in molecule
C...(..... (...C...(...	Molecular branching on carbon atom	++++N---O===	Presence of independent nitrogen and oxygen atoms in molecule
		=.....	Double bond
++++O---B2==	Presence of independent oxygen atom and double bond in molecule	=...(.....	Double bond involved in molecular branching
1.....	Presence of ring in molecule	=...O...(...	Double bond with oxygen atom involved in molecular branching
C...1..... C...1...C...	Presence of ring in molecule with carbon atoms	C...(...=...	Double bond with carbon atom involved in molecular branching
N...C...C...	Ethyl amine fragment	C.....	Carbon atom
C...=..... C...=...C...	Double bond with carbon atom	N.....	Nitrogen atom
		O.....	Oxygen atom
C...N...C...	Sequence of carbon-nitrogen-carbon atoms	N...C.....	Methyl amine group, or sequence of nitrogen-carbon atom
c..... c...c.....	Aromatic carbon in molecular structure	c...(...C...	Branched carbon atom bounded to aromatic carbon
c...C..... c...O.....	Carbon or oxygen atom bounded to aromatic carbon	c...O...C...	Methyl group bounded to aromatic carbon

Based on the results obtained from QSAR modeling, the SMILES notation descriptors associated with molecular fragments that have a positive impact on pIC_{50} for the cytotoxicity of acrylic acid-based dental monomers, leading to a decrease in cytotoxicity, include: “C...C...” (ethyl group) – representing two carbon atoms in sequence in any part of the molecule; “O...C...” (methoxy group) –

denoting a sequence of oxygen and carbon atoms in any part of the molecule; “O...C...C” (ethoxy group) – representing oxygen and two carbon atoms in sequence in any part of the molecule.

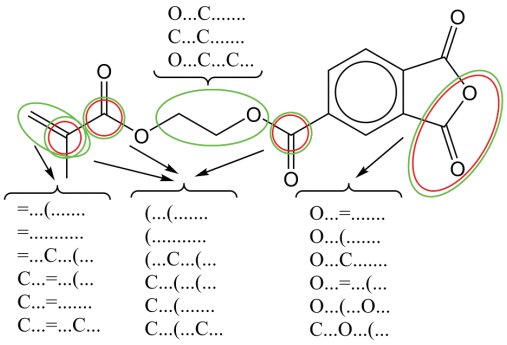

Fig. 4. Molecular fragments contribution to the cytotoxicity of acrylic acid-based dental monomers (green – increase, red – decrease).

In more complex molecular groups, some fragments contribute to an increase in the pIC_{50} value, while others contribute to a decrease. Therefore, to fully understand how these complex molecular fragments influence the cytotoxicity effect, it is essential not only to perform a qualitative analysis of individual molecular fragments but also a quantitative analysis of their *CW* numerical values. For instance, a molecular fragment found in Fig. 2 that incorporates a carboxyl group contains specific subfragments that either exert a detrimental influence on pIC_{50}, such as “C.....” representing a solitary carbon atom or a methyl group, “O.....” signifying an individual oxygen atom, “=.....” indicating the presence of a double bond, “=...(.....” denoting a double bond integrated into molecular branching, and “C a double bond with a carbon atom involved in molecular branching.” In contrast, within the same carboxyl group, there are subfragments with a beneficial effect on pIC_{50}, including “(...(.....” and “(.....” – both linked to molecular branching, “C...(.....” and “(...C...(...” – related to branching on carbon atoms and “C...=.....” and “C...=...C...” – subfragments associated with double bonds featuring carbon atoms. This illustrates how intricate molecular structures can encompass various subfragments that contribute both positively and negatively to the observed cytotoxicity effect, underscoring the necessity for a comprehensive qualitative and quantitative analysis.

CONCLUSION

The primary objective of this research is to create robust QSAR models capable of predicting the cytotoxicity of acrylic acid-based dental monomers with high predictability. This predictability is assessed through the use of various statistical parameters. The conformation-independent models, developed based on optimal descriptors derived from both local graph and SMILES notation invariants, are calculated using the Monte Carlo optimization method. The application

of a variety of statistical techniques allowed for the assessment of the predictive potential and robustness of the developed QSAR models. The validity of these models is confirmed by the numerical values obtained during their validation. The Monte Carlo optimization method effectively identified molecular fragments, which are employed as SMILES notation fragments in QSAR modeling, with both positive and negative effects on the cytotoxicity of acrylic acid-based dental monomers. In conclusion, the methodology presented in this research can be employed to pursue the development of new dental materials with reduced cytotoxicity.

SUPPLEMENTARY MATERIAL

Additional data and information are available electronically at the pages of journal website: https://www.shd-pub.org.rs/index.php/JSCS/article/view/12828, or from the corresponding author on request.

Acknowledgements: This work is supported by the Ministry of Science, Technological Development and Innovation of the Republic of Serbia (Grant No.: 451-03-65/2024-03/ /200113) and the Faculty of Medicine, University of Niš, Republic of Serbia (Internal project No. 70).

И З В О Д

QSAR МОДЕЛОВАЊЕ ЦИТОТОКСИЧНОСТИ ДЕНТАЛНИХ МОНОМЕРА БАЗИРАНИХ НА ДЕРИВАТИМА АКРИЛНЕ КИСЕЛИНЕ ПРИМЕНОМ МОНТЕ КАРЛО ОПТИМИЗАЦИЈЕ

МИРЈАНА БОШКОВИЋ[1], САША СТАНКОВИЋ[1], ЈЕЛЕНА В. ЖИВКОВИЋ[2] и АЛЕКСАНДАР М. ВЕСЕЛИНОВИЋ[2*]

[1]Универзитет у Нишу, Медицински факултет, Катедра Стоматолошка протетика, Булевар др Зорана Ђинђића 81, Ниш и [2]Универзитет у Нишу, Медицински факултет, Катедра Хемија, Булевар др Зорана Ђинђића 81, Ниш

Полимери који се примењују у стоматолошкој пракси често су формирани помоћу деривата акрилне киселине као почетног мономера. Међутим, наведени деривати показују цитотоксичност према различитим типовима ћелија, што је ефекат који мора бити смањен у будућим материјалима. Основни циљ овог истраживања је да се успостави QSAR модел за предвиђање цитотоксичних ефеката деривата акрилне киселине као и да идентификује молекулске фрагменте, молекулске дескрипторе са механичким тумачењем, који имају утицај на цитотоксичност. Основни алгоритам за добијање QSAR модела био је Монте Карло техника оптимизације, а модели су користили конформационо независне молекулске дескрипторе засноване на молекуларном графу и на SMILES нотацији. Различити статистички параметри су коришћени да би се валидирали добијени QSAR модели и добијени резултати указују на добру предиктивност QSAR модела. С обзиром на то да већина база података молекула користи SMILES нотацију за представљање молекулске структуре, представљени QSAR модели могу послужити као брз и ефикасан алат за претрагу нових мономера.

(Примљено 1. марта, ревидирано 15. априла, прихваћено 2. јуна 2024)

REFERENCES

1. I. M. Barszczewska-Rybarek, *Materials (Basel)* **12** (2019) 4057 (https://doi.org/10.3390/ma12244057)
2. N. Moszner, T. Hirt, *J. Polym. Sci. Pol. Chem.* **50** (2012) 4369 (https://doi.org/10.1002/pola.26260)
3. D. Dressano, M. V. Salvador, M. T. Oliveira, G. M. Marchi, B. M. Fronza, M. Hadis, W. M. Palin, A. F. Lima, J. Mech, *Behav. Biomed. Mater*. **110** (2020) 103875 (https://doi.org/10.1016/j.jmbbm.2020.103875)
4. R. Gautam, R. D. Singh, V. P. Sharma, R. Siddhartha, P. Chand, R. Kumar, *J. Biomed. Mater. Res., B* **100** (2012) 1444 (https://doi.org/10.1002/jbm.b.32673)
5. E. C. Kim, H. Park, S. I. Lee, S. Y. Kim, *Basic Clin. Pharm.* **117** (2015) 340 (https://doi.org/10.1111/bcpt.12404)
6. M. Goldberg, *Clin. Oral Investig.* **12** (2008) 1 (https://doi.org/10.1007/s00784-007-0162-8)
7. S. K. Jun, J. R. Cha, J. C. Knowles, H. W. Kim, J. H. Lee, H. H. Lee, *Dent. Mater.* **36** (2020) 157 (https://doi.org/10.1016/j.dental.2019.11.016)
8. J. G. Leprince, W. M. Palin, M. A. Hadis, J. Devaux, G. Leloup, *Dent. Mater.* **29** (2013) 139 (https://doi.org/10.1016/j.dental.2012.11.005)
9. T. Hampe, A. Wiessner, H. Frauendorf, M. Alhussein, P. Karlovsky, R. Bürgers, S. Krohn, *Polymers (Basel)* **14** (2022) 1790 (https://doi.org/10.3390/polym14091790)
10. L. S. Mokeem, I. M. Garcia, M. A. Melo, *Biomedicines* **11** (2023) 1256 (https://doi.org/10.3390/biomedicines11051256)
11. F. Amin, M. A. Fareed, M. S. Zafar, Z. Khurshid, P. J. Palma, N. Kumar, *Coatings* **12** (2022) 1094 (https://doi.org/10.3390/coatings12081094)
12. S. Bandarra, P. Mascarenhas, A. R. Luis, M. Catrau, E. Bekman, A. C. Ribeiro, S. Félix, J. Caldeira, I. Barahona, *Clin. Oral Investig.* **24** (2020) 2691 (https://doi.org/10.1007/s00784-019-03131-4)
13. A. Bakopoulou, T. Papadopoulos, P. Garefis, *Int. J. Mol. Sci.* **10** (2009) 3861 (https://doi.org/10.3390/ijms10093861)
14. M. Cadenaro, T. Maravic, A. Comba, A. Mazzoni, L. Fanfoni, T. Hilton, J. Ferracane, L. Breschi, *Dent. Mater.* **35** (2019) e1 (https://doi.org/10.1016/j.dental.2018.11.012)
15. G. Cervino, M. Cicciù, A. S. Herford, A. Germanà, L. Fiorillo, *Materials (Basel)* **13** (2020) 3350 (https://doi.org/10.3390/ma13153350)
16. I. P. Caldas, G. G. Alves, I. B. Barbosa, P. Scelza, F. de Noronha, M. Z. Scelza, *Dent. Mater.* **35** (2019) 195 (https://doi.org/10.1016/j.dental.2018.11.028)
17. E. N. Muratov, J. Bajorath, R. P. Sheridan, I. V. Tetko, D. Filimonov, V. Poroikov, T. I. Oprea, I. I. Baskin, A. Varnek, A. Roitberg, O. Isayev, S. Curtarolo, D. Fourches, Y. Cohen, A. Aspuru-Guzik, D. A. Winkler, D. Agrafiotis, A. Cherkasov, A.Tropsha, *Chem. Soc. Rev.* **49** (2020) 3525 (https://doi.org/10.1039/d0cs90041a)
18. P. Liu, W. Long, *Int. J. Mol. Sci.* **10** (2009) 1978 (https://doi.org/10.3390/ijms10051978)
19. N. Tripathi, M. K. Goshisht, S. K. Sahu, C. Arora, *Mol. Divers.* **25** (2021) 1643 (https://doi.org/10.1007/s11030-021-10237-z)
20. A. P. Toropova, A. A. Toropov, *Mini Rev. Med. Chem.* **18** (2018) 382 (https://doi.org/10.2174/1389557517666170927154931)
21. A. M. Veselinović, J. B. Veselinović, J. V. Živković, G. M. Nikolić, *Curr. Top. Med. Chem.* **15** (2015) 1768 (https://doi.org/10.2174/1568026615666150506151533)
22. A. K. Halder, A. H. S. Delgado, M. N. D. S. Cordeiro, *Dent. Mater.* **38** (2022) 333 (https://doi.org/10.1016/j.dental.2021.12.014)

23. P. K. Ojha, K. Roy, *Chemometr. Intell. Lab.* **109** (2011) 146 (https://doi.org/10.1016/j.chemolab.2011.08.007)
24. V. Stoičkov, D. Stojanović, I. Tasić, S. Šarić, D. Radenković, P. Babović, D. Sokolović, A. M. Veselinović, *Struct. Chem.* **29** (2018) 441 (https://doi.org/10.1007/s11224-017-1041-9)
25. A. A. Toropov, A. P. Toropova, *Mutat. Res.-Gen. Tox. En*. **819** (2017) 31 (https://doi.org/10.1016/j.mrgentox.2017.05.008)
26. A. M. Veselinović, A. Toropov, A. Toropova, D. Stanković-Đorđević, J. B. Veselinović, *New J. Chem.* **42** (2018) 10976 (https://doi.org/10.1039/C8NJ01034J)
27. P. K. Ojha, K. Roy, *Chemometr. Intell. Lab. Syst.* **109** (2011) 146 (https://doi.org/10.1016/j.chemolab.2011.08.007)
28. P. K. Ojha, I. Mitra, R. N. Das, K. Roy, *Chemometr. Intell. Lab. Syst.* **107** (2011) 194 (https://doi.org/10.1016/j.chemolab.2011.03.011)
29. P. P. Roy, J. T. Leonard, K. Roy, *Chemometr. Intell. Lab. Syst.* **90** (2008) 31 (https://doi.org/10.1016/j.chemolab.2007.07.004)
30. K. Roy, R. N. Das, P. Ambure, R. B. Aher. *Chemometr. Intell. Lab.* **152** (2016) 18 (https://doi.org/10.1016/j.chemolab.2016.01.008)
31. L. I. Lin, *Biometrics* **45** (1989) 255 (https://doi.org/10.2307/2532051)
32. O. Nicolotti, D. Gadaleta, G. F. Mangiatordi, M. Catto, A. Carotti, *IJQSPR* **1** (2016) 45 (https://doi.org/10.4018/IJQSPR.2016010102)
33. P. Gramatica, *QSAR Comb. Sci.* **26** (2007) 694 (https://doi.org/10.1002/qsar.200610151)
34. P. Gramatica, A. Sangion, *J. Chem. Inf. Model.* **56** (2016) 1127 (https://doi.org/10.1021/acs.jcim.6b00088)
35. M. Zivkovic, M. Zlatanovic, N. Zlatanovic, M. Golubović, A. M. Veselinović, *Mini Rev. Med. Chem.* **20** (2020) 1389 (https://doi.org/10.2174/1389557520666200212111428)
36. S. A. Amin, N. Adhikari, S. Gayen, T. Jha, *J. Biomol. Struct. Dyn.* **37** (2019) 4528 (https://doi.org/10.1080/07391102.2018.1552895)
37. S. Ahmadi, S. Lotfi, S. Afshari, P. Kumar, E. Ghasemi, *SAR QSAR Environ. Res.* **32** (2021) 1013 (https://doi.org/10.1080/1062936X.2021.2003429).

Journal of the Serbian Chemical Society
JSCS-info@shd.org.rs • www.shd.org.rs/JSCS
J. Serb. Chem. Soc. 90 (1) S18–S24 (2024) *Supplementary material*

SUPPLEMENTARY MATERIAL TO

Monte Carlo optimization based QSAR modeling of the cytotoxicity of acrylic acid-based dental monomers

MIRJANA BOŠKOVIĆ[1], SAŠA STANKOVIĆ[1], JELENA V. ŽIVKOVIĆ[2] and ALEKSANDAR M. VESELINOVIĆ[2]*

[1]*Department for Prosthetic Dentistry, Faculty of Medicine, University of Niš, Bulevar Dr Zorana Đinđića 81, 18000 Niš, Serbia and* [2]*Departmant of Chemistry, Faculty of Medicine, University of Niš, Bulevar Dr Zorana Đinđića 81, 18000 Niš, Serbia*

J. Serb. Chem. Soc. 90 (1) (2024) 95–107

* Corresponding author. E-mail: aveselinovic@medfak.ni.ac.rs

Table S-I. The SMILES notation of the studied molecules, calculated values for the DCW, experimental data (Ac) – Expr, the values of Ac calculated with the application of CORAL software – Calc, the difference between Expr and Calc – Diff for the built QSPR model.

	SMILES notation	Expr	Split 1				Split 2				Split 3			
			DCW	Calc	Diff.	Set	DCW	Calc	Diff.	Set	DCW	Calc	Diff.	Set
1	OC(COC(=O)C(=C)C)COc1ccc(cc1)C(c1ccc(cc1)OCC(COC(=O)C(=C)C)O)(C)C	4.523	153.6227	4.6717	-0.1487	Tr	131.3798	4.5272	-0.0042	Tr	101.8029	4.6189	-0.0959	Tr
2	O=C(OCCOC(=O)C(=C)C)NCCCCCCNC(=O)OC(C(OC(=O)C(=C)C)(C)C)C	4.046	135.7561	4.1632	-0.1172	Tr	120.7312	4.0288	0.0172	Tr	93.9162	4.1786	-0.1326	Tr
3	CCCCCCCCCCCCCOC(=O)C=C	4	127.3104	3.9229	0.0771	Tr	119.513	3.9718	0.0282	Tr	96.78843	4.339	-0.339	Tr
4	OCCOC(=O)C=C	3.721	85.8679	2.7434	0.9776	Tr	103.3123	3.2134	0.5076	Ts	75.13836	3.1303	0.5907	Tr
5	CCC(COC(=O)C(=C)C)CC	3.481	98.29383	3.097	0.384	Tr	102.7258	3.186	0.295	Tr	68.51583	2.7605	0.7205	Tr
6	CC(=C)C(=O)OCC1CO1	3.432	80.86003	2.6008	0.8312	Tr	101.5913	3.1329	0.2991	Tr	73.62916	3.046	0.386	Tr
7	O=C(C(=C)C)OCCOc1ccccc1	3.319	107.3223	3.354	-0.035	Tr	101.8979	3.1472	0.1718	Tr	78.05005	3.2928	0.0262	Tr
8	CC(COC(=O)C=C)O	3.237	99.58373	3.1337	0.1033	Ts	107.8482	3.4257	-0.1887	Tr	72.10373	2.9608	0.2762	Tr
9	O=C(C(=C)C)OCc1ccccc1	3.194	93.18357	2.9516	0.2424	Tr	101.2897	3.1187	0.0753	Tr	77.69698	3.2731	-0.0791	Ts
10	O=C(C(=C)C)OCC(COC(=O)C(=C)C)(C)C	3.187	106.4787	3.33	-0.143	Tr	102.3464	3.1682	0.0188	Tr	82.20556	3.5248	-0.3378	Tr
11	CCCCCCCCCCCCCOC(=O)C(=C)C	3.174	97.531	3.0753	0.0987	Ts	99.81803	3.0499	0.1241	Tr	73.98246	3.0657	0.1083	Tr
12	CCCCOCCOC(=O)C(=C)C	3.125	92.20183	2.9236	0.2014	Ts	101.7043	3.1381	-0.0131	Tr	71.97876	2.9539	0.1711	Tr
13	O=C(C(=C)C)OCCOC(=O)C(=C)C	2.975	75.04993	2.4355	0.5395	Tr	94.44037	2.7981	0.1769	Ts	60.70989	2.3247	0.6503	Tr
14	CCCCOC(=O)C=C	2.955	104.3175	3.2685	-0.3135	Tr	106.9926	3.3857	-0.4307	Ts	80.88324	3.451	-0.496	Tr
15	O=C(C(=C)C)OCCOCCOC(=O)C(=C)C	2.873	87.5084	2.7901	0.0829	Tr	95.66482	2.8554	0.0176	Tr	68.07138	2.7357	0.1373	Ts
16	C=CC(=O)OCC(C)C	2.87	106.2149	3.3225	-0.4525	Tr	94.80212	2.8151	0.0549	Tr	72.58719	2.9878	-0.1178	Ts
17	OC(COC(=O)C(=C)C)COC(=O)C(=C)C	2.827	80.71603	2.5967	0.2303	Tr	98.43524	2.9851	-0.1581	Ts	67.13854	2.6836	0.1434	Tr
18	O=C(C(=C)C)OCCOCCOCCOC(=O)C(=C)C	2.824	84.61243	2.7076	0.1164	Tr	95.2272	2.835	-0.011	Tr	67.82279	2.7218	0.1022	Tr
19	O=C(C(=C)C)OCCOCCOCCOCCOCCOCCOCCOCCOCCOCCOC(=O)C(=C)C	2.788	81.14627	2.609	0.179	Ts	92.60148	2.7121	0.0759	Tr	66.32961	2.6385	0.1495	Tr
20	O=C(C(=C)C)OCCOCCOCCOCCOCCOCCOCCOCCOCCOC COCCOCCOCCOCCOCCOC(=O)C(=C)C	2.772	78.2578	2.5268	0.2452	Tr	90.41339	2.6096	0.1624	Tr	65.08669	2.5691	0.2029	Tr
21	CC(OC(=O)C(=C)C)CCOC(=O)C(=C)C	2.77	73.47979	2.3908	0.3792	Tr	92.54971	2.7096	0.0604	Tr	68.52136	2.7608	0.0092	Tr
22	CCCOC(=O)C=C	2.759	81.24828	2.6119	0.1471	Ts	100.0274	3.0597	-0.3007	Tr	67.80606	2.7209	0.0381	Tr
23	O=C(C(=C)C)OCCOCCOCCOCCOC(=O)C(=C)C	2.706	83.50628	2.6762	0.0298	Tr	94.78958	2.8145	-0.1085	Tr	67.57421	2.708	-0.002	Ts
24	COC(=O)C=C	2.6	67.60376	2.2236	0.3764	Ts	90.17226	2.5983	0.0017	Ts	64.39926	2.5307	0.0693	Ts
25	CCCCOC(=O)C(=C)C	2.567	83.64036	2.68	-0.113	Tr	88.79469	2.5339	0.0331	Tr	63.37059	2.4733	0.0937	Tr
26	CCOCCOC(=O)C(=C)C	2.565	75.55814	2.4499	0.1151	Ts	86.2699	2.4157	0.1493	Tr	61.63122	2.3762	0.1888	Tr

	SMILES notation	Expr	Split 1				Split 2				Split 3			
			DCW	Calc	Diff.	Set	DCW	Calc	Diff.	Set	DCW	Calc	Diff.	Set
27	CC(COC(=O)C(=C)C)C	2.532	77.15368	2.4954	0.0366	Tr	82.63017	2.2453	0.2867	Tr	62.84333	2.4438	0.0882	Ts
28	O=C(C(=C)C)OCCCCCCOC(=O)C(=C)C	2.442	88.26477	2.8116	-0.3696	Tr	97.62552	2.9472	-0.5052	Ts	69.70968	2.8272	-0.3852	Tr
29	CCOC(=O)C=C	2.432	82.57289	2.6496	-0.2176	Tr	85.66366	2.3873	0.0447	Tr	60.85801	2.333	0.099	Ts
30	CC(=C)C(=O)OCC1CCCO1	2.328	92.03577	2.9189	-0.5909	Tr	98.05556	2.9674	-0.6394	Tr	65.66598	2.6014	-0.2734	Tr
31	CC(=C)C(=O)OCCOC(=O)c1ccc2c(c1)C(=O)OC2=O	2.292	63.64959	2.111	0.181	Tr	84.57794	2.3365	-0.0445	Ts	60.12902	2.2923	-0.0003	Ts
32	CC(COC(=O)C(=C)C)O	2.062	73.87312	2.402	-0.34	Tr	87.70105	2.4827	-0.4207	Tr	61.46598	2.367	-0.305	Ts
33	COCCOC(=O)C(=C)C	2.056	71.08387	2.3226	-0.2666	Ts	83.33848	2.2785	-0.2225	Ts	57.44907	2.1427	-0.0867	Ts
34	CC(=C)C(=O)OCCO	1.997	70.67814	2.3111	-0.3141	Tr	73.44776	1.8155	0.1815	Tr	60.12424	2.292	-0.295	Tr
35	CCCOC(=O)C(=C)C	1.991	63.77341	2.1145	-0.1235	Ts	71.94311	1.7451	0.2459	Ts	53.48796	1.9215	0.0695	Tr
36	O=C(C(=C)C)OCCOCCOCCOCCOCCOCCOCCOCCOCCOCCOCCOCCO CCOCCOCCOCCOCCOCCOCCOCCOCCOCCOCCOCCOCCOC(=O)C(=C)C	1.988	72.21267	2.3547	-0.3667	Tr	84.96481	2.3546	-0.3666	Tr	62.12272	2.4036	-0.4156	Tr
37	CCOC(=O)C(=C)C	1.534	48.05303	1.6671	-0.1331	Ts	65.31183	1.4347	0.0993	Tr	55.24573	2.0197	-0.4857	Tr
38	CN(CCOC(=O)C(=C)C)C	1.057	38.04694	1.3823	-0.3253	Tr	58.02168	1.0934	-0.0364	Ts	41.67586	1.2621	-0.2051	Tr
39	COC(=O)C(=C)C	1.046	44.01846	1.5523	-0.5063	Tr	60.05954	1.1888	-0.1428	Tr	46.13592	1.5111	-0.4651	Tr

Table S-II. The statistical quality of QSAR models developed with the Monte Carlo optimization method for predicting the cytotoxicity of acrylic acid-based dental monomers

	Run	Training set							Test set						
		r^2	CCC	IIC	q^2	RMSE	MAE	F	r^2	CCC	IIC	q^2	RMSE	MAE	F
Split 1	1	0.6442	0.7836	0.5665	0.5936	0.468	0.354	49	0.8815	0.9387	0.5747	0.8203	0.206	0.159	59
	2	0.6663	0.7997	0.5762	0.6137	0.453	0.340	54	0.8936	0.9282	0.5775	0.8419	0.245	0.190	67
	3	0.6439	0.7834	0.7489	0.5879	0.468	0.337	49	0.8815	0.9253	0.6957	0.8285	0.246	0.196	60
	Av	0.6515	0.7889	0.6305	0.5984	0.463	0.344	51	0.8855	0.9307	0.6160	0.8302	0.232	0.182	62
Split 2	1	0.8855	0.9393	0.8646	0.8751	0.247	0.180	209	0.8069	0.8819	0.8977	0.7072	0.272	0.215	33
	2	0.8686	0.9297	0.8698	0.8554	0.265	0.193	178	0.8038	0.8834	0.8964	0.7483	0.278	0.227	33
	3	0.8671	0.9288	0.8691	0.8512	0.267	0.202	176	0.8023	0.8806	0.8957	0.7041	0.278	0.230	32
	Av	0.8737	0.9326	0.8678	0.8606	0.260	0.192	188	0.8043	0.8820	0.8966	0.7199	0.276	0.224	33
Split 3	1	0.8102	0.8952	0.7314	0.7852	0.301	0.227	115	0.8027	0.7968	0.8958	0.6967	0.437	0.374	33
	2	0.7998	0.8888	0.7465	0.7753	0.309	0.235	108	0.7880	0.8098	0.8877	0.6682	0.424	0.336	30
	3	0.7985	0.8880	0.7260	0.7685	0.310	0.227	107	0.7831	0.7920	0.8847	0.6676	0.426	0.336	29
	Av	0.8028	0.8907	0.7346	0.7763	0.301	0.229	110	0.7913	0.7995	0.8894	0.6775	0.429	0.349	31

r^2 – Correlation coefficient; CCC – Concordance correlation coefficient IIC – Index of ideality of correlation q^2 – Cross-validated correlation coefficient RMSE – Root-mean-square deviation; MAE – Mean absolute error F – Fischer ratio; Av – Average value for statistical parameters obtained from three independent Monte Carlo optimization runs

Table S-III. Y-randomization of the best QSAR model (best optimization run) for three independent splits

	Split 1		Split 2		Split 3	
Run	Training	Test	Training	Test	Training	Test
0	0.7779	0.9025	0.9222	0.8107	0.8481	0.856
1	0.0004	0.1169	0.0824	0.0308	0	0.1555
2	0.0002	0.0035	0.021	0.0536	0.0401	0.0423
3	0.0005	0.3662	0.0008	0.0552	0.0113	0.0533
4	0.014	0.1484	0.0412	0.177	0.0079	0.0129
5	0.0001	0.0024	0.0376	0.1078	0.0511	0.0294
6	0.0279	0.0496	0.0001	0.0006	0.0581	0.008
7	0	0.0748	0.0376	0.0631	0.0018	0.0511
8	0.0162	0.1267	0.2047	0.0599	0.033	0.0068
9	0.0367	0.2484	0.0032	0.3614	0.0026	0.2574
10	0.0159	0.2321	0.0114	0.0379	0.009	0.0733
R_r^2	0.0112	0.1369	0.044	0.0947	0.0215	0.069
$^cR_p^2$	0.7723	0.8312	0.9	0.7619	0.8373	0.8208
$^CR_p^2 = R \times (R^2 - R_r^2)^{1/2}$ should be > 0.5						

Table S-IV. The list of SAks together with their correlation weights for the three runs of the Monte Carlo optimization obtained from QSAR model for cytotoxicity of acrylic acid-based dental monomers

SA_k(CW)	CW			SA_k(CW)	CW			SA_k(CW)	CW			SA_k(CW)	CW		
	Run 1	Run 2	Run 3		Run 1	Run 2	Run 3		Run 1	Run 2	Run 3		Run 1	Run 2	Run 3
10001000000	2.04072	1.64329	2.17548	EC0-C...2...	-0.57805	2.13528	0.26973	P4E0C...0-..	0.19057	-0.42875	-0.64271	S2E0O...6-..	2.64238	1.68778	-0.65004
10011000000	-0.68648	-0.89667	-1.64588	EC0-C...3...	0.60777	-0.64754	0.09522	P4E0C...1-..	1.15094	0.14607	0.35132	S2E0O...7-..	2.59459	-1.3961	0.82873
(...(.....	1.86481	2.36047	1.83992	EC0-C...4...	-1.08495	2.88662	4.42322	P4E0C...10-.	-0.30488	-0.88076	2.07319	S3E0C...0-..	2.6031	2.80396	3.19456
(..........	2.38315	0.01164	0.48356	EC0-N...2...	0.71245	1.41515	-0.46103	P4E0C...11-.	0.78769	0.2757	0.1774	S3E0C...1-..	3.26508	1.7543	2.38114
(...C...(...	0.59231	0.23821	0.75957	EC0-N...3...	-0.05248	-0.67878	-0.79341	P4E0C...12-.	2.09153	-0.41509	-0.75097	S3E0C...10-.	1.41755	-0.98002	1.14167
(...O...(...	-1.76475	-0.02351	3.13201	EC0-O...1...	-0.73709	2.01317	-0.78123	P4E0C...2-..	1.45036	1.456	-0.17449	S3E0C...11-.	-1.11642	1.76198	0.61019
++++N---B2==	-0.66841	-0.9578	-0.02689	EC0-O...2...	0.43285	-0.67693	-0.95118	P4E0C...3-..	-0.93113	-0.42538	0.24947	S3E0C...2-..	0.02929	-0.50083	0.31047
++++N---O===	-0.0466	-0.51999	-0.59267	Cmax.0.....	0.07451	-0.90299	-0.78808	P4E0C...4-..	0.08828	0.17332	0.85628	S3E0C...3-..	0.63614	2.14929	-0.42529
++++O---B2==	2.93892	2.29353	4.26808	Cmax.1.....	0.62707	-0.98917	-0.35355	P4E0C...6-..	-0.90566	-0.64323	-0.86677	S3E0C...4-..	-0.86744	2.18077	0.12449
1...(.....	-0.55378	-1.23046	-0.99908	Cmax.2.....	2.15876	2.21378	1.33399	P4E0C...7-..	-0.20717	0.38263	-0.73385	S3E0C...5-..	-0.57557	1.25306	2.41236
1..........	1.72756	3.4168	1.46401	HALO00000000	3.10012	5.12254	0.67608	P4E0C...9-..	1.99289	0.80198	3.80959	S3E0C...6-..	1.32358	-1.46925	-1.79261
1...c...(...	2.01002	-0.86826	-0.95821	N...(.....	-1.54125	-0.74101	-0.71144	P4E0N...0-..	1.63655	2.41321	-0.63807	S3E0C...7-..	-0.86923	3.47435	-0.01045
2..........	-0.69637	2.4027	-0.58136	N...(...C...	-1.47049	-0.96695	-0.76188	P4E0N...2-..	-0.52122	1.13736	-0.98008	S3E0C...8-..	0.09488	3.10096	-1.50905
2...c...(...	0.47004	1.4202	-0.47823	N..........	-1.12924	-1.38708	-0.81376	P4E0O...0-..	-0.30012	0.0685	-0.65479	S3E0C...9-..	-0.48167	-1.05033	-0.85821
=...(.....	-0.73963	-1.82271	-0.56441	N...C...(...	2.89675	-0.07344	-0.63735	P4E0O...1-..	3.0397	1.28555	2.0656	S3E0N...1-..	-0.67174	-1.14393	-0.65369
=..........	-0.0911	-0.84168	0.02385	N...C.....	-0.66218	-1.12418	-1.09708	P4E0O...11-.	-0.55104	1.60997	-0.09848	S3E0N...2-..	0.32892	-1.68074	0.33572
=...2.....	-0.07831	-0.53642	0.64225	N...C...C...	0.35577	1.32927	0.17781	P4E0O...2-..	-4.96228	-5.71882	-2.52658	S3E0N...3-..	-1.91307	1.03169	1.05043
=...C...(...	2.12334	-0.15232	1.48761	O...(...(...	-1.60948	-0.33487	-1.10797	P4E0O...3-..	-0.50319	0.47694	-0.31965	S3E0O...0-..	2.70025	-0.53862	-0.69574
=...O...(...	-0.47436	-0.7329	0.07426	O...(.....	-0.67315	-0.21132	-0.69041	P4E0O...4-..	-0.63363	-0.88632	-1.97634	S3E0O...1-..	0.27918	2.34591	0.23796
C...(...(...	-4.48737	-2.88755	-1.87188	O...(...1...	-1.55361	2.71448	3.41292	P4E0O...6-..	0.84905	2.26782	1.14724	S3E0O...2-..	0.55713	-0.98591	-0.81886
C...(.....	0.85977	0.7236	0.43071	O...(...C...	2.11584	4.06705	2.38901	P4E0O...8-..	2.70512	0.55054	-0.38219	S3E0O...3-..	-1.37363	-1.83098	0.23636
C...(...1...	-0.43911	-1.79311	-0.79008	O...(...O...	-2.33768	-1.1146	-0.78522	NNE0C...100-	-0.49194	-1.60235	-0.5722	S3E0O...4-..	4.46801	4.21327	2.10524
C...(...=...	-0.91602	-0.83295	-0.25098	O..........	-0.53045	-0.64042	-0.79137	NNE0C...109-	0.23401	2.63775	2.20755	S3E0O...5-..	-1.4588	0.24585	0.0096
C...(...C...	-1.41874	-0.16738	-0.75001	O...1.....	2.28796	4.46072	-0.75215	NNE0C...209-	0.12554	0.46501	0.33865	S3E0O...7-..	2.32898	-0.69626	2.68917
C..........	-0.85829	-0.91601	-0.30648	O...=...(...	-0.55988	-1.18035	-0.17877	NNE0C...218-	1.18373	-0.25966	-1.31109	S3E0O...8-..	0.51323	-0.7615	2.23785
C...1.....	2.36179	1.07117	2.38854	O...=.....	-0.96694	-0.80896	-0.23906	NNE0C...300-	1.71752	1.90165	2.03515	Nmax.0.....	1.8318	1.89273	-0.1544
C...1...C...	2.03818	2.30487	0.44927	O...=...2...	4.11841	2.14122	-0.83664	NNE0C...309-	-1.12492	-0.98457	-0.38732	Nmax.1.....	-0.27836	-0.67618	-0.66019
C...2.....	-0.11522	4.24878	0.45511	O...=...C...	2.40021	0.9572	2.39268	NNE0C...318-	-0.73448	-1.45937	0.39744	Nmax.2.....	-1.79641	1.64042	-1.95179

SA_k(CW)	CW			SA_k(CW)	CW			SA_k(CW)	CW			SA_k(CW)	CW		
	Run 1	Run 2	Run 3		Run 1	Run 2	Run 3		Run 1	Run 2	Run 3		Run 1	Run 2	Run 3
C...2...=...	1.27096	-0.6899	0.82935	O...C...(...	1.09343	1.18595	-0.74038	NNE0C...327-	0.2283	0.95106	-0.58411	Omax.1.....	1.38989	1.37447	2.17207
C...=...(...	-0.95726	-0.11894	-0.48055	O...C.....	0.92199	0.50283	0.05931	NNE0C...427-	2.96874	-0.50624	-0.17058	Omax.2.....	-1.51955	-1.87402	-1.92046
C...=.....	4.22321	1.85861	2.46372	O...C...1...	3.25323	3.99833	4.43099	NNE0C...436-	-2.10898	0.76726	1.8355	Omax.3.....	4.26554	2.09267	2.37161
C...=...C...	2.8012	3.20602	1.43809	O...C...2...	-1.1112	0.87075	1.79825	NNE0N...218-	-1.15669	-1.42372	-0.98128	Omax.4.....	0.72815	4.33725	-1.10246
C...C...(...	1.33519	0.6716	0.91631	O...C...C...	0.31427	0.27734	0.32731	NNE0N...327-	0.41046	-0.85664	-0.70549	Omax.6.....	2.46839	2.34804	2.34852
C...C.....	1.22831	0.44223	2.02694	O...c...1...	4.08137	-1.50835	0.20516	NNE0O...109-	-0.20716	1.50682	2.11827	Omax.7.....	2.66992	2.6593	2.31455
C...C...1...	-1.92915	1.26609	-1.55957	P2E0C...0-..	0.24879	0.46539	0.2662	NNE0O...218-	0.58391	0.00576	-0.91952	Omax.8.....	-0.85145	1.52513	-0.63281
C...C...=...	0.76893	0.77539	0.81123	P2E0C...1-..	0.4909	-0.23989	0.30203	NOSP01000000	1.99412	1.31782	2.3857	Smax.0.....	2.35774	4.91929	1.30464
C...C...C...	0.82138	0.9339	0.92997	P2E0C...2-..	0.69635	-1.18758	0.05557	NOSP11000000	-0.38648	-0.62676	-0.51823	c...(.....	-1.1569	-0.55175	-0.60163
C...N...(...	-1.03468	-0.9504	-0.73638	P2E0N...1-..	-0.00182	3.08929	1.52438	S2E0C...0-..	0.52342	0.00279	1.01559	c...(...C...	-0.77989	-0.45582	-0.09065
C...N...C...	1.91526	1.30654	1.68492	P2E0N...2-..	-1.82858	1.14379	2.27136	S2E0C...1-..	0.25801	1.20806	0.81339	c...(...O...	2.23292	-0.89815	-0.58278
C...O...(...	-0.85745	-1.81488	-0.68961	P2E0O...0-..	0.47633	-0.73191	1.03036	S2E0C...2-..	0.04606	0.00094	0.20543	c...(...c...	-1.12445	3.08107	1.33856
C...O...1...	-1.0489	1.51674	2.21203	P2E0O...1-..	-0.36896	-0.74227	0.00983	S2E0C...3-..	-0.52242	-0.0755	-0.65247	c.....	0.13081	1.0173	0.06026
C...O...C...	-0.65933	0.6882	-0.72869	P2E0O...2-..	-0.97739	-0.65778	-0.59931	S2E0C...4-..	0.74275	-2.71042	-0.52924	c...1...(...	-0.55346	-0.71309	-1.28325
C...c...1...	0.34836	-1.96338	2.04929	P2E0O...3-..	-1.65077	-1.82568	-1.67783	S2E0C...5-..	2.17321	-0.2486	0.30416	c...1.....	-0.47171	-0.95229	1.79985
C3.....0...	-0.72705	-1.88642	-0.59877	P3E0C...0-..	-0.07245	0.22551	-0.20371	S2E0C...6-..	-0.89218	-1.31795	0.42055	c...1...c...	1.32654	1.66162	0.07356
C3....H.1...	2.99293	2.31551	2.51151	P3E0C...1-..	1.06332	1.94457	-0.66478	S2E0C...7-..	-0.68778	0.39354	2.26095	c...2.....	-0.77289	4.49669	2.04563
C4.....0...	0.67212	-1.22272	2.18393	P3E0C...2-..	1.44811	0.01957	0.46843	S2E0C...8-..	2.30477	4.43347	-1.74675	c...2...c...	0.60447	3.31636	-0.54616
C5.....0...	4.3235	4.16548	4.3648	P3E0C...3-..	-1.5109	-1.56784	-1.43801	S2E0C...9-..	-0.74215	-0.64691	0.90498	c...C.....	1.89214	0.8456	1.92529
C5....H.1...	-1.78297	-4.67514	-1.47067	P3E0C...4-..	0.49952	0.42785	-0.53465	S2E0N...1-..	-1.03619	-0.66219	-0.68997	c...C...O...	2.35666	1.88731	0.22163
C5...AH.1...	1.35155	-0.46432	-0.52543	P3E0C...5-..	2.3124	3.31191	0.02562	S2E0N...3-..	-0.66226	2.2539	1.04249	c...O.....	0.53269	0.01469	2.60098
C6.....0...	2.27699	1.28413	-0.68345	P3E0N...0-..	1.12737	-1.34512	2.37152	S2E0O...0-..	-0.01955	-0.84339	1.13238	c...O...C...	1.50841	-2.82109	-1.96518
C6...A..1...	0.78966	-0.22067	1.00799	P3E0N...2-..	-0.95411	-0.74931	-0.96078	S2E0O...1-..	2.26042	4.4307	2.44092	c...c...(...	-0.42576	0.9723	-0.59307
C6...A..2...	3.48234	0.93083	-1.05247	P3E0O...0-..	0.64866	-0.92118	0.26571	S2E0O...2-..	0.19888	0.74327	-0.03641	c...c.....	2.06053	0.31807	1.86427
C7.....0...	0.69561	4.4304	2.06093	P3E0O...1-..	2.01562	-0.73381	0.74247	S2E0O...3-..	2.25665	3.43735	1.17877	c...c...1...	-0.83299	-0.7083	-0.116
BOND10000000	1.41096	0.83037	0.01221	P3E0O...2-..	-0.63439	-1.50608	0.57711	S2E0O...4-..	-0.52118	0.29808	-0.89888	c...c...2...	-0.42429	2.28212	0.83626
EC0-C...1...	-0.60445	-1.14516	-0.42115	P3E0O...3-..	-1.90308	0.5397	0.75782	S2E0O...5-..	2.41122	2.44651	2.32521	c...c...c...	-0.05854	2.36627	0.60061

Journal of the Serbian Chemical Society
JSCS-info@shd.org.rs • www.shd.org.rs/JSCS
J. Serb. Chem. Soc. *90* (1) 109–122 (2025)
JSCS–5823
Original scientific paper
Published 4 November, 2024

Preparation, characterization and evaluation of nano manganese dioxide coated on alumina as a new adsorbent for the effective removal of phenol from aqueous samples

SAYED ZIA MOHAMMADI[1], FARIDEH MOUSAZADEH[2]*, LEILA SALAJEGHEH-TEZERJI[1], BATOUL LASHKARI[3] and ELINA BANI-ASADI[2]

[1]Department of Chemistry, Payame Noor University, Tehran, Iran, [2]School of Public Health, Bam University of Medical Sciences, Bam, Iran and [3]Department of New Materials, Institute of Science and High Technology and Environmental Sciences, Graduate University of Advanced Technology, Kerman, Iran

(Received 21 October, revised 14 November 2023, accepted 6 April 2024)

Abstract: An effective sorbent, nano-manganese dioxide coated on alumina (NMO/Al) nanocomposite, as an economical adsorbent, was prepared in the present study. To this end, morphological, chemical and surface characteristics of NMO/Al were determined through various techniques. The NMO/Al nanocomposite could be thus separated effortlessly from water samples using a filter paper and then, the removal of phenol from the wastewater samples was evaluated. Accordingly, various empirical parameters affecting this removal including pH, ionic strength, time, temperature and phenol concentration were examined. In order to investigate the adsorption equilibrium, Langmuir, Freundlich and Temkin equations were utilized. The Langmuir adsorption model had a higher correlation coefficient (R^2) indicating better fit to the adsorption characteristics. Various kinetic models were employed to evaluate the adsorption kinetics of phenol on the NMO/Al nanocomposite. Based on the results, the Elovich model exhibited the best fit with a sorption capacity of 21.34 mg g^{-1}. Additionally, the adsorbed phenol was desorbed from the NMO/Al surface by using ethanol with high efficiency, and then the NMO/Al nanocomposite was used again to remove phenol. The results showed that the NMO/Al nanocomposite could be reused for more than five cycles. Based on the findings, the phenol adsorption process from wastewater using NMO/Al nanocomposite is considered an efficient adsorption approach in a large-scale adsorption system.

Keywords: nano manganese dioxide; alumina; nanocomposite; phenol; removal.

* Corresponding author. E-mail: faridehmousazadeh1398@gmail.com
https://doi.org/10.2298/JSC231021042M

INTRODUCTION

With the growing pace of industrial development, pollution of water resources has become significantly hazardous throughout the world. There are various applications for phenol, such as in medicine, pesticides, explosives, garments, petrochemicals and other fields. However, the usage of phenol generates a significant amount of toxic, carcinogenic and difficult-to-degrade phenol wastewater, which has severe consequences for human health and the environment. Indeed, the treatment of phenol wastewater is of paramount importance.[1] The United States Environmental Protection Agency has classified phenol as a critical pollutant due to its high toxicity and its widespread contamination of water resources.[2] Long--term exposure to phenol can have adverse effects on human organs, including the possibility of causing cancer. As a result, the recommended discharge limit for phenol in surface water is less than 1 μg L^{-1}.[3] Therefore, the treatment of phenol wastewater is an urgent and critical issue.[4] To address this issue, various physical, chemical, and biological processes have been employed for the removal and/or recovery of phenol. Some of these processes include biosorption, electro-fenton, extraction with solvent, electrodialysis, degradation, biodegradation, membrane methods and sorption.[6–10] But most of the mentioned techniques are relatively expensive or had been reported costly in treating secondary toxic sludge. Compared to other processes, absorption is still economically the most profitable method due to its advantages such as simple design, ease of adsorbent regeneration, adsorption capacity and minimum capital investment requirements.

Different adsorbents such as organic framework,[2] activated persulfate,[1,4] bimetallic/carbon nanocomposite,[5] ZnO nanoparticles,[6] nanocomposites,[7] granulated cork,[8] modified SiO_2,[9] magnetic activated carbon-cobalt nanoparticles,[10] non-living Phanerochaete,[11] kaolin/γ-Fe_2O_3,[12] magnetic diatomite[13] and so on, were used for removal of phenol. Alumina (Al_2O_3) is a suitable adsorbent material for treatment of effluents due to its good porosity, and thermal stability, that making it an economical alternative.[14] Moreover, alumina is naturally available and can be easily obtained through chemical reaction from $Al(OH)_3$. To further improve its adsorption efficiency, alumina can be modified through physical or chemical treatment, which increases the density of active sites on its surface. While alumina is a sorbent with many benefits, it can be further improved for enhanced adsorption potential toward organic molecules by modifying it with metals, metal oxides, or other substances. Additionally, due to Lewis acid and base groups on the surface of Al_2O_3, strong interactions between the surface of alumina and metal oxides have been formed and therefore the absorption and catalytic properties of alumina was improved.[15] Previously, manganese dioxide coated on alumina was used to remove arsenic and fluoride ions from water samples, but based on our knowledge this adsorbent has not been used to remove the phenol and in addition,

the method of coating manganese dioxide on alumina in the present work is different from the method of the previous works.[16,17]

In the present study, nano manganese dioxide coated on alumina nanocomposite (NMO/Al) with high absorption capacity was successfully prepared. The NMO/Al nanocomposite was employed for the removal of phenol under various experimental conditions. Furthermore, the impacts of initial adsorbate concentration, contact time, pH and sorbent capacity on the phenol removal were assessed.

EXPERIMENTAL

Reagents and equipment

Phenol was obtained from Merck, and was used to prepare a 1000.0 mg L^{-1} solution in deionized water. Al_2O_3 (0.063–0.2 mm, Merck) was used for the preparation of NMO/Al nanocomposite. The absorbance of phenol was measured using a Varian Cary 50 Scan UV–Vis spectrophotometer with quartz cells. Phenol absorbance values were measured at 270 nm, which is the wavelength of maximum absorbance. pH was measured by Metrohm pH-meter (model 713) with a combined glass electrode (Metrohm). The solutions were agitated by IKA stirrer, model KS (Staufen, Germany). After adsorbing of phenol from sample solution, the NMO/Al was recovered by a filter paper.

X-ray diffraction (XRD) was performed using a Bruker D8 Advance diffractometer with CuKα radiation. The microstructure of NMO/Al was observed using a scanning electron microscope (SEM, Cam Scan MV2300, Cambridge, UK). X-ray photoelectron spectroscopy (XPS) was conducted using an AXIS-Ultra device from Kratos Analytical Ltd. with monochromatic aluminum (Al)/Kα radiation (225 W; 15 mA; 15 kV). Fourier transform infrared (FT-IR) spectra were recorded using a Brucker Tensor 27 spectrometer with the KBr wafer technique.

Preparation of NMO/Al

Manganese dioxide was precipitated onto alumina in an aqueous solution through a reductive reaction:[18]

$$2KMnO_4 + 8HCl \rightarrow 2MnO_2 + 2KCl + 3Cl_2 + 4H_2O \quad (1)$$

To perform this reaction, 4.0 g of potassium permanganate was added to 50 mL of deionized water containing 4.0 g of alumina. Then, 8 mL of concentrated HCl was added dropwise to the mixture while continuously stirring and heating it on a hot plate at 90 °C. The stirring and heating process were continued for 1 h. The coated alumina was then filtered, washed with boiling water, dried in an oven at 80 °C for 6 h, and stored in a bottle for later use.

Phenol removal method

To evaluate the ability of NMO/Al nanocomposite for phenol removal, the tests were done in a batch method at 25 °C and to increase the accuracy of each test, it was repeated 3 times. To determine the highest yield of NMO/Al nanocomposite for phenol removal, the effective parameters on the phenol removal such as contact time, solution temperature, solution pH, ionic strength and phenol concentration were assessed and optimized.

For this assesses, 0.05 g of NMO/Al was added to a solution containing phenol. The Erlenmeyer flasks were agitated (340 rpm) using an IKA stirrer model KS for a certain period of time. After agitation, filter paper was used to separate the NMO/Al from the solution, and then the absorbance of the solution under the filter was measured using an UV–Vis (270 nm).

For assesses of the initial concentration of phenol onto phenol removal, the concentration range of 50 to 150 mg L^{-1} at pH 7 was assessed. For this purpose, a concentration of 50 mg L^{-1} was used to examine the adsorption under other conditions.

The effect of solution pH on the phenol removal was examined over a pH range of 2 to 9. Furthermore, adsorption thermodynamic was assessed at various temperatures (275–309 K). Various concentrations of sodium chloride solution (ranging from 0 to 0.5 mol L^{-1}) were assessed to investigate the salting effect on the phenol removal (Supplementary material to this paper). It should be noted that, the percentage removal (*Re%*) was calculated:

$$Re\% = 100\frac{c_0 - c_t}{c_0} \tag{2}$$

where c_0 (mg L^{-1}) refers to the initial concentration and c_t (mg/L) refers to the amount of phenol at time *t*.

The amount of phenol adsorbed by the NMO/Al nanocomposite after time t (q_t, mg g^{-1}) was calculated:

$$q_t = V\frac{c_0 - c_t}{w} \tag{3}$$

where *V* (L) refers to the volume of solution, and *w* (g) refers to the mass of the adsorbent.

Assesses of desorption

Similar to the adsorption tests, NMO/Al (0.05 g) was added to a phenol solution (50 mg L^{-1}) with a contact time of 60 min at 298 K. After this, filter paper was used to separate the NMO/Al loaded with phenol from the solution, and in the following, deionized water used to wash and remove any unabsorbed traces of phenol.

The consumed NMO/Al nanocomposite, that saturated with phenol, was regenerated using ethanol (10 mL) that added to the phenol-saturated NMO/Al and stirred for 30 min at 298 K and 340 rpm. Once desorption was completed, the adsorbent was separated, washed with deionized water and for the next use, placed in an oven with a temperature of 378 K to dry. To assess the reusability of the NMO/Al, the absorption and desorption process was repeated 5 times.

RESULTS AND DISCUSSION

NMO/Al characterization

The functional groups on the surfaces of alumina and NMO/Al were assessed by FT-IR spectroscopy. FT-IR spectra (shown in Fig. 1a) were recorded using the KBr wafer technique over a range of 400–4000 cm^{-1}. To prepare the wafers, a mixture of 1 mg of the sample and 100 mg of KBr was used.

The absorption bands observed at 3447 and 1617 cm^{-1} in the FT-IR spectra are attributed to the stretching and bending vibrations of adsorbed water molecules (ν(OH)), respectively. The broad peak at 811 cm^{-1} is caused by the Al–O vibration.[19] The appearance of new bands at 458, 517 and 711 cm^{-1} can be attributed to the Mn–O vibration, which makes the NMO/Al nanocomposite spectrum different from the alumina spectrum. Therefore, the presence of MnO_2 on the surface of alumina was confirmed.

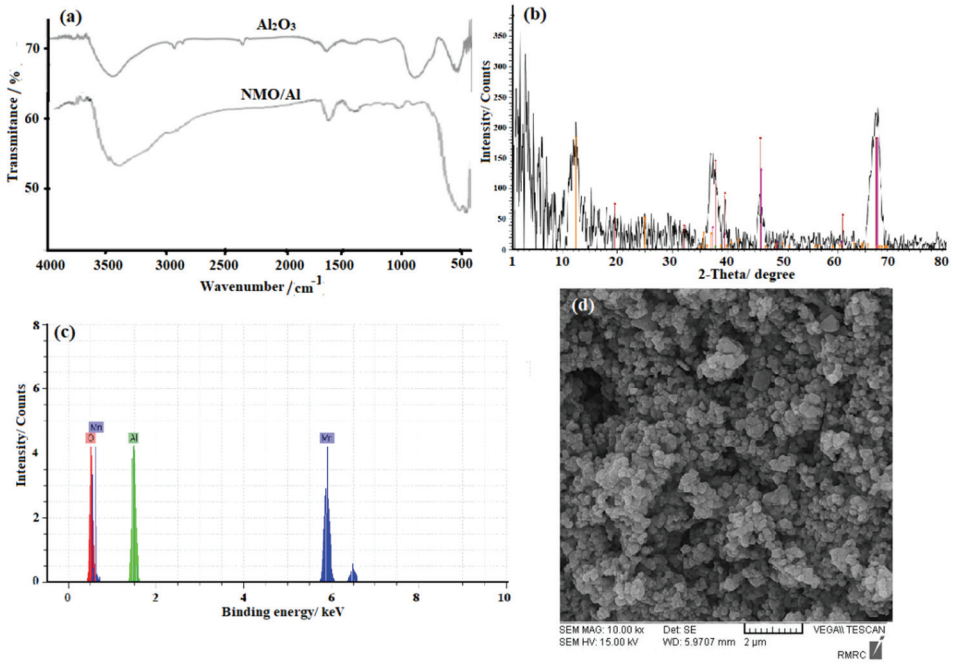

Fig. 1. a) FT-IR spectra of Al_2O_3 and NMO/Al, b) XRD of NMO/Al, c) XPS of NMO/Al and (d) SEM of NMO/Al.

The crystalline structure of the NMO/Al nanocomposite was characterized by XRD analysis (as shown in Fig. 1b). The diffraction peaks present at 2θ values of 32.5, 37.6, 39.6, 45.9, 61.1 and 67.1°, could be related to crystal plates (220), (311), (222), (400), (511) and (440), respectively. These peaks suggest the cubic structure of γ-Al_2O_3 (JCPDS Card no. 01-1303). The calculations made using the Debye––Scherrer equation showed the size of the γ-Al_2O_3 to be 27 nm.

Furthermore, as shown in Fig. 1b, the diffraction peaks present at 2θ values of 12.9, 18.3, 28.8, 37.7, 42.1, 49.9, 56.44, 60.26, 69.7, 71.3 and 73.7°, could be related to crystal plates (110), (200), (310), (211), (301), (411), (600), (521), (541), (222) and (730), respectively. With respect to these results, the successful synthesis of tetragonal crystalline α-MnO_2 was confirmed (standard card JSPDF 44-0141).[20]

Also, X-ray photoelectron spectroscopy (XPS) was used to determine the chemical compositions of the NMO/Al nanocomposite. The presence of Al, Mn and O elements in the NMO/Al nanocomposite was confirmed by using XPS of NMO/Al (Fig. 1c). Quantitative data analysis of the XPS spectra yielded weight ratio of 21.96 % for Al, 22.81 % for Mn and 55.23 % for O in the NMO/Al nanocomposite.

The morphological features of the NMO/Al nanocomposite showed in Fig. 1d. The SEM images of NMO/Al reveal that it has a spherical shape. The porous mic-

rostructure of NMO/Al suggests that it has a large surface area, therefore, it has a good potential to be used as an adsorbent with a high adsorption capacity of pollutants.

The effect of pH

A very important factor in the adsorption process is the pH of the solution because the functional groups on the surface of the adsorbent as well as the chemical structure of the phenol molecule could be affected by pH of solution.[21,22] So, the effect of pH on the removal percentage (*Re%*) of phenol was evaluated in this study over a pH range of 2–9 (Fig. 2a). The results showed that the maximum sorption of phenol occurred in the pH range of 7–9.

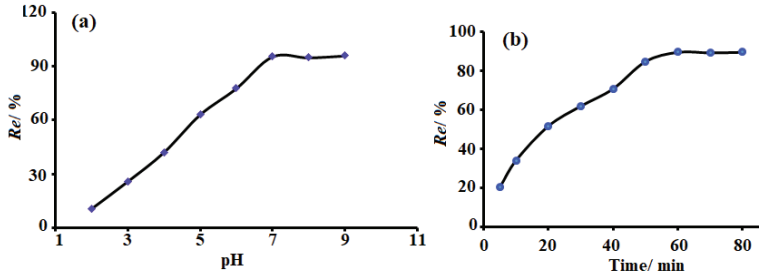

Fig. 2. a) The impact of pH on the adsorption of phenol onto the NMO/Al. Conditions: 25 mL phenol 50.0 mg/L. Agitation time: 60 min. Agitation velocity: 340 rpm. NMO/Al, 0.05 g and b) the impact of contact time on the adsorption of phenol onto the NMO/Al. Conditions have been similar to case a except to the agitating time.

The acid dissociation constant (pK_a) value for phenol was 9.89; therefore, at pHs less than pK_a, phenol molecules exist in non-dissociated state, and the reason for phenol adsorption can be attributed to π–π dispersion interaction, physical adsorption, hydrogen bonding and hydrophobic interaction.[23] With respect to the obtained results, other experiments for removal of phenol were done at pH 7.

The assesses of contact time and initial concentrations

The impacts of initial concentration and contact time on the *Re%* of phenol could be showed in Figs. 2b and 3, respectively.

According to Fig. 2b, the phenol adsorption enhances quickly in the early 30 min and reaches balance at 60 min. With the start of the adsorption process, phenol molecules gradually occupy the active sites on the NMO/Al surface, in the next step, phenol molecules must be transferred from the bulk solution to the active sites on the surface of the NMO/Al nanocomposite. This gradual diffusion would decline the sorption level of phenol after 30 min.

Various initial concentrations of phenol (50, 75, 100, 125 and 150 mg L^{-1}) were also used to examine the impact of initial concentration of phenol on adsorp-

tion by the NMO/Al. According to Fig. 3a, adsorption capacity of phenol by the NMO/Al enhances when initial concentration of phenol increases. By increasing the initial concentration of phenol, the concentration gradient increases and acts as a driving force and as a result causes more absorption of phenol.[22] Clearly, adsorption procedure largely depends on contact time and initial concentration of phenol. Therefore, a contact time (60 min) and a c_0 (50 mg L^{-1}) can be chosen for other experiments.

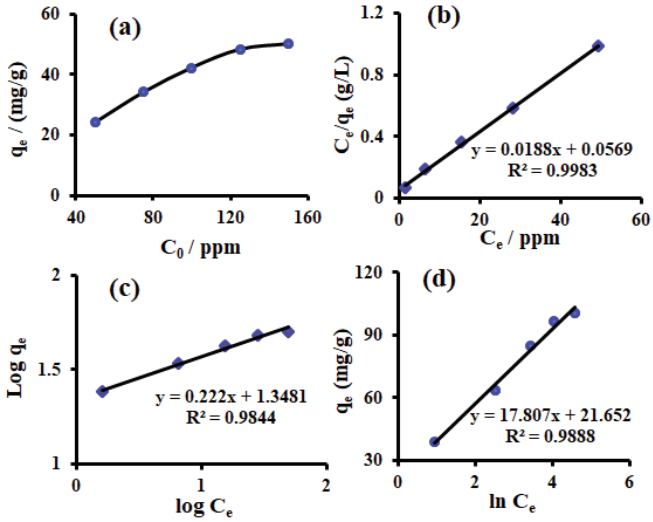

Fig. 3. a) The impact of initial concentrations of phenol, b) Langmuir, c) Freundlich and d) Temkin adsorption isotherms to adsorb phenol onto the NMO/Al at room temperatures.

Adsorption isotherm

To explain the adsorption capacities of phenol on the NMO/Al, the equilibrium experimental data was analyzed to assess the fitness of the data to the Langmuir, Freundlich and Temkin isotherm models. The non-linear Langmuir isotherm model is given below:[24]

$$q_e = \frac{Q_0 K_L c_e}{1 + K_L c_e} \tag{4}$$

In Eq. (4), the equilibrium concentration of phenol (mg L^{-1}) has been denoted to c_e, the adsorbed phenol (mg g^{-1}) in the equilibrium time has been denoted to q_e, the monolayer adsorption capacity of NMO/Al nanocomposite has been denoted to Q_0 (mg g^{-1}) and the Langmuir constant has been denoted to K_L (L mg^{-1}).

The Langmuir model assumes that adsorption occurs on a homogeneous surface with a finite number of identical sites, and the adsorption of one molecule

does not affect the adsorption of another. Using the linear form of Langmuir isotherm model, we can obtain the Langmuir isotherm variables:[24]

$$\frac{c_e}{q_e} = \frac{1}{Q_0 K_L} + \frac{c_e}{Q_0} \tag{5}$$

The plot of c_e/q_e *versus* c_e is a straight line with a slope of $1/Q_0$ and an intercept of $1/Q_0K_L$. The values of Q_0 and K_L can be obtained from the slope and intercept of the linear plot, respectively (as shown in Fig. 3b).

According to Table I, the Langmuir isotherm parameters Q_0 and K_L were determined to be 53.2 mg/g and 0.034 L mg^{-1}, respectively, with a correlation coefficient (R) value of 0.9991. The highest monolayer adsorption capacity for phenol onto the NMO/Al at 298 K was found to be 53.2 mg g^{-1}. This suggests that the NMO/Al has a good adsorption capacity for removing phenol from the aqueous solutions.

TABLE I. The isotherm constants to adsorb phenol onto the surface of NMO/Al

Isotherm model	Parameter	Value
Langmuir	Q / mg g^{-1}	53.2
	K_L / L g^{-1}	0.33
	R^2	0.9983
Freundlich	K_f / mg g^{-1}	22.29
	$1/n$	0.222
	R^2	0.9844
Temkin	K_t / L mol^{-1}	3.37
	B	17.81
	R^2	0.9888

The Freundlich isotherm is another empirical equation used to describe adsorption on a heterogeneous surface. It assumes that the adsorption occurs at sites with different adsorption energies, and the amount of adsorbate adsorbed increases with increasing concentration. The linearized form of the Freundlich isotherm equation is given as:[25]

$$\log q_e = \log K_f + \frac{1}{n} \log c_e \tag{6}$$

where K_f is the Freundlich constant related to the adsorption capacity (mg g^{-1})(L mg^{-1})$^{1/n}$, and n is the Freundlich exponent related to the intensity of adsorption.

The plot of log q_e *versus* log c_e is a straight line with a slope of $1/n$ and an intercept of log K_f. The values of n and K_f can be obtained from the slope and intercept of the linear plot, respectively (as shown in Fig. 3c).

Table I presents the Freundlich isotherm parameters for the adsorption of phenol on the NMO/Al. The value of n, which is an experimental parameter, changes with the degree of inhomogeneity of the bonded phenol on the surface of

adsorbent. The n value greater than 1 indicates the optimal adsorption. The value of K_f indicates the capacity of phenol adsorption. Additionally, the adsorption intensity will be more significant when the n-value is greater.[25]

The linear form of the Temkin isotherm is expressed as:[25]

$$q_e = B \ln K_t + B \ln c_e \tag{7}$$

The adsorbate–adsorbent interactions considered by Temkin isotherm assumes that the heat of adsorption decreases linearly with covering the absorbent surface by the adsorbate substance. In Eq. (7), q_e and c_e have the same definitions as before, B refers to the Temkin constant associated with the adsorption heat and K_t refers to the constant of equilibrium (L mg^{-1}).

The plot of q_e *versus* ln c_e is a straight line with slope of B and an intercept of Bln K_t. B and K_t can be obtained from the slope and intercept of the resulting line, respectively. The linear plot of q_e *versus* ln c_e for the adsorption of phenol on NMO/Al was showed in Fig. 3d.

Table I provides the Temkin constants and R^2 value for the adsorption of phenol on the NMO/Al. These constants give us information about the adsorption heat and maximum binding energy of the adsorbate on the adsorbent.

Table I indicates that the Langmuir model provides a better fit to the experimental data, as evidenced by its higher R^2 value. The maximum monolayer adsorption capacity for phenol on the NMO/Al was found to be 53.2 mg g^{-1} at 25 °C. Since the value of n in the Freundlich equation (4.504) is between 1 and 10, the absorption of phenol is favorable.[25]

Kinetic examination

To assess phenol adsorption kinetics on the NMO/Al, the intraparticle diffusion model (IPD), the Lagergren;s pseudo-first and second-order models and the Elovich model were evaluated. The pseudo-first order model is as follows:[26]

$$\log(q_e - q_t) = \ln q_e - K_1 t \tag{8}$$

In Eq. (8), K_1 is the rate constant of the pseudo-first order sorption (min^{-1}). The value of q_e and K_1 can be determined from the intercept and the slope of the plot of log ($q_e - q_t$) *versus* t, as shown in Fig. 4a.

Pseudo second-order model is defined as follows:[26]

$$\frac{dq_t}{dt} = k_2 (q_e - q_t)^2 \tag{9}$$

Rearranging the variables gives:

$$\frac{dq_t}{(q_e - q_t)^2} = k_2 dt \tag{10}$$

When Eq. (10) has been integrated in the boundary conditions $t = 0$ ($q = 0$) to $t = t$ ($q = q_t$):

$$\frac{t}{q_t} = \frac{1}{k_2 q_e^2} + \frac{t}{q_e} \tag{11}$$

In the above equation, k_2 represents the rate constant of pseudo-second order adsorption (g/(mg min)). The value of q_e and k_2 can be also calculated from slope and intercept of plot (t/q_t *versus* t), as shown in Fig. 4b.

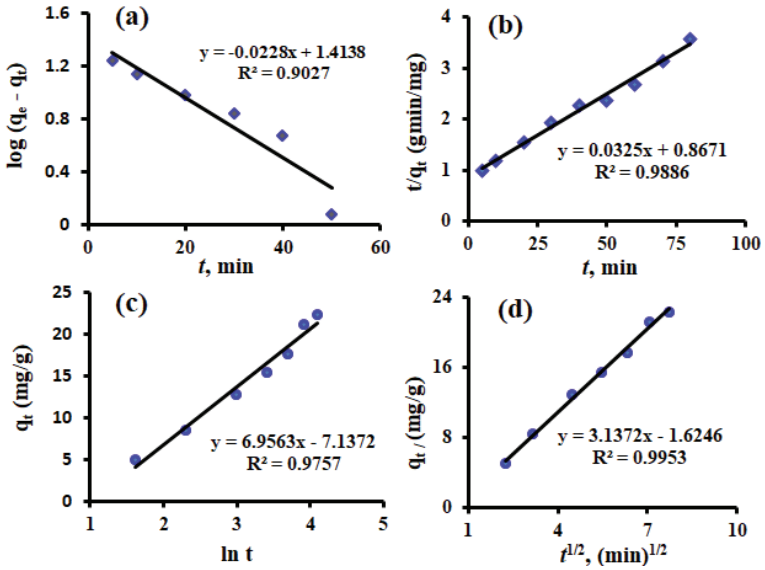

Fig. 4. The phenol adsorption kinetic onto the NMO/Al at room temperature: a) pseudo-first order,b) pseudo-second order, c) Elovich and d) intraparticle diffusions plots.

The Elovich equation was also used to qualitatively describe the chemisorption process.[25] The linear form of the Elovich model is expressed as:

$$q_t = \frac{1}{\beta}\ln \alpha\beta + \frac{1}{\beta}\ln t \tag{12}$$

In Eq. (12), α (g mg^{-1} min^{-1}) refers to the sorption rate and β (g mg^{-1}) refers to activation energy of chemisorption. Chemisorption is a process in which the adsorbate molecules are bonded to the surface of the adsorbent through chemical bonds. The sorption rate represents the rate at which the adsorbate molecules are chemically bonded to the surface of the adsorbent. The activation energy represents the minimum energy required for the adsorbate molecules to overcome the energy barrier and form chemical bonds with the adsorbent surface.

The values of α and β can be determined from the plot of q_t *versus* ln t, as shown in Fig. 4c.

In the intraparticle diffusion model, the plot of q_t *versus* $t^{1/2}$ gives a straight line, which can be expressed as:[26]

$$q_t = K_{id} t^{1/2} + C \quad (13)$$

In this equation, the rate constant of intraparticle diffusion (mg g^{-1} $min^{-1/2}$) was denoted to K_{id} and the intercept of the line denoted to C (Fig. 4d).

The resulted kinetic parameters from these models summarizes in Table II. The calculated q_e value for the Elovich model is in close agreement with the experimental q_e value, indicating a good fit of this model to the experimental data. The K_{id} for phenol was 3.14 mg g^{-1} $min^{-1/2}$, which shows the high tendency of the NMO/Al for removal of phenol.[27]

TABLE II. Kinetics constants for phenol sorption onto the NMO/Al

Kinetic model	Coefficient	Value
	q_e experimental (mg g^{-1})	22.38
Pseudo-first order	k_1 / min^{-1}	0.023
	q_e calculated (mg g^{-1})	4.11
	R^2	0.9027
Pseudo-second order	k_2 / g mg^{-1} min^{-1}	0.0012
	q_e calculated (mg g^{-1})	30.77
	R^2	0.9886
Elovich model	α / mg g^{-1} min^{-1}	19.40
	β / g mg^{-1}	0.144
	q_e calculated (mg g^{-1})	21.34
	R^2	0.9757
Intra-particle diffusion model	K_{id} / mg g^{-1} $min^{-1/2}$)	3.14
	q_e calculated (mg g^{-1})	22.7
	R^2	0.9953

NMO/Al reusability

Adsorbent reusability is a leading factor in the environmentally-friendly and economical process of adsorption. The problem with contaminated adsorbent disposal to the environment may be thus decreased due to adsorbent reusability. The results showed that the *Re%* of phenol in cycles 1 to 5 were 97.2, 94.7, 89.6, 85.1 and 80.3, respectively, that indicating the excellent reusability of NMO/Al.

Treatment of wastewater sample

The real wastewater samples were collected from an industrial center in Kerman Province, Iran, and then examined for the respective content using inductively coupled plasma-optical emission spectrometry (ICP-OES) as shown in Table III. In the next step, real wastewater samples were spiked with phenol (50 mg L^{-1}) and

treated with the NMO/Al under optimized conditions. The mixture was then separated and analyzed for metal ion levels and phenol content using ICP-OES and spectrophotometer, respectively (Table III). The results showed that the NMO/Al was highly efficient in removing phenol and some metal ions from the wastewater samples.

TABLE III. Application of the NMO/Al to remove phenol from wastewater sample

Component	Concentration before treatment[a], mg L^{-1}	Concentration after treatment, mg L^{-1}	*Re%*
Phenol	50.0	3.2	93.6
Cr	5.3	0.6	88.7
Pb	5.4	0.7	87.0
Cu	8.1	0.8	90.1
Ni	6.2	0.9	85.5
Cd	4.5	0.5	88.9
Mn	4.3	Not detect	100
Co	5.2	Not detect	100
As	3.7	Not detect	100

[a]Original sample spiked with 50 mg L^{-1} of phenol

CONCLUSION

In this study, a novel and effective adsorbent was developed by chemically depositing MnO_2 nanoparticles onto the surface of alumina. The results obtained from FT-IR, SEM, XRD and XPS analyses confirmed the successful grafting of MnO_2 nanoparticles onto the alumina surface. The applicability of the NMO/Al as a new adsorbent was further confirmed by the ability to effectively remove phenol from an effluent sample. The Langmuir isotherm model well indicated the equilibrium data, and the highest phenol adsorption capacity on the NMO/Al was reported by 53.2 mg g^{-1}. The desorption experiment results showed that the NMO/Al adsorbent can be recovered and reused for up to five cycles. In the further works, the NMO/Al nanocomposite could be magnetized using iron oxide or cobalt oxide nanoparticles and then used to remove various contaminants from contaminated samples.

SUPPLEMENTARY MATERIAL

Additional data and information are available electronically at the pages of journal website: https://www.shd-pub.org.rs/index.php/JSCS/article/view/12633, or from the corresponding author on request.

Acknowledgements. The current study was conducted thanks to the support of Payame Noor University. The Bam University of Medical Sciences, Bam, Iran, provided financial assistance (project no. 98000075), which the authors gratefully thank.

И З В О Д

ПРИПРЕМА, КАРАКТЕРИЗАЦИЈА И ЕВАЛУАЦИЈА НАНО-МАНГАН-ДИОКСИДА КОЈИ ОБЛАЖЕ ГЛИНИЦУ, КАО НОВОГ АДСОРБЕНТА ЗА ЕФИКАСНО УКЛАЊАЊЕ ФЕНОЛА ИЗ ВОДЕНИХ УЗОРАКА

SAYED ZIA MOHAMMADI[1], FARIDEH MOUSAZADEH[2], LEILA SALAJEGHEH-TEZERJI[1], BATOUL LASHKARI[3] и ELINA BANI-ASADI[2]

[1]Department of Chemistry, Payame Noor University, Tehran, Iran, [2]School of Public Health, Bam University of Medical Sciences, Bam, Iran u [3]Department of New Materials, Institute of Science and High Technology and Environmental Sciences, Graduate University of Advanced Technology, Kerman, Iran

Ефикасан сорбент, нано-манган-диоксид на нанокомпозиту глинице (NMO/Al) припремљен је као економичан адсорбент у овом раду. У том циљу, различитим техникама су одређене морфолошке, хемијске и површинске карактеристике NMO/Al. NMO/Al нанокомпозит се може без напора одвојити од узорака воде помоћу филтер папира, да би затим било процењено уклањање фенола из узорака отпадне воде. Сходно томе, испитани су различити емпиријски параметри који утичу на ово уклањање укључујући pH, јонску јачину, време, температуру и концентрацију фенола. Да би се испитала адсорпциона равнотежа, коришћене су Langmuir, Freundlich и Temkin једначине. Langmuir адсорпциони модел је имао већи коефицијент корелације (R^2), што указује на боље уклапање у карактеристике адсорпције. За процену кинетике адсорпције фенола на NMO/Al нанокомпозиту коришћени су различити кинетички модели. На основу резултата, Elovich модел је показао најбоље слагање са капацитетом сорпције од 21,34 mg g^{-1}. Додатно, адсорбовани фенол је ефикасно десорбован са NMO/Al површине коришћењем етанола, а затим је NMO/Al нанокомпозит поново коришћен за уклањање фенола. Резултати су показали да се NMO/Al нанокомпозит може користити у више од пет циклуса. На основу налаза, процес адсорпције фенола из отпадне воде коришћењем NMO/Al нанокомпозита се сматра ефикасним адсорпционим приступом у систему адсорпције великих размера.

(Примљено 21. октобра, ревидирано 14. новембра 2023, прихваћено 6. априла 2024)

REFERENCES

1. Q. Yu, M. Tang, G. Liu, M. Liu, J. Ye, *Chem. Eng. Process* **186** (2023) 109313 (https://doi.org/10.1016/j.cep.2023.109313)
2. A.K. Mohammed, J.K. Ali, M.B.S. Kuzhimully, M.A. Addicoat, S. Varghese, M. Baias, E. Alhseinat, D. Shetty, *Chem. Eng. J.* **466** (2023) 143234 (https://doi.org/10.1016/j.cej.2023.143234)
3. P. Kazemi, M. Peydayesh, A. Bandegi, T. Mohammadi, O. Bakhtiari, *Chem. Eng. Res. Des.* **92** (2014) 375 (https://doi.org/10.1016/j.cherd.2013.07.023)
4. F. Khoshtinat, T. Tabatabaie, B. Ramavandi, S. Hashemi, *Chemosphere* **283** (2021) 131265 (https://doi.org/10.1016/j.chemosphere.2021.131265)
5. S. Zarin, Z. Aslam, A. Zahir, M. Shahzad Kamal, A. Ghaffar Rana, W. Ahmad, S. Ahmed, *J. Iranian Chem. Soc.* **15** (2018)2689 (https://doi.org/10.1007/s13738-018-1457-1)
6. R. Sridar, U. Uma Ramanane, M. Rajasimman, *Environ. Nanotechnol. Monitor. Manage.* **10** (2018) 388 (https://doi.org/10.1016/j.enmm.2018.09.003)
7. K.A. Hernández-Hernández, J. Illescas, M.C. Díaz-Nava, S. Martínez-Gallegos, C. Muro-Urista, R.E. Ortega-Aguilar, E. Rodríguez-Alba, E. Rivera, *Appl. Clay Sci.* **157** (2018) 212 (https://doi.org/10.1016/j.clay.2018.01.020)

8. M. Mallek, M. Chtourou, M. Portillo, H. Monclús, K. Walha, A. ben Salah, V. Salvadó, *J. Environ. Manage.* **223** (2018) 576 (https://doi.org/10.1016/j.jenvman.2018.06.069)
9. X. Yang, X. Liu, W. Tang, Y. Gao, H. Ni, J. Zhang, *Korean J. Chem. Eng.* **34** (2017) 723 (https://doi.org/10.1007/s11814-016-0311-3)
10. S.Z. Mohammadi, Z. Darijani, M.A. Karimi, *J. Alloys Compd.* **832** (2020) 154942 (https://doi.org/10.1016/j.jallcom.2020.154942)
11. T. Pernyeszi, V. Farkas, A. Felinger, B. Boros, I. Dékány, *Environ. Sci. Pollut. Res.* **25** (2018) 8550 (https://doi.org/10.1007/s11356-017-1120-x)
12. N.S. Mirbagheri, S. Sabbaghi, *Microporous Mesoporous Mater.* **259** (2018) 134 (https://doi.org/10.1016/j.micromeso.2017.10.007)
13. Y. Yu, Z. Hu, Y. Wang, H. Gao, *Int. J. Miner. Process.* **162** (2017) 1 (https://doi.org/10.1016/j.minpro.2017.02.001)
14. M. Aazza, H. Ahlafi, H. Moussou, H. Maghat, *J. Environ. Chem. Eng.* **5** (2017) 3418 (https://doi.org/10.1016/j.jece.2017.06.051)
15. C. di Luca, F. Ivorra, P. Massa, R. Fenoglio, *Chem. Eng. J.* **268** (2015) 280 (https://doi.org/10.1016/j.cej.2015.01.074)
16. E. Deschamps, V.S.T. Ciminelli, P.G. Weidler, A.Y. Ramos, *Clays Clay Miner.* **51** (2003) 197 (https://doi.org/10.1346/CCMN.2003.0510210)
17. S.M. Maliyekkal, A.K. Sharma, L. Philip, *Water Res.* **40** (2006) 3497 (https://doi.org/10.1016/j.watres.2006.08.007)
18. O.A. Elhefnawy, W.I. Zidan, M.M. Abo-Aly, E.M. Bakier, G.A. Al-Magid, *Spectrosc. Lett.* **47** (2014) 131 (https://doi.org/10.1080/00387010.2013.773519)
19. K. Atrak, A. Ramazani, S. Taghavi Fardood, *J. Mater. Sci. Mater. Electron.* **29** (2018) 8347 (https://doi.org/10.1007/s10854-018-8845-2)
20. X. Wan, S. Yang, Z. Cai, Q. He, Y. Ye, Y. Xia, G. Li, J. Liu, *Nanomaterials* **9** (2019) 847 (https://doi.org/10.3390/nano9060847)
21. S.Z. Mohammadi, H. Hamidian, L. Karimzadeh, Z. Moeinadini, *Arab. J. Chem.* **9** (2016) S1290 (http://dx.doi.org/10.1016/j.arabjc.2012.02.002)
22. Y.-D. Liang, Y.-J. He, T.-T. Wang, L.H. Lei, *J. Water Process Eng.* **27** (2019) 77 (https://doi.org/10.1016/j.jwpe.2018.11.013)
23. Y. Zhou, X. Liu, L. Tang, F. Zhang, G. Zeng, X. Peng, L. Luo, Y. Deng, Y. Pang, J. Zhang, *J. Hazard. Mater.* **333** (2017) 80 (https://doi.org/10.1016/j.jhazmat.2017.03.031)
24. S. Z. Mohammadi, Z. Safari, N. Madady, *J. Inorg. Organomet. Polym. Mater.* **30** (2020) 3199 (https://doi.org/10.1007/s10904-020-01485-x)
25. S. Z. Mohammadi, N. Mofidinasab, M. A. Karimi, A. Beheshti, *Int. J. Environ. Sci. Technol.* **17** (2020) 4815 (https://doi.org/10.1007/s13762-020-02767-0)
26. S. Z. Mohammadi, N. Mofidinasab, M. A. Karimi, F. Mosazadeh, *Water Sci. Technol.* **82** (2020) 829 (https://doi.org/10.2166/wst.2020.375)
27. S. Z. Mohammadi, M. A. Karimi, S. N. Yazdy, T. Shamspur, H. Hamidian, *Quim Nova* **37** (2014) 804 (https://www.scielo.br/j/qn/a/yGw8SYRs7w5ZdY7w6S4f4hR/?lang=en).

Journal of the Serbian Chemical Society
JSCS-info@shd.org.rs • www.shd.org.rs/JSCS
J. Serb. Chem. Soc. 90 (1) S25 (2025)
Supplementary material

SUPPLEMENTARY MATERIAL TO

Preparation, characterization and evaluation of nano manganese dioxide coated on alumina as a new adsorbent for the effective removal of phenol from aqueous samples

SAYED ZIA MOHAMMADI[1], FARIDEH MOUSAZADEH[2]*, LEILA SALAJEGHEH-TEZERJI[1], BATOUL LASHKARI[3] and ELINA BANI-ASADI[2]

[1]Department of Chemistry, Payame Noor University, Tehran, Iran, [2]School of Public Health, Bam University of Medical Sciences, Bam, Iran and [3]Department of New Materials, Institute of Science and High Technology and Environmental Sciences, Graduate University of Advanced Technology, Kerman, Iran

J. Serb. Chem. Soc. 90 (1) (2024) 109–122

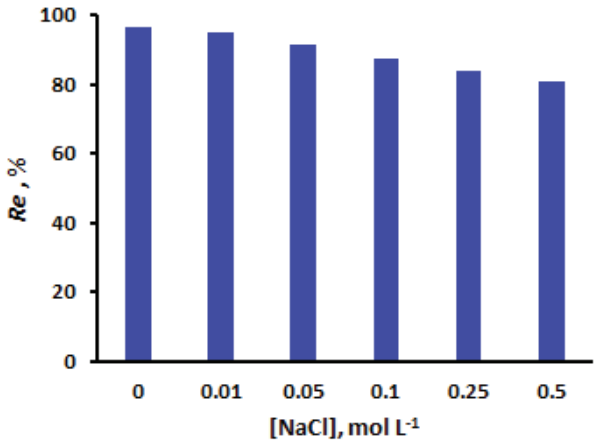

Fig. S-1. Ionic strength impact on adsorption of phenol onto the NMO/Al.

* Corresponding author. E-mail: faridehmousazadeh1398@gmail.com

Journal of the Serbian Chemical Society
JSCS-info@shd.org.rs • www.shd.org.rs/JSCS
J. Serb. Chem. Soc. *90* (1) 123–135 (2025)
JSCS–5824
Original scientific paper
Published 9 November, 2024

Green synthesis, characterization and biochemical properties of waste walnut (*Juglans regia* L.) inner shell-based silver nanoparticles

MERVE CAN[1] and MERVE KESKİN[2]*

[1]*Graduate Education Institute, Department of Biotechnology, Bilecik Seyh Edebali University, Bilecik, Türkiye and* [2]*Vocational School of Health Services, Bilecik Seyh Edebali University, Bilecik, Türkiye*

(Received 10 November, revised 28 December 2023, accepted 3 March 2024)

Abstract: Sustainability is important for future ecology and the increase of waste in recent years negatively affects sustainability. The management of waste and using them in the technology field could be a solution for sustainability. Nanotechnology is a developing technology aiming to improve the physical, chemical and biological properties of matter with the size of 1–100 nm. Nanoparticles could be synthesized by different methods such as physical, biological, and chemical. The green synthesis (biological synthesis) method is the most preferred when compared to chemical and physical methods because it is eco-friendly, energy-saving, cheaper, less waste-producing, easy to scale, sustainable and biologically compatible. Walnut is a versatile fruit with its leaves, dry and green fruit, timber, inner/outer shell and outer peel. Its inner shell and outer peel are not used as food and are waste. In this study, a waste walnut inner shell was used to synthesize silver nanoparticles (WS-AgNPs). WS-AgNPs were synthesized by green technique, characterized and biochemical properties were determined. WS-AgNPs exhibited the maximum absorbance at 460nm with 46–51 nm size and they inhibited urease enzyme by 82.16±1.30 %. It was clear that herbal-based wastes could be used in nanotechnology and have the potential to be used in medicine.

Keywords: waste management; green synthesis; silver nanoparticles; *H. pylori*; antioxidant.

INTRODUCTION

Sustainability is defined as the ability to continue the functions, processes, and productivity of ecology and ecological systems in the future.[1] It has been emphasized in recent studies that the world's resources and the environment are moving toward the limit of depletion as a result of human activities.[1] With the

* Corresponding author. E-mail: merveozdemirkeskin@gmail.com
https://doi.org/10.2298/JSC231110023C

increasing population and developing technology, the amount of waste is also increasing due to the variety of materials produced. According to the report published by the Turkish Statistical Institute (TUIK) on December 23, 2021, a total of 104.8 million tons of waste was generated in thermal power plants, manufacturing industry areas, organized industrial zones, mining enterprises, health centres and households throughout. 30 Million tons of this waste was generated in 2020. The total amount of waste was reported nearly 94.9 million tons in 2018 and increased by 10.5 % in 2021 compared to 2018.[2] The amount of waste per capita for Turkey was 1.16 kg per day in 2018. The total amount of processed waste increased by 22 % compared to 2018.[2] Considered from this perspective, sustainability can only be achieved by using the resources provided by nature at a pace that allows them to renew themselves.[1] For this purpose, it is important to develop production processes that use inputs with low environmental impacts, have high efficiency, contain little or zero waste, and do not create pollution. Waste prevention, also known as zero waste, is an approach that includes the most efficient use of resources, reducing the amount of waste generated and recycling waste.[3] It is clearly seen that preventing the increase in the amount of waste or recycling waste is extremely important. Studies should be carried out within the scope of the principles of sustainable cities and communities and responsible production and consumption, which are among the sustainable development goals. One of the important studies carried out within the scope of sustainability is the production of waste-based nanoparticles by green synthesis technique and their introduction into the field of technology.

Nanotechnology is a new technology that allows the processing of particles in sizes between 1–100 nm.[4,5] Nanotechnology is widely used in medicine, dentistry, drug delivery systems, many biomedical applications, the environment and engineering. Silver nanoparticles (AgNP) are important with their properties such as chemical stability, conductivity and catalytic and antibacterial activities. Compared to other elements, silver has a more antimicrobial effect and it is the least toxic element. AgNPs can be synthesized by many different methods such as chemical, biological and physical. The most common is the biological synthesis method, and it is also known as green synthesis. The green synthesis is the most preferred because it is ecologically friendly, energy-saving, cheaper, less waste-producing, easy to scale, sustainable, using no toxic chemicals and has biological compatibility.[5] In addition to the use of bacteria, mould, yeast, algae and plants as a reducing and stabilizing agent, it is not toxic due to the absence of chemicals. Nanoparticles could be synthesized faster than other applications by green synthesis. It is the most preferred method due to its biocompatibility. Silver nanoparticles could be synthesised by the green synthesis technique.[6] The silver nanoparticles are used in antimicrobial application areas, separation of toxic compounds, biosensors, environment and various treatment systems.[7–9] In addit-

ion to these, silver nanoparticles have an applications in areas like the prevention of diseases in agriculture, the rapid elimination of existing diseases, increasing the ability of plants to absorb nutrients from the soil in agriculture, antibacterial and odour-repellent textile products, anti-scratch car paints, dirt-repellent coatings, transparent protective sunscreens and self-cleaning glass silver.[4–9]

Walnut is a versatile fruit with its leaves, dry and green fruits, inner membrane and outer shell. Walnut is a widely consumed nut because it contains valuable nutrients and oils. Its fruit could be used as food but its inner membrane and outer shell are waste not used in any application (Fig. 1).

Fig. 1. Inner shell of walnut.

In this study, the waste inner shell of walnut was used as an electron precursor and the potential of employing waste walnut was examined *via* nanotechnology. For this purpose, waste inner shell-based silver nanoparticles were synthesized, characterized and biochemical properties were determined. Thus, the walnut inner shell was used in nanotechnology within the scope of sustainability and evaluated for use in different applications.

EXPERIMENTAL

WS-AgNPs were synthesized according to Keskin (2022) with minor modifications.[10] For this purpose, walnut inner shell extract and 0.05 M silver nitrate ($AgNO_3$) solution were mixed in a dark flask at a 1:1 volume ratio. The mixture was stirred for ~2 h at room temperature. The changes of color to dark brown were noted and confirmation of nanoparticle synthesis was done by UV absorption spectroscopy (Hach, DR/4000U) between 250 and 750 nm. The UV scanning was performed for each 30 min and the maximum absorbance at maximum wavelength of each scan was graphed. At the end of the synthesis, centrifugation was performed for 15 min at 9000 rpm with a high-speed centrifuge device to precipitate AgNPs from the aqueous medium. The resulting AgNPs were washed with distilled water to wash off impurities and dried at 75 °C. Obtained nanoparticles were characterized by scanning electron microscopy (SEM, ZEISS/Supra 40 VP), Fourier transform infrared spectroscopy (FTIR) (Thermo Fisher) and energy dispersive X-ray (EDX).

*Total phenolic content of walnut (*Juglans regia *L.) inner shell extract and WS-AgNPs*

The total phenolic content of natural products could be determined according to the Folin method.[11,12] The phenolic compounds and Folin–Ciocâlteu reagent become a colored complex and give a maximum absorbance at 765 nm. Gallic acid (GA) is usually used as a standard to produce a calibration curve.[11,12] The results are represented in mg of GA equivalent (GAE) per g. The analyses were performed in triplicate.

Antioxidant activity of WS-AgNPs

2,2-Diphenyl-1-picrylhydrazyl (DPPH) radical scavenging activity. DPPH radical is a commercially available radical and a 100 μM methanol solution of this radical was used in the experiments.[13] WS-AgNPs sample solutions were prepared at different concentrations (0.25, 0.5, 1, 1.25 and 1.5 mg mL^{-1}). Equal volumes (750 μL) of DPPH solution and WS-AgNPs sample solutions (different concentrations) were mixed and kept at room temperature for 50 min. At the end of the time, absorbance was recorded at 517 nm where DPPH gives maximum absorbance. These absorbance values were plotted against the corresponding concentrations and SC_{50} values were calculated and expressed against the Trolox standard.[13] The analysis was performed for walnut inner shell extract and all analyses were performed in triplicate.

Iron reduction capacity (FRAP). FRAP method is the most commonly used method for the determination of the antioxidant capacity of natural products and is based on the principle that antioxidant substances in natural products reduce iron (III) ions in Fe(III)–TPTZ complex.[14] Fe(III) reduced by antioxidant substances present in solution gives absorbance at 593 nm. The results were expressed in μM $FeSO_4 \cdot 7H_2O$.

Urease inhibition. Urease (E. C 3.5.1.5) is an enzyme that converts urea to ammonia and carbon dioxide. The formation of urea was determined using the indophenol method.[15] 200 μL Jack Bean urease, 500 μL buffer (100 mM urea, 0.01 M K_2HPO_4, 1 mM EDTA and 0.01 M LiCl, pH 8.2), and 100 μL inner shell extract were incubated for 20 min at room temperature. After incubation, phenol solution (550 μL, 1 % phenol, and 0.005 % sodium nitroprusside) and alkaline mixture (650 μL, 0.5 % sodium hydroxide and 0.1 % NaOCl) were added to the tubes and absorbance were recorded at 625 nm after 50 min. IC_{50} values were determined using standards at different concentrations. The same procedure was performed for WS-AgNPs at different concentrations (0.25, 0.5, 1, 1.25 and 1.5 mg mL^{-1}). All analyses were performed in triplicate.

RESULTS AND DISCUSSION

The population growth and the difficulties in disposing of the increasing amount of waste are catastrophic to the environment and climate conditions. For a sustainable environment, it is important to recycle waste and bring it into the field of technology. Organic solid waste management and ecological worries have been escalating in recent days.[16] Hence, fruit wastes, such as fruit peels, and other organic fractions of domestic solid wastes may be used effectively in nanotechnology-based applications.[17–19] In this study, silver nanoparticles were obtained by green synthesis technique using walnut inner membrane, which is produced in significant amounts in our country and its use is quite limited. Different parts of walnut contain linolelaidic acid, 1-heptatriacotanol, oleamide, ethyl isoalcoholate, hexadecanoic acid, cinnamic acid, brassica sterol acetate and *β*-sitosterol.[20–23] It was stated that specially walnut inner shell is rich in polysaccharides and polyphenols and contains also fat, protein, amino acids, flavonoids, saponins and alkaloids.[24] The fact that the walnut inner membrane is rich in bioactive components indicates that it may be an important agent in silver nanoparticle synthesis (Fig. 2).

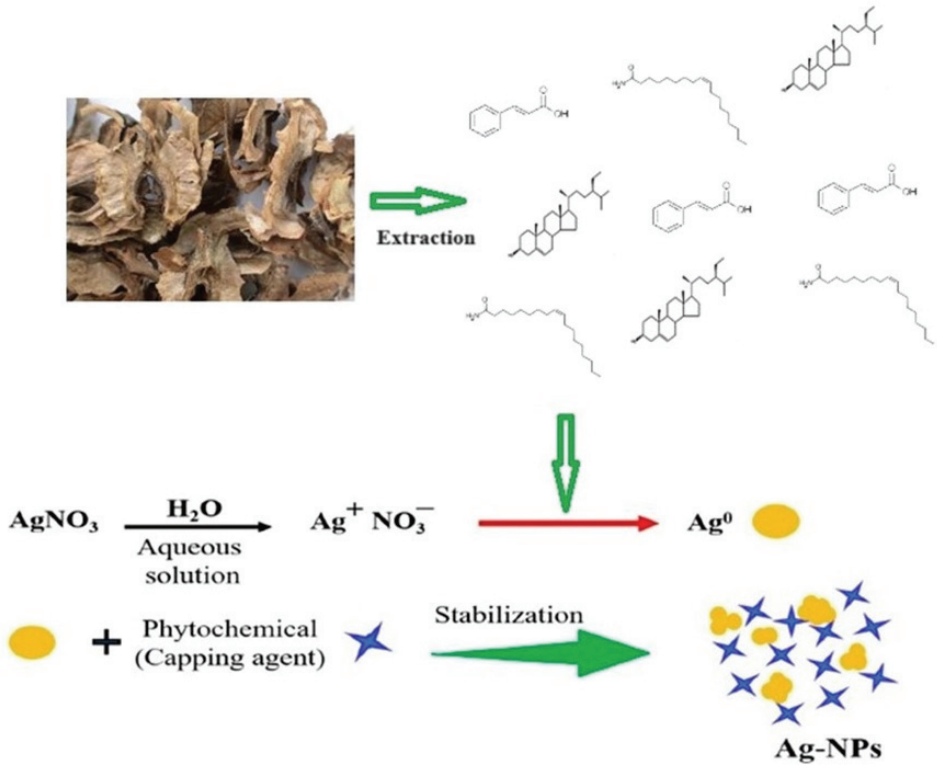

Fig. 2. Potential mechanism of synthesis of WS-AgNPs.[25]

The optical properties of synthesized nanoparticles were determined using a UV–Vis spectrophotometer. It was determined that the obtained nanoparticles gave maximum absorbance at 460 nm (Fig. 3). The reduction of Ag^+ to Ag was defined by intermittently measuring the absorption spectra of the reaction solution using a UV–Vis spectrophotometer. Usually, due to the excitation of free electrons, AgNPs would display a surface plasmon resonance (SPR) band at 450––550 nm,[16] 400–500nm[26] and 430 nm.[27] In the current study, the SPR value of WS-AgNPs was detected at 460 nm. The obtained data in this study is similar to the previously reported AgNPs synthesis result.[16,28–30]

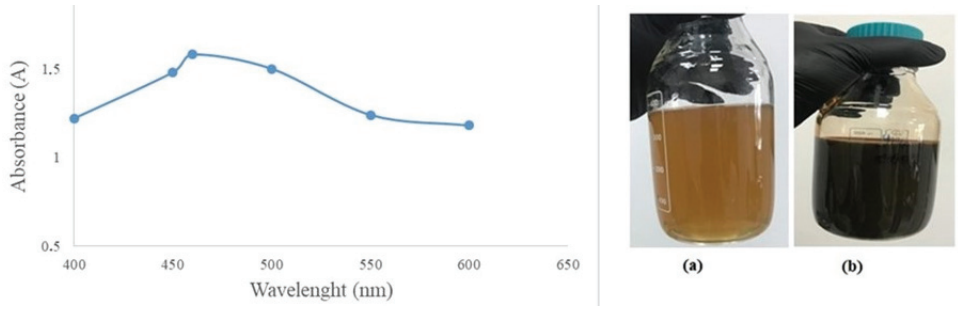

Fig. 3. UV spectrum of WS-AgNPs; a) Walnut inner shell extract; b) WS- AgNPs solution.

Functional groups of walnut inner shell extract and WS-AgNPs supernatant were determined using FT-IR and the results were shown in Figs. 4 and 5, respectively. FTIR data allow us to compare walnut inner shell extract and WS-AgNPs supernatant functional groups to determine possible reactions. As seen in Figs. 4 and 5, there were changes at 2122.54 cm^{-1} band and there was a new band at 1065.98 cm^{-1}. The band at 3200 to 3400 cm^{-1} represents O–H stretching groups.[31] In the study, silver nanoparticles were synthesized from maize (*Zea mays* L.) extract. According to this study, AgNPs had differences at functional groups of 3336.64–3334.57 cm^{-1} O–H bands and there are no differences at 1636.82–1636.48 cm^{-1} C–C bands.[31] It was clear that the functional groups and maximum absorbance of AgNPs vary over a wide range and the results obtained in this study were compatible with the literature.[16,28–31]

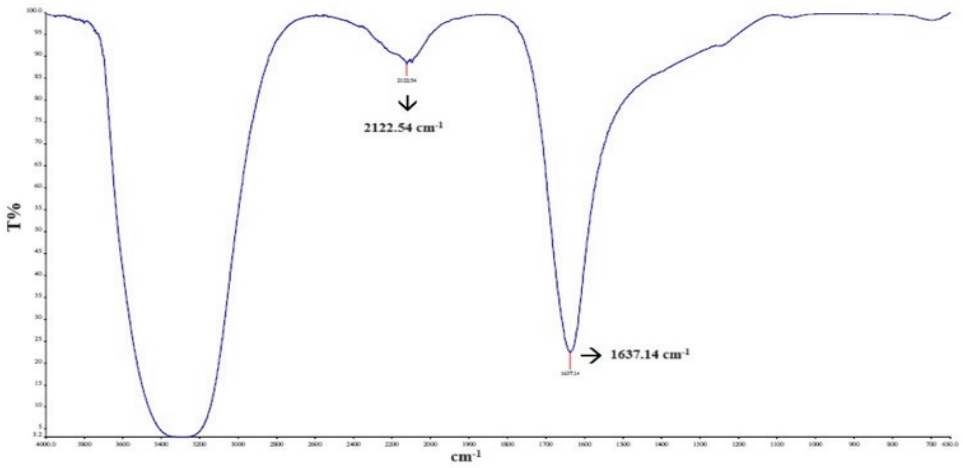

Fig. 4. Walnut inner shell extract FT-IR data.

The size of nanoparticles varied between 46 and 51 nm (Fig. 6). The histogram was obtained by using Fig. 6. In another study, *Tribulus terrestris* based

silver nanoparticles were synthesized and particle size was determined in a range between 15 and 65 nm.[32] In the literature, AgNPs were obtained in different sizes such as 14.3–14.7,[29] 16.7,[30] 12.63,[31] 46.26[32] and 65.92.[33] It was seen that particle sizes of silver nanoparticles could be changed in a wide range.[26–33]

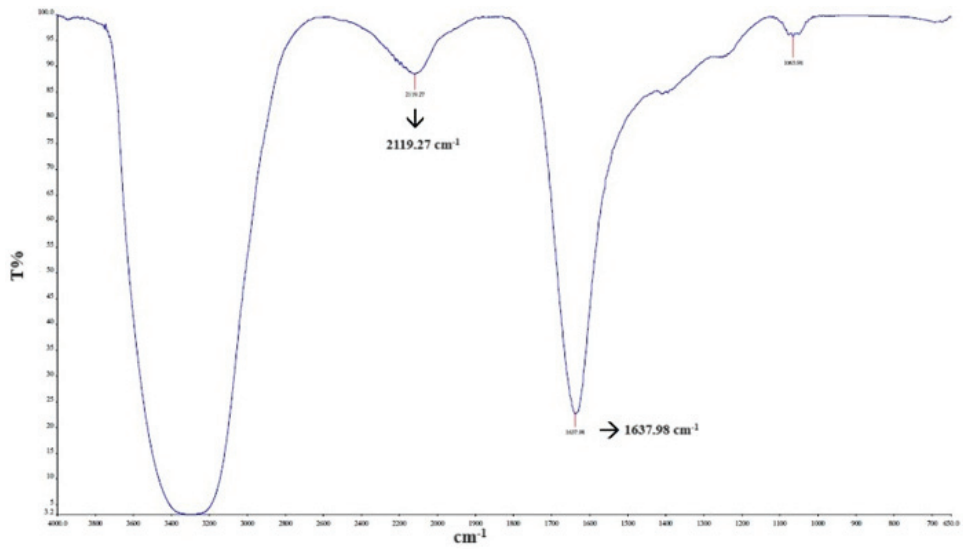

Fig. 5. WS-AgNPs supernatant FT-IR data.

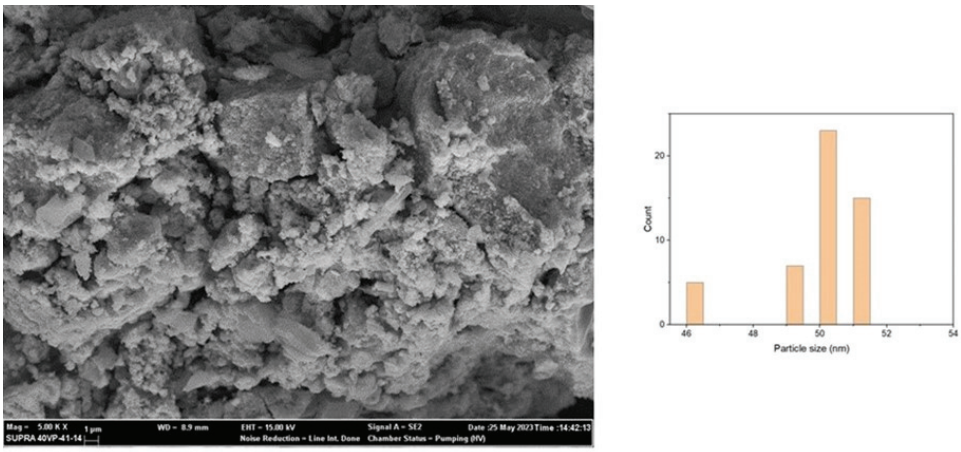

Fig. 6. SEM image and histogram of WS-AgNPs.

The WS-AgNPs had a peak at 3 keV in EDX analyses (Fig. 7). EDX analysis for silver nanoparticles usually shows characteristic peaks in EDX spectra around 3 keV due to surface plasmon resonances with weak carbon, oxygen and

nitrogen peaks.[34] In this study, silver nanoparticles showed a strong well-defined signal at 3 keV.

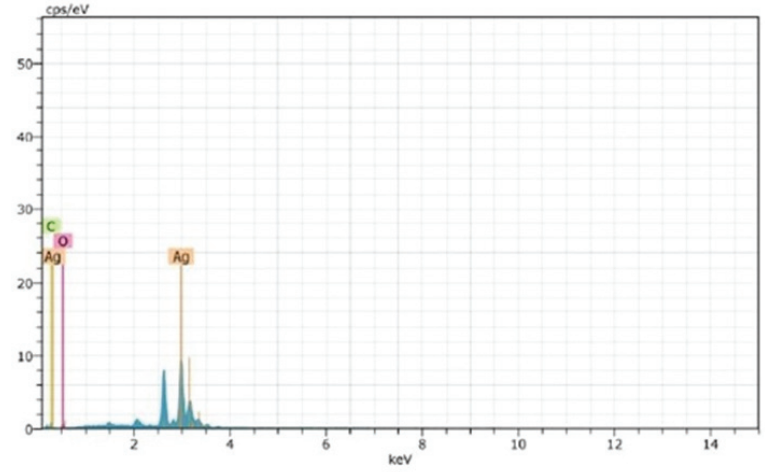

Spectrum: 3352

Element	Series	unn. C [wt.%]	norm. C [wt.%]	Atom. C [at.%]	Error (1 Sigma) [wt.%]
Silver	L-series	57.09	91.95	61.66	1.85
Oxygen	K-series	4.20	6.76	30.58	1.09
Carbon	K-series	0.80	1.29	7.76	0.26
	Total:	62.08	100.00	100.00	

Fig. 7. EDX results of WS-AgNPs.

The total phenolic content of walnut inner shell extract and WS-AgNPs were determined as 21.33±0.18 and 27.63±0.22 mg GAE/g DW and the inhibition effect of urease enzyme was calculated as 52.83±1.19% and 82.16±1.30 %, respectively (Table I). In a study, *Asphodelus aestivus* Brot. aerial part extract-based silver nanoparticles were synthesized and antioxidant activity was determined. It was reported that the AgNPs (67.54 %) had a good inhibition effect according to plant extract (31.82 %) for DPPH.[35] In another study, *Primula vulgaris* based silver nanoparticles were synthesized and the total phenolic content and antioxidant activity of NPs were determined. The antioxidant activity of AgNPs, biosynthesized using *P. vulgaris* flower extract, was found 90.6 %.[36] It was clear that the antioxidant activity and total phenolic content could be changed in a wide range and our results were compatible with the literature.[35–42]

Helicobacter pylori is the most common infectious bacteria affecting almost half of the world's population with diseases such as gastritis, peptic ulcers and gastric cancer. While proton pump inhibitors, antibiotic combinations, and bismuth compounds are used in the first-line treatment of patients infected with *H. pylori* and symptomatic patients, treatment is usually unnecessary in symptom-

-free patients due to the risk of reinfection in a short time.[43] Despite all these treatment options, H. *pylori* infection is still an important health problem due to antibiotic resistance.

TABLE I. Biochemical properties of Walnut inner shell extract and WS-AgNPs

Sample	Total phenolic content mg GAE g^{-1} DW sample	FRAP μM TE g^{-1}	DPPH %	Urease inhibition %
Walnut inner shell extract	21.33±0.18	107.44±2.04	72.71±0.98	52.83±1.19
WS-AgNPs	27.63±0.22	181.12±1.89	85.23±1.02	82.16±1.30

H. *pylori* in order to survive, in the stomach strong acid pH, needs to reach the mucus layer. The flagella and the urease enzyme secreted by the bacterium enable it to reach the mucus layer. The urease enzyme breaks down urea secreted by gastric epithelial cells into ammonia and the ammonia released causes an increase in the pH of the stomach and provides a suitable environment for the bacteria to survive. Therefore, inhibition of the urease enzyme is very important. In this study, the synthesized nanoparticles inhibited the urease enzyme by 82.16±1.30 %. Borase *et al.* synthesized silver nanoparticles based on *Ficus carica* in their study and stated that the extract and silver nanoparticles inhibited ammonium formation by 4.73 % and nearly 80 %, respectively.[44] Amin *et al.* synthesized silver nanoparticles based on *Solanum xanthocarpum* L. and found that the nanoparticles inhibited the urease enzyme by 64 %.[45] Gul *et al.* synthesized silver nanoparticles based on *Ricinus communis* and reported that the nanoparticles inhibited the urease enzyme by 94.2 %.[25] Many studies are showing that silver nanoparticles obtained by using different herbal sources have many effects such as antimicrobial, antioxidant, etc. (Table II). In this study, it was determined that the particles obtained had antioxidant activity and inhibited the urease enzyme.

TABLE II. Synthesis of AgNPs by using different sources

Biological source	UV absorbance, nm	Av. size, nm	Biomedical application	Reference
Honey	443/456	14.3/14.7	Antibacterial activity	29
Aristolochia bracteolata Lam	430	16.7	Antioxidant and antibacterial activities	30
Zea mays L.	461.25	12.63	Antimicrobial activity	31
Tagetes erecta L.	422	46.26	Antioxidant activity	32
Glycosmis mauritiana	435	65.92	Antioxidant activity, antimicrobial activity and enzyme inhibition properties	33
Solanum xanthocarpum L.	406	4 to 18	Antioxidant activity and enzyme inhibition properties	45
Mikania cordata	451	26.8–46.0	Antioxidant and antibacterial activities	46

TABLE II. Continued

Biological source	UV absorbance, nm	Av. size, nm	Biomedical application	Reference
Tribulus terrestris	400–450	21–73	Antioxidant activity and enzyme inhibition properties	47
Humulus lupulus L.	450	30.60 to 36.72	Antioxidant activity and enzyme inhibition properties	48
Parsley stem	460	31	Antioxidant activity	49
Citrullus colocynthis	450	10–45	Antioxidant and anti-gout activities	50
This study	460	46–51	Antioxidant activity and enzyme inhibition properties	–

CONCLUSION

Walnut is a widely consumed nut because it contains valuable nutrients and oils. Due to the consumption of walnuts as food, the inner shell of the walnut remains a significant amount of waste along with its phytochemicals. In this study walnut inner shell-based silver nanoparticles were synthesized, characterized and biochemical properties determined. It was shown by this study that herbal-based wastes could be used in nanotechnology for different purposes. The walnut inner shell extract was used as an electron processor to synthesize WS--AgNPs. After detailed characterization, it was determined that WS-AgNPs are a good antioxidant and urease inhibitor. It could be concluded that WS-AgNPs had potential as an antimicrobial agent and could be used in many applications for health benefits.

Acknowledgements. This study is a part of Merve Can's Master Thesis and a part of this study was presented in Third International Congress on Biological and Health Sciences (Online, 14-16 April 2023). The study was supported by Bilecik Şeyh Edebali University (BAP) with project number of 2022-02.BŞEÜ.01-03.

ИЗВОД

ЗЕЛЕНА СИНТЕЗА, КАРАКТЕРИЗАЦИЈА И БИОХЕМИЈСКА СВОЈСТВА НАНОЧЕСТИЦА СРЕБРА НА БАЗИ ОТПАДНЕ УНУТРАШЊЕ ЉУСКЕ ОРАХА (*Juglans regia* L.)

MERVE CAN[1] и MERVE KESKİN[2]

[1]*Graduate Education Institute, Bilecik Seyh Edebali University, Bilecik, Türkiye u* [2]*Vocational School of Health Services, Bilecik Seyh Edebali University, Bilecik, Türkiye*

Одрживост је важна за будућу екологију, а пораст отпада последњих година негативно утиче на одрживост. Управљање отпадом и његово коришћење у области технологије могло би да буде решење за одрживост. Нанотехнологија је технологија у развоју, која се примењује за побољшање физичких, хемијских и биолошких својстава материје величине 1–100 nm. Наночестице се могу синтетизовати различитим методама као што су физичке, биолошке и хемијске. Метода зелене синтезе (биолошке синтезе) је најповољнија у поређењу са хемијским и физичким јер је еколошки прихватљива, штедљива, јефтинија, мање ствара отпад, лака за скалирање, одржива и биолошки компатибилна. Орах је воће које

има разноврсну употребу, од листова, сувог и зеленог воћа, дрвета, унутрашње/спољне љуске и коре. Његова унутрашња и спољашња љуска се не користе као храна и представљају отпад. У овој студији, отпадна унутрашња љуска ораха коришћена је за синтезу сребрних наночестица (WS-AgNP). WS-AgNP су синтетизоване зеленом техником, окарактерисане и одређена су им биохемијска својства. Честице WS-AgNP величине 46–51 nm су показале максимум апсорпције на 460 nm, и инхибирале су ензим уреазу за 82,16±1,30 %. Очигледно је да се отпад на бази биљака може користити у нанотехнологији и да такође има потенцијал да се користи у медицини.

(Примљено 10. новембра, ревидирано 28. децембра 2023, прихваћено 3. марта 2024)

REFERENCES

1. V. A. Yavuz, *Mustafa Kemal Univer. J.Soc. Sci. Inst.* **7** (2010) 63 (https://dergipark.org.tr/en/pub/mkusbed/issue/19556/208640)
2. TUİK (2023), https://www.tuik.gov.tr/ (access date: 21.05.2023)
3. Sıfır Atık (2023), https://sifiratik.gov.tr/ (access date: 21.05.2023)
4. M. Beykaya, A. Çağlar, *Akü Femübid* **16** (2016) 631 (https://doi.org/10.5578/fmbd.34220)
5. M. Keskin, G. Kaya, S. Bayram, A. Kurek-Górecka, P. Olczyk, *Molecules* **28** (2023) 2762 (https://doi.org/10.3390/molecules28062762)
6. M. Rafique, I. Sadaf, M. S. Rafique, M. B. Tahir, *Art. Cells Nanomed. Biotech.* **45** (2017) 1272 (https://doi.org/10.1080/21691401.2016.1241792)
7. V. Thamilselvi, K. V. Radha, *IOSR J. Pharm* **7** (2017) 21 (https://doi.org/10.9790/3013-0701012127)
8. M. Murphy, K. Ting, X. Zhang, C. Soo, Z. Zheng, *J. Nanomat.* (2015) 5 (https://doi.org/10.1155/2015/696918)
9. A. C. Burduşel, O. Gherasim, A. M. Grumezescu, L. Mogoantă, A. Ficai, E. Andronescu, *Nanomaterials* **8** (2018) 681 (https://doi.org/10.3390/nano8090681)
10. M. Keskin, *El-Cezeri* **9** (2022) 266 (https://doi.org/10.31202/ecjse.963670)
11. V. L. Singleton, R. Orthofer, R. M. Lamuela-Raventós, *Methods Enzymol*. **299** (1999) 152–178 (https://doi.org/10.1016/S0076-6879(99)99017-1)
12. V.L. Singleton, J.A. Rossi, *Am. J. Enol. Viticult*. **16** (1965) 144 (https://doi.org/10.5344/ajev.1965.16.3.144)
13. P. Molyneux, *Songklanakarin J. Sci. Technol*. **26** (2004) 211 (https://sjst.psu.ac.th/inc_viewpage.php?link=journal/26-2/07-DPPH.pdf&id=214&t=Paper%20PDF&act=load)
14. I.F. Benzie, J.J. Strain, *Meth. Enzym.* **299** (1999) 15 (https://doi.org/10.1016/s0076-6879(99)99005-5)
15. Ş. Keskin, Y. Şirin, H. E. Çakir, M. Keskin, *S. Afr. J. Bot.* **120** (2019) 170 (https://doi.org/10.1016/j.sajb.2018.04.017)
16. G. Das, J.K. Patra, T. Debnath, A. Ansari, H. S. Shin, *PloS ONE* **14** (2019) e0220950 (https://doi.org/10.1371/journal.pone.0220950)
17. S. Ahmed, M. Ahmad, B.L. Swami, S. Ikram, *J. Adv. Res.* **7** (2016) 17 (https://doi.org/10.1016/j.jare.2015.02.007)
18. M. Reenaa, A.S. Menon, *Int. J. Curr. Microb. App. Sci.* **6** (2017) 2358 (https://doi.org/10.20546/ijcmas.2017.606.337)

19. B. A. Omran, H. N. Nassar, N.A. Fatthallah, A. Hamdy, E.H. El-Shatoury, N.S. El-Gendy, *Energy Sources, A* **40** (2018) 227 (https://doi.org/10.1080/15567036.2017.1410597)
20. S. Zhao, J. Niu, L. Yun, K. Liu, S. Wang, J. Wen, H. Wang, Z. Zhang, *HortScience* **54** (2019) 275 (https://doi.org/10.21273/HORTSCI13381-18)
21. H. Han, S. Wang, M. Rakita, Y. Wang, Q. Han, Q. Xu, *Food Nutrit. Sci.* **9** (2018) 1034 (https://doi.org/10.4236/fns.2018.98076)
22. A. Medic, J. Jakopic, A. Solar, M. Hudina, R. Veberic, *Biology* **10** (2021) 535 (https://doi.org/10.3390/biology10060535)
23. S. Askin, H. Askin, E. Dursun, E. Palabiyik, H. Uguz, Ö. Cakmak, K. Koc, *Cytokine* **153** (2022) 155861 (https://doi.org/10.1016/j.cyto.2022.155861)
24. Y. Zhan, M. Ma, Z. Chen, A. Ma, S. Li, J. Xia, Y. Jia, *Foods* **12** (2023) 3379 (https://doi.org/10.3390/foods12183379)
25. A. Gul, A. Shaheen, I. Ahmad, B. Khattak, M. Ahmad, R. Ullah, A. Bari, S. S. Ali, A. Alobaid, M. M. Asmari, H .M. Mahmood, *Biomolecules* **11** (2021) 206 (https://doi.org/10.3390/biom11020206)
26. Y. He, F. Wei, Z. Ma, H. Zhang, Q. Yang, B. Yao, Z. Huang, J. Li, C. Zenga, Q. Zhang, *RSC Advances* **7** (2017) 39842 (https://doi.org/10.1039/c7ra05286c)
27. B. Mousavi, F. Tafvizi, S. Zaker Bostanabad, *Art. Cells Nanomed. Biotech.* **46** (2018) 499 (https://doi.org/10.1080/21691401.2018.1430697)
28. J. M. Ashraf, M. A. Ansari, H. M. Khan, M. A. Alzohairy, I. Choi, *Sci. Rep.* **6** (2016) 20414 (https://doi.org/10.1038/srep20414)
29. G. Matar, G. Akyuz, E. Kaymazlar, M. Andaç, *Bioint. Res. App. Chem.* **13** (2023) 195 (https://doi.org/10.33263/briac132.195)
30. R. Chinnasamy, K. Chinnaperumal, T. Cherian, K. Thamilchelvan, B. Govindasamy, C. Vetrivel, V. Perumal, P. Willie, P. Krutmuang, *Biomass Conv. Bioref.* (2023) 1 (https://doi.org/10.1007/s13399-023-03750-8)
31. A. Eren, M. F. Baran, *App. Eco. Env. Res.* **17** (2019) 4097 (https://doi.org/10.15666/aeer/1702_40974105)
32. R. Erenler, C. Temiz, I. Yildiz, Y. Yanar, C. Ozyigit, *J. Optoel. Adv. Mat.* **23** (2021) 503 (https://joam.inoe.ro/articles/green-synthesis-and-characterization-of-silver-nanoparticles-from-tagetes-erecta-flowers/fulltext)
33. M. Govindappa, H. Farheen, C.P. Chandrappa, R.V. Rai, V.B. Raghavendra, *Adv. Nat. Sci: Nanosci. Nanotech.* **7** (2016) 035014 (https://doi.org/10.1088/2043-6262/7/3/035014)
34. J. S. Moodley, S. B. N. Krishna, K. Pillay, Sershen, P. Govender, *Adv. Nat. Sci: Nanosci. Nanotech.* **9** (2018) 015011 (https://doi.org/10.1088/2043-6254/aaabb2)
35. T. Fafal, P. Taştan, B. S. Tüzün, M. Ozyazici, B. Kivcak, *S. Af. J. Bot.* **112** (2017) 346 (https://doi.org/10.1016/j.sajb.2017.06.019)
36. B. Erdem, H. Çiftçi, Y. Şahin, *Muş Alparslan Üniversitesi Fen Bilimleri Dergisi* **10** (2022)1013 (https://doi.org/10.18586/msufbd.1126542)
37. T. Kokila, P. S. Ramesh, D. Geetha, *Ecotox. Env. Safety* **134** (2016) 467 (https://doi.org/10.1016/j.ecoenv.2016.03.021).
38. M. R. C. Sytu, D. H. Camacho, *BioNanoScience* **8** (2018) 835
39. E. N. Gecer, *J. Inorg. Organomet. Polym. Mat.* **31** (2021) 4402 (https://doi.org/10.1007/s10904-021-02057-3)
40. M. Mani, S. Pavithra, K. Mohanraj, S. Kumaresan, S. S. Alotaibi, M. M. Eraqi, A. D. Gandhi, R. Babujanarthanam, M. Maaza, K. Kaviyarasu, *Env. Res.* **199** (2021) 111274 (https://doi.org/10.1016/j.envres.2021.111274)

41. T. Sivakumar, *Int. J. Bot. Stud.* **6** (2021) 476 (https://www.botanyjournals.com/assets/archives/2021/vol6issue3/6-3-76-159.pdf)
42. W. G. Shousha, W. M. Aboulthana, A. H. Salama, M. H. Saleh, E. A. Essawy, *Bull. Nat. R. Centre* **43** (2019) 1 (https://doi.org/10.1186/s42269-019-0221-8)
43. E. Dilmaç, M. Sucu, T. Günbatan, İ. Gürbüz, *Mersin Üniversitesi Tıp Fakültesi Lokman Hekim Tıp Tarihi ve Folklorik Tıp Dergisi* **13** (2023) 98 (https://doi.org/10.31020/mutftd.1184609)
44. H. P. Borase, R. B. Salunkhe, C. D. Patil, R. K. Suryawanshi, B. K. Salunke, N. D. Wagh, S. V. Patil, *Biotech. App. Biochem.* **62** (2015) 780 (https://doi.org/10.1002/bab.1341)
45. M. Amin, F. Anwar, M. R. S. A. Janjua, M. A. Iqbal, U. Rashid, *Int. J. Mol. Sci.* **13** (2012) 9923 (https://doi.org/10.3390/ijms13089923)
46. M. Khatun, Z. Khatun, M.R. Karim, M.R. Habib, M.H. Rahman, M.A. Aziz, *Food Chem. Adv.* **3** (2023) 100386 (https://doi.org/10.1016/j.focha.2023.100386)
47. C. C. M. Figueiredo, A. da Costa Gomes, L. C. Zibordi, F. O. Granero, V. F. Ximenes, N. M. Pavan, L. P. Silva, C. da S. M. Sonvesso, A. E. Job, N. Nicolau-Junior, R. M. G. da Silva, *Food Bioprod. Proc.* **138** (2023) 150 (https://doi.org/10.1016/j.fbp.2023.01.010)
48. M. Keskin, *Acta Sci. Pol. Hort. Cult.* **21** (2022) 11 (https://doi.org/10.24326/asphc.2022.4.2)
49. O.B. Boga, H. Kara, E.B. Kurbanoglu, *Int. Conf. Frontiers Acad. Res.***1** (2023) 162 (https://as-proceeding.com/index.php/icfar/article/view/61)
50. S. Karunakaran, R. Hari, *Avicenna J. Med. Biotech.* **14** (2022) 303 (https://doi.org/10.18502/ajmb.v14i4.10485).